STUDY OF COMPUTATIONAL AND EXPERIMENTAL METHODOLOGIES FOR CRACKS RECOGNITION OF VIBRATING SYSTEMS USING MODAL PARAMETERS

Irshad Ahmad Khan

Study of Computational and Experimental Methodologies for Cracks Recognition of Vibrating Systems using Modal Parameters

Thesis Submitted to the

Department of Mechanical Engineering National Institute of Technology, Rourkela

for award of the degree

of

Doctor of Philosophy

by

Irshad Ahmad Khan

under the guidance of

Prof. Dayal R. Parhi

Department of Mechanical Engineering

National Institute of Technology Rourkela

Orissa (India)-769008

September 2015

Declaration

I hereby declare that this dissertation is my own work and that, to the best of my knowledge and belief. This dissertation contains my original work, no material has been taken from previous published or written by another neither person nor material which to a substantial extent has been accepted for the award of any other diploma or degree of the university. Wherever contributions of others are involved, every effort is made to indicate this clearly, with due reference to the literature, and acknowledgement of collaborative research and discussions.

(***Irshad Ahmad Khan***)

Date:

CERTIFICATE

This is to certify that the thesis entitled, ***"Study of Computational and Experimental Methodologies for Cracks Recognition of Vibrating Systems using Modal Parameters",*** *being submitted by Mr. Irshad Ahmad Khan to the Department of Mechanical Engineering, National Institute of Technology, Rourkela, for the partial fulfillment of award of the degree Doctor of Philosophy, is a record of bona fide research work carried out by him under my supervision and guidance.*

This thesis is worthy of consideration for award of the degree of Doctor of Philosophy in accordance with the regulation of the institute. To the best of my knowledge, the results embodied in this thesis have not been submitted to any other University or Institute for the award of any degree or diploma.

Prof. Dayal R. Parhi

(Supervisor)

Acknowledgements

I would never have been able to finish my dissertation without the guidance of my committee members, help from friends, and support from my family.

I would like to express my deepest gratitude to my advisor, Dr. Dayal R Parhi, for his guidance, caring, patience, and providing me with an excellent atmosphere for research. I have been amazingly lucky to have Dr. Parhi as my advisor, mentor and friend. His patience and support helped me to overcome the most difficult crisis in my life and finish this dissertation.

I am grateful to Prof. Sunil Kumar Sarangi, Director of National Institute of Technology, Rourkela for giving me an opportunity to work under the supervision of Prof. Dayal R. Parhi. I am thankful to Prof. S. S. Mahapatra, Head of the Department, Department of Mechanical Engineering and Prof. K. P. Maity former Head of the Department, Department of Mechanical Engineering, National Institute of Technology, Rourkela for his moral support and valuable suggestions regarding my academic requirements.

It's a great opportunity to express my gratefulness and love to my wife, Firoza Khan. She is always there standing by me with her support, encouragement, patience and love through the good times and bad. I thank to my Nine months old daughter, Ms. Daniya Khan, for her charming smile, which gives me inner strength and happiness during my research work.

This dissertation is dedicated to my parents. My Mom and Dad are a constant source of love, support, motivation and strength all these years. Their constant support and love provides me, strength and an ability to tackle challenges head on.

Lastly, I would like to thank my all lab mates who had given me the timely help and encouragement in completing thesis work.

Last, but not the least, I thank the one above all of us, the omnipresent God, for giving me the strength during the course of this research work.

Irshad Ahmad Khan

Abstract

Mostly the structural members and machine elements are subjected to progressive static and dynamic loading and that may cause initiation of defects in the form of crack. The cause of damage may be due to the normal operation, accidents or severe natural calamities such as earthquake or storm. That may lead to catastrophic failure or collapse of the structures. Thereby the importance of identification of damage in the structures is not only for leading safe operation but also to prevent the loss of economy and lives. The condition monitoring of the engineering systems is attracted by the researchers and scientists very much to invent the automated fault diagnosis mechanism using the change in vibration response before and after damage. The structural steel is widely used in various engineering systems such as bridges, railway coaches, ships, automobiles, etc. The glass fiber reinforced epoxy layered composite material has become popular for constructing the various engineering structures due to its valuable characteristics such as higher stiffness and strength to weight ratio, better damage tolerance capacity and wear resistance. Therefore, layered composite and structural steel have been taken into account in the current study. The theoretical analysis has been performed to measure the vibration signatures (Natural Frequencies and Mode Shapes) of multiple cracked composite and structural steel. The presence of the crack in structures generates an additional flexibility. That is evaluated by strain energy release rate given by linear fracture mechanics. The additional flexibility alters the dynamic signatures of cracked beam. The local stiffness matrix has been calculated by the inverse of local dimensionless compliance matrix. The finite element analysis has been carried out to measure the vibration signatures of cracked cantilever beam using commercially available finite element software package ANSYS. It is observed from the current analysis, the various factors such as the orientation of cracks, number and position of the cracks affect the performance and effectiveness of damage detection techniques. The various automated artificial intelligent (AI) techniques such as fuzzy controller, neural network and hybrid AI techniques based multiple faults diagnosis systems are developed using vibration response of cracked cantilever beams. The experiments have been conducted to verify the performance and accuracy of proposed methods. A good agreement is observed between the results.

Keywords: Natural Frequency, Mode shape, Fuzzy, Neural network, Vibration response.

Table of Contents

List of Tables

List of Figures

Nomenclature

Although all the primary symbols used in this dissertation are defined in the text as they occur, a list of them is presented below for easy reference. On some occasions, a single symbol is used for different meanings depending on the context and thus sometimes uniqueness is lost. The contextual explanation of the symbol at its appropriate place of use is hoped to eliminate the confusion.

English Symbol

L	Length of the beam
B	Width of the beam
H	Thickness of the beam
L_e	Length of an element
a_1, a_2	Depth of crack
L_1, L_2	Location of the crack
A	Cross-sectional area of the beam
E	Elastic Modulus
G	Rigidity Modulus
u, v, θ	Nodal displacement of composite beam element
F, S, M	Applied system force for composite beam element
K_{el}	Stiffness matrix for composite beam element
M_e	Mass matrix for composite beam element
K_I, K_{II} ,K_{III}	Stress intensity factors
j	Strain Energy release rate
C	Compliance coefficient matrix
T	Transformation matrix
K_{crack}	Stiffness matrix for composite beam
A_{11}	Axial compliance
$A_{12}= A_{21}$	Coupled axial and bending compliance
A_{22}	Bending compliance
$\bar{A}_{11}$	Dimensionless form of A_{11}
$\bar{A}_{12} = \bar{A}_{21}$	Dimensionless form of $A_{12}= A_{21}$

$\bar{A}_{22}$	Dimensionless form of A_{22}
$R_{i\ (i = 1to\ 18)}$	Unknown coefficients of matrix R
i, j	Variables
$Q_{I,i}(i=1, 2)$	Stress intensity factors for F_i loads
$P_{i\ (i = 1, 2)}$	Experimentally calculated function
$F_{i\ (i = 1, 2)}$	Axial force (i=1), Bending moment (i=2)
K'	Stiffness matrix for first crack position
K''	Stiffness matrix for second crack position
K	Stiffness matrix for free vibration
$u_i(i=1,2)$	Normal functions (longitudinal) $u_i(x)$
$v_i(i=1,2)$	Normal functions (transverse) $v_i(x)$
x	X co-ordinate of the beam
y	Y co-ordinate of the beam

Greek Symbols

υ	Poisson's Ratio
ρ	Mass Density
α	Angle of fibers
ω_n	Natural frequency
ψ_1	Relative first crack depth (a_1/H)
ψ_2	Relative second crack depth (a_2/H)
β_1	Relative first crack location (L_1/L)
β_2	Relative second crack location (L_2/L)
Λ	Minimum (min) operation
$\forall$	For every
ϵ	Complement
μ	Degree of association

CHAPTER 1

Introduction

The assessment of damages present in the structures attracts the attention of scientists and engineers since last few decades. The presence of damage in the form of crack in structural components and machine elements, if not recognised immediately? will be severe threat to the integrity of the system and may cause loss of assets as well as human lives. The prediction of damage in form of crack is important not only for safety but also for the economic growth of industries. The quantitative change in dynamic response of structures before and after the damage can be used for crack identification. This chapter highlights the various methods those have been implemented for fault diagnosis of vibrating structures. The first part of this chapter addresses the background and motivation from the analysis of various crack diagnosis techniques. The second part describes the aim and objectives of the current research and novelty of the work. The organization of this thesis is depicted in the last section of the current chapter.

1.1 Motivation for the development of fault diagnosis techniques

Usually, damage may occur in the structural members due to normal operations, accidents, and severe natural calamities such as earthquake or storms. These may produce structural damage such as cracks, which can lead to sudden failure and breakdown of the structures. The development of health monitoring techniques such as vibration based damage detection methods is most significant to avoid sudden and unexpected failure of the engineering systems. The engineering structures are one of the most important elements of the modern society. Any disruption present in these structures may lead to the loss of assets as well as the loss of life. It is, therefore, most important to ensure the safe and uninterrupted performance of the engineering structures by periodic monitoring.

In the literature, many methods are available for the assessment of faults present in the engineering structures. Some of these methods are expensive because of their installation and maitenance cost like ultrasonic testing, magnetic particles testing and few are less sensitive as they require more time and presence of geometrical constraints for techniques (liquid penetrant testing). The vibration analysis-based method has high sensitivity, low

installation and operation cost so that it can be effectively used as fault diagnosis tool. The researchers have measured the change in vibration features of structures before and after damage to develop the Artificial Intelligent (AI) techniques based fault detection models. The AI techniques are modelled with an objective of fast and accurate measurement of damages/cracks present in the structures.

AI techniques (fuzzy logic system and neural network models) and hybrid fuzzy-neuro models have been designed and analyzed in current research for prediction of multiple cracks present in the structures to ensure the smooth and safe operation by capturing the modal response.

1.2 Aim and objective of the dissertation

The quantification and localization of damage are important in any engineering system associated with aerospace, civil and mechanical engineering. The engineering systems must be free from damage to ensure the safe and smooth operation. The presence of cracks in engineering system may lead to sudden and unexpected failure of systems. This damage or crack must be identified early to prevent catastrophic failure. The beam-like structures are commonly used as a structural element in various engineering systems (composite and steel structure, industrial machine) and these elements are subjected to static and dynamic loading.

The uses of the composite materials are rapidly increased in aerospace, civil and mechanical engineering over the past few years. Now composite materials have become a major constituent of various engineering systems due to their valuable features such as high stiffness and strength to weight ratios, better wear and fatigue resistance and damage tolerance capacity. The different types of damage may be detected in composite materials such as delamination, matrix cracking and fiber breaking. The presences of these damages in composite structures reduce the strength and stiffness and may lead to the catastrophic failure of the structure. The vibration analysis based methods is preferable over a non-destructive testing for damage detection in fibre reinforced composite (FRC) and isentropic materials (structural steel) beam. However vibration based methods are used worldwide for identification of damage. The objectives of dissertation are:

- To develop AI based structural health monitoring techniques using vibration parameters of multiple cracked cantilever composite and steel beams. In the current study, a literature review has been carried out in the domain of damage detection

methods applied in the various engineering system. It is observed that the results obtained by researchers are not systematically applied to the development of methods for the identification multiple crack present in the composite structures.

- In the present analysis, an effort has been carried out to design and analyze novel multiple crack identification methods such as theoretical, numerical (FEM), experimental and AI techniques using modal parameters of intact and damage cantilever composite and steel beams.
- The results derived from various proposed methods such as theoretical, numerical (FEM), experimental, fuzzy logic, neural networks and hybrid fuzzy-neuro models have been compared with the experimental results and a close judgment has been reported.

1.3 Novelty of the work

In the present study, Theoretical, Numerical, Experimental and AI techniques are employed for identification of multiple damages of the composite and steel beams. The vibration signatures (Natural Frequencies and Mode Shapes) are extracted from theoretical and finite element methods. The first three natural frequencies and mode shapes are used as input parameters to AI models and outputs are relative first and second crack locations and depths. The identification of multiple cracks using AI techniques with first three natural frequencies and mode shapes is a unique combination as inputs to AI based models for composite structure.

In this thesis various hybrid AI techniques based models such as Fuzzy-BPNN, Fuzzy-RBFNN and Fuzzy-KSOM have been developed and designed for identification of multiple cracks in steel and composite structures.

1.4 Organization of dissertation

The current dissertation is organized as follows.

Chapter1 gives the introduction on the effect of damage/crack on modal parameters of engineering systems and discussion about methods being employed by researchers for estimation of the damage of different engineering applications. The aim and objective of thesis and motivation to carry out the present research is also reported in this chapter.

Chapter 2 is the literature review section. It represents the discussion based on development and analysis of faults diagnosis methods using vibration analysis and AI

techniques. This section discusses the classification of methods in the domain of damage detection and also explains the reasons behind the direction of the current study.

Chapter 3 deals with the theoretical analysis of cantilever composite and steel beam to measure the modal indicators (natural frequencies and mode shapes) individually in two sections. The presence of crack generates local flexibility at the vicinity of crack, that upsets the modal response (observed reduction in natural frequencies and change in mode shapes). The changes in modal responses can be used to localize and quantify the crack in engineering structures. The authentication of results obtained from the theoretical model has been verified with the experimental results and good agreement is observed between the results.

Chapter 4 provides information regarding the application of the finite element method for identification of damage present in cantilever beam by capturing change in modal responses. These deviations in the modal indicators are used as information to recognize crack locations and depths. The results obtained from the numerical simulation are compared with theoretical and experimental results for validation.

Chapter 5 discusses the application of the fuzzy logic system for identification of damage in cantilever beam. The detailed procedure for development of the fuzzy system is outlined in this chapter. The architectures of various membership functions such as Triangular, Gaussian, and Trapezoidal are briefly discussed. The results obtained from different fuzzy models have been compared with experimental results to verify the performance of the fuzzy system.

Chapter 6 introduces the artificial neural network techniques such as Back Propagation Neural Network (BPNN), Radial Basis Function Neural Network (RBFNN) and Kohonen Self Organizing Maps (KSOM) for prediction of crack locations and depths of multiple cracked cantilever composite and steel beams. The procedures adopted for the development of three types of neural models with their architectures are outlined in the present chapter.

Chapter 7 gives the outline of a hybrid fuzzy-neuro model for prediction of crack intensities and severities in engineering systems. The procedure employed to design the fuzzy part and neural part of the fuzzy-neural model is presented. The analysis and comparisons of results derived from various hybrid fuzzy-neuro models and the experimental test are presented.

Chapter 8 presents the experimental procedure along with details of experimental instruments used in the analysis. The results obtained from the experimental investigation are compared with different analysis results discussed in the present thesis.

Chapter 9 presents a comprehensive review and analysis of outcomes obtained from various proposed methods cited in the current research.

Chapter 10 provides the conclusions derived from different methods of fault diagnosis being adopted in current research and suggests the scope of present work in future.

CHAPTER 2

Literature Review

In the current chapter a comprehensive study of different damage detection methodologies such as vibration based classical methods, finite element methods, wavelet transform method and AI techniques based methods used for identification of damage to the structural and machine components are discussed. In this chapter the findings and developments done by researchers and scientists during the past few decades in the field of condition monitoring of the structural and machine elements are presented.

2.1 Introduction

The scientific and research communities give more attention to the structural integrity monitoring because unpredicted failure of structural members may cause reduced economy and loss of human life. The literature review section describes the study of the published work in the fields of condition monitoring techniques, fault detection methods, damage detection algorithm and vibration response analysis methods. Firstly vibration based damage identification methods are described, followed by Finite Element Analysis (FEA), discreet wavelet transform and sensors based method. The artificial intelligence techniques such as fuzzy system, artificial neural network, genetic algorithm, Adaptive Neuro Fuzzy Inference System (ANFIS) and hybrid AI methods for damage detection in structural members and machine elements are also discussed and analyzed in the detail. The literature gives a direction to move forward in the present research. The aim of the present research is to design and develop an artificial intelligent technique based algorithm, which can be used to detect multiple cracks in the beam like dynamic structures.

2.2 Study of structural integrity monitoring techniques

Scientists and researchers have developed many methodologies for the prediction of damage in different fields of engineering and science. The vibration analysis based methods are found to be quite satisfactory for integrity monitoring of cracked dynamic structures. Since last three decades extensive research have been done by scientists and

researchers in the area of vibration based damage detection methods and significant growth has been reported in the field of engineering. A wide range of techniques, methodologies and algorithms are invented to solve various problems of different structures.

Doebling et al. [1] have presented the detail review of vibration based damage identification and structural health diagnosis methods up to 1996. Dimarogonas [2] has also presented a review article on various damage detection methods reported by researcher (between 1971-1993). Sohn et al. [3] have presented an updated version of review article on the available literature upto 2001. In above discussed articles vibration response is the parameters were considered to classify the damage detection methods. Carden and Fanning [4] have presented review article on the available literature of different damage detection methods, which are published in 1996-2003.But in the above papers damage identification methodologies based on soft computing AI technique have not been addressed. In this chapter, the different methodologies of damage identification in cracked vibrating structures have been described briefly. The different methodologies proposed by various researchers and scientists for condition monitoring can be classified as:

2.2.1 Classic methods for identification of damage

In the present section, classical methods such ultrasonic testing based methods, function response based methods, energy operator based method, analytical methods, and algorithms based methods, etc. for fault detection are discussed. The research works related to the above methodologies are discussed below.

A review paper to study and compare several damage detection methodologies based on natural frequencies, modal strain energy and modal curvature analysis of a damaged Euler–Bernoulli beam has been presented by Dessi and Camerlengo [5]. They have divided all selected techniques into two classes: one includes techniques that require data from literatures for estimating structural changes due to damage; the second category contains the modified Laplacian operator and the fractal dimension. No reverse identification technique has been reported in the above paper. A multiple damage detection method based on Wavelet Transform (WT) and Teager Energy Operator (TEO) of beams has been described by Cao et al. [6]. The WT & TEO based curvature mode shape structures provide greater resistance to noise and more sensitivity to damage in comparison with the conventional curvature mode shape. They observed that proposed

WT & TEO curvature mode shape based method actually detect multiple damages even in small size in beams in high-noise environment. Wang [7] has developed a new damage identification factor called Difference of nearby Difference Curvature Indicator (DNDCI) for single-span beams. The proposed DNDCI is very sensitive to the damage region or nearby measuring points and also there is no need of any pre-knowledge of the non-damage beam. The proposed model is compared with examples from literature for validation purpose. He has observed that DNDCI can be applied to the actual single-span beams supported by bearings.

A numerical analysis of delaminated composite Timoshenko beams for getting the vibration response under consideration of constant amplitude moving force has been presented be Kargarnovin et al. [8]. They have derived Governing differential equations of motion for proposed model, and delaminated area is modeled using a piecewise-linear spring principle. The Ritz method is employed to calculate the dynamic response of the beam for the free and forced vibrations and compared with the corresponding available literatures. They have also studied the effects of several variables (force, velocity, lamina ply angle, single de-lamination size, its span-wise and/or thickness-wise location) on vibration parameters and forced critical speed. Argatov et al. [9] have presented a new method to detect localized large-scale internal damage in imperfect bolted joint structures. They have used the structural damping and the equivalent linearization of the bolted lap joint response to separate the combined boundary damage from localized large-scale internal damage. In the development of method, they have illustrated the longitudinal vibrations in a thin elastic bar with both ends attached by lapped bolted joints with different levels of damage. They have found that proposed method can be used for the estimation of internal damage severity if the crack location is recognized. Kargarnovin et al. [8] and Argatov et al. [9] have presented the analysis on damage structures but they have not discussed about damage detection using soft computing technique.

Casini and Vestroni [10] have analyzed the nonlinear modal data of a two degree of freedom piecewise-linear oscillator with two damage parameters and two discontinuity boundaries in the configuration plane. The system can be used to model the dynamics of linear systems colliding with elastic obstacles as well as an asymmetrically multi-cracked cantilever beam vibrating in bending mode and hence demonstrating a bilinear stiffness.

Carr and Chapetti [11] have studied the influence of a surface fatigue crack on the vibration characteristics of T-welded plates and the results are compared to the control of machined through thickness cuts to the dynamic response of cantilever beams. They have

analyzed the influence of fatigue cracks growth on the natural frequencies and compared to experimental data with two and three dimensions results of numerical modeling. The results of their analysis showed the capacity of experimental technique to detect fatigue cracks relatively sooner than another method under study. The output of the proposd method can be used to design a robust AI model for relatively fast identification of fatique crack. An Experimental Modal Analysis (EMA) of structures to get vibration parameters under vibrational excitation has been proposed by Farshidi et al. [12]. The EMA is used without contact to assess the structural dynamics of a beam by exciting a beam cantilever structure using a collimated air pulse controlled by a solenoid valve. They have measured the reflected beam air wave surface by an array of microphones. They have stated that the experimental tests demonstrate the effectiveness of their proposed methodology for both accurate and cost-effective measurement of structural dynamics in translation and rotation degrees of excitation using a non-contact sensor and engine.

Rezaee and Hassannejad [13] have used perturbation method for vibration analysis of a simply supported beam with fatigue breathing crack. The cracked simply supported beam is modeled as a nonlinear single degree of freedom system. They have observed from the results; that damping factor is sensitive to the crack depth and location. Moreover, the presence of the super harmonics of the fundamental frequency in the response spectra of the cracked beam discloses the nonlinear dynamic behavior of the cracked beam, which can be used as a crack indicator in structural health monitoring applications. A damage assessment technique for the non-destructive detection and size assessment of open cracks in beam structures has been developed by Faverjon and Sinou [14]. The constitutive relation error updating method is used for the recognition of the crack's location and size in a simply-supported beam. The transverse open crack is modeled through the introduction of the flexibility due to the presence of the crack (by reducing the second moment of area of the element at the crack's location). They have analyzed about a crack in simply supported shaft but have not depicted the methodology for reverse identification. Mazanoglu et al. [15] have performed a non-uniform vibration analysis of Euler - Bernoulli beams with open multiple cracks and using energy-based method and Rayleigh - Ritz approximation method. They have measured the change in strain on the cracked beam due to bending. They also analyzed the Euler - Bernoulli beam through the finite element program and compared the results with the analytical method and found that the results are in good agreement.

Lee [16] has proposed a damage detection methodology for beam structures with multiple cracks using the Newton-Rapson method, and he has assumed the cracks present in the system as rotational springs. A method to measure the local flexibility matrix and stress intensity factor of cracked beam to develop an algorithm for damage identification has been proposed by He et al. [17]. They have developed the method by dividing the number of split tube thin rings. Ebersbach and Peng [18] have prepared an expert system for the condition monitoring of fixed plant machinery, using proven industry method. They have observed that developed system can be used to detect failure with high precision using the dynamic response of the system Finite element methods and wavelets transform method were used to find the size and severity of cracks. A damage detection method using vibration characteristics of a circular arc in both damaged and undamaged models using the theoretical analysis and compared the results with the experimental analysis to design has been developed by Cerri et al. [19]. They have used the natural frequencies and mode shapes to develop the damage detection model with the assumption, the arch act as a torsion spring on the cracked section. Shin et al. [20] have analyzed the vibration response of circular arcs with variable cross section. They have represented the equation for deriving the natural frequency of the system under different boundary conditions, with the application of generalized differential quadrature method and the differential transformation process. The results from their proposed method were compared with literature. A new crack detection technique based on the Amplitude Deviation Curve (ADC) or Slope Deviation Curve (SDC) approach which is upgraded version of Operational Deflection Shape (ODS) has been proposed by Babu and Sekhar [21]. They have revealed the effectiveness of SDC over ODS for small cracks detection.

Benfratello et al. [22] have presented numerical and experimental investigations in order to assess the ability of non-Gaussianity measures to detect the presence and position of a crack. The Monte Carlo method is applied to evaluate in the time domain the higher order statistics of a cantilever beam modeled by finite elements. They have used the skew ness coefficient of degrees of freedom of rotation for the purpose of identifying a crack in the damaged structure. Sinha [23] has analyzed the nonlinear dynamic behavior of the mechanical system using higher order spectra tools for detecting the presence of higher harmonics in the signals obtained from the system. He has found that the misaligned axis of rotation of the shaft and crack exhibits a nonlinear behavior due to the presence of higher harmonics spectra in the signal. According to them, the tools of higher order spectra can be actually used for condition monitoring of rotatory mechanical systems.

Viola et al. [24] have studied the dynamic behavior of multi-step and multi- damaged circular arcs using different boundary conditions. They have proposed the analytical and numerical solutions for multi-stepped damage and undamaged circular arches. The analytical solution is based on the Euler characteristic exponent procedure involving the roots of characteristic polynomials while the numerical method is focused on the generalized differential quadrature method and the generalized differential quadrature element technique.

Humar et al. [25] have presented a survey on some of common vibration base crack detection techniques and discovered the drawbacks in them. The presence of cracks in the structure has badly affected the modal response, stiffness, and damping. They have found that most of the vibration-based damage detection techniques, fail to perform when applied to real structures due to the inherent difficulties. They have presented computer simulation studies of some of the techniques and suggested the conditions under which they may or may not run. They have concluded that all practical challenges found in a real system cannot be simulated by computer applications entirely doing crack base vibration assessment methods of a challenging course. In [18-25] it is reported that crack and damage have major role on the vibration signatures of the structures. It is also observed in the above papers that no systematic approach has been given for prediction of multiple cracks and damages in structures. A new technique for identification of cracks in the beam based on instantaneous frequency and empirical mode decomposition has been proposed by Loutridis et al. [26]. The dynamic behavior of the structure has been investigated both theoretically and experimentally under harmonic excitation. They have observed that the variation of the instantaneous frequency increases with increasing depth of the crack and these changes were used to estimate the size of the crack. Wang et al. [27] have investigated coupled bending and torsional vibration of a fiber-reinforced composite cantilever with an edge. They have analyzed the composite cantilever beam with a surface crack and found that the variation in vibration responses depends on two parameters, i.e. the crack location and material properties (fiber orientation and fiber volume fraction). They have concluded that the change in frequency can be efficiently used to detect the crack position and measure its severity. An experiment was conducted by them to authenticate the results obtained by the proposed method. But in the above paper methodololy for localization and severity of crack has not been addressed.

Douka and Hadjileontiadis [28] have studied the nonlinear dynamic behavior of a cantilever beam theoretically and experimentally by using time–frequency analysis

instead of the traditional Fourier analysis. They have analyzed the simulated and experimental response data by applying empirical mode decomposition and Hilbert transform method. They found that proposed methodology can accurately analyze the nonlinearities due to the presence of a breathing crack. But thoroughly experimental validation of results is required for authecation of proposed Hilbert transform method. The effects of cracks in anti-resonances of a double cracked cantilever beam using analytical and experimental methods have been investigated by Douka et al. [29]. They have recognized the cracks of the cracked beam using anti-resonance shift. The results of theoretical analysis have been authenticated using the results obtained from the experiments of Plexiglas beam for detecting the cracks. This paper has not addressed soft computing AI technique for crack identification.

Cerri and Ruta [30] have investigated a circular arc articulated plan for the development of a structural damage detection technique to study the changes in the natural frequency of the system. They have discussed two different methods for crack detection. First method based is on comparison of the change of the natural frequency, which is obtained from the experimental and theoretical analysis and the second method is based on a joint intersection of the curves obtained from the modal equations. The equation of curve can be written as:

$$k_r(\psi) = -\frac{G_2(\zeta_{e,r})}{G_1(\psi, \zeta_{e,r})} \tag{2.1}$$

Where subscript e represents experimental data and variable ψ denotes the damage location and k_r is the damage intensity value corresponding to the r^{th} eigenvalue of the damage arc. The experimental Eigen value can be obtained from following relation:

$$\zeta_{e,r}^{D} = \zeta_{r}^{U}\left(\omega_{e,r}^{D} \Big/ \omega_{e,r}^{U}\right) \tag{2.2}$$

Where $\omega_{e,r}^{D}$ and $\omega_{e,r}^{U}$ are the natural frequencies in damage and un-damage state of the structure.

A non-destructive technique for damage detection in structures has been developed by Owolabi et al. [31]. Experimental investigations were performed at the crack location and crack intensity for fixed beams and simply supported beams. They have measured the changes in the first three natural frequencies and their amplitudes to predict the crack in a beam structure. But in this paper analysis is not given for computation AI technique. An exact solution approach based on the Laplace transform to analyze the bending free

vibration of a cantilever laminated composite beam with surface cracks has been described Song et al. [32] . They have used the principle of Hamilton variational together with the Timoshenko beam model to develop the technique for the detection of damage crack in the composite structure. The effects of various parameters such as the ply angle, fiber volume fraction, crack number, position and depth on the vibration characteristics of the beam has been discussed in detail. Zou et al. [33] have proposed a modified version of the local flexibility of a cracked rotor system which more suitable for the theoretical model. They have studied the dynamic behavior of the cracked rotor to design for forward application as a crack diagnostic model.

Patil and Maiti [34] have proposed a method for damage recognition in a of slender Euler-Bernoulli beam using frequency measurement and the transfer matrix method. They have considered cracks as rotating springs in the analytical method for identification of cracks. A damage detection algorithm to predict the damage intensity and measure its severity using the change in modal parameters of a continuous two beam span has been presented by Kim and Stubbs [35]. They have reviewed two algorithms and eliminated some of the assumptions and limitations of these methods and developed a new algorithm for damage recognition. They have found that new proposed method has a higher accuracy than reviewed two algorithms for damage detection. In [34-35] it is reported that application of computational AI techniques is not addressed. Chinchalkar [36] has developed a general numerical method to detect fault using finite element method. His approach is based on measuring the first three natural frequencies of the cracked beam. The proposed method for fault detection accommodates different boundary conditions and with wide variations in the depth of the crack. Xia and Hao [37] have proposed a technique for identification of the damage; select the subset points to measure corresponding modes. They have used two factors to detect the cracks: the sensitivity of a residual vector for structural damage and damage to the sensitivity of the measured noise. They have concluded that the developed method is independent of the state of damage and can detect damage using the undamaged state of the structure.

Messina et al. [38] proposed Multiple Damage Location Assurance Criterion (MDLAC) correlation coefficient with the help of two metheds of recognizing the size of damage in structural components. The sensivity of frequency of each mode at each damage position is the parameter of designing the proposed method. MDLAC is termed as a statistical correlation between change in frequency predicted by analytical method (δF_a) and change in frequency measured by experintal investigation (δF_e). The change in analytical

frequency (δF_a) can be measured as a function of the damage extent vector (δD). The magnitude of the damage is obtained by searching for damage extent vector (δD) which maximizes the MDLAC value:

$$MDLAC(\{\delta D\}) = \frac{\left|\{\delta F_e\}^T \cdot \{\delta F_a(\{\delta D\})\}\right|^2}{\left(\{\delta F_e\}^T \{\delta F_e\}\right) \cdot \left(\{\delta F_a(\{\delta D\})\}^T \cdot \{\delta F_a(\{\delta D\})\}\right)} \quad (2.3)$$

The MDLAC coeficiant is a pratical approach to datremine the damage extent which is verified by numerical and experimental analysis results. This proposed MDLAC approach only requires the measurement of change in natural frequency of damage and non-damage structure and can be utilized as a powerful tool for detection of damage extent in term of both the locatiom and size of damage at single and multiple places. In [34-38], it is observed that though the damage has major role in functioning of system, but analysis on damage identification required in this paper.

2.2.2 Finite element methods used for crack identification

The finite element method is applied by various researchers for identification cracks of the faulty dynamic structures, which are described in this section:

Xu et al. [39] have proposed a crack identification method using curvatures and continuous wavelet transforms finite element analysis of beams. A uniform acrylonitrile butadiene styrene cantilever beam with crack has been used in the experimental analysis to know the fidelity of the proposed method. They have found a good agreement between the finite element analysis and experimental analysis results. Wang et al. [40] have performed experimental and numerical analysis of a laminated T700/BA9912 composite under low-velocity impact to analyze the damage behavior. The 3D Hashin damage criterion and the cohesive zone model are used in the finite-element investigation, and the numerical simulation displays the de-lamination, matrix damage, and fiber breakage present in the composite material. A Non-Damage Inspection (NDI) method is performed to evaluate the effectiveness of numerical models. They have found that the predicted size and shape of the de-lamination area well agreed with the NDI result and the fiber breakage in the bottom layers of the laminates are in good agreement with the experimental analysis. An analytical discrete element technique and finite element method to determine the dynamic response of the un-damped Euler Bernoulli beam with breathing cracks under a point moving mass has been presented by Ariaei et al. [41]. The

effect of the moving mass, velocity, location and size of the crack on beam deflection is investigated.

A 3D finite element method to find out plane normal and shearing stresses over critical surfaces of adhesively bonded single lap joints with FRP composite adherends has been analysed by Panigrahi [42]. The stress distribution over mid surface of the adhesive layer of damaged and non-damaged model has been compared with the literature. The parameters of vibration and stress distribution obtained in [41-42] can be used to designed soft computing AI models for recognition of damage. Potirniche et al. [43] have applied finite element method using ABAQUS software for fatigue and fracture application. Two dimensional elements with edge crack are considered in the analysis. They have determined the stiffness matrix of the crack element from the Castiglione's first principle and compared the results of the proposed method with results obtained from the physical method and they have found good agreement between the results. A non-destructive damage detection method to study the influence of a crack on the dynamic response of a cantilever beam subjected to bending has been described by Hearndon et al. [44]. They have created a cracked finite element model to compute the influence of damage location and severity on the stiffness of structures. Due to presence of crack, the change in beam deflection is observed, which leads to the reduction of the global stiffness of the beam, upset the vibration responses. This property has been used by authors in structural health monitoring purpose.

Al-said [45] has proposed a mathematical model to identify crack location and depth in stepped cantilever Euler Bernoulli beam carrying a rigid disk at its tip. He has described lateral vibration of the beam using a simple mathematical model combined with mode method and long-range equation. The proposed FEA based method is capable of recognition of crack location and depth. Andreausa et al. [46] have studied the non-linear response of a cantilever cracked beam subjected to harmonic loading with two dimensional finite element formulations which is capable to display a breathing crack behavior via a frictionless contact model of the interacting surfaces. A numerical technique to analyze the free vibration analysis of uniform and stepped cracked beam with circular cross section has been presented by Kisa and Gurel [47]. The beam was assumed to be detached in two parts from crack section, the finite element and component mode synthesis method used in analysis to achieve the goal. The modal parameters of a cracked beam obtained from the free vibration analysis, which can be used in the crack identification process. A finite element method for crack identification of the beam for

free and forced response analysis has been proposed Karthikeyan et al. [48]. A transverse surface crack is considered in the Timoshenko beam model. Chasalevris and Papadopoulos [49] have presented an inverse crack identification method using the dynamic behavior of a shaft with two transverse surface cracks. They have proposed that the identification method gives not only the depth and the location of the crack, but also the regular orientation of crack around axes of shafts.

Nahvi and Jabbari [50] have presented analytical and experimental approach for identification of crack by vibration measurement. An experimental investigation is performed of the cracked cantilever beam excited by hammer and vibration responses recorded by accelerometer moving along the length of the beam. To recognize the crack contours of normalized frequency was plotted in term of relative crack depth and crack location. They have recognized crack depth and crack location by the intersection of contours with constant natural frequency planes. Law and Lu [51] have proposed crack detection method of a beam structure with Dirac delta function and based dynamic measurement in the time domain. The proposed method was based on model superposition and optimization technique with regularization on the solution. They have compared proposed identification damage algorithm with experimental analysis.

Vibration parameters (natural frequencies and mode shapes) of cracked beam using finite element method have been calculated by Zheng and Kessissoglou [52]. They added overall flexibility matrix to a flexibility matrix of the heavy beam instead of local flexibility to obtain total flexibility matrix. They have found that the overall flexibility matrix gives more accurate vibration parameters than local flexibility matrix. It is reported that overall flexibility of system can be used for identification of damage present in the structures.

A Single Damage Indicator (SDI) factor to localize and quantify a crack in beam like structure by relating with fractional change in natural frequency has been proposed Kim and stubb [53]. They have proposed two models one for crack location and another for crack depth by using the parameter fractional change in modal energy to change in natural frequencies due to presence of crack. In the first model, (crack location model) fractional change in measured the eigenvalue (*Zi*) and FEM based theoretical modal sensivity of the i^{th} modal stiffness corresponding to j^{th} element F_{ij} is described respectively. The theoretical modal curvature is determined from a third order interpolation function of displacement modeshape. This can be defined as:

$$Z_i = \delta\omega_i^2 \big/ \omega_i^2 \tag{2.4}$$

$$F_{ij} = K_{ij} \big/ K_i = \frac{\int_{x_j}^{x_{j+1}} \{\varphi''\}^2 dx}{\int_0^L \{\varphi''\}^2 dx} \tag{2.5}$$

Then they introduced an error index parameter to localize the error for i[th] mode and j[th] location is expressed as:

$$e_{ij} = \frac{Z_i}{\sum_{k=1}^{NM} Z_k} - \frac{F_{ij}}{\sum_{k=1}^{NM} F_{kj}} \tag{2.6}$$

where NM denotes numbers of measured vibration modes. A expression for single damage indicator is defined to detect the damage position for all mode of vibration.

$$SDI_j = \left[\sum_{i=1}^{NM} e_{ij}^2\right]^{-1/2} \tag{2.7}$$

The damage a_j at known position can be expected using the sensitivety equation in the crack size model. The crack depth can be recognized from damage parameter a_i and this model is based on linear fracture mechanics principle. The robustness of crack detection model has been evaluated by experimental investigation.

Saavendra and Cuitino [54] have presented the dynamic behavior of different multi-beams systems containing a transverse crack using theoretical and experimental analysis. An additional flexibility introduces at the vicinity of the crack is evaluated using strain energy release rate given by linear fracture mechanics theory. A new cracked finite element stiffness matrix is deduced due to the additional flexibility and used in the finite element method of the crack system. A procedure for detection of cracks in structures using modal test data has been proposed by Viola et al. [55]. They have examined the crack depth and crack position by changes in the dynamic behavior of cracked structures. Due to crack local flexibility introduced in the structure so that the dynamic response changed. But analysis of soft computing AI technique in above paper can be make a systematic approach for damage recognition.

2.2.3 Artificial intelligence techniques used for crack identification

In this section different types of Artificial intelligence techniques used in the field of identification of fault in present in faulty structures have described briefly as follow:

2.2.3.1 Fuzzy Inference System

Sugumaran and Ramachandran [56] have introduced the use of decision tree of a fuzzy classifier for selecting the best pair histogram feature that distinguishes the fault condition of the roller bearing from is given samples formed. The modal response from a piezoelectric transducer is recorded for the different types of errors (good bearing, bearing with inner race fault, bearing with outer race fault, and inner & outer race fault) of the bearing and it has used to generate the fuzzy rules. A fuzzy classifier is built and tested with measured data. The results have found to be satisfactory. A new surface cracks identification method based non-phenomenological inverse problems; especially in the case of AC field measurement has been introduced by Hasanzadeh et al. [57]. Their method is based on a formal framework of aligning electromagnetic probe responses by using the concept of similarity measures created by a fuzzy recursive least square algorithm as a learning methodology. They have stated that, the proposed technique provides a means to compensate for the lack of sufficient samples in available crack databases for prediction of crack in structures. They have shown that the combination of this fuzzy inference method and the method of the adaptation for different crack shapes provides sufficient means as a priori empirical knowledge for the training system.

A novel Fuzzy Robust Wavelet Support Vector Classifier (FRWSVC) based on a wavelet function and developed an Adaptive Gaussian Particle Swarm Optimization (AGPSO) algorithm to search the optimal parameters of the unknown FRWSVC has been designed by Wu and Law [58]. The experimental analysis results that apply the hybrid diagnostic model are based on the FRWSVC and the AGPSO algorithm. But as further analysis, use of hybrid fuzzy-BPNN model may give better results. Chandrasekhar and Ganguli [59] have revealed that the geometry and measurement uncertainty significant problem in recognition of the damage. The Curvature Damage Factor (CDF) of a cantilever beam is used as damage indicators in the analysis. They have used Monte Carlo method to determine the changes in the damage indicator study due to uncertainty in the geometric properties of the beam. The results obtained from the simulation are used for the development and testing of the fuzzy logic. In this publication, the uncertainty associated with the fuzzy logic system for the detection of structural damage has been directed. Saravanan et al. [60] have presented a technique; based on the acquired of the machinery to effectively diagnose the state of inaccessible moving components inside the machine proposed vibration signals. The proposed method has designed using a fuzzy classifier

and a decision tree to automatically generate rules from the feature set. They have tested fuzzy classifier with representative data and the results are found quite promising.

Two novel approaches to improve the performance of the online fuzzy classifier have been presented by Angelov et al. [61]. They have developed the fuzzy system for handwritten image recognition as well as on a real-life problem of the image classification context, where images should be classified into good and bad ones during an on-line and interactive production process. In [60-61] it is found that fuzzy classifier is one of the powerful soft-computing techniques, which can be used for assessment of damage. Kim et al. [62] have presented a computer aided diagnosis system for crack concrete structures with fuzzy set theory. The fuzzy training and operation performed based on built-in rules on the crack symptoms expressed as linguistic term and some numeric data and calculates reliability values and reinforcing values for each crack cause. Finally, the system integrates the previous diagnostic results using the Choquet fuzzy integral, calculates final reliability values and ranks the crack causes. They have expected that proposed system can be used as an effective crack diagnosis tool for both experts and non-experts in the regular inspection of RC structures.

A non-destructive testing and evaluation technique for detection of defects in materials using a fuzzy logic approach has been proposed Reza et al. [63]. The method proposed by them shows that there is less dependency between the variation of density and size of a defect and variations of noise density and distribution. Proposed approach reduces the noise and drift, leading to a better detection of defects. From the analysis of above paper, it is reported that fuzzy logic can be systematically applied for the crack identification of structures. Boutros and Liang [64] have developed fuzzy fused index (FFI) for reliable health recognition of machine component which is a fusion of four conditions-monitoring indicators based on fuzzy logic and Sugeno-style inference engine. Authors have successfully tested and validated in two different applications which are tool condition monitoring in milling operations and bearing condition assessment.

De Miguel and Blázquez [65] have designed a decision module based on fuzzy logic for model-based fault diagnosis in a DC motor. A fault detection and isolation system based on the input and output parameters have successfully applied in laboratory devices to reduce the uncertainty due to disturbances and modelling errors. The experimental estimation of the sensitivities of the residual equations has used to estimate the fault size. A mobile robot navigation control system based on fuzzy inference system has been described by Parhi [66]. Fuzzy rules embedded in the controller of a mobile robot enable

it to avoid obstacles in a cluttered environment that includes other mobile robot so that the robots do not collide with one another. Mohanta et al. [67] have developed a fuzzy Markov model for the maintenance planning of a captive power plant taking into account the various parameters that develops the failure repair cycle.

2.2.3.2 Artificial neural network techniques

In curent section different types of Artificial Neural Network (ANN) based techniques used for crack detection are described. ANN is used as a capable technique for damage detection.

A Back Propagation Neural Network (BPNN) technique for condition monitoring of cracked beam has been designed by Rakideh et al. [68]. They have extracted the first three natural frequencies of the beam using analytical method and fed these natural frequencies to BPNN model to predict the crack location and crack depth. They have concluded that the neural network is a powerful method to determine the location and depth of the crack. Also, the capability of prediction accuracy has increased with increasing the numbers of the natural frequencies. But an experimental verification is required in above paper. An artificial neural network based approach for identification of damage in an industrial welding robot has been proposed by Eski et al. [69]. To achieve the objective, an experimental setup is fabricated to accumulate the related data and the accelerations of welding robot, which has six degrees of freedom, are examined. They have concluded that RBNN is a capability to analyze the accelerations of manipulator joints during a prescribed trajectory. Schlechtingen and Santos [70] have proposed a comparison of results obtained from three different models, are the regression based model and two artificial neural network based models, which are a full signal reconstruction and an autoregressive normal behavior model used for fault identification of a wind turbine bearing. After the comparison of results, they have found all three proposed models were capable to identify initial faults. They have determined the neural network based approaches give best fault visibility with less computational time with comparison to regression based approach.

Multi Layers Perceptron (MLP) and Self Organizing Map (SOM) neural network based classifier for prognosis of fault of three phase induction motor and evaluated the performance of classifiers have been developed by Ghate and Dudul [71]. The different number of learning rules and transfer functions has investigated for different number of hidden layers. The simple statistical parameters used as input feature space and principal

component analysis are used for reduction of input dimensionality. They have also tested their approach with noise and found the performance of the proposed method satisfactory. As the further analysis RBFNN may give better results than MLP and SOM. Fan et al. [72] have presented a fault detection and diagnosis strategy for local system of air handling units. The strategy consists of two stages which are the fault detection stage and the fault diagnosis stage, respectively. In the first stage, the neural network fault detection model is used by them for generating estimates of sensor values and they have compared to actual values to produce residuals. The design neural network fault detection model has trained using an abundance of characteristic information from the historical data in the system. They have concluded that the trained neural network model can detect the abnormal condition in the system.

Saravanan et al. [73] have evaluated the effectiveness of wavelet-based features for fault diagnosis of a gear box using artificial neural network (ANN) and Proximal Support Vector Machines (PSVM). They have found PSVM has superiority over ANN in classification of features. Paviglianiti et al. [74] have proposed a detection and isolation sensor faults in a robotic manipulator. The proposed methods can trackle the influence of outer disturbances and uncertainties of the model. The dynamics of the proposed model have enhanced by using a radial basis function type of neural network. A new damage detection technique by using the Auto Regressive (AR) with a back propagation neural network has been developed by Wang et al. [75]. They have found the difference in the values of AR coefficients, which indicates AR coefficients of ideal signal for normal machine are deducted from faulty machines. The results obtained by them are compared with the three methods, which include the difference of AR coefficients with BPNN, the AR coefficients with BPNN and the distance of AR coefficients method for 23 samples. The authors have found that the difference of AR coefficients with BPNN were superior to AR coefficients with BPNN and distance of AR coefficient methods.

A fault identification and health monitoring techniques for a gear-set using continuous wavelet transform and neural network technique has been presented by Wu and Chan [76]. In the proposed fault diagnosis technique, sound emission of the gear-set is used for evaluation. A continuous wavelet transform technique combined with a feature selection of energy spectrum is used for examining fault signals in a gear-set of machines. They have concluded that the sound emission from the system can be used for promising fault diagnosis and condition monitoring of the rotating machines. Mehrjoo et al. [77] have proposed a damage detection methodology to assess the damage intensities of joints in

truss bridge structure using soft-computing technique i.e. back propagation neural network. But thorough experimental validation is required in above papers [76-77].The Modal frequency parameters such as natural frequencies and mode shapes are fed as input to BPNN for evaluation of damage intensities of joints in truss bridge structure. Just-Agosto et al. [78] have developed a fault detection technique using the Bayesian probabilistic neural network. A combination of vibration and thermal parameters sent to neural network as input data to detect fault in sandwich composite. A fault diagnosis and condition monitoring technique for internal combustion engine using Discrete Wavelet Transform (DWT) and neural network has been presented by Wu and Liu [79]. They have combined the DWT technique with feature selection of the energy spectrum of diagnosis of faults in rotating engines.

A faults detection methodology for structures using modal parameters and statistical neural network model has been presented by Bakhary et al. [80]. They have considered the effect of uncertainties in developing ANN model, by applying Rosenblueth's point estimate method verified by Monte Carlo simulation, the statistics of the stiffness parameters are estimated. But thorough experimental verification is needed in the above paper. A neural network based methodology for condition monitoring of axial flow fan blades has been presented by Oberholster and Heyns [81]. They have developed a methodology in two stages, in the first stage. The Neural networks are trained on features extracted from on-line blade vibration signals measured on an experimental test structure. In the second stage, neural networks trained on Numerical Frequency Response Function (NFRF) features obtained from a Finite Element Model (FEM) of the test structure. They have concluded that numerical approach is more preferable to the experimental approach where it is less costly to construct, update and test an FEM than to test an experimental or operational structure by means of damage simulation and suggested methodology can handle the online damage classification using sensor for the test structures. But in above paper deviation of results is not discussed. Yeung and Smith [82] have investigated a damage detection methodology, using pattern recognition of the vibration signature and unsupervised Probabilistic Resource Allocating Network (PRAN). They have found that sensitivity of the neural networks can be adjusted so that a satisfactory rate of damage detection can be achieved even in the presence of noisy signals.

A health monitoring of the cantilever beam containing transverse surface crack using neural network techniques has been developed by Suresh et al. [83]. They have calculated modal frequency parameters for different crack locations and depths using analytical

method and these modal parameters are used to train the neural network to detect the damage severity and intensity. A comparative study on the performance neural networks, such as multi-layer perception network, radial basis function network is done by authors. The authors have found that radial basis function network performance is better than multi-layer perception network. Kao and Hung [84] have presented structural condition monitoring technique using a supervised learning type of Neural System Identification Networks (NSINs).They first identified the undamaged and damaged states of a structural system using NSINs then trained NSINs has used to generate free vibration responses with the same initial condition or impulsive force of structures. In [83-84] it is reported that thorough experimental verification is needed for the authentication of results.

2.2.3.3 Genetic algorithms system

In the process of identification of crack in structural and machine component, the genetic algorithm is one of most effective soft computing technique. The genetic algorithm is based methodologies are discussed in this segment.

Zheng et al. [85] have proposed a crack detection method in beam with double or triple cracks as well as four cracks using a Hierarchical Genetic Algorithm (HGA). The predicted crack locations and sizes are in good agreement with the actual cracked beam. They have observed the numerical simulation reveals the HGA substantially reduces the total number of FE computation required and they are many orders smaller compared to conventional GA and also demonstrate the advantages of HGA over GA. A reverse crack detection technique using automated genetic algorithms in beam-like structures with a single transverse edge crack has been presented by Mehrjoo et al. [86]. The vibration signatures of beam calculated with the help of new developed theoretical models and results of proposed model compare with the two-dimensional (2D) finite element analysis results as well as available experimental measurements. They have used known vibration signatures as inputs to the genetic controller to predict the crack location and crack depth. The proposed model is verified through various examples available on cracked beams with different damage configuration. They have found that the present algorithm is able to identify various crack configurations in a cracked beam.

Meruane and Heylen [87] have presented a hybrid real-coded genetic algorithm as a powerful tool to solve optimization problems to quantify and locate the structural damage. The performance of the five basic functions based on nodal data that they studied. In addition, the authors have proposed the use of damaging penalization that

satisfactory false detection avoids damage by experimental noise or numerical errors. They have tested and found that this approach achieves a much more accurate solution than traditional optimization methods, the effectiveness of the proposed technique on a three dimensional space frame with single and multiple damage scenarios. A new feature extraction and selection scheme for hybrid fault diagnosis of gearbox based on S transform, non-negative matrix factorization, mutual information and multi-objective evolutionary genetic algorithms has been developed by Li et al. [88]. The S transforms function has adapted to the vibration signals for different fault condition of the transmission system and the non-negative matrix factorization is obtained to use to extract features from the time-frequency representation. The genetic algorithm is used for accurate classification of hybrid faults of the gearbox. The results of the experiments as described, showed that the proposed feature extraction and selection scheme demonstrate to be an effective and efficient tool for hybrid fault diagnosis of the gearbox.

Nobahari and Seyedpoor [89] have proposed an effective optimization method using genetic algorithms for quantification multiple damage in structural members based on the changes in the natural frequency. They have applied finite element analysis to evaluate the mandatory natural frequencies. A modified genetic algorithm with two new operators such as health and simulator operators is presented to accurately identification of the locations and extent of the damage. A crack detection tool in structural elements using a genetic algorithm optimization process, taking into account the existence of contact between the interfaces of the crack has been developed by Buezas et al. [90]. They have used bi and three-dimensional models addressed to the dynamics of a structural element with a transverse breathing crack. The experiment being performed with a damaged beam and the resultant data is used as input for the fault diagnosis of genetic algorithm. But as further analysis, use of hybrid technique may give better results. A real time fault detection method using the adaptive features extraction algorithm in gearbox to deal with non-stationary faulty signals has been developed by Hussain and Gabbar [91]. They have concluded that their suggested novel method is based on the combination of conventional one-dimensional and multi-dimensional search method that compared with evolutionary algorithms such as genetic algorithms showed high performance and accurate fault detection results. Han et al. [92] have studied on the important sensors for chiller Automated Fault Detection and Diagnosis (AFDD) application, based on feature selection techniques and machine learning methodology. Mutual information based filter has adopted for a preliminary idea about how the number of features affects the AFDD

performance. The results show that the eight functions / sensors, centered around the core cooling cycle and by the proposed method, selected surpass the other three feature subsets using the linear discriminant analysis.

A two-stage identification method to identify a number of cracks and their positions and size on a shaft has been presented by Singh and Tiwari [93]. In the first stage, a multi-crack detection and its quantification and localization algorithm are developed. The transverse forced vibration analysis has performed on a non-rotating cracked shaft with the help of the finite element method by using the Timoshenko beam theory. This stage of the algorithm gives the number of cracks and their approximate locations over the shaft. In the second stage of the algorithm, the size and the accurate location of cracks are obtained by using multi-objective genetic algorithms. But in the above paper deviation of results is not addressed. A new multi-dimensional hybrid intelligent diagnosis method to recognize automatically different categories and levels of gear damage has been proposed by Lei et al. [94]. The Hilbert transform, wavelet packet transforms and empirical mode decomposition method are used on gear vibration signals to extract additional fault characteristic data. They have generated multi-dimensional feature sets (time-domain, frequency-domain and time–frequency-domain features) are combined with genetic algorithms to recognize gear health conditions. The method proposed by the authors can be applied to the collected features to identify the gear damage type and damage levels.

A fault diagnosis technique to detect faults in rolling element bearing using a combination of fast kurtogram and genetic algorithm has been proposed by Zhang and Randall [95]. The fast kurtogram gives rough estimation of analysis parameters effectively. The Genetic algorithms have strong capability for optimization, but are slow unless initial parameters are close to optimal. Therefore, the authors present a model and algorithm to design the parameters for optimal resonance demodulation using the combination of first kurtogram for initial estimates, and a genetic algorithm for final optimization. The feasibility and the effectiveness of the proposed method are demonstrated by experiment and give better results than the classical method of arbitrarily choosing a resonance to demodulate. Perera et al. [96] have used genetic algorithm for solving multi-objective optimization for detecting the damage. They have compared genetic algorithm optimizations based on aggregate functions with Pareto optimality. Xiang et al. [97] have developed a novel crack detection method for detecting crack position and depth in a shaft with the application of Rotating Rayleigh-Euler and Rayleigh-Timoshenko beam elements of B-spline wavelet. According to them, the first three frequencies are measured

to find the crack depths through genetic algorithms. The authentication of the method is validated by some numerical examples and experimental data, and it has found that the method is able to detect the crack in a shaft.

A fault diagnosis method based genetic algorithms for cracked beam like structures has been developed by Baghmisheh et al. [98]. An analytical and numerical method used to model the cracked beam and to get natural frequencies of the cantilever beam respectively. The identification of the crack location and depth in the cantilever beam is done using optimization technique, and Binary and Continuous Genetic Algorithms (BGA, CGA) are used to find the optimal location and depth by minimizing the cost function which is based on the difference of measured and calculated natural frequencies. But in this paper error percentage of results is not reported. Zhang et al. [99] have used genetic programming (GP) to detect faults in the rotating machinery. They have compared the results of GP with other techniques such as artificial neural network and support vector machines (SVM). The authors have found that performance of GP equal to or better compared to ANN and SVM. He et al. [100] have developed a shaft crack detection method by mean of finite element method and genetic algorithms. They have concluded that proposed method has potential to solve a wide range of inverse identification problems in an effective and efficient way. Friswell et al. [101] have developed damage detection methodology based on a Genetic Algorithm (GA) and summarized intrinsic sensitivity method for determining the location of damage of the structures. The GA has used by them in order to optimize the discrete variables damaged area and intrinsic sensitivity method used to optimize the extent of damage.

2.2.3.4 Adaptive Neuro Fuzzy Inference System (ANFIS) technique

In this section a discussion about ANFIS technique applied for condition monitoring as well as a classification problem by researchers in various fields of engineering is carried out.

A novel analytical technique, based on the ANFIS, for supplier selection decision-making problem for textile firm has been presented by Guneri et al. [102]. The proposed algorithm consists of two main steps on the basis of available database: input selection with ANFIS, and these selected inputs used to construct the ANFIS controller. They have found that the constructed ANFIS controller can be successfully applied to the supplier selection type of decision making problem in industries.

Boyacioglu and Avci [103] have presented an Adaptive Network Fuzzy Inference System based mechanism for predicting the stock price index return of the Istanbul Stock Exchange (ISE). They have concluded that the economists can be applied ANFIS successfully for forecasting the stock price index return. Vairappan et al. [104] have proposed an upgraded version of ANFIS with self-feed backs using batch type local search learning. The developed mechanism enhanced the ability of the conventional ANFIS in handling time-varying occurrence data. The introduction of self-feed backs enables the ANFIS to be embedded with memory in order to overcome the limitation of its static problem. They have revealed the modified ANFIS can be effectively used with dynamic properties such as the time-series data. A model based on ANFIS for prediction of the white layer thickness and the average surface roughness in wire electrical discharge machine has been proposed by Çaydas et al. [105]. The input parameters of ANFIS model are pulse duration, open circuit voltage, dielectric flushing pressure and wire feed rate. An experimental analysis had performed to verify the authentication of results predicted by the proposed model. From the study of above paper, it is concluded that ANFIS model can be systematically applied for the identification of single crack present in the structure. Jassar et al. [106] have designed an Adaptive Neuro-fuzzy Inference System (ANFIS) can be used to design closed-loop control for space heating systems. The aim of the authors has enhanced the overall performance of heating systems, in terms of energy efficiency and thermal comfort. They found that the average air temperature results estimated by using the designed ANFIS model are close proximity with experimental results.

Lei et al. [107] have presented a new method for fault diagnosis based on Multiple Adaptive Neuro-fuzzy Inference System (MANFIS) is applied to rolling element bearings, and the testing results of the MANFIS model represent the proposed model can identify different fault classifications and severities, which has a better classification performance compared to the individual classifiers based on ANFIS. They have studied the efficiency of the proposed feature selection method based on the improved distance evaluation technique is also demonstrated by the testing results. An ANFIS based technique for a Static Var Compensator (SVC) to improve the damping of power systems in the presence uncertainty of load model parameters has been developd by Ellithy and Al-Naamany [108]. ANFIS is trained over a wide range of typical load parameters in order to adapt the gains of the SVC stabilizer. A MATLAB platform is used for simulation to analyze the effectiveness of the proposed ANFIS SVC stabilizer. They

concluded on the basis simulation results, the tuned gains of the SVC stabilizer using the ANFIS can give better damping than the conventional fixed-gains SVC stabilizer.

2.2.3.5 Hybrid AI techniques used for crack identification

This chapter reviewes the various hybrid AI techniques applied for detecting damage of structural and machine elements briefly.

Zhu et al. [109] have proposed an ANFIS and integrated wavelet real-time filtering algorithm based helicopter structural damage identification method when the frequency and magnitude of harmonic excitation are constant. They have found that proposed integrated method can be effectively utilized for identifications of several unknown damages and small damages of structures and also it can be used to recognize both the time and the location when the structural damage occurs unpredictably. A Wavelet based Adaptive Neuro fuzzy Inference System (WANFIS) to measure the nonlinear behavior of the structure–MR damper systems has been developed by Mitchell et al. [110] . They have observed new WANFIS approach is effective in exhibiting the nonlinear behavior of the structure–MR damper system subjected to a variety of natural hazards while resulting in shorter training times in comparison with ANFIS model. Beena and Ganguli [111] have presented fault detection algorithms for cantilever beam using fuzzy cognitive map and neural network based on Hebbian-learning. The continuum mechanics and finite element method have been used to extract the vibration responses (First six natural frequencies) from cantilever beam. The developed technique works quite well for structural damage even in the presence of noise.

Salahshoor et al. [112] have proposed an innovative fault detection method using three ANFIS classifiers for industrial power plants. Each ANFIS classifier is devised to detect and diagnose a group category of four stream turbine faults. To organize an overall list of 12 faults into three fault categories, possessing time series similarities in their symptoms, a preliminary set of conceptual and experimental studies is conducted. A nonlinear system identification method to detect process fault of a cement rotary kiln has been proposed by Sadeghian and Fatehi [113]. To identify the various operation points in the rotary kiln, a locally Neuro-fuzzy model is used, which is trained by LOLIMOT algorithm. Eslamloueyan [114] has proposed a Hierarchical Artificial Neural Network (HANN) for detection of faults of Tennessee–Eastman process (TEP). The first step in designing the HANN is to divide the fault pattern space into a few sub-spaces through using fuzzy C-means clustering algorithm. For each sub-space of fault patterns a specific

agent is trained in order to make fault diagnosis. A supervisor agent is designed to specialize in the selection of the relevant fault diagnostic agent. The feed forward multilayer perceptron networks have used for developing diagnostic and supervisor agents.

A bearing fault diagnosis technique based on multi scale entropy and adaptive neuro fuzzy inference system to measure the nonlinearity presents in a bearing system has been developed by Zhang et al. [115]. They have performed an experimental investigation on electrical motor bearing with three different fault categories and several levels of fault severity. The results obtained from the experimental analysis have used to design and train the ANFIS system for fault identification of the bearing system. But as further analysis fuzzy-RBFN can give better results if used in the above paper. Simon and Hungerbuhler [116] have presented a comparative study of three AI techniques suited to perform classification tasks. The neural network trained using Levenberg–Marquardt and the Levenberg–Marquardt method with Bayesian regularization, the Neuro-Fuzzy model based on clustering and grid partition, and the Takagi–Sugeno fuzzy models for the pattern recognition based data analysis of the existing industrial batch dryer. A fault diagnostic technique using Neuro-fuzzy approach to pattern classification of rotating machinery has been presented by Zio and Gola [117]. They have used this method to get high rate of correct classification model. The efficiency of the proposed hybrid model is verified by applying to a motor bearing system and the results obtained are satisfactory.

Yang et al. [118] have developed a fault detection method based on adaptive neuro-fuzzy inference system in combination with classification and regression tree. The ANFIS model is trained with the data sets obtained from vibration signals and the current signals of the induction motors. They have concluded that the developed ANFIS model is capable to diagnose the fault present in the induction motors. Quteishat and Lim [119] have proposed a Fuzzy Min-Max (FMM) network, which is a supervised neural network classifier that forms hyper-boxes for prediction and classification problems. This method is applied to the extraction of rule set from FMM to warrant the predicted results. The outputs of FMM are compared with results measured from a power generation plant for fault recognition with the help of sensors. Fang et al. [120] have shown performance of a structural health monitoring tool of based on frequency response and neural network. The dynamic steepest descent algorithm and the fuzzy steepest descent algorithm have used to improve the training rate of ANN. They have investigated a tunable steepest descent algorithm using a heuristics approach, which improves the convergence speed

significantly without sacrificing the algorithm ease and the computational time. They have concluded that the neural network technique can assess the damage condition with high accuracy. As the further study, application of fuzzy-RBFNN hybrid technique along with experimental data may give better result.

A feature selection based network system to diagnose the various types of faults in the gearbox has been designed by Hajnayeb et al. [121]. The authenticity of the proposed method is verified by experimental analysis. The results of feature selection method are compared with genetic algorithm results. They have found a close proximity between the results. Firpi and Vachtsevanos [122] have presented a genetically programmed artificial features extraction based method for identification of the faults of the gearbox. The artificial features extracted from vibration parameters, which is sensed by accelerometer to identify and detect a crack fault a crack fault in a gearbox of a helicopter's main transmission.

Han et al. [123] have proposed an automated fault diagnosis method for induction motors through the combination of Discrete Wavelet Transform (DWT), feature extraction, GA and ANN techniques. The DWT improve the quality of signal to noise ratio at preprocessing features are extracted from motor stator current during reducing data transfers. GA is extracted most significant features from the available features database and also optimized the ANN structure characteristics. Samanta [124] has presented a study on gear fault detection using Artificial Neural Networks (ANNs) and Support Vector Machines (SMVs). The vibration parameters of a rotating machine with damage and non-damage gears are processed for feature extraction. He has used extracted features from damage and non-damage gears as inputs to both classifiers (ANNs and SVMs) for the state recognition of gear box. The extracted features optimized using a genetic algorithm.

Samanta et al. [125] have presented a comparative study of the performance of the bearing fault detection techniques using two classifiers namely artificial neural networks and support vector machines. The vibration analysis performed to get the vibration signal of a rotating machine with defective and non-defective bearing processes for feature extraction. The extracted features from original and processed signals are used as inputs to the classifier for two senses (normal and fault) detection. The number of nodes in hidden layers (for ANNs) and width of radial basis function along with selected input features are optimized using a genetic algorithm. Jack and Nandi [126] have examined and compared the performance of artificial neural networks and support vector machines

classifier in two sense faults and no-fault recognition of the bearing assembly. They have used a genetic algorithm based feature selection process to improve the overall performance of both the proposed techniques.

A hybrid fuzzy-genetic system to damage detection in both single and multiple cracked Timoshenko beam has been designed by Aydin and Kisi [127]. They have optimized the fuzzy membership function using genetic algorithms for hybridization process to get, the more accurate damage position. The natural frequencies and maxima of rotational mode shape deviations fed as input to the integrated system. The efficiency of design, integrated model is evaluated through several error measurements. They have observed that predicted hybrid model results have good fidelity with theoretical models. A Fuzzy v-Support Vector Classifier Machine (Fv-SVCM) which is new version of support vector machine to establish the non-linear diagnosing system of car assembly line has been designed by Wu [128]. The Fv-SVCM mode can easily handle the fuzzy fault detection pattern with highly precision compared to the fuzzy - neural network. Therefore Fv-SVCM diagnosed fault with input parameters successfully and support vector classifier machine extends the application scope. In the above paper thorough experimental verification is required for the authentication of results.

Pawar and Ganguli [129] have developed a structural health monitoring technique based genetic fuzzy system for global online damage detection of composite helicopter rotor blades using displacement and force based measurement deviations between damage and healthy condition and for local online damage detection using strain energy. Yuan and Chu [130] have proposed an Artificial Immunization Algorithm (AIA) to optimize the parameters in the support vector machine (SVM). The AIA is a new optimization method based on the biological immune principle of humans and other animals. It can effectively prevent premature convergence and guarantee the diversity of solution. With the optimized parameters of AIA, the total capacity of the SVM classifier is improved. The fault diagnosis of turbo pump rotor shows that the SVM optimized by AIA give higher recognition accuracy than normal SVM. A hybrid genetic-fuzzy system to detect damage location and its extent has been analyzed by Pawar and Ganguly [131]. A finite element method is used to get change in natural frequencies between damage and healthy cantilever beam. A fuzzy system is developed using these changes in natural frequencies and genetic algorithm use to optimize the fuzzy rule base and membership functions. But as further analysis, use of fuzzy-neuro hybrid technique along with experimental data may give better result.

2.2.4 Miscellaneous methods used for crack identification

Some miscellaneous algorithms and methods are also used for identification of damage are briefly depicted in this section.

Hosseinabadi et al. [132] have proposed a new wavelet network based technique for structural damage identification using the guided ultrasonic wave. A Fixed Grid Wavelet Network (FGWN) algorithm developed for feature extraction and pattern recognition to quantitatively characterize damage in a thick steel beam. The FEM simulation data used for training the FGWN; however the FEM simulation and experimental data used for testing the FGWN damage identification algorithm. A novel leak identification method to localize the leak in pipelines carrying crude oils and liquid fuels using rough set theory and support vector machine has been proposed by Mandal et al. [133]. An artificial Bee Colony Algorithm (ABC) and a Particle Swarm Optimization (PSO) technique have used to design SVM. The results obtained from the ABC algorithm compared with PSO technique, results and observed close proximity between them. They have observed that proposed method is capable of localizing leaks in pipelines successfully.

Bacha et al. [134] have presented a new method for fault classification in a power transformer using Dissolved Gas Analysis (DGA) and multi-layer support vector machine classifier. The effectiveness of SVM diagnosis is analyzed with polynomial and Gaussian functions. The real data sets are used to investigate its viability of the DGA methods, fault classification in power transformer oil. The experimental investigation results show the efficiency of the proposed model for predicting the DGA method in the power transformer oil. A condition-based maintenance model for industrial machines by computing the remaining life of the machine component with the help support vector machine has been developed by Kim et al. [135]. To validate the feasibility of the proposed model, real life fault, historical data from the bearings of high pressure-liquefied natural gas pumps was analyzed and used to obtain the optimal prediction of remaining useful life. The obtained results were very promising and showed that the proposed prognosis system based on health state probability estimation has the potential to be used as an estimation tool for remnant life prediction in industrial.

A K-means clustering algorithms for the automated diagnosis of defective rolling element bearings has been designed byYiakopoulos et al. [136]. They have said that K-means clustering is an unsupervised learning procedure, that method can be directly executed in the vibration indices. Thus, the need for training the method with data measured on the

particular systems under defective bearing conditions is excluded. They have found that, the proposed K-means clustering based method is effective for localization of damages present in the bearing systems. Jun [137] has developed a fault detection system in a swine wastewater treatment plant using Dynamic Time Warping (DTW) and discriminant analysis with Oxidation–Reduction Potential (ORP) and Dissolved Oxygen (DO) values. He has found that the ORP method performs better than other two methods which have used for diagnosis of fault present in the system. Fagerholt et al. [138] have performed an experimental and numerical investigation on the fracture behavior of a cast aluminium alloy. They have used the classical flow theory for modeling the fracture in the alloy. They have also used Digital Image Correlation (DIC) to collect the data about the displacement and strain field in the specimen. They found the results derived from the numerical measurement are good agreement with the experimental data.

Cusido et al. [139] have proposed a different signal processing method, integrated wavelet and power spectral density techniques, giving the power detail density as a fault factor. The method demonstrates good theoretical and experimental results. Bachschmid et al. [140] have used the model of a turbo-generator unit to perform a numerical sensitivity analysis, in which the vibrations of the shaft-line, and more in detail the vibrations of the shaft in correspondence to the bearings, have calculated for all possible positions of the crack along the shaft-line, and for several different values of the depth of the crack. They have established a relation between the dynamic response and the position of crack location and depth present in the system. Dilena and Morassi [141] have demonstrated the natural frequency and anti-resonant frequency shifts contains certain generalized Fourier coefficients of the stiffness variation due to presence of damage. According to them the results of numerical simulations on rods with localized or diffused cracks are in good agreement with theory. They have concluded that the experimental results show that the inverse problem solution, noise and modeling errors on anti-resonances amplified strongly than the natural frequency data used.

A novel Laplacian model to form an improved damage identification algorithm has been proposed by Cao and Qiao [142]. The novel Laplacian model exhibits apparent advantages such as high-noise insusceptibility, insightful in damage revealment, and visualized damage presentation over the standard Laplace operator. They have measured the curvature of mode to model the damage detection tool. The results derived from the proposed Laplacian concept have been compared with experimental results. Curadelli et al. [143] have presented a new technique to assess structural damage by means of the

instantaneous damping coefficient due to higher sensitivity from natural frequencies or modal shapes to damage using a wavelet transform. They have found important changes in damping parameters of damage structure, though experimental and numerical simulation. Also represent the wavelet transform effectively applied in a procedure for instantaneous frequencies and damping identification of the free vibration parameters.

Friswell [144] has reviewed about application of inverse method to localize and quantify the crack using modal indices. He has stated in the present research, uncertain parameters present in the models have to be identified. He has discussed number of problems with the application of this method for the assessment of damage, including modeling error, environmental efforts, damage localization and regularization. A new concept of Nonlinear Output Frequency Response Functions (NOFRFS) to identify the cracks present in beams like vibrating structures using modal indices has been introduced by Peng et al. [145]. They found the NOFRFS are a sensitive indicator to notify the presence of cracks. They have reported that this method establishes a basis for the application of NOFRF models in identification of cracks present in the structures. Rus and Gallego [146] have proposed a work based on hyper singular shape sensitivity boundary integral equation for the solution of the inverse problem for localization of crack. The performance, accuracy and sensitivity of the proposed method have been verified by the simulated/experimental results.

Pakrashi et al. [147] have developed a new wavelet–kurtosis based damage detection method for different crack depth ratios and crack positions, including the effects of varying signal to noise ratio. An experimental analysis carried out in damaged aluminium beam with open cracks of different configuration for validation of the proposed method. The damaged shape of beam expected by using a novel video camera based pattern recognition technique. They have concluded that the integration wavelet analysis with a kurtosis based damage assessment can be effectively utilized for structural damage detection purpose under the presence of measurement noise. A novel method for assessment of crack in beam like dynamic structures based on kurtosis has been presented by Hadjileontiadis et al. [148]. They have stated the crack can be localizing by measurement of unexpected changes in the spatial variation of response and the size of the crack can be measured by estimation of Kurtosis. The performance proposed method has been verified by experiments on crack Plexiglas beams. They have concluded that the proposed kurtosis-based crack estimation technique is more effective and efficient than the available crack detection in literature due to low computational complexity.

Kyricazoglou et al. [149] have presented a method to localize the fault in composite laminates by computing the slope deflection curve of composite beams in flexure. They have provided the mechanism of fault diagnosis and location of damage from a comparison of dynamic features response from the faulty vibrating laminates. They found in their research slope deflection curve is an encouraging technique for assessment of initial damage in composites.

Agrawalla [150] thesis research is carried out only for single crack present in the structures. In his thesis, there is no elaborate discussion of theory of composite beam, FE method. He has also not done analysis for multi cracked composite structures and hybrid techniques. Dash [151] has done initial study on cracked structure using simple neural network. He has not given any analysis on composite structure and has not done elaborative study on FE analysis. But in the current research new hybrid methodology such as Fuzzy-RBFNN, Fuzzy-KSOM and Fuzzy-BPNN have been considered for multiple crack identification. The Fuzzy-RBFNN is found to the best among all techniques derived in the current research work. An error 3.5 % is found between the results obtained from Fuzzy-RBFNN and experimental analysis.

2.3 Summary

The literature review presents an overview of fault diagnosis techniques based on vibration analysis for isotropic material and orthotropic (composite) material. It is observed that Theoretical, FEM, and AI based methods are used for identification of damage of isotropic materials for single crack scenario. Only few research papers are available for multiple cracks detection of isotropic material structures and for the composite structures it is still unreported using AI techniques. The AI techniques can be used more effectively for fault diagnosis. But it is observed that the potential of AI based methods are not completely explored to design the intelligent multiple fault detection model in the engineering systems.

In the present research, a systematic approach has been carried out to design AI based techniques such as fuzzy logic, neural networks (BPNN, RBFNN & KSOM) and various hybrid fuzzy-neuro models for prediction of fault intensities and severities present in the composite and steel beams. The desired parameters to design and train the AI models have been derived from theoretical, finite element and experimental analysis of cantilever beam.

CHAPTER 3

Theoretical Analysis of Multiple Cracked Cantilever Beam for Measurement of Dynamic Response

The presence of damage in the form of crack in a structural component is a serious threat to the integrity of structures as well the safety of human life. Several methods are available in literature used for assessment of the damage in form crack to prevent the catastrophic failure of structures. The vibration based methods are most successfully applied for recognition of the damage [1]. It is observed that dynamic response, e.g. natural frequencies and mode shapes of structure changes due to damage [31].

3.1 Introduction

The vibration response of the cracked structure has been investigated successfully by researchers [1-5]. The vibration response is very sensitive to crack location and its intensity. The researchers and scientists have analyzed that effect of cracks on vibration responses of faulty structure. These changes in vibration responses can be efficiently utilized for developing the crack detection method. In this chapter a systematic theoretical approach is used to analyze the effect of multiple cracks on vibration responses of two types of cantilever beams, one is made up of glass-epoxy composite material and another is of structural steel. The flexibility of the cracked composite beam element is calculated by considering the cracks as massles substitute spring. The flexibility of spring can be calculated by using fracture mechanics and Castigliano theorem [152]. The transformation function of the cracked composite beam element has been calculated by finite element method. Three nodes are taken on a cracked composite beam element with three degrees of freedom for each node. The flexibility and transformation function of the cracked composite beam element are used to find the stiffness of a beam which is subsequently used to calculate the dynamic response of the cracked composite beam.

The linear fracture mechanics theory has been used to calculate the stress intensity factor and strain energy release rate for cracked steel beam element, which is further used to derive dimension-less compliance matrices and local stiffness matrices. The dynamic

response of multiple cracked steel beam has been calculated by using stiffness matrix. The robustness of the proposed theoretical model has been established by comparing the results with the experimental analysis results.

3.2 Analysis of dynamic response of cracked composite beam

3.2.1 Calculation of stiffness and mass matrices for composite beam element

The method suggested by Krawczuk [153] can be used to find the stiffness and mass matrices of the composite beam element. Out of assumed three nodes in an element, one node is taken in the middle and two at the extreme ends of the element. There are three degrees of freedom at each node $\delta = \{u, v, \theta\}$ as shown in figure 3.1 (a) , the applied system forces $F= \{F_1, S_1, M_1, F_2, S_2, M_2, F_3, S_3, M_3\}$ and corresponding displacements $\delta = \{u_1, v_1, \theta_1, u_2, v_2, \theta_2, u_3, v_3, \theta_3\}$ are shown in figure 3.1(b). The stiffness matrix for a three-node composite beam element with three degrees of freedom at each node, for case of bending in x-y plane, is given as follows [153].

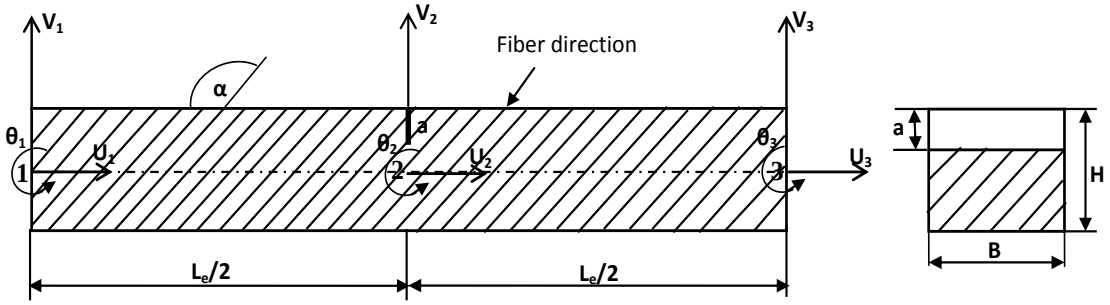

Figure 3.1(a) Nodal displacements in element coordinate system

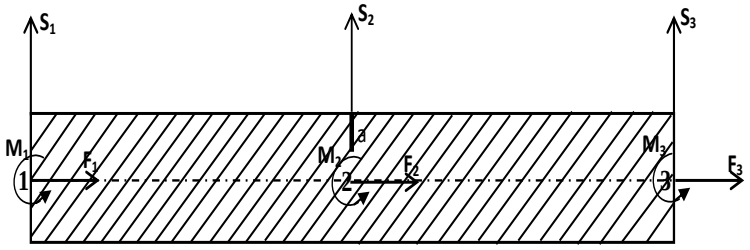

Figure 3.2(b) Applied forces on beam element

$$K_{el} = \left[q_{ij} \right]_{(9\times 9)} \tag{3.1}$$

Where q_{ij} (i, j=1… 9) are shown as

$$
\left.
\begin{aligned}
&q_{11} = q_{77} = 7BH\bar{Q}_{11}/3L_e,\\
&q_{12} = q_{21} = -q_{78} = -q_{87} = 7BH\bar{Q}_{13}/3L_e,\\
&q_{13} = q_{31} = -q_{79} = -q_{97} = BH\bar{Q}_{13}/2L_e,\\
&q_{47} = q_{74} = -q_{14} = -q_{41} = 8BH\bar{Q}_{11}/3L_e,\\
&q_{15} = -q_{51} = -q_{42} = q_{24} = -q_{48} = -q_{84} = -q_{57} = -q_{75} = 8BH\bar{Q}_{13}/3L_e,\\
&q_{16} = q_{61} = -q_{34} = -q_{43} = q_{49} = q_{94} = -q_{67} = -q_{76} = 2BH\bar{Q}_{13}/3,\\
&q_{17} = q_{71} = BH\bar{Q}_{11}/3L_e\\
&q_{18} = q_{81} = q_{27} = q_{72} = BH\bar{Q}_{13}/3L_e\\
&q_{73} = q_{37} = -q_{19} = -q_{91} = BH\bar{Q}_{13}/6,\\
&q_{22} = q_{88} = 7BH\bar{Q}_{11}/3L_e\\
&q_{23} = q_{32} = -q_{89} = -q_{98} = BH\bar{Q}_{13}/2,\\
&q_{25} = q_{52} = -q_{58} = -q_{85} = -8BH\bar{Q}_{33}/3L_e,\\
&q_{26} = q_{62} = q_{59} = q_{95} = -q_{53} = q_{35} = -q_{86} = -q_{68} = 2BH\bar{Q}_{33}/3,\\
&q_{28} = q_{82} = BH\bar{Q}_{33}/3L_e,\\
&q_{38} = q_{83} = -q_{29} = -q_{92} = BH\bar{Q}_{33}/6,\\
&q_{45} = q_{54} = 16BH\bar{Q}_{13}/3L_e,\\
&q_{44} = 16BH\bar{Q}_{11}/3L_e,\\
&q_{55} = 16BH\bar{Q}_{33}/3L_e,\\
&q_{33} = q_{99} = BH(7H^2\bar{Q}_{11}/36L_e + L_e\bar{Q}_{33}/9),\\
&q_{36} = q_{63} = q_{69} = q_{96} = BH(-2H^2\bar{Q}_{11}/9L_e + L_e\bar{Q}_{33}/9),\\
&q_{39} = q_{93} = BH(H^2\bar{Q}_{11}/36L_e - L_e\bar{Q}_{33}/18),\\
&q_{66} = BH(4H^2\bar{Q}_{11}/9L_e + 4L_e\bar{Q}_{33}/9),\\
&q_{46} = q_{56} = 0
\end{aligned}
\right\} \qquad (3.2)
$$

Where B, H, L_e are the dimension of the composite beam element, $\bar{Q}_{11}$, $\bar{Q}_{13}$ and $\bar{Q}_{33}$ are stress constants and given as [154].

$$
\left.
\begin{aligned}
&\bar{Q}_{11} = \bar{C}_{11}m^4 + 2(\bar{C}_{12} + 2\bar{C}_{33})m^2n^2 + \bar{C}_{22}n^4,\\
&\bar{Q}_{13} = (\bar{C}_{11} - \bar{C}_{12} - 4\bar{C}_{33})m^3n + \bar{C}_{12} - \bar{C}_{22} - 2\bar{C}_{33}mn^3\\
&\bar{Q}_{33} = (\bar{C}_{11} - 2\bar{C}_{12} + \bar{C}_{22} - 2\bar{C}_{33})m^2n^2 + \bar{C}_{33}(m^4 + n^4),
\end{aligned}
\right\} \qquad (3.3)
$$

Where m=cosα, n=sinα and C_{ij} terms are determined from the relation [155]

$$
\bar{C}_{11} = \frac{E_{11}}{(1 - \nu^2 E_{22}/E_{11})},\ \bar{C}_{22} = \bar{C}_{11}E_{22}/E_{11},\ \bar{C}_{12} = \nu_{12}\bar{C}_{22},\quad \bar{S}_{33} = G_{12} \qquad (3.4)
$$

Where E_{11}, E_{22}, G_{12} and v_{12} are the mechanical properties of the composite and can be determined as shown in [154].

$$E_{11} = E_f\varphi + E_m(1-\varphi);\ E_{22} = E_m\left[\frac{E_f + E_m + (E_f - E_m)\varphi}{E_f + E_m - (E_f - E_m)\varphi}\right],$$

$$v_{12} = v_f\varphi + v_m(1-\varphi);\ G_{12} = G_m\left[\frac{G_f + G_m + (G_f - G_m)\varphi}{G_f + G_m - (G_f - G_m)\varphi}\right]$$

The mass matrix of the composite beam element can be given as [153]

$$M_{el} = \left[M_{ij}\right]_{(9\times 9),} \tag{3.5}$$

Where M_{ij} (i, j=1… 9) are shown as

$$\left.\begin{aligned}
&m_{11} = m_{22} = m_{77} = m_{88} = m_{14} = m_{41} = 2\rho BHL_e/15,\\
&m_{17} = m_{71} = m_{28} = m_{82} = -\rho BHL_e/30,\\
&m_{23} = m_{32} = -m_{38} = -m_{83} = -m_{89} = -m_{98} = \rho BHL^2{}_e/180,\\
&m_{68} = m_{86} = -m_{26} = -m_{62} = \rho BHL^2{}_e/90,\\
&m_{33} = m_{99} = \rho BHL_e(L^2{}_e/1890 + H^2/90),\\
&m_{66} = 2\rho BHL_e(L^2{}_e/1890 + H^2/90),\\
&m_{36} = m_{63} = m_{69} = m_{96} = \rho BHL_e(-L^2{}_e/945 + H^2/180),\\
&m_{39} = m_{93} = \rho BHL_e(L^2{}_e/1890 - H^2/90),\\
&m_{44} = m_{55} = 8\rho BHL_e/15,\\
&m_{12} = m_{21} = m_{13} = m_{31} = m_{15} = m_{51} = m_{16} = m_{61} = m_{18} = m_{81} = m_{19}\\
&= m_{91} = m_{24} = m_{42} = m_{27} = m_{72} = m_{34} = m_{43} = m_{35} = m_{53} = m_{37}\\
&= m_{73} = m_{45} = m_{54} = m_{46} = m_{64} = m_{48} = m_{84} = m_{49} = m_{94} = m_{56} = m_{65}\\
&= m_{57} = m_{75} = m_{59} = m_{95} = m_{67} = m_{76} = m_{78} = m_{87} = m_{79} = m_{97} = 0
\end{aligned}\right\} \tag{3.6}$$

3.2.2 Calculation of stiffness matrix for cracked composite beam element

According to the St. Venant's principle, the stress field is influenced only in the vicinity of the crack. The additional strain energy generates due to presence of crack, which changes flexibility coefficients expressed by stress intensity factors, can be derived by Castigliano's theorem in the linear elastic range. In this study, the bending-stretching

effect due to mid-plane asymmetry encouraged by the cracks is neglected. The coefficients of compliance C_{ij} are derived from the strain energy release rate (J), which induced by cracks developed by Griffith–Irwin theory [156]. J can be expressed as;

$$J = \frac{\partial U(P_{i,} A)}{\partial A} \tag{3.7}$$

Where A = area of the crack section, F_i = corresponding loads, U = strain energy of the beam due to presence of crack and can be written as [155].

$$U = \int_A \left(D_1 \sum_{i=1}^{i=N} K_{Ii}^2 + D_{12} \sum_{i=1}^{i=N} K_{Ii} \sum_{j=1}^{j=N} K_{IIj} + D_2 \sum_{i=1}^{i=N} K_{IIi}^2 + D_3 \sum_{i=1}^{i=N} K_{IIIi}^2 \right) dA \tag{3.8}$$

Where: K_I, K_{II} and K_{III} are the stress intensity factors for fracture modes of opening, sliding and tearing type of crack. D_1, D_{12}, D_2 and D_3 are the coefficients depending on the material parameters [155].

$$\left.\begin{aligned} D_1 &= -0.5\bar{d}_{22}\,\mathrm{Im}\left(\frac{s_1+s_2}{s_1 s_2}\right), \\ D_{12} &= \bar{d}_{11}\,\mathrm{Im}(s_1 s_2), \\ D_2 &= 0.5\bar{d}_{11}\,\mathrm{Im}(s_1+s_2), \\ D_3 &= 0.5\,\bar{d}_{44}\,\bar{d}_{55} \end{aligned}\right\} \tag{3.9}$$

The coefficients s_1, s_2 and $\bar{d}_{ij}$ can be measured from following equation [154].

$$\bar{d}_{11}s^4 - 2\bar{d}_{16}s^3 + (2\bar{d}_{12} + \bar{d}_{66})s^2 - 2\bar{d}_{26}s + \bar{d}_{22} = 0$$

Where $\bar{d}_{ij}$ constants can be calculated as

$$\left.\begin{aligned} \bar{d}_{11} &= d_{11}m^4 + (2d_{12} + d_{66})m^2n^2 + d_{22}n^4, \\ \bar{d}_{22} &= d_{11}n^4 + (2d_{12} + d_{66})m^2n^2 + d_{22}m^4, \\ \bar{d}_{12} &= (d_{11} + d_{22} - d_{66})m^2n^2 + d_{12}(m^4 + n^4), \\ \bar{d}_{16} &= (-2d_{11} + 2d_{12} + d_{66})m^3n + (d_{22} - 2d_{12} - d_{66})mn^3, \\ \bar{d}_{26} &= (-2d_{11} + 2d_{12} + d_{66})mn^3 + (d_{22} - 2d_{12} - d_{66})m^3n, \\ \bar{d}_{66} &= 2(2d_{11} - 4d_{12} + 2d_{22} - d_{66})n^2m^2 + d_{66}(m^4 + n^4) \end{aligned}\right\} \tag{3.10}$$

Where $m = \cos\alpha$; $n = \sin\alpha$ and d_{ij} are compliance constants of the composite along the principal axes. The d_{ij} can be related to the mechanical constants of the material by

$$d_{11} = \frac{1}{E_{11}}(1 - v_{12}^2 \frac{E_{22}}{E_{11}}), \quad d_{22} = \frac{1}{E_{22}}(1 - v_{23}^2), \quad d_{12} = \frac{-v_{12}}{E_{11}}(1 + v_{23}^2) \tag{3.11}$$

$$d_{66} = 1/G_{12}, \quad d_{44} = 1/G_{23}, d_{55} = d_{66}$$

The stress intensity factors, K_I, K_{II} and K_{III} expressed as [155]:

$$K_{ji} = \sigma_i \sqrt{\pi a} Y_j(\xi)\ F_{ji}(a/H) \tag{3.12}$$

Where σ_i = stress for the corresponding fracture mode, $F_{ji}(a/H)$ = correction factor for the finite specimen size; $Y_j(\xi)$ =correction factor for the anisotropic material [155], a = crack depth and H= element height. The correction factors $Y_j(\xi)$ and $F_{ji}(a/H)$ (j= x, xx and i= 1, 6) can be calculated from following equations

$$\left.\begin{aligned}
&F_{X1} = F_{X4} = F_X = \sqrt{\tan\Omega/\Omega}[0.752 + 2.02\ (a/H) + 0.371\ (1-\sin\Omega)^3]/\cos\ \Omega\ ,\\
&F_{X2} = F_{X3} = F_{X5} = F_{X6} = F_{XX} = \sqrt{\tan\Omega/\Omega}[0.923 + 0.199(1-\sin\Omega)^4]/\cos\ \Omega\ ,\\
&F_{XX2} = F_{XX5} = F_{XX1} = \left[1.122 - 0.561\ (a/H) + 0.85\ (a/H)^2 + 0.18\ (a/H)^3\right]/\sqrt{1-a/H}\ ,\\
&Y_X(\xi) = 1 + 0.1\ (\xi-1) - 0.016\ (\xi-1)^2 + 0.002\ (\xi-1)^3\ ,\\
&Y_{XX}(\xi) = 1
\end{aligned}\right\} \tag{3.13}$$

Where Ω=Πa/H, Additional displacement due to crack, according to the Castigliano's theorem [152], in the direction of the load P_i, is

$$u_i = \frac{\partial U(P_i, A)}{\partial P_i} \tag{3.14}$$

Substituting the Eq. (3.7) into Eq. (3.14), displacement and strain energy release rate J can be related as follows:

$$u_i = \frac{\partial}{\partial P_i} \int_A J(P_i, A)\ dA \tag{3.15}$$

The flexibility coefficients, which are highly depend on the stress intensity factors and the shape and size of crack and, can be written as [156]:

$$c_{ij} = \frac{\partial u_i}{\partial P_j} = \frac{\partial^2}{\partial P_i \partial P_j} \int_A J(P_i, A)\, dA = \frac{\partial^2 U}{\partial P_i \partial P_j}\ , \tag{3.16}$$

The compliance coefficient matrix derived from the above equation, can be assumed according to the displacement vector $\delta = \{u, v, \theta\}$ as

$$C = \left[c_{ij}\right]_{(6\times 6)} \tag{3.17}$$

Where C_{ij} (i, j=1 to 6) are derived by using eqs. (3.7)- (3.16).

The transformation matrix [T] for cracked element is calculated by using the equation of overall equilibrium of elemental forces is shown in figure 3.1(b). The final transformation matrix is;

$$[T]^t = \begin{bmatrix} 1 & 0 & 0 & 0 & 0 & 0 \\ 0 & 1 & 0 & 0 & 0 & 0 \\ 0 & 0 & 1 & 0 & 0 & 0 \\ -1 & 0 & 0 & -1 & 0 & 0 \\ 0 & -1 & 0 & 0 & -1 & 0 \\ 0 & L_e/2 & -1 & 0 & L_e/2 & -1 \\ 0 & 0 & 0 & 1 & 0 & 0 \\ 0 & 0 & 0 & 0 & 1 & 0 \\ 0 & 0 & 0 & 0 & 0 & 1 \end{bmatrix} \quad (3.18)$$

Hence the stiffness matrix of a cracked beam element can be obtained as

$$K_{Crack} = [T][C]^{-1}[T]^t \quad (3.19)$$

The model parameters of composite beam can be calculated by the characteristic equation of vibration and can be written as;

$$\left|[K] - \lambda[M]\right| \bar{x} = 0 \quad (3.20)$$

Where λ= function of natural frequency, $\bar{x}$ = function of mode shape, and M= mass per unit length

The natural frequency of the beam can be computed as;

$$f = \sqrt{\lambda} \quad (3.21)$$

The variation of natural frequencies for I, II and III modes of vibration with different crack locations and depths respectively have been shown in figures 3.2(a), 3.2(b) and 3.2(c). It is seen that the relative natural frequency for first mode of vibration is on increasing trend while for other two modes attains minimum and maximum value at different crack locations.

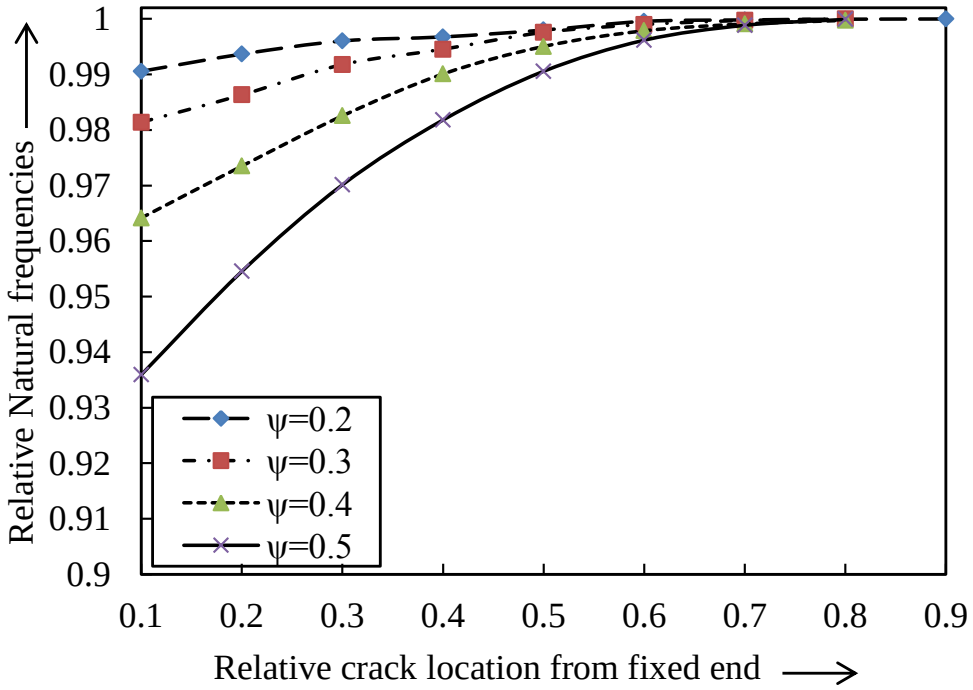

Figure 3.2(a) Relative natural frequencies vs. Relative crack location from the fixed end for I-mode of vibration

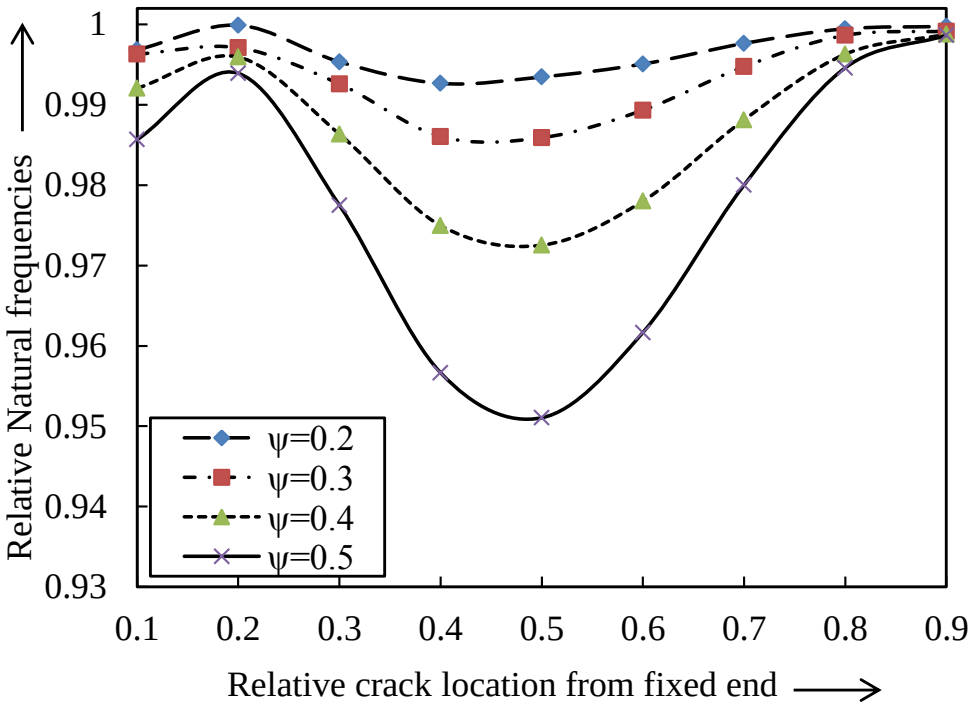

Figure 3.2(b) Relative natural frequencies vs. Relative crack location from the fixed end for II-mode of vibration

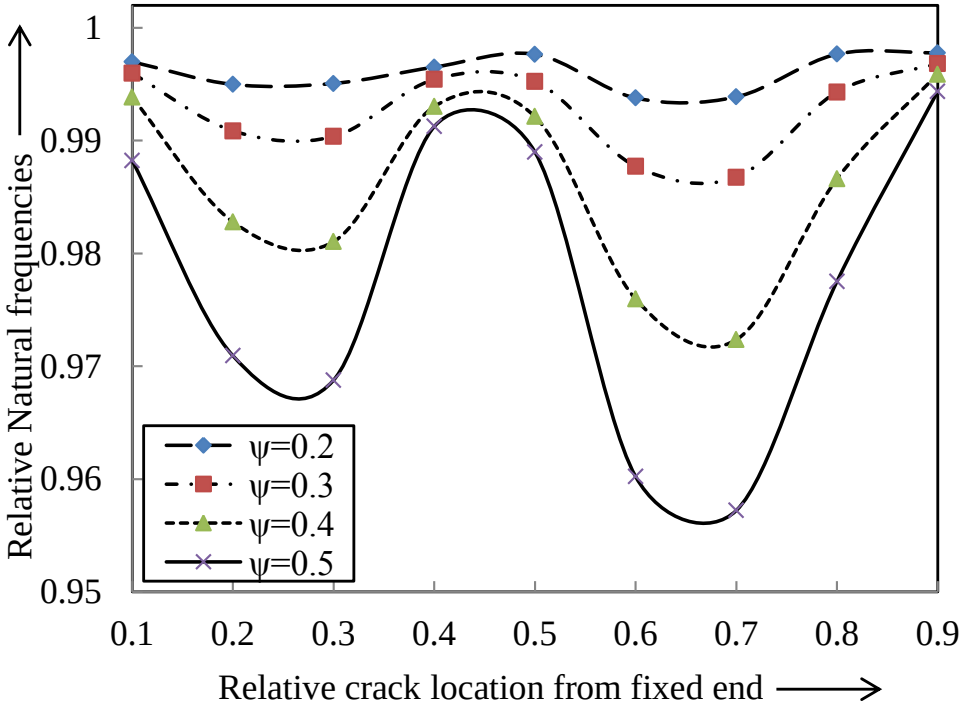

Figure 3.2(c) Relative natural frequencies vs. Relative crack location from the fixed end for III-mode of vibration

The theoretical analysis results for the 1st , 2nd and 3rd mode shapes for non-cracked and cracked composite beam are shown in figures 3.3, 3.4 and 3.5 and the orientation of the cracks are β_1=0.25, β_2=0.5, ψ_1=0.1667 and ψ_2=0.5. The magnified view at the vicinity of the first and second crack for 1st, 2nd and 3rd mode of vibration are shown in figures 3.3(b), 3.3(c), 3.4(b), 3.4(c), 3.5(b) and 3.5(c). A sudden jump has been observed in relative amplitudes at crack locations. These changes in amplitudes will be helpful in the prediction of crack locations and intensities.

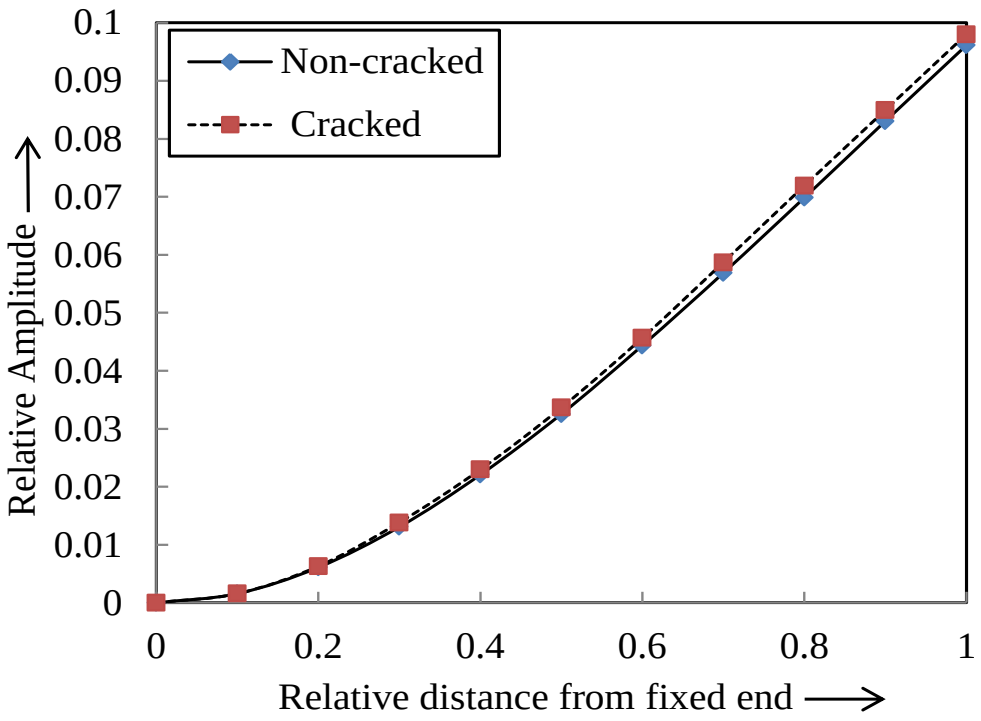

Figure 3.3(a) Relative Amplitude vs. Relative distance from fixed end (1st mode of vibration) β_1=0.25, β_2=0.5, ψ_1=0.1667& ψ_2=0.5

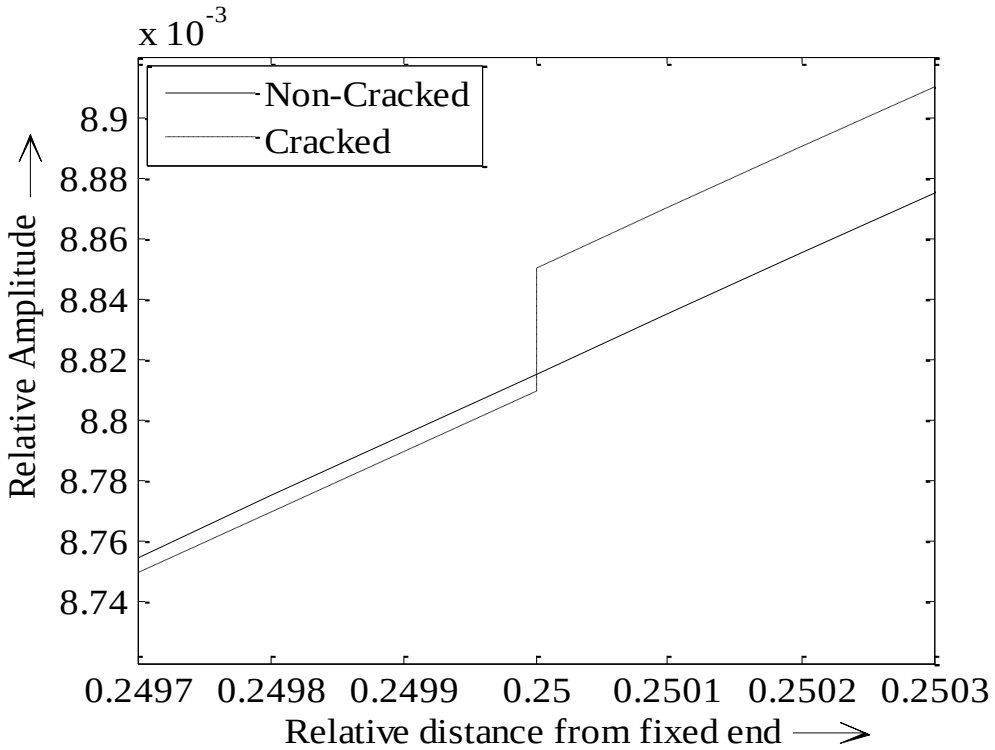

Figure 3.3(b) Magnified view at the first crack location (β_1=0.25)

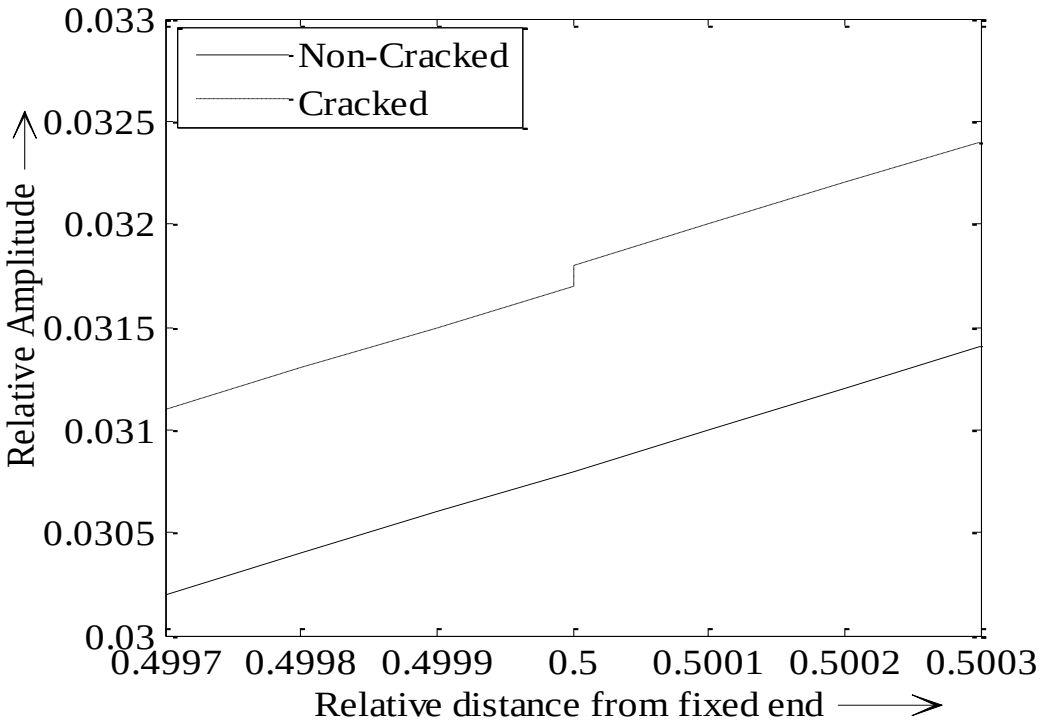

Figure 3.3(c) Magnified view at the second crack location (β_1=0.5)

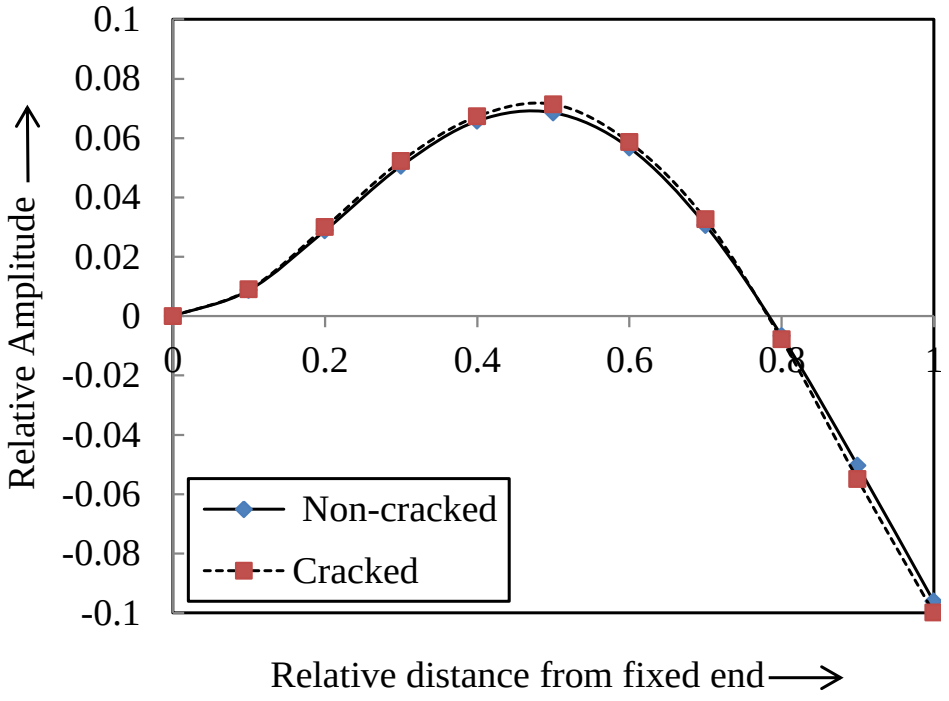

Figure 3.4(a) Relative Amplitude vs. Relative distance from fixed end (2^{nd} mode of vibration), β_1=0.25, β_2=0.5, ψ_1=0.1667 & ψ_2=0.5

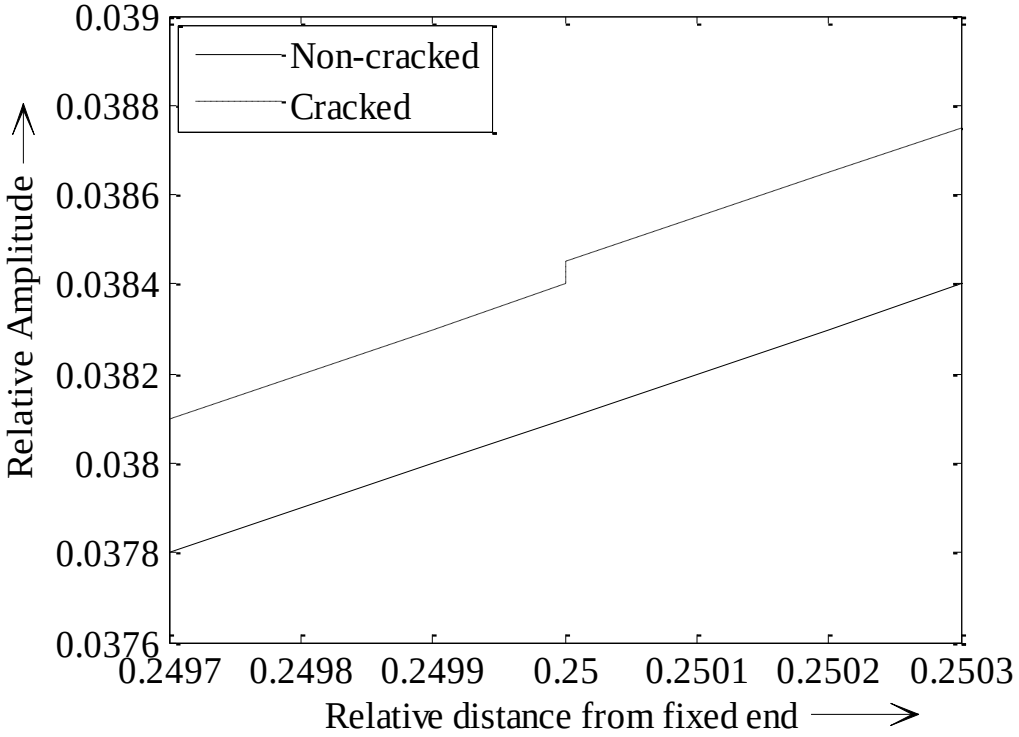

Figure 3.4(b) Magnified view at the first crack location (β_1=0.25)

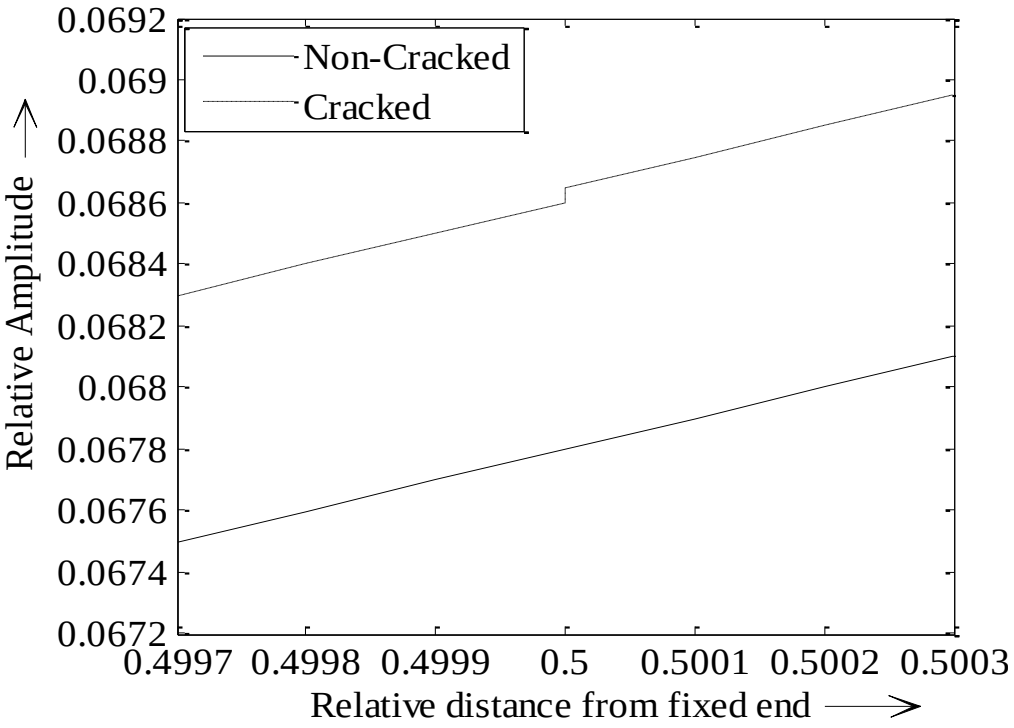

Figure 3.4c Magnified view at the second crack location (β_1=0.5)

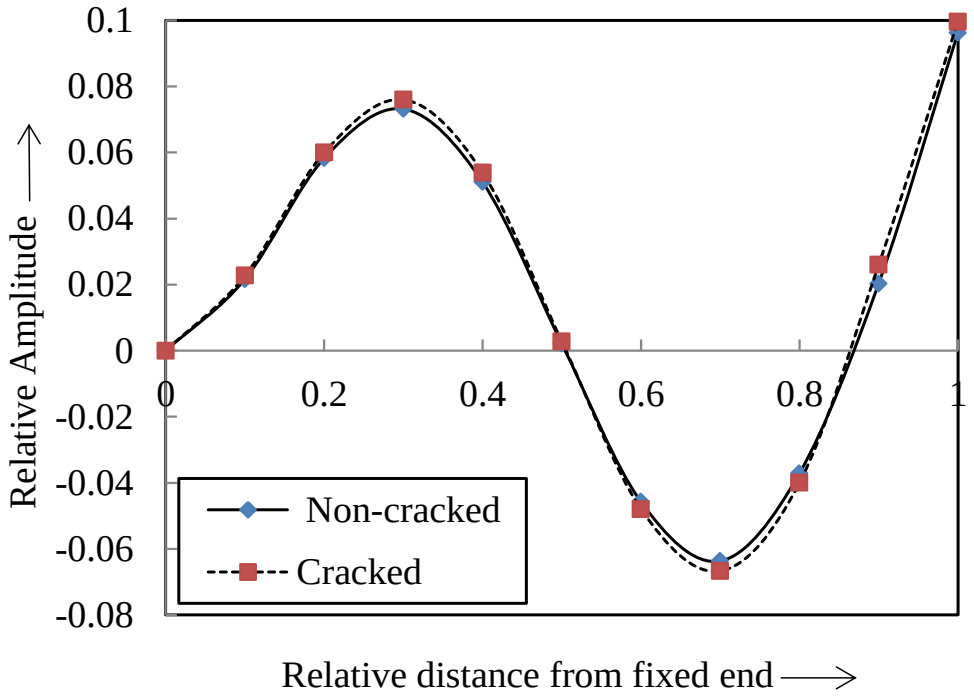

Figure 3.5(a) Relative Amplitude vs. Relative distance from fixed end (3rd mode of vibration) β_1=0.25, β_2=0.5, ψ_1=0.1667 & ψ_2=0.5

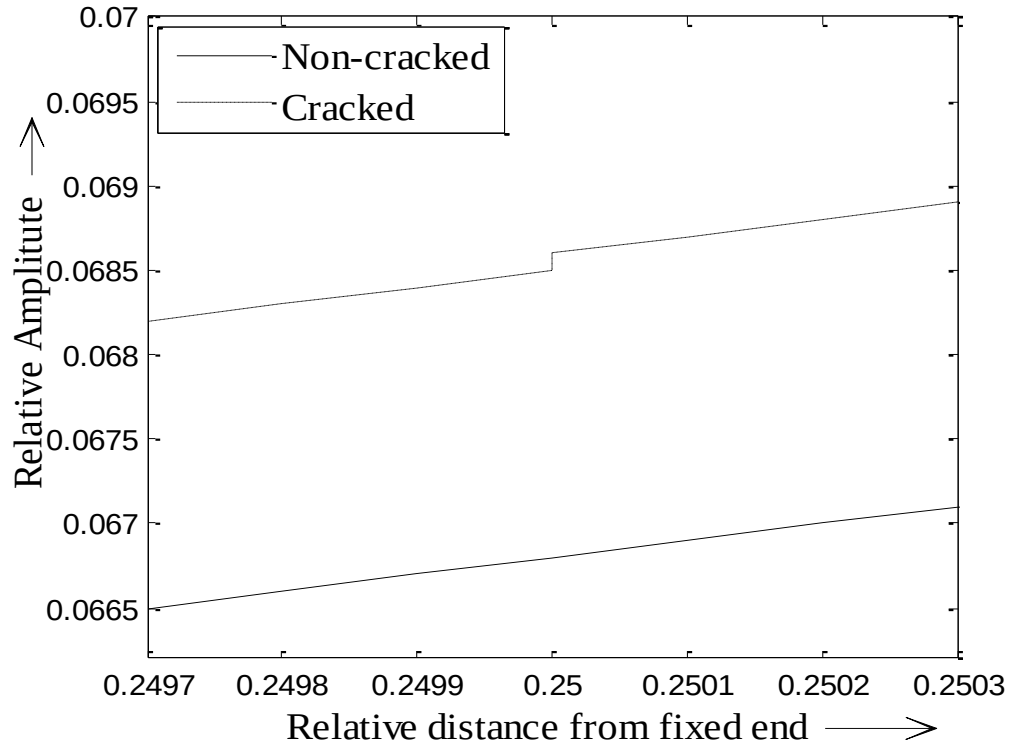

Figure 3.5(b) Magnified view at the first crack location (β_1=0.25)

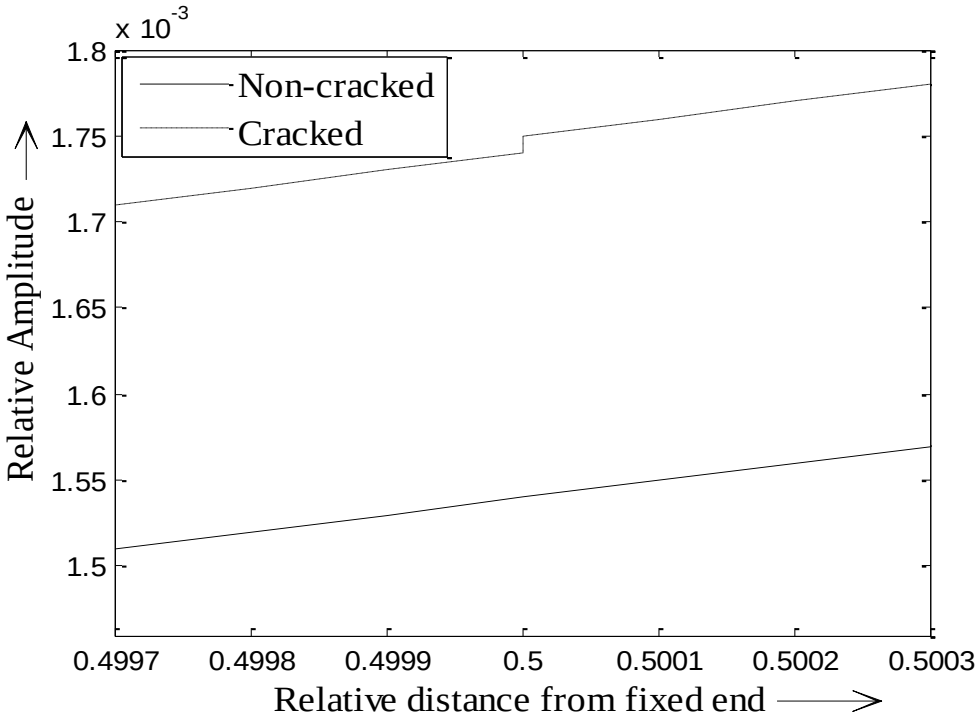

Figure 3.5(c) Magnified view at the second crack location (β_1=0.5)

3.3 Analysis of dynamic response of cracked structural steel beam

A theoretical model has been presented to extract the dynamic response (natural frequencies and mode shapes) of the multiple cracked steel beam. During the analysis of the theoretical results, a noticeable change is observed in the first three mode shapes, especially in the vicinity of crack locations.

3.3.1 Determination of the local flexibility and local stiffness matrix of a cracked steel beam

A cracked cantilever beam is subjected to axial force (F_1) and bending (F_2) as shown in figure 3.6 (a). Two transverse cracks of depth 'a_1' and 'a_2' are presence on the surface of the beam of width 'B' and height 'H' introduce a local flexibility, this can be defined in matrix form, and the size of the matrix depends on the degree of freedom. The cross-sectional view is also shown in figure 3.6 (b).

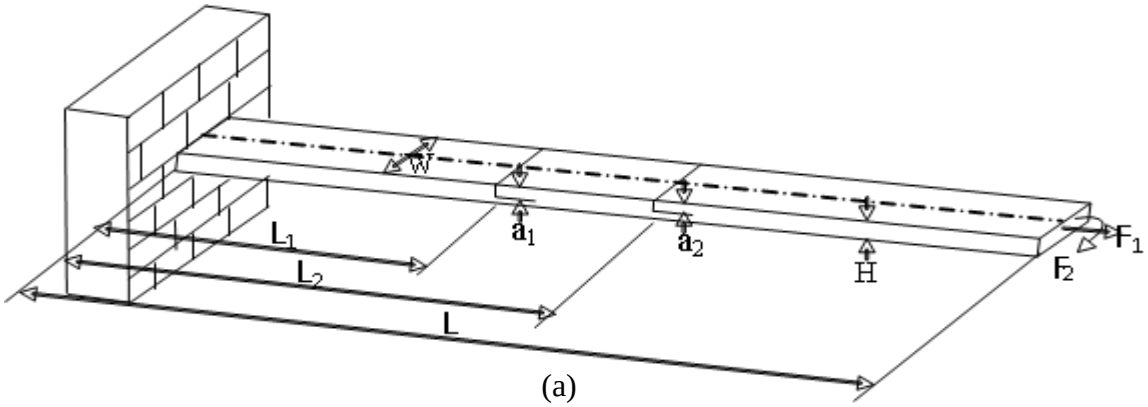

(a)

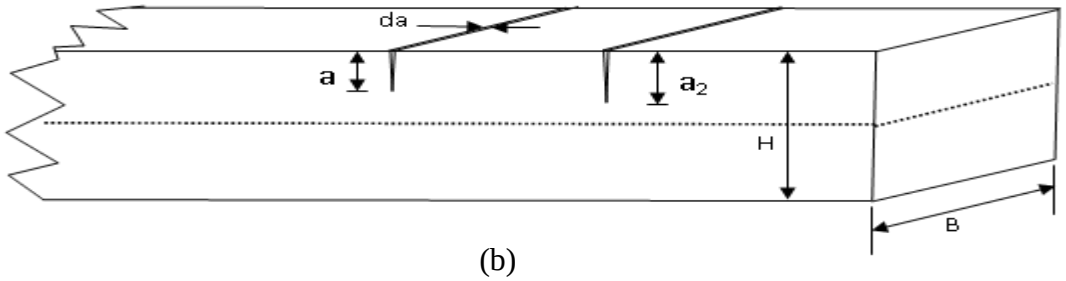

(b)

Figure 3.6 Geometry of beam: (a) Multiple cracked cantilever beam and (b) cross-sectional view of the beam

The strain energy release rate at cracked segment can be written according to Tada [158] as;

$$J = \frac{1}{\varphi'}(Q_{I1} + Q_{I2})^2, \tag{3.22}$$

Where $\frac{1}{\varphi'} = \frac{1-\nu^2}{\varphi}$ (for plane strain condition);

$= \frac{1}{\varphi}$ (for plane stress condition)

The Stress intensity factors $Q_{I1,}$ Q_{I2} are for mode I (opening of the crack) for load load F_1 and F_2 respectively. The values of stress intensity factors from earlier studies [158] are;

$$\frac{F_1}{HB}\sqrt{\pi a}(P_1(\frac{a}{H})) = Q_{I1}, \frac{6F_2}{H^2 B}\sqrt{\pi a}\,(P_2(\frac{a}{H})) = Q_{I2} \tag{3.23}$$

The expressions for F_1 and F_2 are as follows

$$P_1(\frac{a}{H}) = (\frac{2H}{\pi a}\tan(\frac{\pi a}{2H}))^{0.5}\left\{\frac{0.752 + 2.02(a/H) + 0.37(1-\sin(a\pi/2H))^3}{\cos(\pi a/2H)}\right\} \tag{3.24}$$

$$P_2(\frac{a}{H}) = (\frac{2H}{\pi a}\tan(\frac{\pi a}{2H}))^{0.5}\left\{\frac{0.923 + 0.199(1-\sin(a\pi/2H))^4}{\cos(\pi a/2H)}\right\} \tag{3.25}$$

Assuming U_e is the strain energy due to presence of crack. The additional displacement along the force F_i according to the Castigliano's theorem is;

$$\frac{\partial U_e}{\partial F_i} = u_i \tag{3.26}$$

Strain energy will have, $U_e = \int_0^{a_1} J\, da = \int_0^{a_1} \frac{\partial U_e}{\partial a}\, da$ (3.27)

Where $J = \frac{\partial U_e}{\partial a}$, the strain energy density functions.

From eqs. (3.26) and (3.27), we have;

$$\frac{\partial}{\partial F_i}\left[\int_0^{a_1} J(a)\, da\right] = u_i \tag{3.28}$$

The flexibility, influence co-efficient A_{ij} by definition is;

$$A_{ij} = \frac{\partial u_i}{\partial F_j} = \frac{\partial^2}{\partial F_j \partial F_i}\int_0^{a_1} J(a)\, da \tag{3.29}$$

And can be expressed as;

$$\frac{HB}{\varphi'}\frac{\partial^2}{\partial F_j \partial F_i}\int_0^{\psi_1} (Q_{l2} + Q_{l1})^2\, d\psi = A_{ij} \tag{3.30}$$

Using eq. (3.25) the compliance A_{11}, A_{22}, A_{12} $(=A_{21})$ are as follows;

$$A_{11} = \frac{BH}{\varphi'}\int_0^{\psi_1} \frac{\pi a}{B^2 H^2} 2(F_1(\psi))^2\, d\psi = \frac{2\pi}{B\varphi'}\int_0^{\psi_1} \psi (F_1(\psi))^2\, d\psi \tag{3.31}$$

$$A_{12} = A_{21} = \frac{12\pi}{\varphi' BH}\int_0^{\psi_1} \psi F_1(\psi) F_2(\psi))\, d\psi \tag{3.32}$$

$$A_{22} = \frac{72\pi}{\varphi' BH^2}\int_0^{\xi_1} \psi F_2(\psi) F_2(\psi))\, d\psi \tag{3.33}$$

The dimension-less form of the influence co-efficient will be;

$$\overline{A_{11}} = A_{11}\frac{B\varphi'}{2\pi};\ \overline{A_{12}} = A_{12}\frac{\varphi' BH}{12\pi} = \overline{A_{21}}\ ;\ \overline{A_{22}} = A_{22}\frac{\varphi' BH^2}{72\pi} \tag{3.34}$$

The inversion of compliance matrix will lead to the formation of local stiffness matrix and can be written as;

$$Q=\begin{bmatrix} A_{11} & A_{12} \\ A_{21} & A_{22} \end{bmatrix}^{-1}=\begin{bmatrix} Q_{11} & Q_{12} \\ Q_{21} & Q_{22} \end{bmatrix} \tag{3.35}$$

The stiffness matrices for the first and second crack location can be obtained as follows:

$$Q'=\begin{bmatrix} Q'_{11} & Q'_{12} \\ Q'_{21} & Q'_{22} \end{bmatrix}=\begin{bmatrix} A'_{11} & A'_{12} \\ A'_{21} & A'_{22} \end{bmatrix}^{-1} \text{ And } Q''=\begin{bmatrix} Q''_{11} & Q''_{12} \\ Q''_{21} & Q''_{22} \end{bmatrix}=\begin{bmatrix} A''_{11} & A''_{12} \\ A''_{21} & A''_{22} \end{bmatrix}^{-1} \tag{3.36}$$

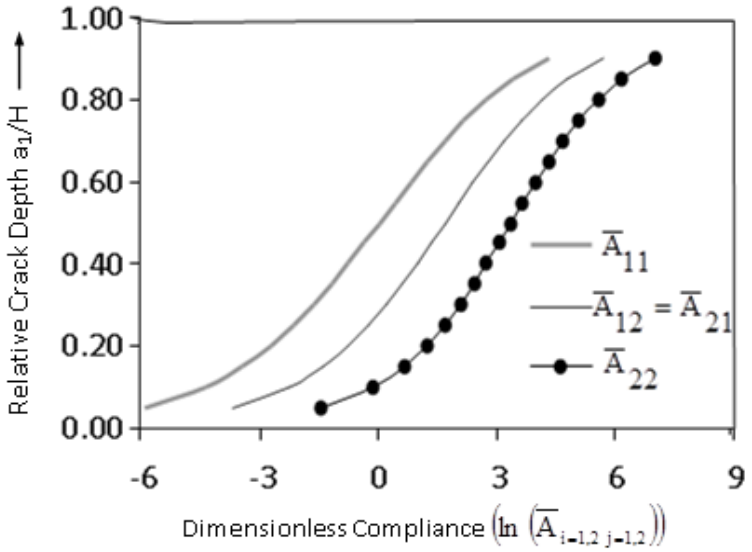

Figure 3.7 Relative crack depths (a_1/H) vs. Dimensionless Compliance $\left(\ln\left(\overline{A}_{i=1,2\ j=1,2}\right)\right)$

The variations of dimensionless compliances with respect to relative crack depth have been shown in figure 3.7 and from the graph it is observed that the dimensionless compliance increases with increase in relative crack depths.

3.3.2 Vibration analysis of the multiple cracked cantilever steel beams

In this section double crack cantilevers beam with length 'L' width 'B' and depth 'H' is shown in figure 3.8. The locations of cracks are 'L_1' and 'L_2' from the fixed end and the crack depths are 'a_1'and 'a_2'. The amplitudes of longitudinal vibration have been taken as $u_1(x, t)$, $u_2(x, t)$, $u_3(x, t)$ and amplitudes of bending vibration have been considered as $v_1(x, t)$, $v_2(x, t)$, $v_3(x, t)$ for the section-1(before 1st crack), section-2 (in between the cracks), section-3 (after the 2nd crack) respectively as shown in figure 3.8.

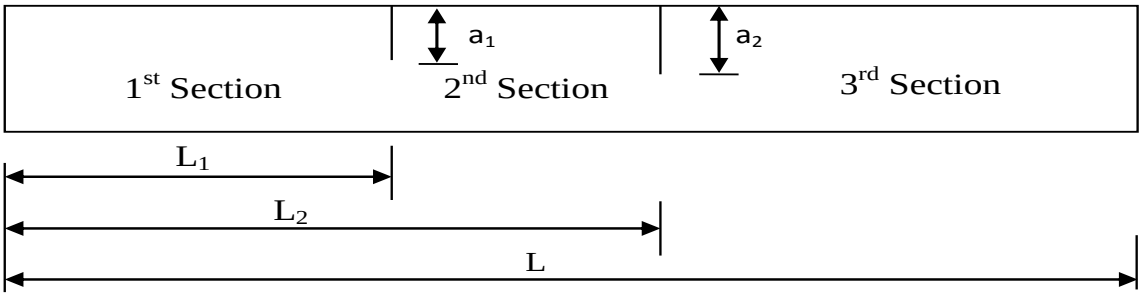

Figure 3.8 Front view of the cracked cantilever beam

The following are the expressions of normal functions of the system

$$\left.\begin{aligned}
&\bar{u}_1(\bar{x}) = R_1 \cos(\bar{Q}_u \bar{x}) + R_2 \ \sin(\bar{Q}_u \bar{x}) \\
&\bar{u}_2(\bar{x}) = R_3 \cos(\bar{Q}_u \bar{x}) + R_4 \ \sin(\bar{Q}_u \bar{x}) \\
&\bar{u}_3(\bar{x}) = R_5 \cos(\bar{Q}_u \bar{x}) + R_6 \ \sin(\bar{Q}_u \bar{x}) \\
&\bar{v}_1(\bar{x}) = R_5 \cosh(\bar{Q}_v \bar{x}) + R_6 \sinh(\bar{Q}_v \bar{x}) + R_7 \cos(\bar{Q}_v \bar{x}) + R_8 \ \sin(\bar{Q}_v \bar{x}) \\
&\bar{v}_2(\bar{x}) = R_9 \cosh(\bar{Q}_v \bar{x}) + R_{10} \sinh(\bar{Q}_v \bar{x}) + R_{11} \cos(\bar{Q}_v \bar{x}) + R_{12} \ \sin(\bar{Q}_v \bar{x}) \\
&\bar{v}_3(\bar{x}) = R_{15} \cosh(\bar{Q}_v \bar{x}) + R_{16} \sinh(\bar{Q}_v \bar{x}) + R_{17} \cos(\bar{Q}_v \bar{x}) + \bar{Q}_{18} \sin(\bar{K}_v \bar{x})
\end{aligned}\right\} \quad (3.37)$$

Where: $\bar{x} = \frac{x}{L}$, $\bar{u} = \frac{u}{L}$, $\bar{v} = \frac{v}{L}$, $\beta_1 = \frac{L_1}{L}$, $\beta_2 = \frac{L_2}{L}$, $\bar{Q}_u = \frac{\omega L}{C_u}$, $C_u = \left(\frac{\varphi}{\rho}\right)^{1/2}$, $\bar{Q}_v = \left(\frac{\omega L^2}{C_y}\right)^{1/2}$

The constants R_i, (i=1, 18) are to be calculated by using boundary conditions. The following are the boundary conditions for the cantilever beam;

$\bar{u}_1(0)=0;\ \bar{v}_1(0)=0;\ \bar{v}_1'(0)=0;\ \bar{u}_3'(1)=0;\ v_3''(1)=0;\ v_3'''(1)=0.$

At the cracked section:

$\bar{u}'_1(\beta_1) = \bar{u}'_2(\beta\beta)\ \ \bar{v}_1(\beta_1)=\bar{v}_2(\beta_1);\ \ \bar{v}_1'(\beta_1)=\bar{v}_2''(\beta_1);\ \ \bar{v}_1'''(\beta_1)=\bar{v}_2'''(\beta_1)$

$\bar{u}'_2(\beta_2)=\bar{u}'_3(\beta_2);\ \ \bar{v}_1(\beta_2)=\bar{v}_2(\beta_2);\ \ \bar{v}_1'(\beta_2)=\bar{v}_2''(\beta_2);\ \ \bar{v}_1'''(\beta_1)=\bar{v}_2'''(\beta_1)$

The expression in equation (3.38) can be found out because of the discontinuity of axial deformation to the right and left of the first crack location at the distance L_1 from the fixed end of the cantilever beam. Also at the cracked section, we have;

$$A\varphi \frac{du_1(L_1)}{dx} = q'_{11}(u_2(L_1) - u_1(L_1)) + q'_{12}\left(\frac{dv_2(L_1)}{dx} - \frac{dv_1(L_1)}{dx}\right) \quad (3.38)$$

Multiplying $\frac{A\varphi}{Lq'_{11}q'_{12}}$ on both sides of the equation (16) we get;

$$M_1 M_2 \bar{u}_1'(\beta_1) = M_2(\bar{u}_2(\beta_1) - \bar{u}_1'(\beta_1)) + M_1(\bar{v}_2'(\beta_1) - \bar{v}_1'(\beta_1)) \quad (3.39)$$

The expression in equation (3.39) can be found out because of the discontinuity of slope to the left and right of the crack at the crack section.

$$\varphi I \frac{d^2 v_1(L_1)}{dx^2} = q'_{21}(u_2(L_1) - u_1(L_1)) + q'_{22}\left(\frac{dv_2(L_1)}{dx} - \frac{dv_1(L_1)}{dx}\right) \quad (3.40)$$

Multiplying $\frac{\varphi I}{L^2 q'_{22} q'_{21}}$ on both sides of the equation (3.40) we get;

$$M_3 M_4 \bar{v}_1''(\beta_1) = M_4(\bar{v}_2'(\beta_1) - \bar{v}_1'(\beta_1)) + M_3(\bar{u}_2(\beta_1) - \bar{u}_1(\beta_1)) \quad (3.41)$$

Similarly, considering the second crack we can have;

$$M_5 M_6 \bar{u}_2'(\beta_2) = M_6(\bar{u}_3(\beta_2) - \bar{u}_2(\beta_2)) + M_5(\bar{v}_3'(\beta_2) - \bar{v}_2'(\beta_2)) \quad (3.42)$$

$$M_7 M_8 \bar{v}_2''(\beta_2) = M_8(\bar{v}_3'(\beta_2) - \bar{v}_2'(\beta_2)) + M_7(\bar{u}_3(\beta_2) - \bar{u}_2(\beta_2)) \quad (3.43)$$

Where $M_1 = \varphi E/(Lq'_{11});\ M_2 = A\varphi/q'_{12}\ ;\ M_3 = \varphi I/(Lq'_{22}),M_4 = \varphi I/(L^2 q'_{21})$

$M_5 = A\varphi/(Lq''_{22});\ M_6 = A\varphi/q''_{23}\ ;\ M_7 = \varphi I/(Lq''_{33}),M_8 = EI/(L^2 q''_{32})$

By using the normal functions, equation (3.37) with the laid down boundary conditions as mentioned above, the characteristic equation of the system can be expressed as;

$$\left|\bar{K}\right| = 0 \quad (3.44)$$

This determinant is a function of natural frequency (ω), the relative locations of the crack and the local stiffness matrix (Q) which in turn is a function of the relative crack depth.

Where $\bar{K}$ is a 18x18 matrix and is expressed as;

$$[\bar{K}] = \begin{bmatrix}
0 & 0 & 0 & 0 & 0 & 0 & 0 & 0 & 0 & 0 & 0 & 0 & 1 & 0 & 0 & 0 & 0 & 0 \\
1 & 0 & 1 & 0 & 0 & 0 & 0 & 0 & 0 & 0 & 0 & 0 & 0 & 0 & 0 & 0 & 0 & 0 \\
0 & 1 & 0 & 1 & 0 & 0 & 0 & 0 & 0 & 0 & 0 & 0 & 0 & 0 & 0 & 0 & 0 & 0 \\
0 & 0 & 0 & 0 & 0 & 0 & 0 & 0 & 0 & 0 & 0 & 0 & 0 & 0 & 0 & 0 & -T_1 & T_2 \\
0 & 0 & 0 & 0 & 0 & 0 & 0 & 0 & G_3 & G_4 & -G_7 & -G_8 & 0 & 0 & 0 & 0 & 0 & 0 \\
0 & 0 & 0 & 0 & 0 & 0 & 0 & 0 & G_4 & G_3 & G_8 & -G_7 & 0 & 0 & 0 & 0 & 0 & 0 \\
0 & 0 & 0 & 0 & 0 & 0 & 0 & 0 & 0 & 0 & 0 & 0 & -T_6 & T_5 & T_6 & -T_5 & 0 & 0 \\
G_1 & G_2 & G_5 & G_6 & -G_1 & -G_2 & -G_5 & -G_6 & 0 & 0 & 0 & 0 & 0 & 0 & 0 & 0 & 0 & 0 \\
G_1 & G_2 & -G_5 & -G_6 & -G_1 & -G_2 & G_5 & G_6 & 0 & 0 & 0 & 0 & 0 & 0 & 0 & 0 & 0 & 0 \\
G_2 & G_1 & G_6 & -G_5 & -G_2 & -G_1 & -G_6 & G_5 & 0 & 0 & 0 & 0 & 0 & 0 & 0 & 0 & 0 & 0 \\
0 & 0 & 0 & 0 & 0 & 0 & 0 & 0 & 0 & 0 & 0 & 0 & 0 & 0 & -T_4 & T_3 & T_4 & -T_3 \\
0 & 0 & 0 & 0 & G_9 & G_{10} & G_{11} & G_{12} & -G_9 & -G_{10} & -G_{11} & -G_{12} & 0 & 0 & 0 & 0 & 0 & 0 \\
0 & 0 & 0 & 0 & G_9 & G_{10} & -G_{11} & -G_{12} & -G_9 & -G_{10} & G_{11} & G_{12} & 0 & 0 & 0 & 0 & 0 & 0 \\
0 & 0 & 0 & 0 & G_{10} & G_9 & G_{12} & -G_{11} & -G_{10} & -G_9 & -G_{12} & G_{11} & 0 & 0 & 0 & 0 & 0 & 0 \\
-S_3 & -S_4 & S_5 & -S_6 & S_3 & S_4 & -S_5 & S_6 & 0 & 0 & 0 & 0 & S_1 & -S_2 & T_5 & T_6 & 0 & 0 \\
S_7 & S_8 & -S_9 & -S_{10} & -S_{11} & -S_{12} & S_{13} & -S_{14} & 0 & 0 & 0 & 0 & S_{15} & S_{16} & -S_{15} & -S_{16} & 0 & 0 \\
0 & 0 & 0 & 0 & V_3 & V_4 & -V_5 & V_6 & -V_3 & -V_4 & V_5 & -V_6 & 0 & 0 & V_1 & V_2 & -T_3 & -T_4 \\
0 & 0 & 0 & 0 & V_7 & V_8 & -V_9 & -V_{10} & -V_{11} & -V_{12} & V_{13} & -V_{14} & 0 & 0 & V_{15} & V_{16} & -V_{15} & -V_{16}
\end{bmatrix} \quad (3.45)$$

Where

$T_1 = Sin\overline{Q}_u; T_2 = Cos\overline{Q}_u; T_3 = Cos(\overline{Q}_u \beta_2); T_4 = Sin(\overline{Q}_u \beta_2); T_5 = Cos(\overline{Q}_u \beta_1); T_6 = Sin(\overline{Q}_u \beta_1);$

$G_1 = Cosh(\overline{Q}_y \beta_1); G_2 = Sinh(\overline{Q}_y . \beta_1); G_3 = Cosh(\overline{Q}_y); G_4 = Sinh(\overline{Q}_y); G_5 = Cos(\overline{Q}_y \beta_1);$

$G_6 = Sin(\overline{Q}_y \beta_1); G_7 = Cos(\overline{Q}_y); G_8 = Sin(\overline{Q}_y); G_9 = Cosh(\overline{Q}_y \beta_2); G_{10} = Sinh(\overline{Q}_y \beta_2);$

$G_{11} = Cos(\overline{Q}_y \beta_2); G_{12} = Sin(\overline{Q}_y \beta_2); M_1 = AE/(LQ'_{11}); M_2 = AE/Q'_{12}; M_3 = EI/(LQ'_{22});$

$M_4 = EI/(L^2 Q'_{21}); M_{12} = M_1/M_2; M_{34} = M_3/M_4; S_1 = T_5 - M_1 \overline{Q}_u T_6; S_2 = T_6 + M_1 \overline{Q}_u T_5;$

$S_3 = M_{12} S_{11}; S_4 = M_{12} S_{12}; S_5 = M_{12} S_{13}; S_6 = M_{12} S_{14}; S_7 = M_3 \overline{Q}_y{}^2 G_1 + S_{11};$

$S_8 = M_3 \overline{Q}_y{}^2 G_2 + S_{12}; S_9 = M_3 \overline{Q}_y{}^2 G_5 + S_{13}; S_{10} = M_3 \overline{Q}_y{}^2 G_6 - S_{14}; S_{11} = \overline{Q}_y G_2; S_{12} = \overline{Q}_y G_1;$

$S_{13} = \overline{Q}_y G_6; S_{14} = \overline{Q}_y G_5; S_{14} = \overline{Q}_y G; S_{15} = M_{34} T_5; S_{16} = M_{34} T_6; M_5 = AE/(LQ''_{22});$

$M_6 = AE/Q''_{23}; M_7 = EI/(LQ''_{33}); M_8 = EI/(L^2 Q''_{32}); M_{56} = M_5/M_6; \; M_{78} = M_7/M_8;$

$V_1 = T_3 - M_5 \overline{Q}_u T_4; V_2 = T_4 + M_5 \overline{Q}_u T_3; V_3 = M_{56} V_{11}; V_4 = M_{56} V_{12}; V_5 = M_{56} V_{13}; V_6 = M_{56} V_{14};$

$V_7 = M_7 \overline{Q}_y{}^2 G_9 + V_{11}; V_8 = M_7 \overline{Q}_y{}^2 G_{10} + V_{12}; V_9 = M_7 \overline{Q}_y{}^2 G_{11} + V_{13}; V_{10} = M_7 \overline{Q}_y{}^2 G_{12} - V_{14};$

$V_{11} = \overline{Q}_y G_{10}; V_{12} = \overline{Q}_y G_9; V_{13} = \overline{Q}_y G_{12}; V_{14} = \overline{Q}_y G_{11}; V_{15} = M_{78} T_3; V_{16} = M_{78} T_4$

The theoretical analysis results for first three mode shapes for non-cracked and cracked steel beam are shown in figures 3.9,3.10, and 3.11 for cracks orientation β_1=0.25, β_2=0.5, ψ_1=0.1667 and ψ_2=0.5. Magnified view at the vicinity of the first and second crack for first three mode of vibration are shown in figures 3.9(b), 3.9(c), 3.10(b), 3.10(c), 3.11(b) and 3.11(c). A sudden jump has been observed in relative amplitudes at crack locations; these changes in amplitudes will be helpful in the prediction of crack location and its intensity.

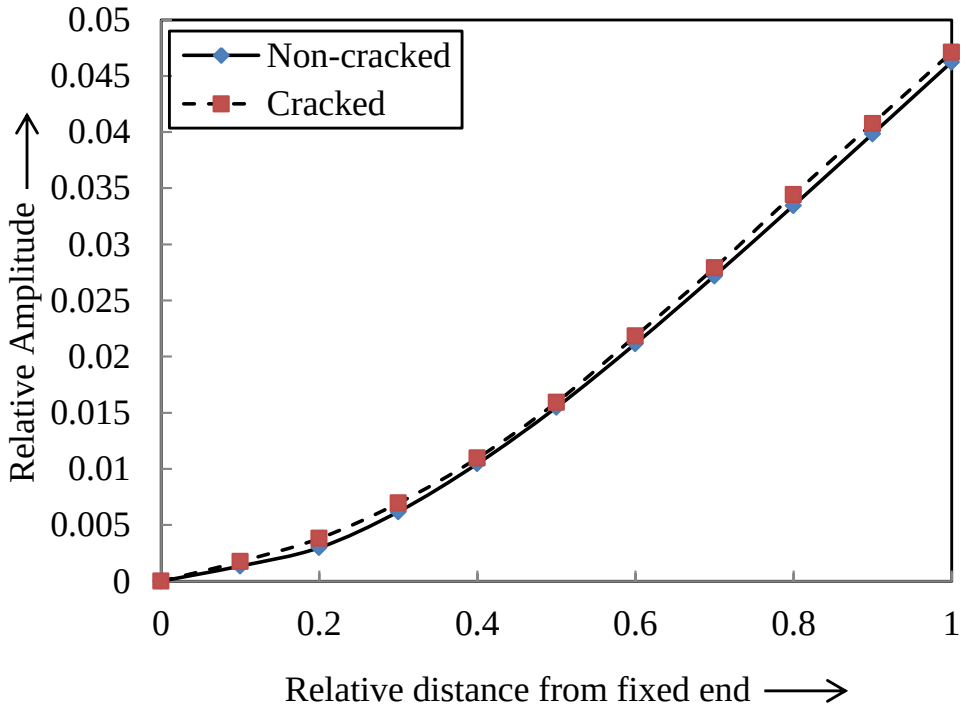

Figure 3.9(a) Relative Amplitude vs. Relative distance from fixed end (1st mode of vibration) β_1=0.25, β_2=0.5, ψ_1=0.1667 & ψ_2=0.5

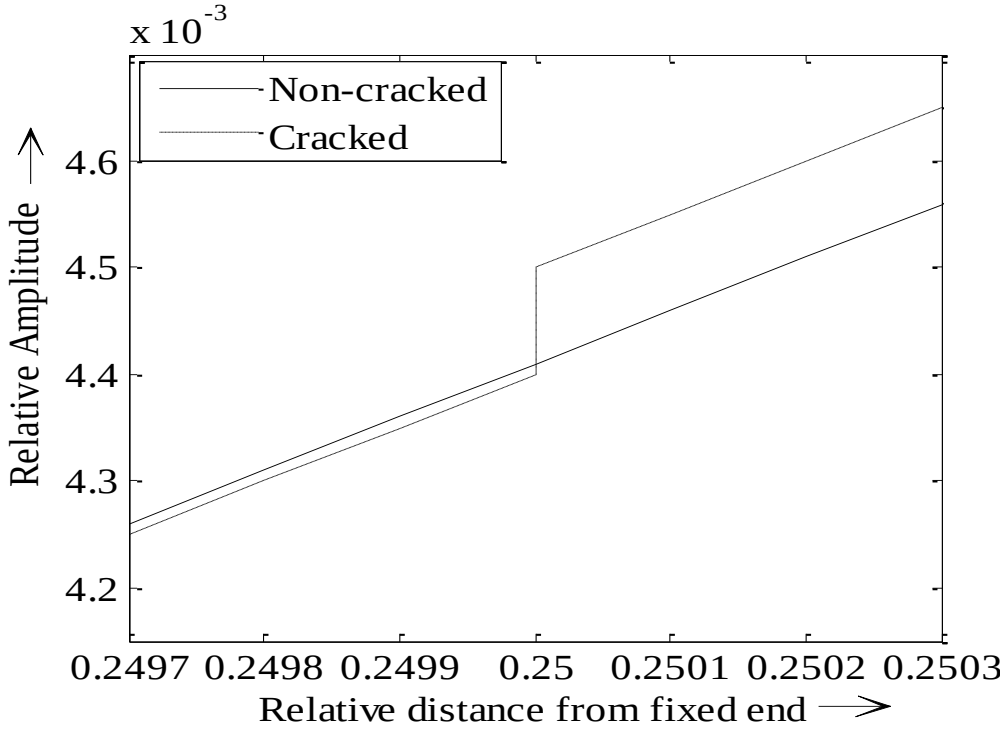

Figure 3.9(b) Magnified view at the first crack location (β_1=0.25)

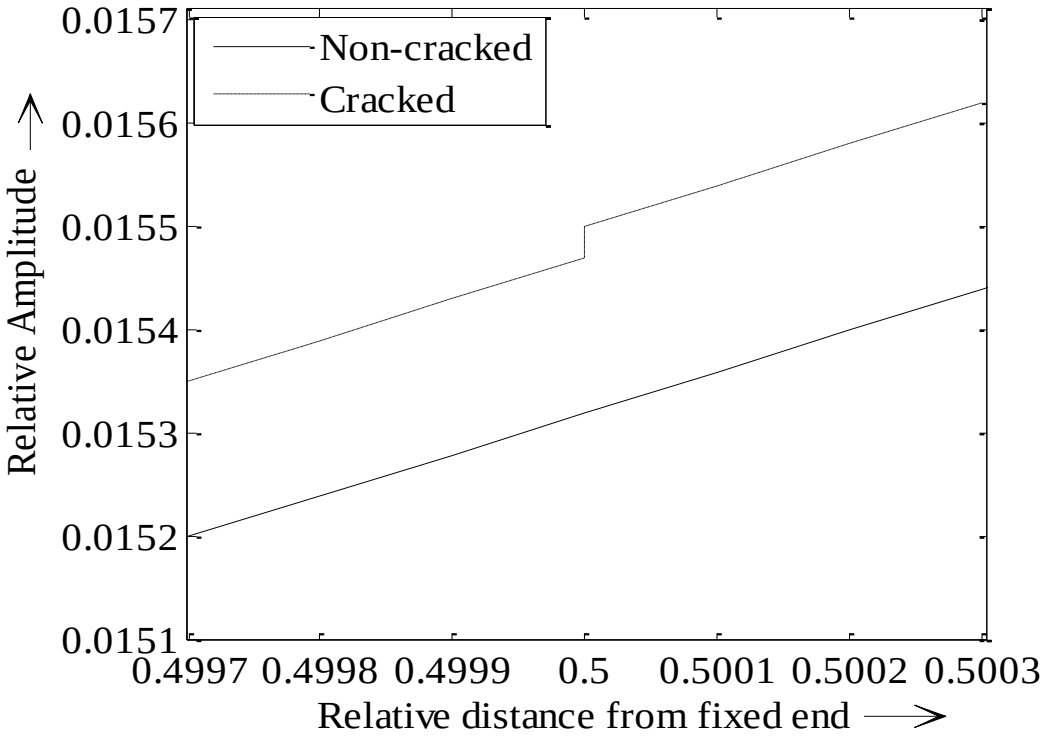

Figure 3.9(c) Magnified view at the second crack location (β_1=0.5)

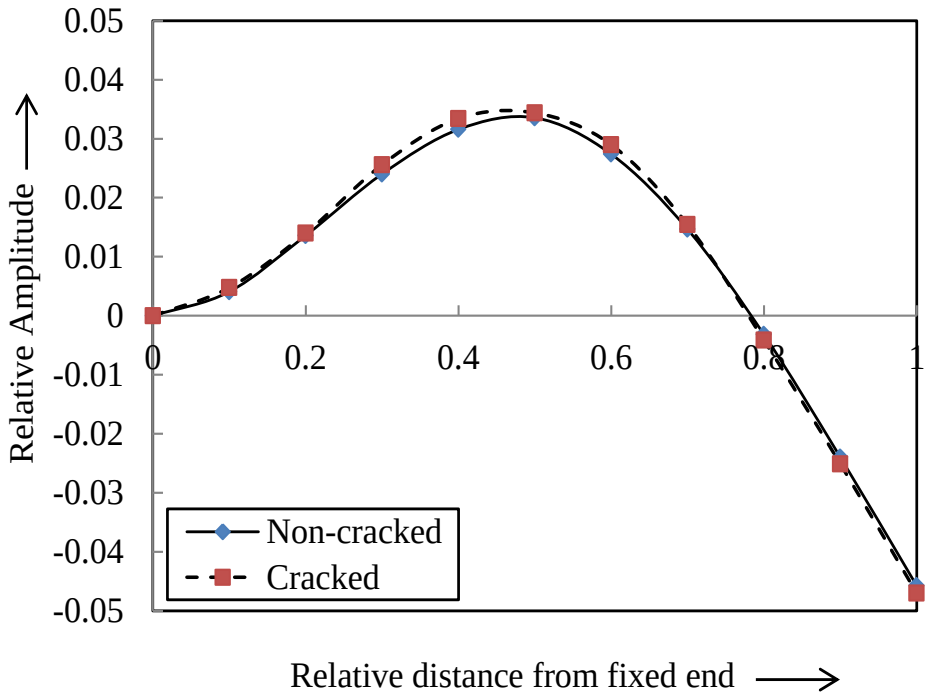

Figure 3.10(a) Relative Amplitude vs. Relative distance from fixed end (2nd mode of vibration) β_1=0.25, β_2=0.5, ψ_1=0.1667 & ψ_2=0.5

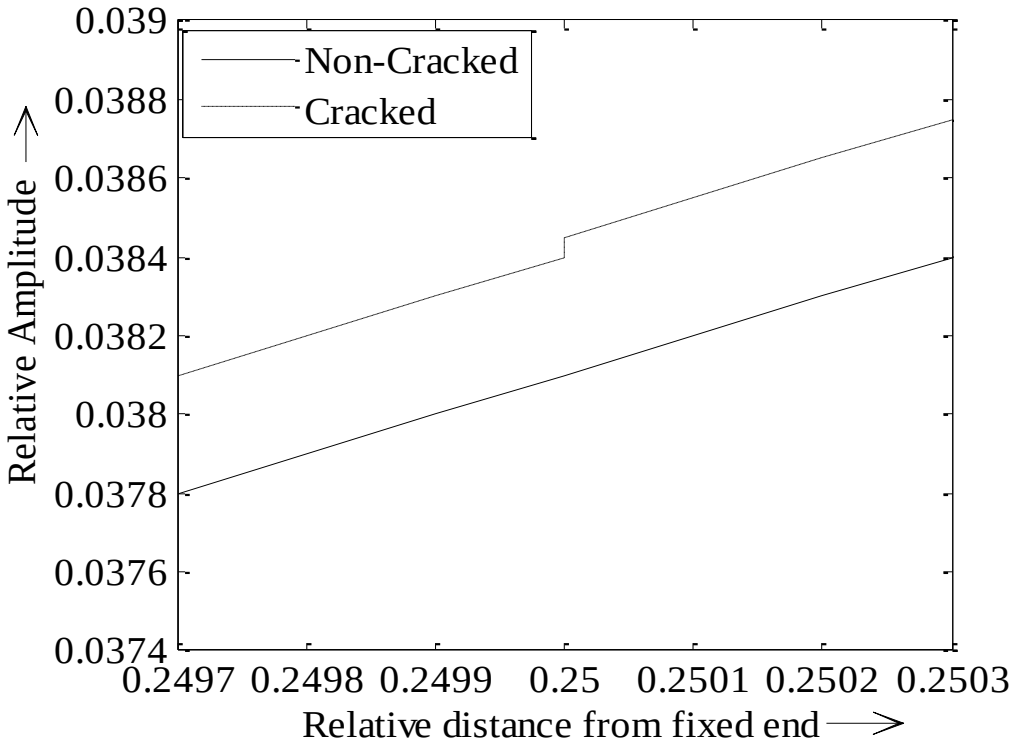

Figure 3.10(b) Magnified view at the first crack location (β_1=0.25)

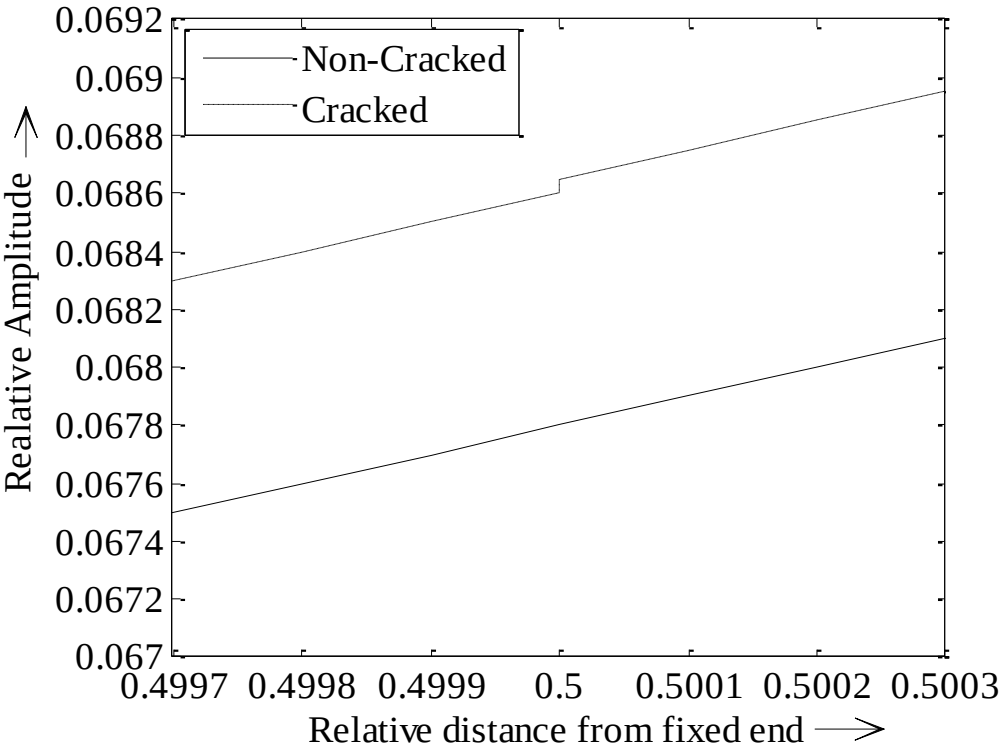

Figure 3.10(c) Magnified view at the second crack location (β_1=0.5)

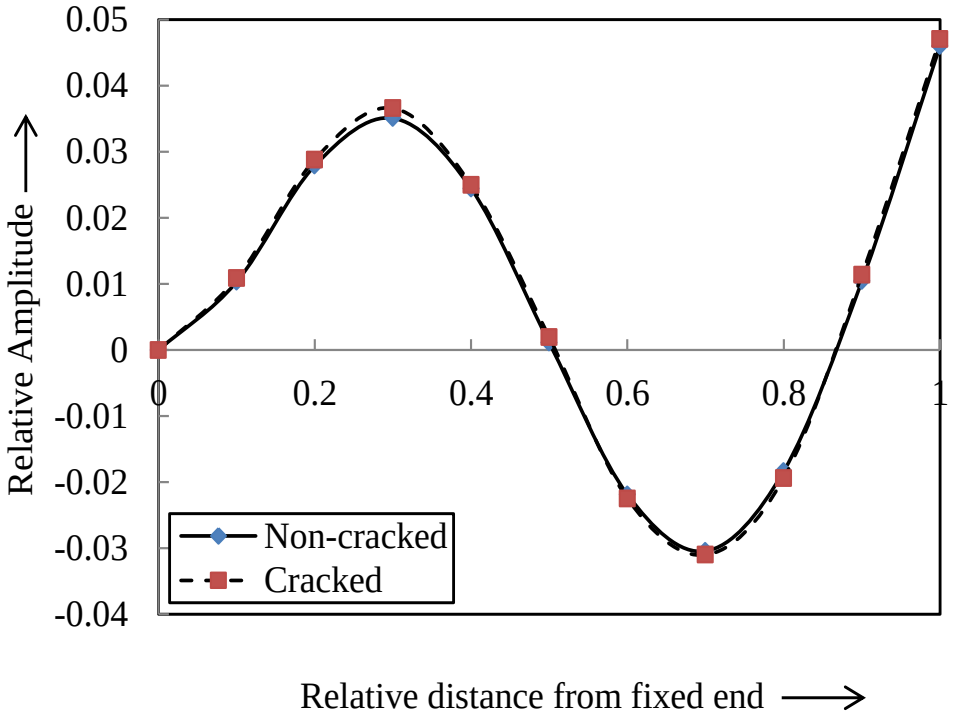

Figure 3.11(a) Relative Amplitude vs. Relative distance from fixed end (3rd mode of vibration) β_1=0.25, β_2=0.5, ψ_1=0.1667 & ψ_2=0.5

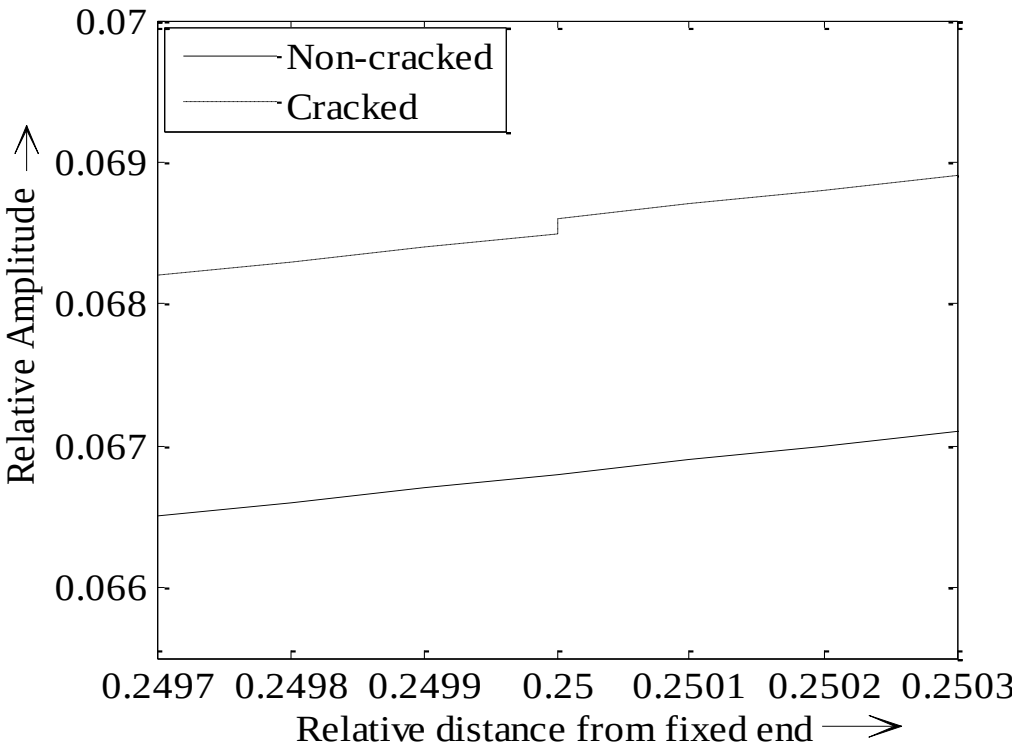

Figure 3.11(b) Magnified view at the first crack location (β_1=0.25)

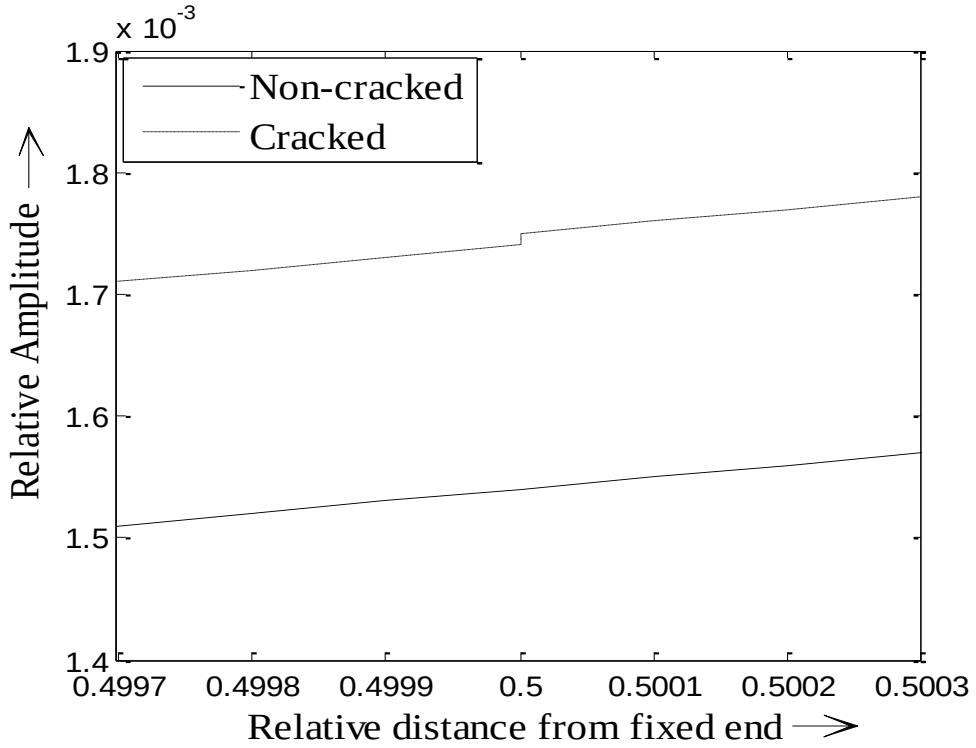

Figure 3.11(c) Magnified view at the second crack location (β_1=0.5)

3.4 Evaluation and comparison of experimental and theoretical analysis results

3.4.1 Analysis of experimental results and theoretical results of composite beam

The glass fibers reinforced epoxy composite beam with dimension (800x50x6 mm) has been considered in analysis for evaluation of vibration response. The numbers of experiments have been conducted on specimens with various configurations of first and second crack locations and its size to measure the first three mode shapes and corresponding natural frequencies. The schematic block diagram experimental setup is shown in figure 3.12. The experimental investigation has been performed to obtain mode shapes for three sets of 1st and 2nd relative crack location and relative crack depth: first set is 0.25, 0.5 (crack location) and 0.1667, 0.5 (crack depth), second set is 0.1875, 0.4375 (crack location) and 0.5, 0.416 (crack depth) and third set is 0.3125, 0.5625 (crack location) and 0.333, 0.25 (crack depth) has been compared with the theoretical analysis for cracked and non-cracked composite beam. The comparisons are plotted for the first set in figures 3.13(a) to 3.13(c).

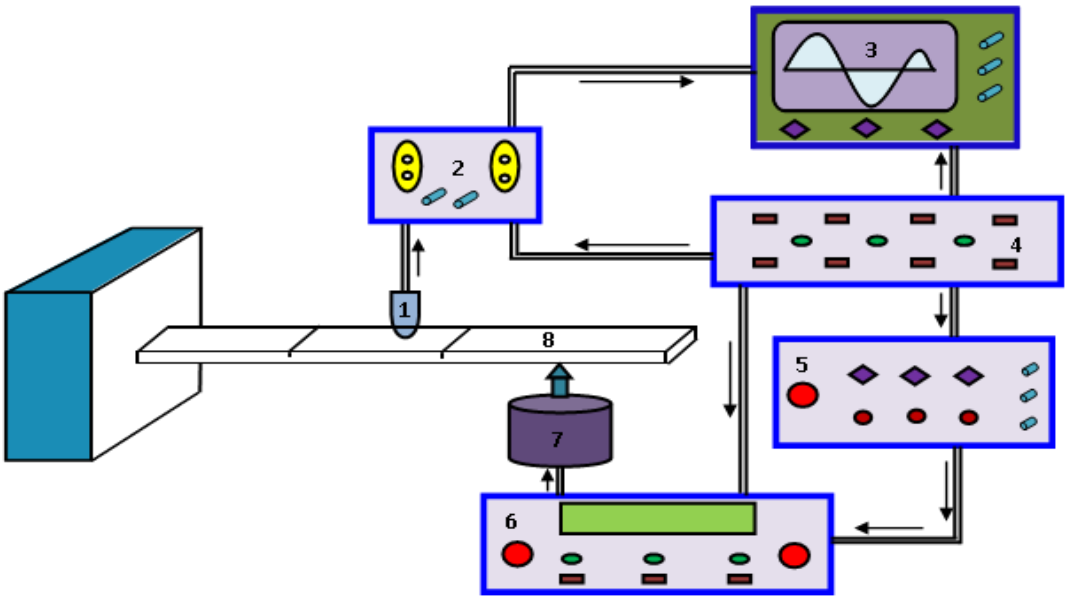

Figure 3.12 Schematic block diagram of experimental set-up

1. Delta tron Accelerometer; 2. Vibration analyzer; 3. Vibration indicator embedded with Pulse Labshop software; 4. Power Distribution box; 5. Signal generator; 6. Power amplifier; 7. Vibration Shaker; 8. Cracked beam with foundation

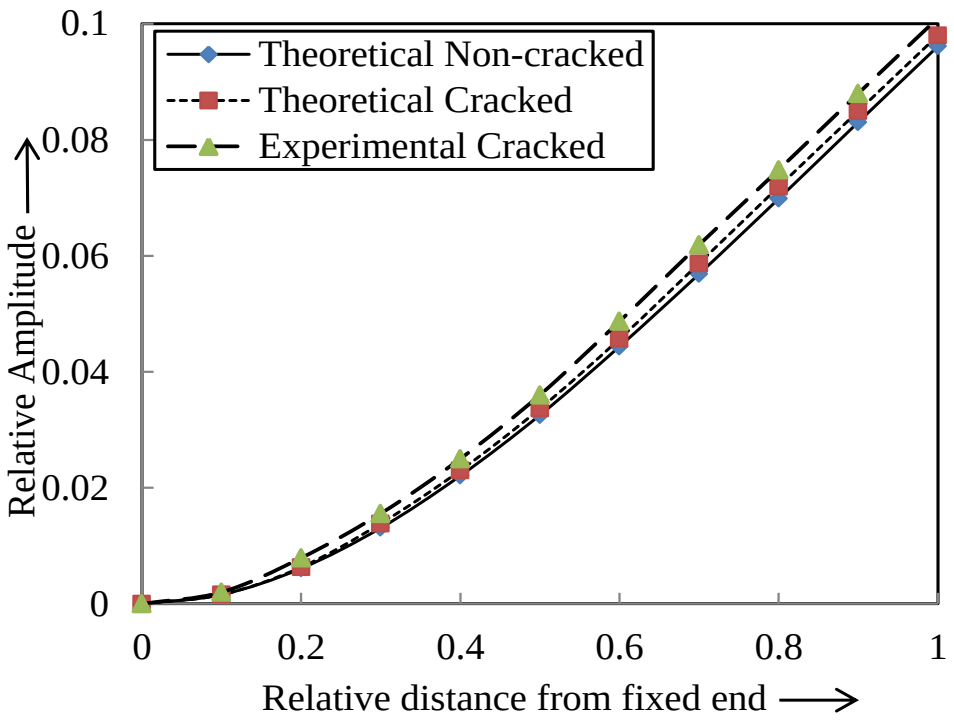

Figure 3.13(a) Relative Amplitude vs. Relative distance from fixed end (1st mode of vibration) β_1=0.25, β_2=0.5, ψ_1=0.1667 & ψ_2=0.5

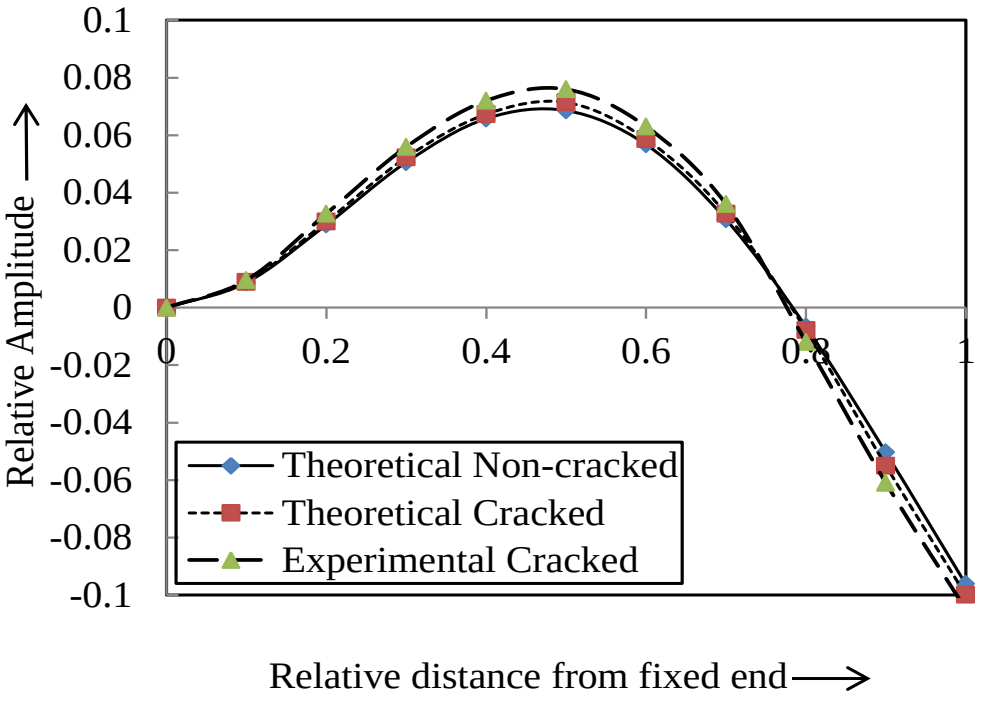

Figure 3.13(b) Relative Amplitude vs. Relative distance from fixed end (2nd mode of vibration) β_1=0.25, β_2=0.5, ψ_1=0.1667 & ψ_2=0.5

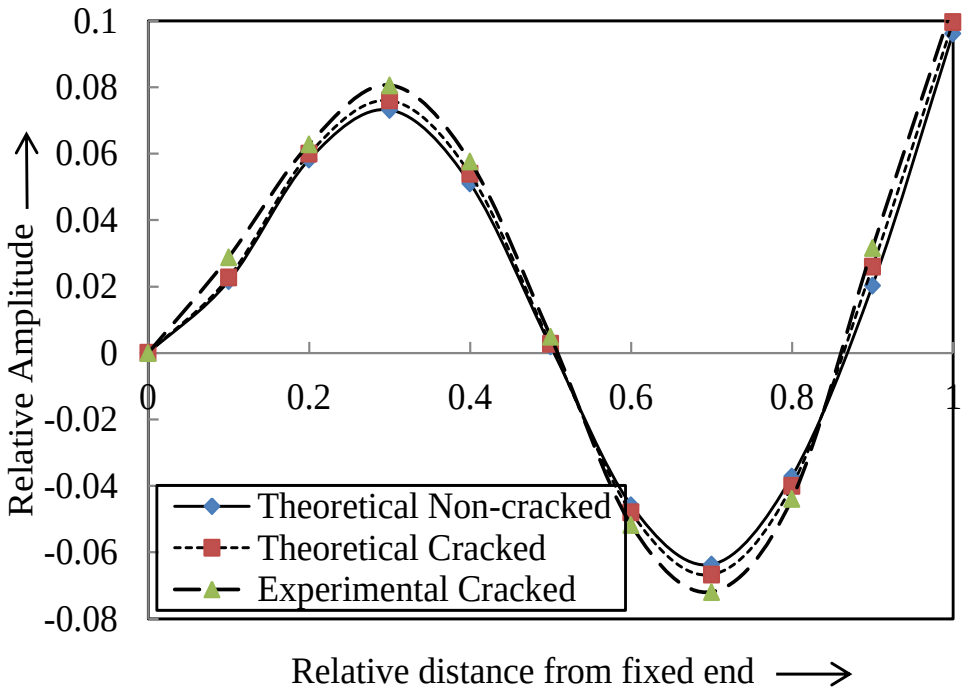

Figure 3.13(c) Relative Amplitude vs. Relative distance from fixed end (3rd mode of vibration) β_1=0.25, β_2=0.5, ψ_1=0.1667 & ψ_2=0.5

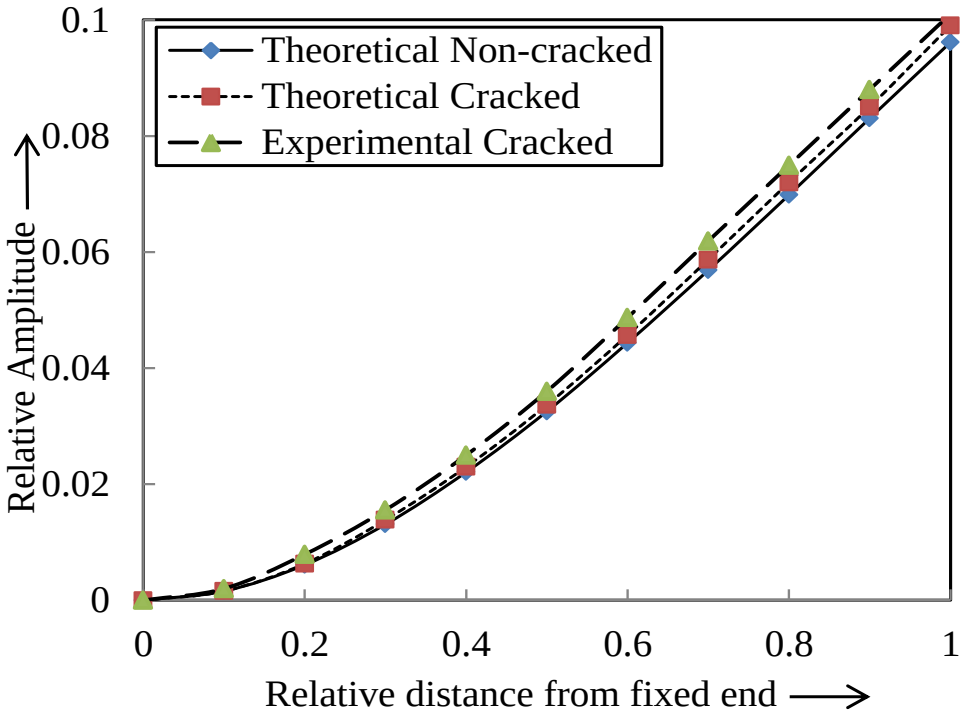

Figure 3.14(a) Relative Amplitude vs. Relative distance from fixed end (1st mode of vibration) β_1=0.1875, β_2=0.4375, ψ_1=0.5 & ψ_2=0.416

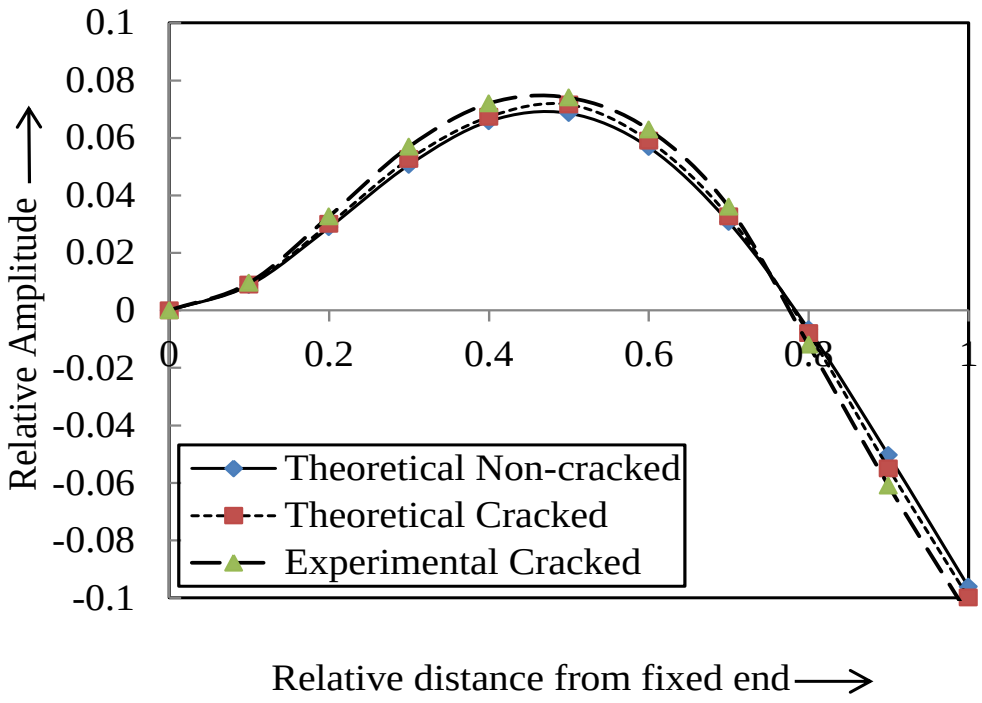

Figure 3.14(b) Relative Amplitude vs. Relative distance from fixed end (2nd mode of vibration) β_1=0.1875, β_2=0.4375, ψ_1=0.5 & ψ_2=0.416

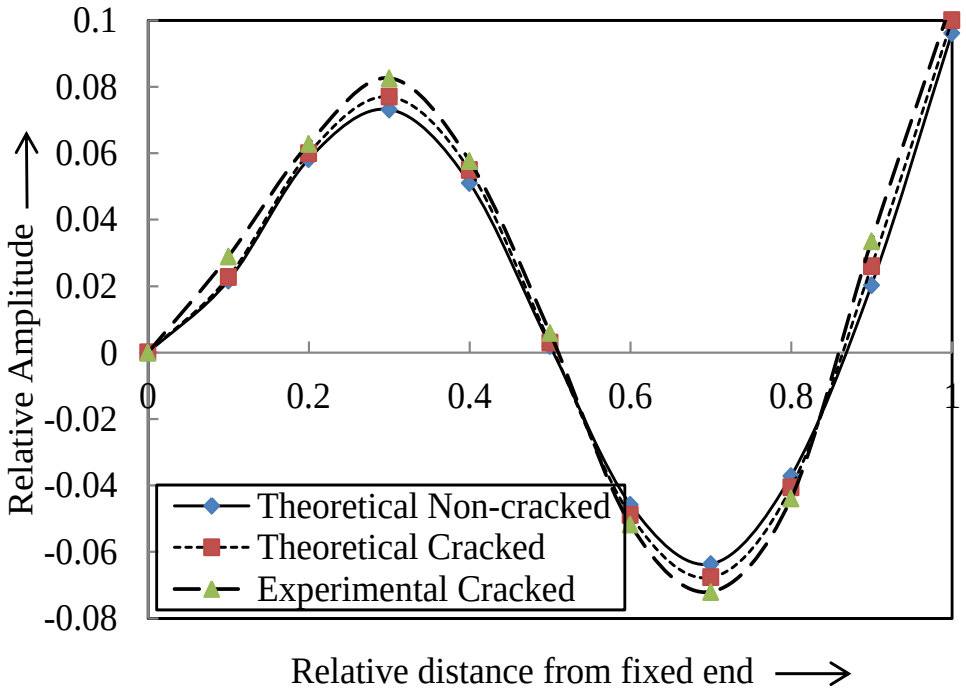

Figure 3.14(c) Relative Amplitude vs. Relative distance from fixed end (3rd mode of vibration) β_1=0.1875, β_2=0.4375, ψ_1=0.5 & ψ_2=0.416

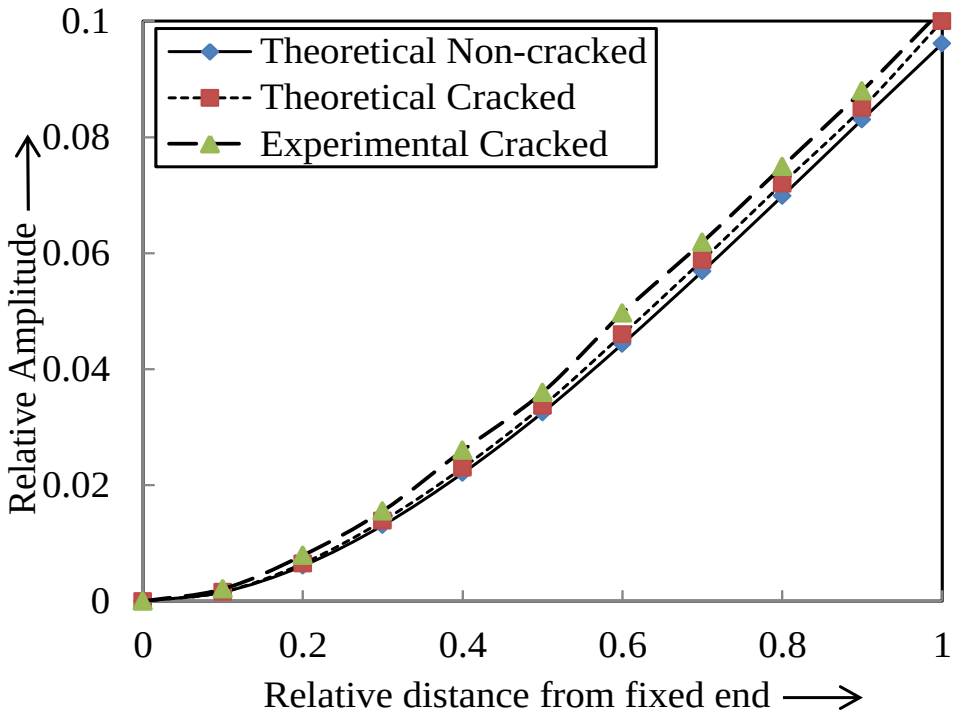

Figure 3.15(a) Relative Amplitude vs. Relative distance from fixed end (1st mode of vibration) β_1=0.3125, β_2=0.5525, ψ_1=0.333& ψ_2=0.25

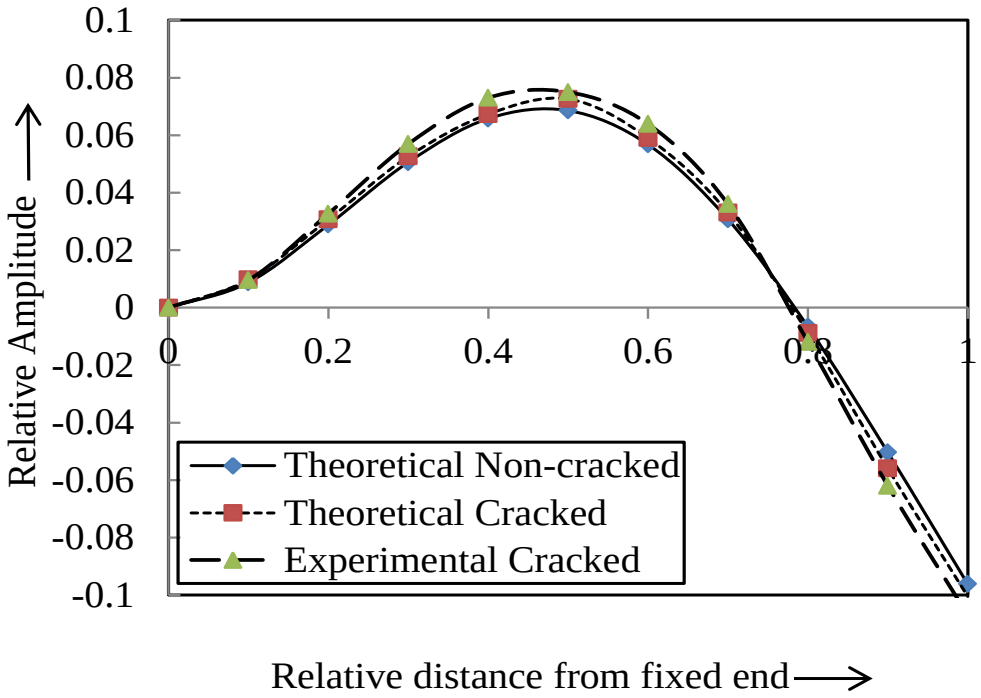

Figure 3.15 (b) Relative Amplitude vs. Relative distance from fixed end (2nd mode of vibration) β_1=0.3125, β_2=0.5525, ψ_1=0.333& ψ_2=0.25

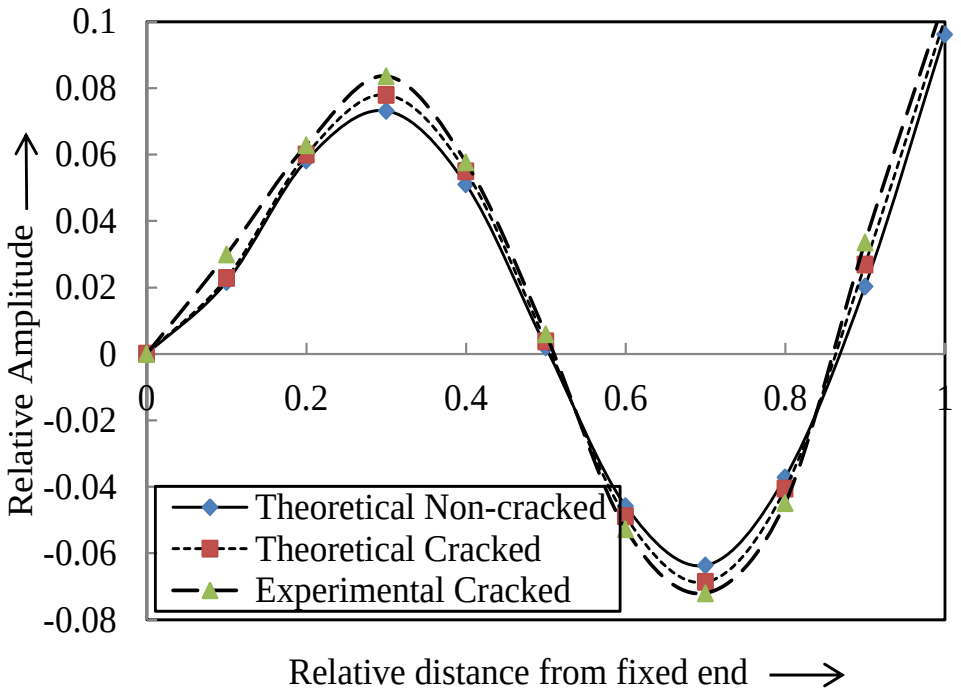

Figure 3.15(c) Relative Amplitude vs. Relative distance from fixed end (3rd mode of vibration) β_1=0.3125, β_2=0.5525, ψ_1=0.333&

3.4.2 Analysis of experimental results and theoretical results for steel beam

The structural steel beam with dimension (800x50x6 mm) as discussed in the previous section has been considered in the analysis for evaluation of vibration response. Many cracked specimens are collected with different configurations of first and second crack locations and depths and are used to conduct the experiments for identifying the first three mode shapes and corresponding natural frequencies. The schematic block diagram experimental setup is shown in figure 3.12.

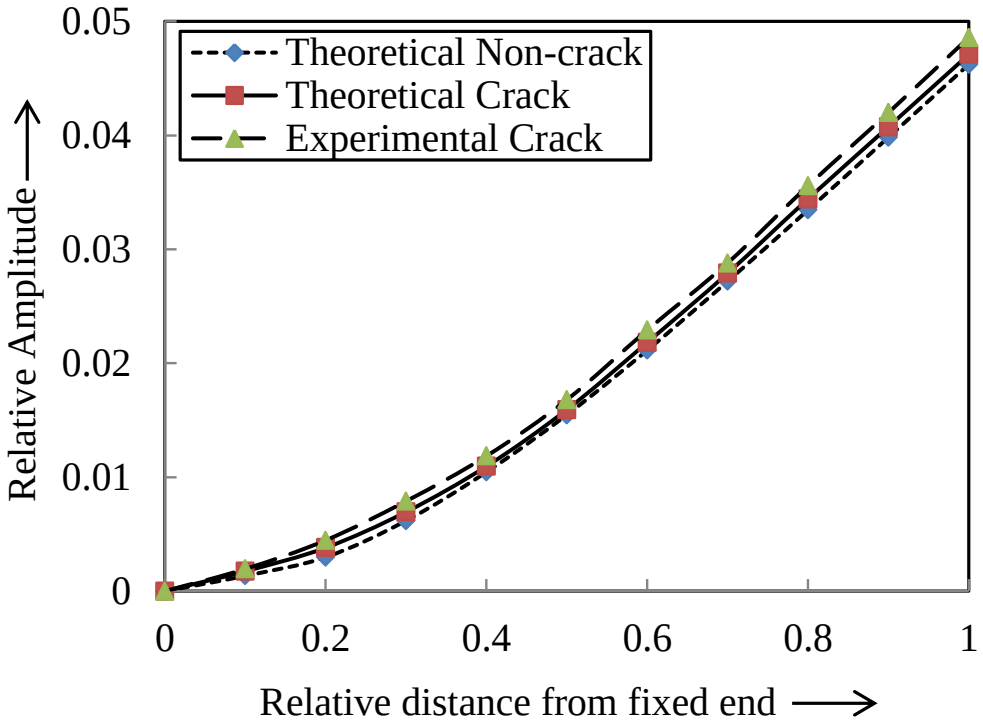

Figure 3.16a Relative Amplitude vs. Relative distance from fixed end (1st mode of vibration) β_1=0.25, β_2=0.5, ψ_1=0.1667 & ψ_2=0.5

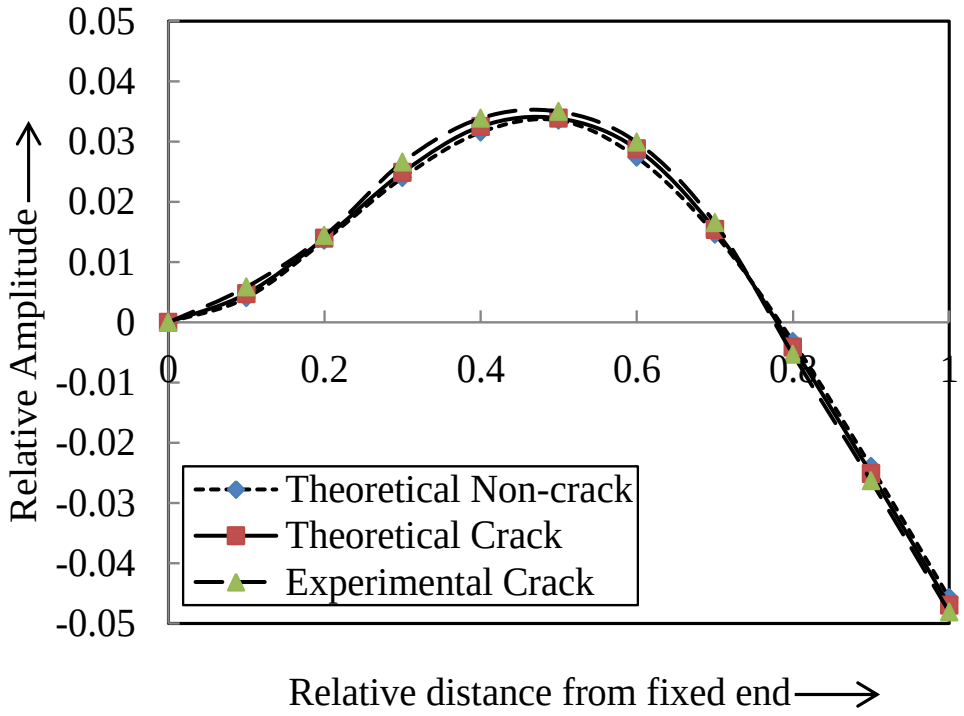

Figure 3.16b Relative Amplitude vs. Relative distance from fixed end (2nd mode of vibration) β_1=0.25, β_2=0.5, ψ_1=0.1667 & ψ_2=0.5

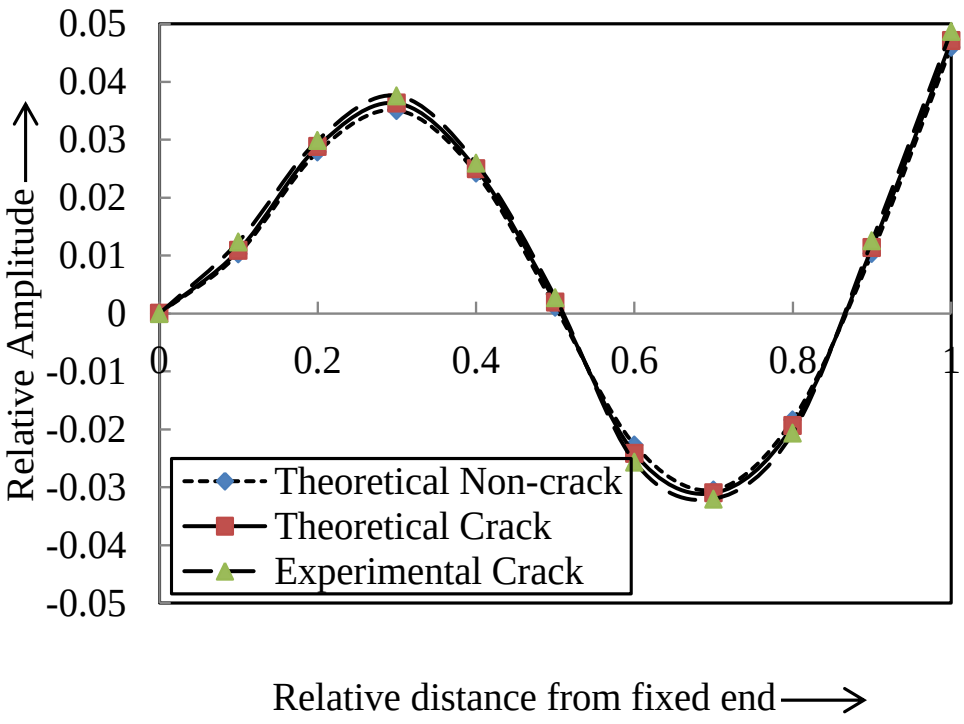

Figure 3.16c Relative Amplitude vs. Relative distance from fixed end (3rd mode of vibration) β_1=0.25, β_2=0.5, ψ_1=0.1667 & ψ_2=0.5

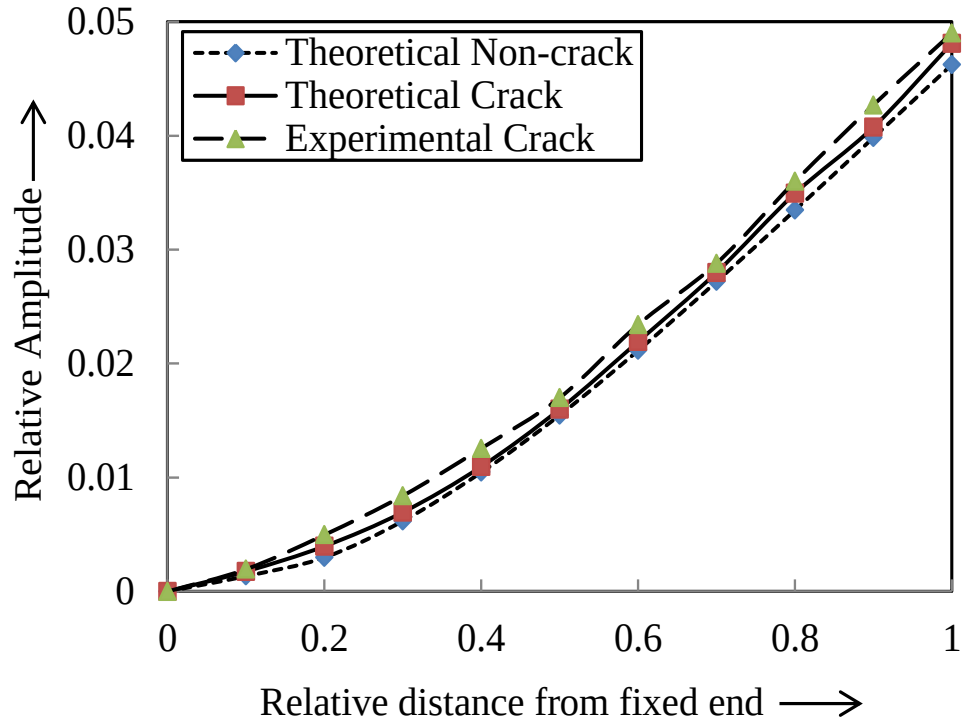

Figure 3.17a Relative Amplitude vs. Relative distance from fixed end (1st mode of vibration) β_1=0.1875, β_2=0.4375, ψ_1=0.5 & ψ_2=0.416

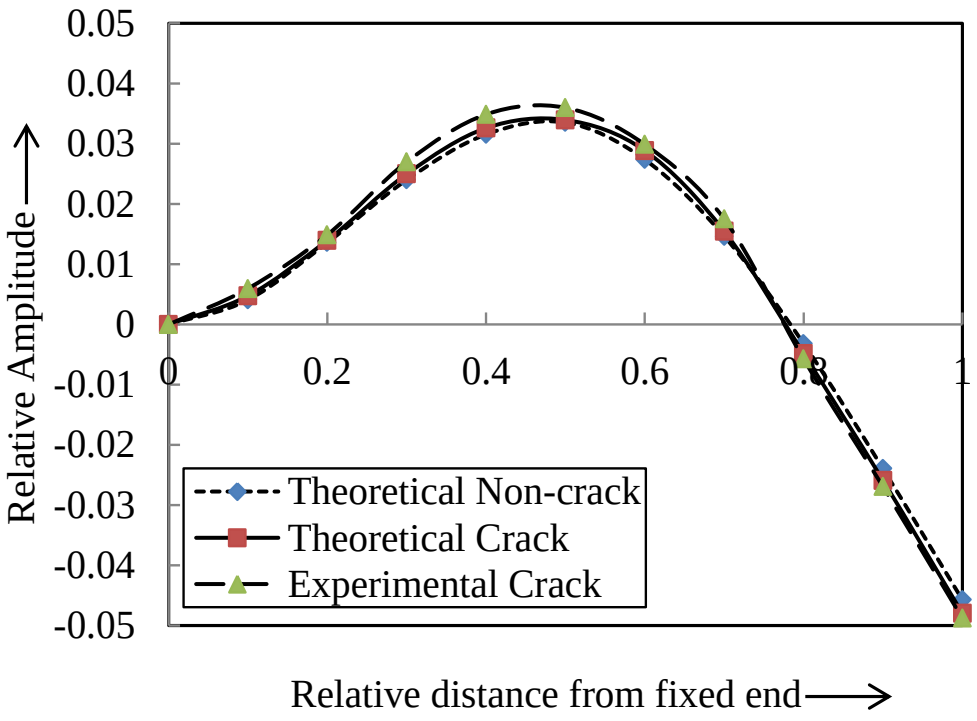

Figure 3.17b Relative Amplitude vs. Relative distance from fixed end (2nd mode of vibration) β_1=0.1875, β_2=0.4375, ψ_1=0.5 & ψ_2=0.416

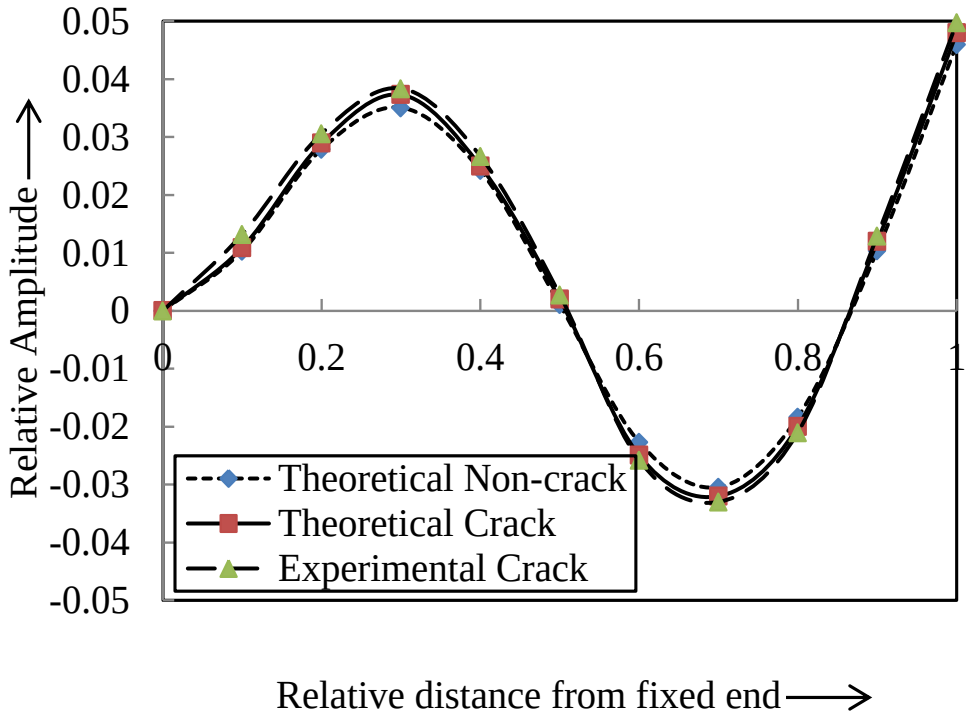

Figure 3.17c Relative Amplitude vs. Relative distance from fixed end (3rd mode of vibration) β_1=0.1875, β_2=0.4375, ψ_1=0.5 & ψ_2=0.416

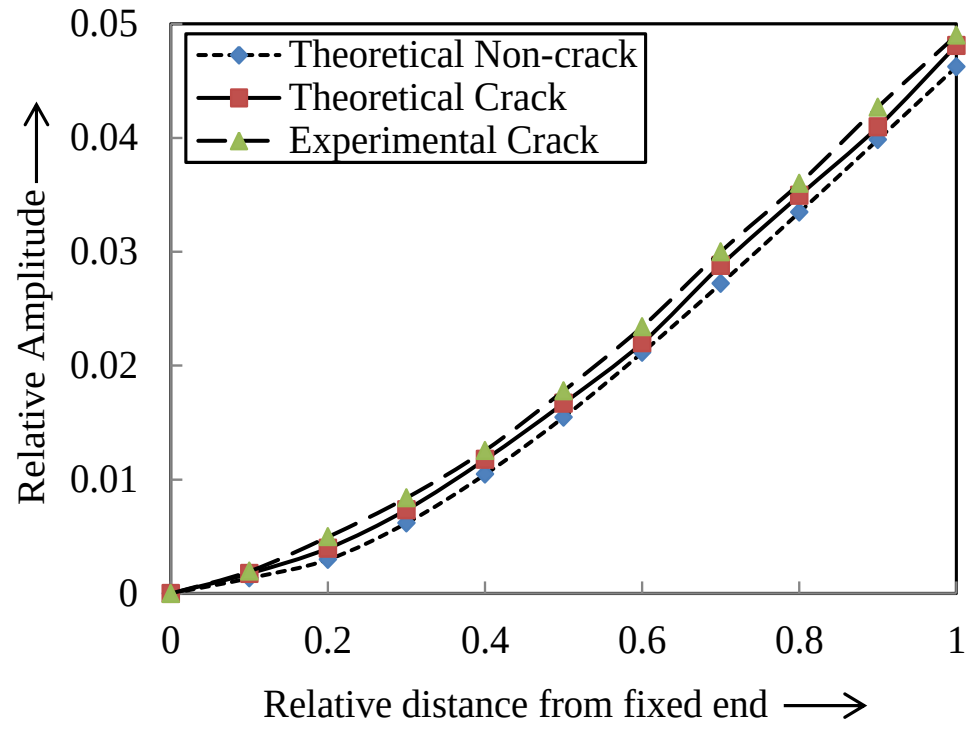

Figure 3.18a Relative Amplitude vs. Relative distance from fixed end (1st mode of vibration) β_1=0.3125, β_2=0.5525, ψ_1=0.333& ψ_2=0.25

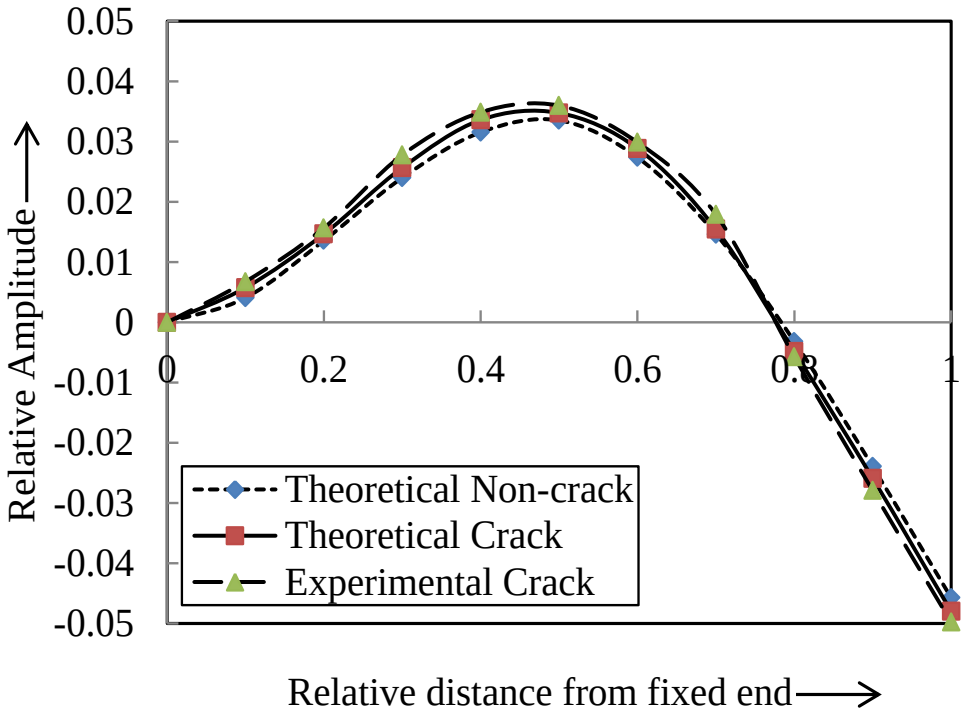

Figure 3.18b Relative Amplitude vs. Relative distance from fixed end (2nd mode of vibration) β_1=0.3125, β_2=0.5525, ψ_1=0.333& ψ_2=0.25

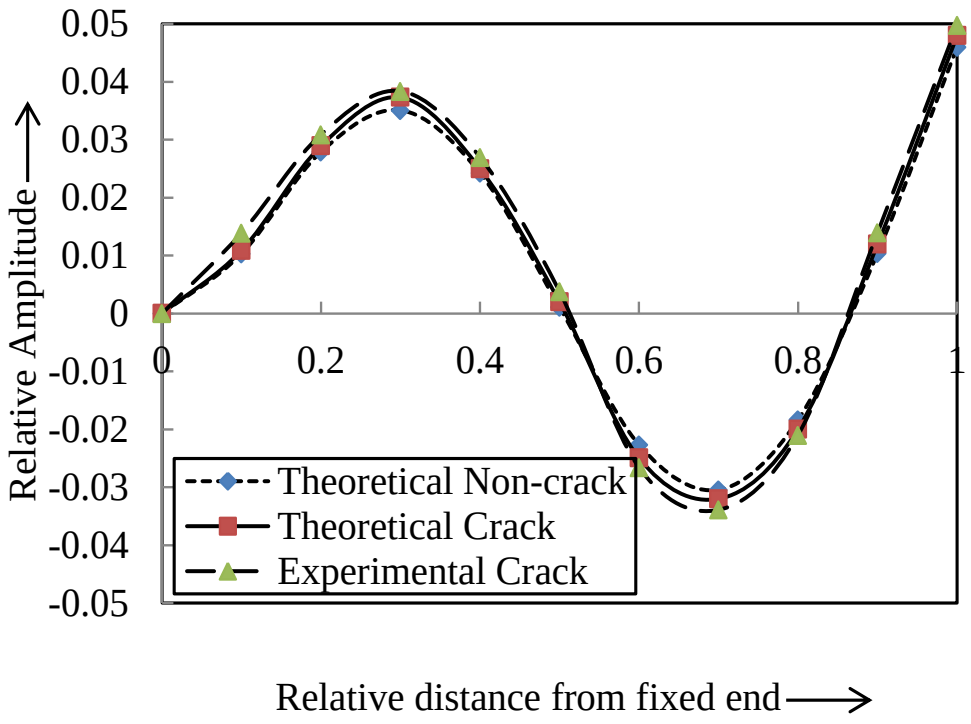

Figure 3.18c Relative Amplitude vs. Relative distance from fixed end (3rd mode of vibration) β_1=0.3125, β_2=0.5525, ψ_1=0.333& ψ_2=0.25

3.5 Comparison and validation of theoretical analysis results and experimental analysis results

The fidelity and performance of the theoretical model has been verified by experimental test, performed on the glass fibers reinforced epoxy composite and steel composite beam. The results of first three mode shapes obtained from theoretical and experimental analysis are compared for cracked composite beam in figures 3.12 to 3.14 and for cracked steel beam in figures 3.15 to 3.17. The theoretical analysis results and experimental investigation results are compared in this section, only ten results from the available data pool is represented in table 3.1 for composite beam and in table 3.2 for steel beam.

The relative natural frequency and relative mode shape difference used in the analysis can be defined as follows.

$$\text{Relative natural frequency} = \frac{(\text{Natural frequency of cracked beam})}{(\text{Natural frequency of noncracked beam})}$$

$$\text{Relative mode shape difference} = \frac{(\text{Amplitude of noncracked - Amplitude of cracked beam})}{(\text{Amplitude of noncracked beam})}$$

The first three relative natural frequencies are presented in the first three columns of tables 3.1 and 3.2 whereas relative mode shapes of first three mode of vibration are presented in the fourth, fifth and sixth columns of the tables. The relative first crack depth, relative first crack location, relative second crack depth and relative second crack location obtained from theoretical analysis are displayed in seventh, eighth, ninth and tenth column respectively. The relative first crack depth, relative first crack location, relative second crack depth and relative second crack location obtained from experimental test are displayed in eleventh, twelfth, thirteenth and fourteenth column of both tables respectively.

Table 3.1 Comparison of the results between Theoretical and Experimental analysis (composite)

Relative 1st natural frequency "rfnf"	Relative 2nd natural frequency "rsnf"	Relative 3rd natural frequency "rtnf"	Relative 1st mode shape difference "rfmd"	Relative 2nd mode shape difference "rsmd"	Relative 3rd mode shape difference "rtmd"	Experimental relative 1st crack location "rfcl" 1st crack depth "rfcd" 2nd crack location "rscl" 2nd crack depth "rscd"				Theoretical relative 1st crack location "rfcl" 1st crack depth "rfcd" 2nd crack location "rscl" 2nd crack depth "rscd"			
						rfcl	rfcd	rscl	rscd	rfcl	rfcd	rscl	rscd
0.99607	0.99700	0.99829	0.00013	0.00203	0.00240	0.1875	0.1667	0.4375	0.250	0.180	0.160	0.421	0.241
0.98098	0.99557	0.99892	0.00275	0.00456	0.01064	0.125	0.4167	0.8750	0.333	0.120	0.401	0.842	0.320
0.99651	0.99425	0.99796	0.00079	0.00264	0.00101	0.3125	0.1667	0.5000	0.250	0.301	0.160	0.481	0.241
0.99001	0.99318	0.98710	0.00145	0.00571	0.00508	0.250	0.4167	0.5625	0.1667	0.241	0.401	0.541	0.160
0.98809	0.98584	0.98255	0.00288	0.01210	0.01352	0.375	0.5000	0.750	0.250	0.361	0.481	0.722	0.241
0.99672	0.98724	0.99719	0.00176	0.00332	0.00594	0.4375	0.2500	0.5625	0.333	0.421	0.241	0.541	0.320
0.99788	0.97843	0.97519	0.00284	0.01222	0.02349	0.5625	0.333	0.6875	0.500	0.541	0.320	0.661	0.481
0.99874	0.99877	0.99628	0.00026	0.00475	0.01519	0.625	0.0833	0.875	0.4167	0.601	0.080	0.842	0.401
0.99114	0.99799	0.99803	0.00010	0.00166	0.00183	0.1875	0.250	0.3125	0.250	0.180	0.241	0.301	0.241
0.99701	0.98999	0.99803	0.00153	0.00464	0.00239	0.4375	0.333	0.5625	0.1667	0.421	0.320	0.541	0.160
Average percentage of deviation										3.82	3.83	3.78	3.77
Total percentage of deviation										3.80			

Table 3.2 Comparison of the results between Theoretical and Experimental analysis (Steel)

Relative 1st natural frequency "rfnf"	Relative 2nd natural frequency "rsnf"	Relative 3rd natural frequency "rtnf"	Relative 1st mode shape difference "rfmd"	Relative 2nd mode shape difference "rsmd"	Relative 3rd mode shape difference "rtmd"	Experimental relative 1st crack location "rfcl" 1st crack depth "rfcd" 2nd crack location "rscl" 2nd crack depth "rscd"				Theoretical relative 1st crack location "rfcl" 1st crack depth "rfcd" 2nd crack location "rscl" 2nd crack depth "rscd"			
						rfcl	rfcd	rscl	rscd	rfcl	rfcd	rscl	rscd
0.99939	0.99813	0.99978	0.00013	0.00106	0.00411	0.125	0.1667	0.250	0.3333	0.120	0.159	0.239	0.319
0.99980	0.99768	0.99664	0.00035	0.00108	0.00073	0.250	0.0833	0.500	0.1667	0.239	0.080	0.478	0.159
0.99952	0.97803	0.98418	0.00341	0.00134	0.02088	0.375	0.250	0.625	0.500	0.359	0.239	0.598	0.478
0.99889	0.99881	0.99932	0.00041	0.00224	0.00310	0.1875	0.3333	0.3125	0.1667	0.179	0.319	0.299	0.159
0.99906	0.98250	0.99800	0.00293	0.00965	0.00839	0.4375	0.500	0.6875	0.25	0.418	0.478	0.657	0.239
0.99958	0.99129	0.99869	0.00123	0.00187	0.00670	0.5625	0.3333	0.8125	0.0833	0.538	0.319	0.777	0.080
0.99971	0.98183	0.98589	0.00272	0.00638	0.00962	0.500	0.4167	0.75	0.500	0.478	0.398	0.717	0.478
0.99473	0.98761	0.98721	0.00239	0.00786	0.01099	0.3125	0.500	0.5625	0.3333	0.299	0.478	0.538	0.319
0.99230	0.99003	0.99182	0.00149	0.00455	0.00673	0.4375	0.250	0.6625	0.4167	0.418	0.239	0.633	0.398
0.99677	0.98931	0.99459	0.00152	0.00540	0.00865	0.625	0.4167	0.875	0.3333	0.598	0.398	0.837	0.319
Average percentage of deviation										4.35	4.37	3.38	4.36
Total percentage of deviation										4.4			

3.6 Discussion

This section is subjected to discussion on analysis of results derived in the theoretical and experimental evaluation. This chapter is divided in two categories; first part is theoretical analysis of cantilever beam then its experimental validation and second part is the theoretical analysis and its verification by experimental test for structural steel.

The nodal displacement of composite beam element and applied force on the beam element are shown in figures 3.1(a) and 3.1(b) respectively. The variation of first three natural frequencies with crack locations and depths are presented in figures 3.2(a)-3.2(c). Figures 3.3 to 3.5 represents noticeable deviation in first three consecutive mode shapes of cracked and intact composite beam and magnified view at the vicinity of first crack (figures 3.3(b), 3.4(b) & 3.5(b)) and second crack (figures 3.3(c), 3.4(c) & 3.5(c)). A sudden jump is observed in mode shape behavior at the crack position. It is the signal of noticeable change in mode shape behavior due to presence of crack in the structure. The significant variations in the mode shapes have been observed with increase in crack depth and are shown in figure 3.3(a) to 3.3(c).

Figures 3.6(a) and 3.6(b) represents multiple cracked cantilever beam of structural steel and cross-sectional view of cantilever beam respectively. It is observed that the dimensionless compliance constant increases with increase in the depth of crack due to reduction in stiffness at the crack location.

Similar to the composite structure, steel beam also depicted the variation in the mode shapes for cracked and intact beam and are displayed in the figures 3.9 to 3.11 and magnified view near the first and second crack position are shown in the figures 3.9(b), 3.10(b), 3.11(b), 3.9(c), 3.10(c) & 3.11(c). It is found that there is significant deviation in the mode shape due to presence of cracks. Figure 3.12 presents schematic block diagram of experiment setup. A comparison and verification of the results derived from theoretical model are plotted with results of experimental examination and are shown in the figures 3.13 to 3.15 (for composite) and figures 3.16 to 3.18 (for structural steel). The results derived from theoretical and experimental observation are displayed in tabular form with first three modal parameters (natural frequencies and mode shapes) and relative crack location and crack depth in the tables 3.1 and 3.2 for composite beam and steel bream respectively.

3.7 Summary

The conclusions are drawn in this section from the results derived from theoretical and experimental examination in this chapter. The modal parameters (natural frequencies and mode shapes) upset due to presence of crack in the structure. It can be seen in the magnified view at the crack locations. The vibration signatures derived from theoretical model have been verified with the results of experimental investigation and a close proximity is found between them for both composite and structural steel beam. The total percentage of deviation of the theoretical analysis is 3.8% for composite beam and 4.4% for structural steel. The deviation in the dynamic behavior of the structure can be used as the factor for diagnosis of the damage and dynamic characteristics can also be used for modelling the inverse method for identification of damage. The proposed method can be successfully applied for the design of smart artificial intelligent techniques for online measurement of the damage present in the structures. In the successive chapters various artificial intelligent based techniques have been discussed for identification of multiple cracks present in composite and steel beam.

CHAPTER 4

Finite Element Analysis of Multiple Cracked Cantilever Beam for Measurement of Dynamic Response

The presence of cracks in the rotor, shaft and structural components are serious risk to the integrity of system. This may cause of destruction and collapse of the structures. The detection of crack in early stage of the system is beneficial. In the last two decades many researchers and engineers have developed several methods and presented many models for prediction of crack, based on vibrational behaviors of damage structures. The vibration based methods are used for identification of damage; offer some advantages over other conventional methodologies. These methods can help to detect crack location and depth using vibrational data, obtained from cracked structure. The presence of crack in structures generates flexibility at the vicinity of crack which causes the reduction of natural frequencies and change in mode shapes. Hence it may be possible to detect crack location and intensity by measuring the change in vibration parameters. This chapter introduces finite element analysis for identification of multiple cracks present in the beam like structures. The results of finite element analysis have been compared with theoretical analysis and experimental analysis results to secure the robustness of proposed numerical method. Finally it is concluded that proposed finite element method can be successfully applied for multiple crack detection of structures.

4.1 Introduction

Automation of damage detection techniques in different engineering system can be termed as systematic approach to predict and quantify the damage present in the system. The concerned of the failure analysis of faulty beam structure is to secure the overall safety and performance of the system. The vibrational response of faulty structural members can be effectively used to seize the damage feature such as crack location and crack depth. The researchers have been proposed various damage detection methods based on thermal radiation, energy, discreet wavelet and numerical methods such as artificial intelligent and finite element methods. In the past few decades scientists have

developed a model for single crack structure based on the finite element method and found that the performance of finite element method is better as compared to the theoretical model designed for crack diagnosis. So this method can be used to diagnose the crack parameters such as crack location and crack depth of the system using modal response of the system.

In the present section finite element method has been used to find crack locations and depths for multiple cracked composite and structural steel beams. It is found that the presence of cracks on the beam structure potentially affect the dynamic behavior of the beam. The finite element results have been compared to that of theoretical and experimental analysis results and a close proximity between the results is found.

4.2 Analysis of finite element method

The finite element method is a powerful finite element method that can be used to solve complex problem using interpolation or approximation method. The finite element method is a systematic approach for solving the complicated problems. So the finite element method can be applied in vibrating structures with different boundary conditions to get approximate solution. In the finite element analysis, whole structure is first divided in small parts in various shapes. These small parts known as elements and procedure employed to divide the structures in small parts is called discretization and generation of the regular shape pattern in the structure is called meshing. The efficiency of finite element method is dependent on the quality of the mesh. Each element of finite element model has corner points that connect to another element called nodes. Each finite element associated with equation of motion and that can be easily interpolated. The solutions of each finite element are combined together to get global mass and stiffness matrices, which describes the vibration response of the structure. The global mass and stiffness matrices can be analyzed to get vibrational parameters of the structure.

The finite element analysis of cantilever beam has been done using ANSYS software. ANSYS is commercially available finite element analysis software with capacity of solving wide range of complex problems. The application of ANSYS is spread over many fields of engineering and technology such as structural, thermal, mechanical, electromagnetic and computational fluid dynamics. The modelling and simulation of composite and steel cantilever beam has been done in ANSYS using multi-physics

platform. The first three natural frequencies and relevant mode shapes have been extracted from block lanczos, mode extraction method [159].

The following steps are involved in order to solve the any problem using finite element software.

(1) Preprocessing Phase: This section of the ANSYS involves the selection of type of the element with respect to problem types. The ANSYS also provides the CAD modelling facility. Meshing process is the most important feature of FE analysis, which is generated in this section using mapped meshing feature of the ANSYS.

(2) Solution Phase: Applying the boundary conditions and load on the structural component are the most significant feature of this section. ANSYS then attempts to solve the equation of motion of the system element. The selection of mode extraction method is also very important parameter of this solution phase. The block lanczos, mode extraction method is taken in the present investigation.

(3) Post processing phase: This section allows the review of the results. The post processing is most significant tool for viewing the results after the solution phase. These results may be in form of color contour plot and graphical representation of the stress, thermal, buckling, electromagnetic, vibration and computation fluid dynamics analysis etc.

4.3 Finite element analysis of composite beam

The finite element analysis software ANSYS is powerful numerical technique for extraction of vibration response of cracked and non-cracked composite beam. The additional flexibility is generates at the vicinity of the crack. This flexibility changes the dynamic of cracked composite beam. The change in the vibration response between cracked and non-cracked structure has been observed in terms of natural frequencies and mode shapes.

The numerical analysis for glass fiber reinforced epoxy composite has been done using ANSYS finite element analysis software package. The finite element model of cracked composite beam model, Meshing at the crack tip, Layer stacking of composite beam and ANSYS generated mode shape models has been shown in appendix A.

4.3.1 Selection and description of element in the analysis

The modelling and the simulation of composite beam are done in ANSYS platform. The selection of element is significant approach in ANSYS. In the current investigation 3D

Solid shell190 (SOLSH 190) element is taken in the analysis. The SOLSH 190 element is allowed to create crack at any extent in laminated structures. The SOLSH 190 is mostly used for layered structural application such as construction of sandwich and laminated shell with a wide range of thickness. This element has eight nodes and each node has three degree of freedom (Translation in X, Y and Z direction) and total twenty four degree of freedom of the each element. The geometrical configuration of SOLSH 190 is shown figure 4.1[159].

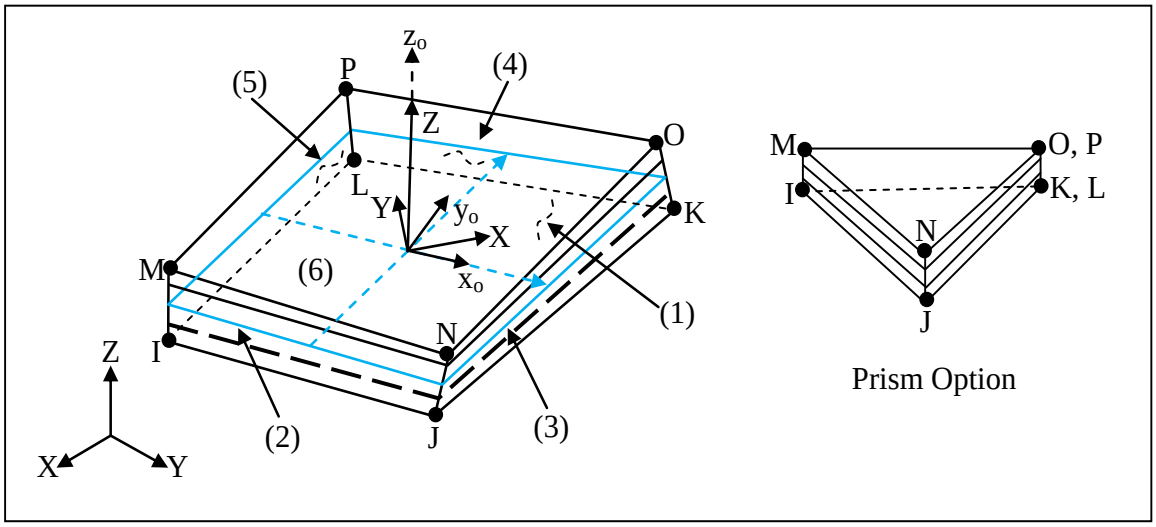

Figure 4.1 Geometrical configuration of SOLSH 190

4.3.2 The properties of material and selection of the crack orientation

The different sets of orientation of the cracks (in term of location and depth) are taken for composite and structural steel and are in the following patterns:

The relative crack locations (β_1,β_2) for composite beam are (0.182,0.424); (0.121,0.848); (0.303,0.485);(0.242,0.545); (0.363,0.727); (0.424,0.545); (0.545,0.666); (0.606,0.848); (0.182,0.303); (0.424,0.545).

The relative crack locations (β_1 ,β_2) for steel beam are (0.121,0.241); (0.241,0.483); (0.362,0.603); (0.181,0.302);(0.422,0.663); (0.543,0.784); (0.483,0.724); (0.302,0.543); (0.422,0.639); (0.603,0.844).

1st relative crack depth ($\psi_1=a_1/H$) taken between 0.0833 to 0.5 at step size of 0.0833

2nd relative crack depth ($\psi_2=a_2/H$) taken between 0.0833 to 0.5 at step size of 0.0833

The following dimensions of the beam are used in the current section: Length of the Beam (L) = 800mm; Width of the beam (W) = 50mm; Thickness of the Beam (H) = 6mm

The individual material properties of the fiber (glass) and matrix (epoxy) are depicted in table 4.1.

Table 4.1 Material properties of Glass fiber- reinforced epoxy composite

	Fiber (Glass)	Matrix (Epoxy)
Elastic Modulus (Gpa)	$E_f = 72.4$	$E_m = 3.45$
Rigidity Modulus (Gpa)	$G_f = 29.67$	$G_m = 1.277$
Poisson's Ratio	$\upsilon_f = 0.22$	$\upsilon_m = 0.35$
Mass Density (gm-cm^{-3})	$\rho_f = 2.6$	$\rho_m = 1.2$

The results of finite element analysis for first three mode shape of cracked composite beam are displayed with that of theoretical and experimental results for authentication of finite element analysis are shown in figures 4.2(a) to 4.2(c) and table 4.1 represents a comprehensive comparison of results of all proposed theoretical, numerical and experimental analysis.

4.3.3 Mesh convergence study

The mesh convergence testing is very significant parameter of finite element analysis. This begins with a mesh discretization and then comparison of successive results within threshold difference value between the previous results. Now repeat the problem with a finer mesh (i.e. more elements) and then compare the results with the previous test. If the results are nearly similar (approx. less than 5%), then the first mesh is probably good enough for that particular geometry, loading and constraints. If the results differ by a large amount then, it will be necessary to try a finer mesh yet. If there is no significant change in results observed, when the mesh size 2×2, then the current mesh size is taken into account. Similarly mesh convergence study has been opted for structural steel beam. The mesh convergence testing results for composite beam is shown in table 4.2.

Table 4.2 Mesh convergence study for composite beam

S. No.	Mesh Size	Natural Frequency (Hz)			Amplitude (mm)		
		I	II	III	I	II	III
1	16×16	7.602	47.597	131.854	132.860	132.813	132.755
2	8×8	6.940	43.452	120.370	121.289	121.246	121.193
3	4×4	6.404	40.099	111.084	111.931	111.892	111.843
4	2×2	6.105	38.226	105.895	106.703	106.665	106.619

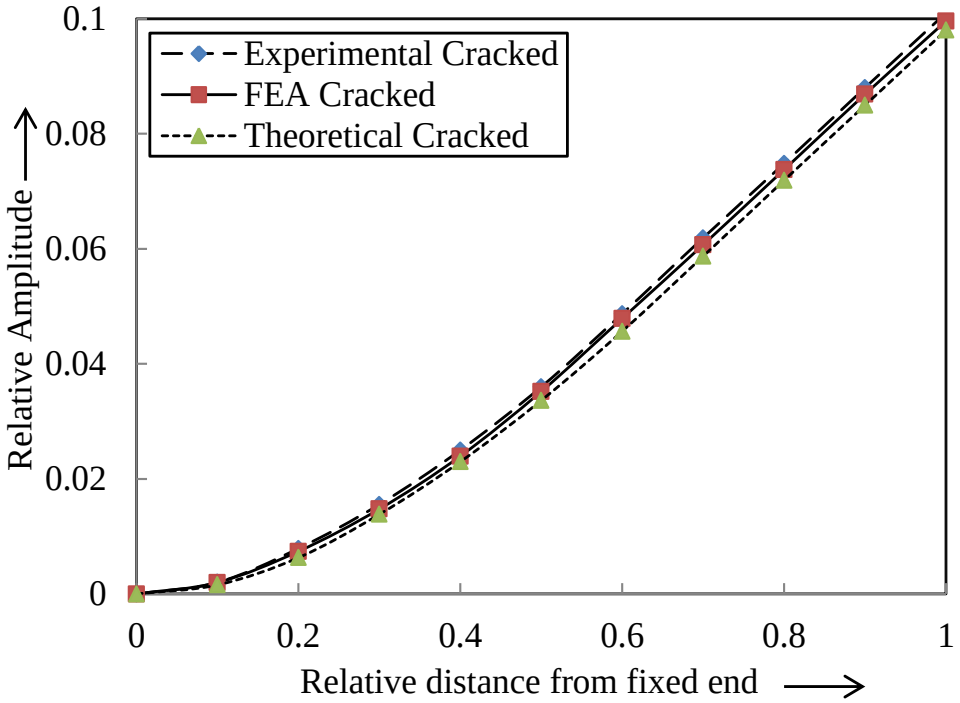

Figure 4.2(a) Relative Amplitude vs. Relative distance from fixed end (1st mode of vibration) β_1=0.25, β_2=0.5, ψ_1=0.1667 & ψ_2=0.5

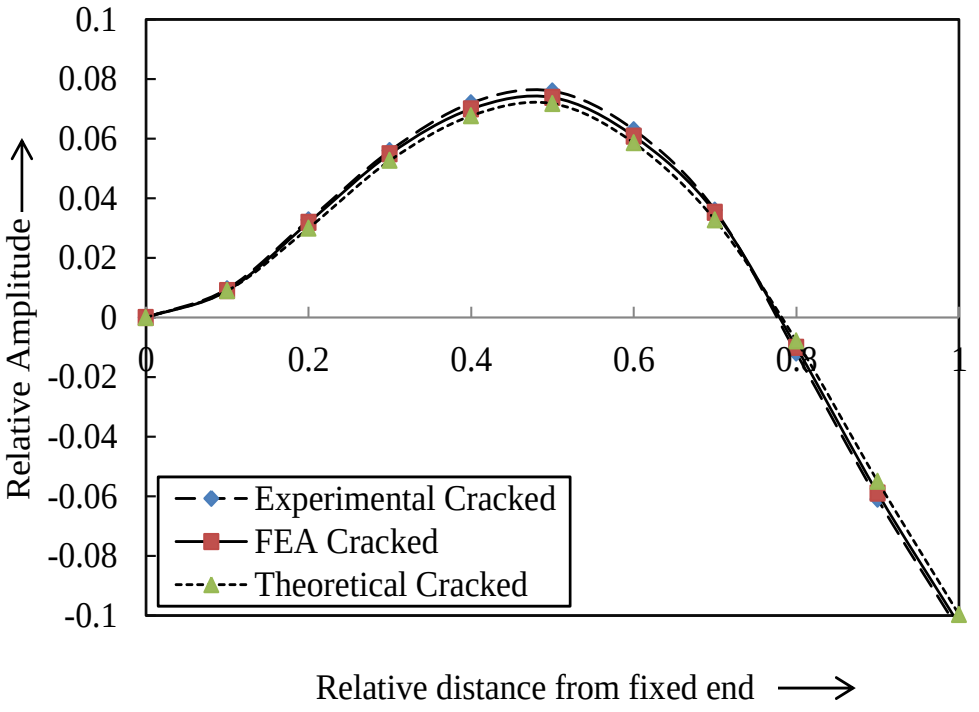

Figure 4.2(b) Relative Amplitude vs. Relative distance from fixed end (2nd mode of vibration) β_1=0.25, β_2=0.5, ψ_1=0.1667 & ψ_2=0.5

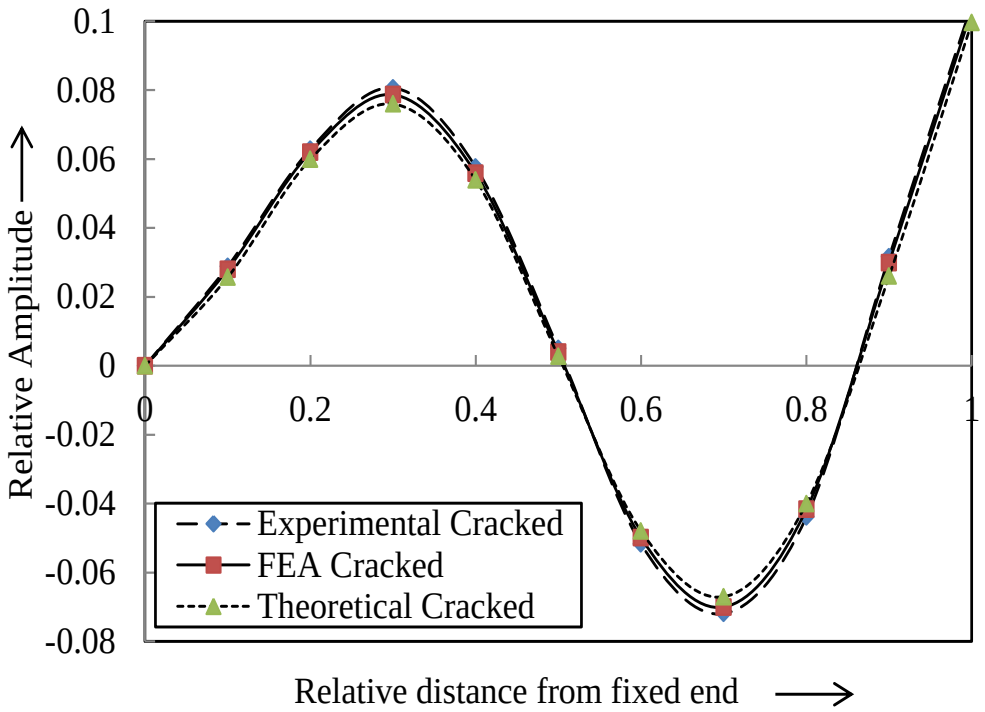

Figure 4.2(c) Relative Amplitude vs. Relative distance from fixed end (3rd mode of vibration) β_1=0.25, β_2=0.5, ψ_1=0.1667 & ψ_2=0.5

4.4 Finite element analysis of steel beam

The finite element analysis is performed for studying the modal response of a dynamic beam structure. The natural frequencies and mode shapes are the most important parameters in designing a structure under the dynamic and complex loading conditions. The finite element analysis is performed by using the ANSYS software in the frequency domain to find change in behaviours of vibration parameters. The presence of damage in the form of crack alters the vibration indices. The change in behaviour of vibration characteristics can be applied to develop the structural health monitoring techniques.

4.4.1 Selection and description of element in the analysis

The selection of the elements is significant in the ANSYS. A higher order 3-D, 8-node element (Specified as SOLID185 in ANSYS) with three degrees of freedom at each node: translations in the nodal x, y, and z directions are selected and used throughout the analysis. The SOLID185 can be used in 3-D modeling of solid structures. The SOLID185 has plasticity, hyper elasticity, stress stiffening, creep, large deflection, and large strain capabilities. It also has mixed formulation capability for simulating deformations of

nearly incompressible elastic plastic materials, and fully incompressible hyperplastic materials. The geometry and node locations of element are shown in figure 4.3 [157].

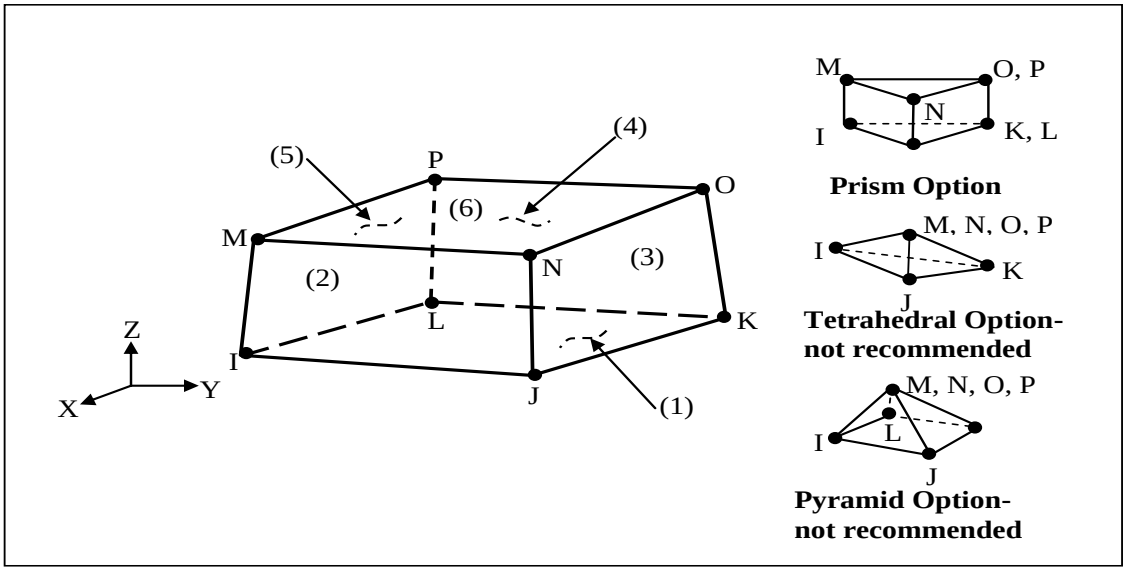

Figure 4.3 Geometry of SOLID185 element

4.4.2 The material properties and dimensions of beam

The following dimensions of the beam are used in the current section:

Length of the Beam (L) = 800mm; Width of the beam (W) = 50mm; Thickness of the Beam (H) = 6mm

The material properties of the structural steel used in the analysis are shown in the table 4.3

Table 4.3 Material properties of structural steel

Young's Modulus (E)	200Gpa
Poission ratio's (ν)	0.3
Density (ρ)	7850 kg/m^3

The first three mode shapes for cracked beam derived from finite element based finite element analysis are plotted along with theoretical and experimental analysis results of cracked steel beam and the orientation of cracks (β_1=0.25, β_2=0.5, ψ_1=0.1667 and ψ_2=0.5) is shown in the figure 4.4a-4.4c.

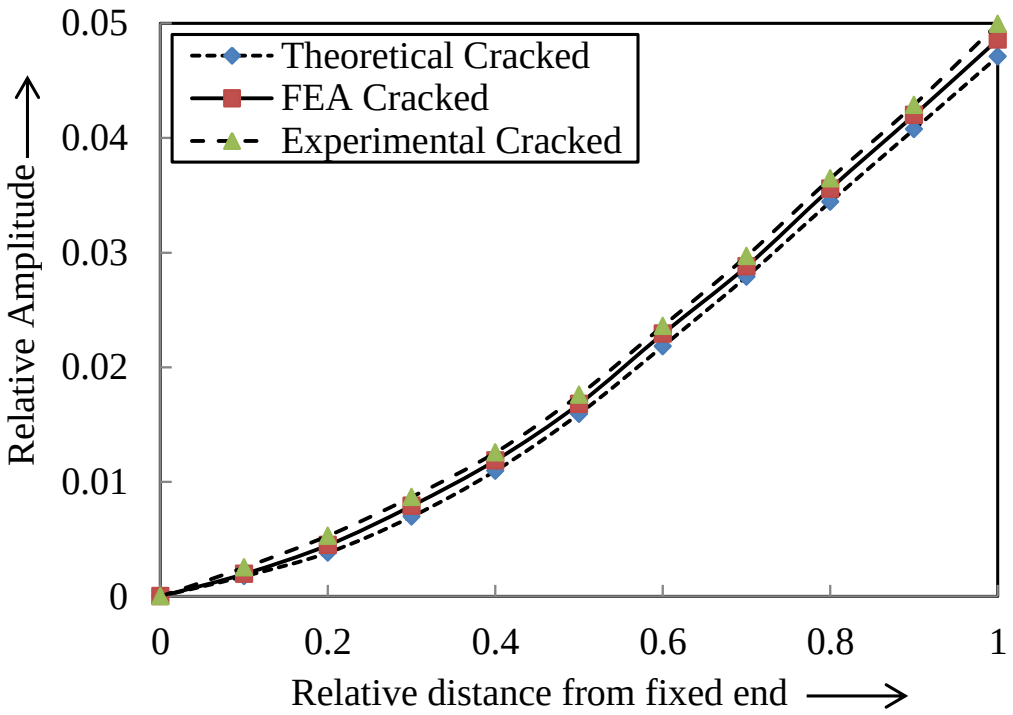

Figure 4.4a Relative Amplitude vs. Relative distance from fixed end (1st mode of vibration) β_1=0.25, β_2=0.5, ψ_1=0.1667 & ψ_2=0.5

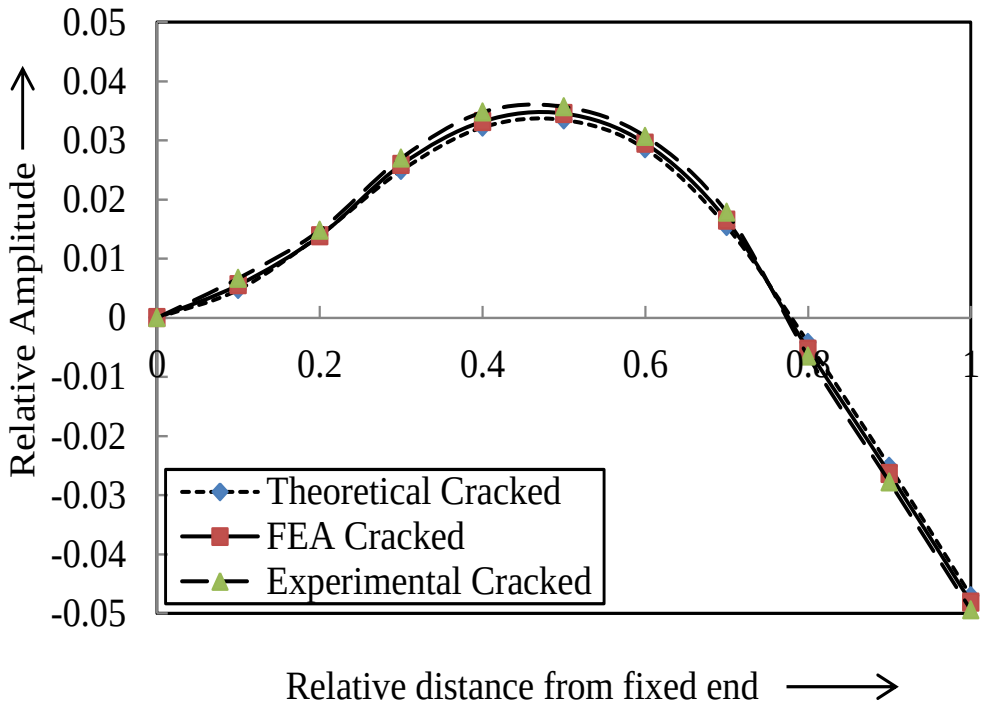

Figure 4.4b Relative Amplitude vs. Relative distance from fixed end (2nd mode of vibration) β_1=0.25, β_2=0.5, ψ_1=0.1667 & ψ_2=0.5

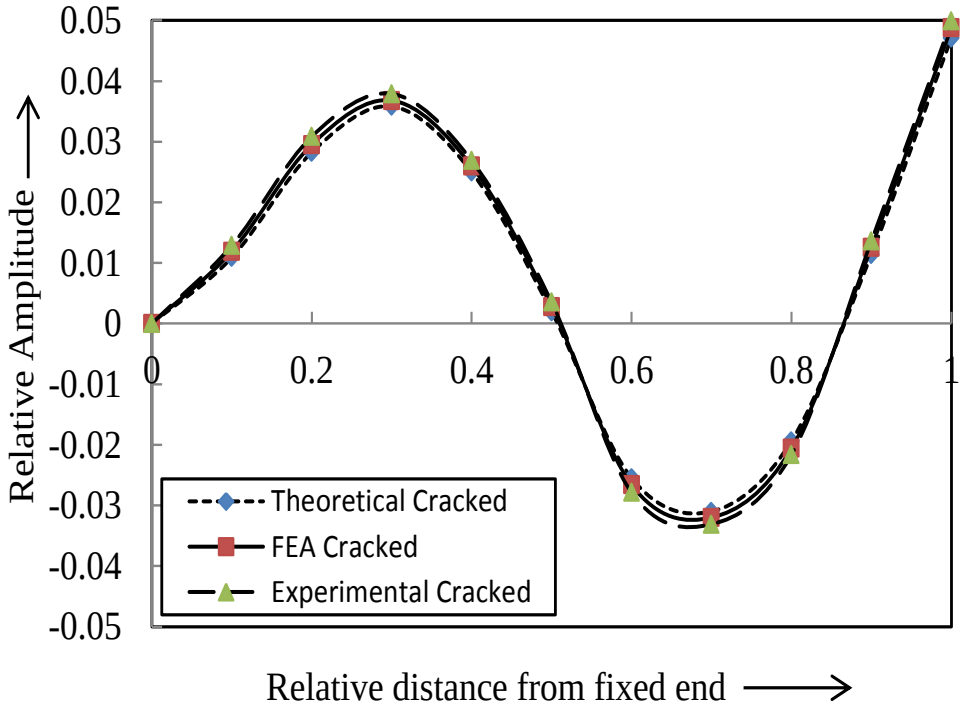

Figure 4.4c Relative Amplitude vs. Relative distance from fixed end (3rd mode of vibration) β_1=0.25, β_2=0.5, ψ_1=0.1667 & ψ_2=0.5

Table 4.4 Comparison of the results among Theoretical, FEA and Experimental analysis (Composite beam)

Relative 1st natural frequency "rfnf"	Relative 2nd natural frequency "rsnf"	Relative 3rd natural frequency "rtnf"	Relative 1st mode shape difference "rfmd"	Relative 2nd mode shape difference "rsmd"	Relative 3rd mode shape difference "rtmd"	Experimental relative 1st crack location "rfcl" 1st crack depth "rfcd" 2nd crack location "rscl" 2nd crack depth "rscd"				FEA relative 1st crack location "rfcl" 1st crack depth "rfcd" 2nd crack location "rscl" 2nd crack depth "rscd"				Theoretical relative 1st crack location "rfcl" 1st crack depth "rfcd" 2nd crack location "rscl" 2nd crack depth "rscd"			
						rfcl	rfcd	rscl	rscd	rfcl	rfcd	rscl	rscd	rfcl	rfcd	rscl	rscd
0.99607	0.99700	0.99829	0.00013	0.00203	0.00240	0.1875	0.1667	0.4375	0.250	0.182	0.162	0.424	0.242	0.180	0.160	0.421	0.241
0.98098	0.99557	0.99892	0.00275	0.00456	0.01064	0.125	0.4167	0.8750	0.333	0.121	0.404	0.848	0.323	0.120	0.401	0.842	0.320
0.99651	0.99425	0.99796	0.00079	0.00264	0.00101	0.3125	0.1667	0.5000	0.250	0.303	0.162	0.485	0.242	0.301	0.160	0.481	0.241
0.99001	0.99318	0.98710	0.00145	0.00571	0.00508	0.250	0.4167	0.5625	0.1667	0.242	0.404	0.545	0.162	0.241	0.401	0.541	0.160
0.98809	0.98584	0.98255	0.00288	0.01210	0.01352	0.375	0.5000	0.750	0.250	0.363	0.485	0.727	0.242	0.361	0.481	0.722	0.241
0.99672	0.98724	0.99719	0.00176	0.00332	0.00594	0.4375	0.2500	0.5625	0.333	0.424	0.242	0.545	0.323	0.421	0.241	0.541	0.320
0.99788	0.97843	0.97519	0.00284	0.01222	0.02349	0.5625	0.333	0.6875	0.500	0.545	0.323	0.666	0.485	0.541	0.320	0.661	0.481
0.99874	0.99877	0.99628	0.00026	0.00475	0.01519	0.625	0.0833	0.875	0.4167	0.606	0.081	0.848	0.404	0.601	0.080	0.842	0.401
0.99114	0.99799	0.99803	0.00010	0.00166	0.00183	0.1875	0.250	0.3125	0.250	0.182	0.242	0.303	0.242	0.180	0.241	0.301	0.241
0.99701	0.98999	0.99803	0.00153	0.00464	0.00239	0.4375	0.333	0.5625	0.1667	0.424	0.323	0.545	0.162	0.421	0.320	0.541	0.160
Average percentage of deviation										3.08	2.99	3.06	3.05	3.82	3.83	3.78	3.77
Total percentage of deviation										3.10				3.80			

Table 4.5 Comparison of the results among Theoretical, FEA and Experimental analysis (Steel beam)

Relative 1st natural frequency "rfnf"	Relative 2nd natural frequency "rsnf"	Relative 3rd natural frequency "rtnf"	Relative 1st mode shape difference "rfmd"	Relative 2nd mode shape difference "rsmd"	Relative 3rd mode shape difference "rtmd"	Experimental relative 1st crack location "rfcl" 1st crack depth "rfcd" 2nd crack location "rscl" 2nd crack depth "rscd"				FEA relative 1st crack location "rfcl" 1st crack depth "rfcd" 2nd crack location "rscl" 2nd crack depth "rscd"				Theoretical relative 1st crack location "rfcl" 1st crack depth "rfcd" 2nd crack location "rscl" 2nd crack depth "rscd"			
						rfcl	rfcd	rscl	rscd	rfcl	rfcd	rscl	rscd	rfcl	rfcd	rscl	rscd
0.99939	0.99813	0.99978	0.00013	0.00106	0.00411	0.125	0.1667	0.250	0.3333	0.121	0.161	0.241	0.322	0.120	0.159	0.239	0.319
0.99980	0.99768	0.99664	0.00035	0.00108	0.00073	0.250	0.0833	0.500	0.1667	0.241	0.080	0.483	0.161	0.239	0.080	0.478	0.159
0.99952	0.97803	0.98418	0.00341	0.00134	0.02088	0.375	0.250	0.625	0.500	0.362	0.241	0.603	0.483	0.359	0.239	0.598	0.478
0.99889	0.99881	0.99932	0.00041	0.00224	0.00310	0.1875	0.3333	0.3125	0.1667	0.181	0.322	0.302	0.161	0.179	0.319	0.299	0.159
0.99906	0.98250	0.99800	0.00293	0.00965	0.00839	0.4375	0.500	0.6875	0.25	0.422	0.483	0.663	0.241	0.418	0.478	0.657	0.239
0.99958	0.99129	0.99869	0.00123	0.00187	0.00670	0.5625	0.3333	0.8125	0.0833	0.543	0.322	0.784	0.080	0.538	0.319	0.777	0.080
0.99971	0.98183	0.98589	0.00272	0.00638	0.00962	0.500	0.4167	0.75	0.500	0.483	0.402	0.724	0.483	0.478	0.398	0.717	0.478
0.99473	0.98761	0.98721	0.00239	0.00786	0.01099	0.3125	0.500	0.5625	0.3333	0.302	0.483	0.543	0.322	0.299	0.478	0.538	0.319
0.99230	0.99003	0.99182	0.00149	0.00455	0.00673	0.4375	0.250	0.6625	0.4167	0.422	0.241	0.639	0.402	0.418	0.239	0.633	0.398
0.99677	0.98931	0.99459	0.00152	0.00540	0.00865	0.625	0.4167	0.875	0.3333	0.603	0.402	0.844	0.322	0.598	0.398	0.837	0.319
Average percentage of deviation										3.76	3.52	3.51	3.49	4.35	4.37	3.38	4.36
Total percentage of deviation										3.50				4.4			

4.5 Discussion

The brief discussion on the outcome of proposed finite element method has been presented in this section.

It is noticed that presence of damage in the form of crack in the structure alters the vibration response. It can be seen in the magnified view of mode shapes at the crack location. The various step involved in the ANSYS to solve any problem are discussed. These steps are: preprocessing phase, solution phase and post processing phase. The selection of the element is very important to get the most refined results from the ANSYS. The SOLSH190 element is chosen for composite beam. The geometrical configuration of SOLSH190 is shown in the figure 4.1. Similarly SOLID185 has been selected for structural steel. The geometry of element and nodal position is shown in figure 4.3. The individual material properties of composite constituent and material properties of structural steel are presented in tables 4.1 and 4.3 respectively. The mesh convergence testing is presented in table 4.2. The results derived from finite element method are authenticated by results obtained from experimental test for composite structure as well as for structural steel beam. The results for first three consecutive mode shapes obtained from finite element analysis are plotted with corresponding mode shapes derived from theoretical and experimental diagnosis for cracked composite and are shown in figures 4.2(a)-4.2(c). Similarly graphs are plotted for structural steel has been shown in figures 4.4(a)-4.4(c). The results for relative first crack depth and crack position and relative second crack depth and crack position are derived from theoretical, FEA and experimental examination corresponding to relative 1^{st}, 2^{nd} & 3^{rd} natural frequencies and mode shapes are presented in table 4.4 and 4.5 for composite and steel beam respectively. It is observed that results are in good agreement.

4.6 Summary

The conclusions are drawn in this section from the results derived from numerical method. The simple, effective and robust finite element method is presented to analyze the multiple cracks in the composite and structural steel beam. It is observed that the modal response obtained from finite element analysis show the deviation between cracked and intact beam model. This can be observed in figures B1 (a) and B1(c).

The modal response such as first three consecutive mode shapes and natural frequencies are derived from finite element method and found to be of close proximity with results obtained from theoretical and experimental observations as shown in figure 4.2-4.4. The total percentage of deviation of finite element analysis is 3.10% for composite beam and 3.50% for structural steel. The dynamic response derived from finite element analysis can be utilized to design and develop the fault diagnosis and condition monitoring techniques based on artificial intelligent techniques such as fuzzy logic and various types of neural networks. The data obtained from FEA are subsequently used in hybrid fuzzy-neural techniques as training patterns for prediction of crack locations and depths. The artificial intelligent techniques based structural health monitoring algorithms have been discussed in the upcoming chapters.

CHAPTER 5

Study of Fuzzy System for Identification of Multiple Cracks of Cantilever Beam

The presence of damage is a grave threat to the integrity of the system, which leads to reduce the life and may cause the failure of the system. Hence, it is needed to develop the online automated method to predict the damage effectively, present in the engineering system. It is well-established fact that the presence of crack in the system upset the vibration parameters (e.g. Change the natural frequencies and mode shapes). So these changes can be effectively used to locate damage severity and intensity. On the ground of these modifications in vibration parameters, automated AI techniques can be used to detect the crack locations and crack depths to avoid the catastrophic failure of engineering systems.

In the current chapter, fuzzy logic system has been applied to forecast the structural damage in the form of crack.

5.1 Introduction

Fuzzy Logic System (FLS) was first developed by Mamdani and Assilan around 1975 [160], although L A Zadeh [161] has presented the concept of fuzzy set in 1965. Essentially, Fuzzy Logic (FL) is a multi-value logic, which permits interval qualities to be characterized by linguistic expressions like yes/no, high/low, true/false. In the most recent couple of decades, specialists is utilized the FL approach for applications, such as feature extraction, identification and classification of geometrical properties and so on. FLS can mimic the human conduct by taking the distinctive thinking modes keeping in mind the end goal to make the computer system act like humans. The investigation of the imprecision and vulnerability underlies the exceptional human capacity to comprehend different engineering applications. FL can determine mapping principles regarding words instead of numbers. Another essential idea in FLS is the fuzzy if–then rule which is for the most part utilized as a part of the advancement of the fuzzy rule-based system. FLS can show nonlinear capacities of self-assertive many-sided quality to a desired level of precision. FLS is an advantageous approach to guide a data space to output space and is

one of the apparatuses used to model multi-inputs, multi-outputs systems. Henceforth the fuzzy methodology can be adequately utilized as a crack diagnostics tool for multiple cracked systems.

In the current section, the Fuzzy Logic Controller (FLC) has been used for multiple cracks of a beam of composite and steel material. The FLC has been modeled with six input variables such as relative first three consecutive natural frequencies and relative first three consecutive mode shape difference. Moreover, four output variables such as relative first and second crack location, relative first and second crack depth are taken for diagnosis of multiple cracks. Various fuzzy linguistic terms and fuzzy membership functions such as Triangular, Trapezoidal and Gaussian have been utilized to build up the proposed multiple cracks recognition technique. The rule base is designed for FLC with the help of vibration response and which is obtained from the numerical analysis. The robustness of FLC for diagnosis of multiple cracks has been compared with theoretical, numerical and experimental analysis results. It is observed that the proposed fuzzy model can be successfully applied for the diagnosis of the structural damage.

5.2 Overview of Fuzzy logic system

The fuzzy logic technique is a popular computing system based on the concept of fuzzy set theory, fuzzy reasoning, and fuzzy if-then rules. The application of fuzzy logic is found successfully in wide variety of fields such as bioinformatics, pattern recognition, business, data classification, automatic control, decision analysis, robotics, expert systems and time series prediction. A fuzzy logic controller primarily takes a decision by nonlinear mapping of the input information in a scalar output, using fuzzy rules. The mapping could be possible through fuzzy if–then rules, input/output membership function, a total of output sets, and de-fuzzification. An FLC can be taken as a congregation of autonomous multi-data, single-output network. The FLC mainly contains four parts: the fuzzifier, inference engine, rules base, and de-fuzzifier. The rule base of the FLC can be created using the numeric information. Once the fuzzy rules are developed, FLC becomes a system that gives output data, after processing the input data using fuzzy rules and fuzzy linguistic expressions. The fuzzifier takes data values and checks the level of relationship with each of the fuzzy sets through the membership functions. The FLC changes crisp inputs into crisp outputs. The fuzzy logic system consists of five stages to complete the operation. These are as follows;

Stage 1: Feed input data to FLS

The input data is fed to FLS. The fuzzy system distinguishes the degree of association of input variables using fuzzy rule database and membership functions. That is called fuzzification of input data.

Stage 2: Functions of Fuzzy Operator

The fuzzy system measures the degree of association of each fuzzified input data that satisfies for each rule of the fuzzy rule base. If the rule exists between more than one membership functions, the fuzzy operator gets a single value of the rule.

Stage 3: Apply the algorithm for generation of rules

The fuzzy membership function is reshaped through an algorithm, which is a parameter of a fuzzy set. A function is associated for reshaping the output, related to the forerunner.

Stage 4: Clustering the results

Each rule of the fuzzy database produces a result that is integrated to get a decision from fuzzy logic system. The clustering of each rule base results leads to an aggregated fuzzy set as output.

Stage 5: Defuzzification

In the defuzzification layer of FL system a method like a centre of gravity, mean of maxima and weighted average is applied in order to convert the fuzzified value to crisp value.

5.2.1 Selection of fuzzy membership function

The fuzzy membership function plays a significant role in the modeling of the fuzzy logic controller. The fuzzy membership function describes the fuzzy set and provides a measure of the degree of similarity or inaccurate dependencies of an element to a fuzzy set also. The Triangular, Gaussian, Trapezoidal, Bell-shaped, etc. are the membership functions mostly used in the fuzzy logic analysis, but any other type of membership functions can also be used. The fuzzy set elements with a non-zero degree of membership recognized as support are know as the core of the fuzzy set. The membership functions are usually called μF (x) is shown in the following figures. Where μ is the degree of the weight of the element x in the fuzzy set F., The height or size of the membership function is typically referred to zero to one. Therefore, each component of the fuzzy set fit with a

degree in the range of [0, 1]. The following three types of membership function selected in the present analysis are address below.

(1) Triangular membership function

The Triangular membership function is shown in figure 5.1 (a). The Triangular membership function $\mu_F(x)$ has three vertices 'a', 'b' and 'c' of the fuzzy set 'F'. The degree of membership is equivalent to zero at point 'a' & 'c' and degree of membership is equal to one at point 'b'. The mathematical exemplification of the fuzzy triangular membership function $\mu_F(x)$ can be described below.

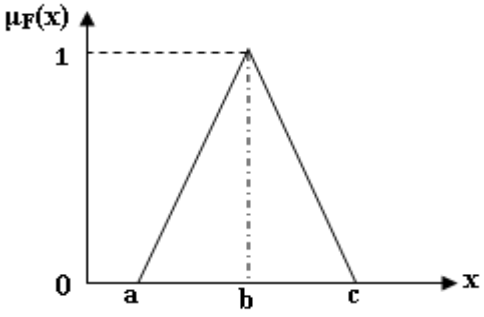

$$\mu_F(x) = \begin{cases} 0 \text{ if } x \le a \\ (x- a) / (b- a) \text{ if } a \le x \le b \\ (a- x) / (a- b) \text{ if } b \le x \le e \\ 0 \text{ if } x \ge a \end{cases}$$

Figure 5.1(a) Triangular membership function

(2) Gaussian membership function

The fuzzy Gaussian membership function is shown in figure 5.1 (b). The mathematical exemplification of the fuzzy Gaussian membership function can be described as below.

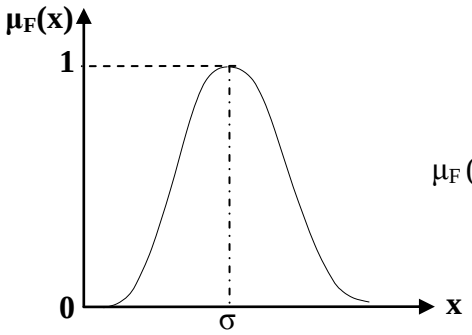

$$\mu_F(x, \sigma, w, n) = \text{Exp}\left[-0.5\{(x - \sigma)/w\}^n\right]$$

Figure 5.1(b), Gaussian membership function

Where σ = center; w= width; n=fuzzification factor

(3) Trapezoidal membership function

The fuzzy trapezoidal membership function is shown in figure 5.1 (c). The trapezoidal membership function has two base points (a, b) and two shoulder points (c, d). A mathematical expression of the trapezoidal membership function is described as follow.

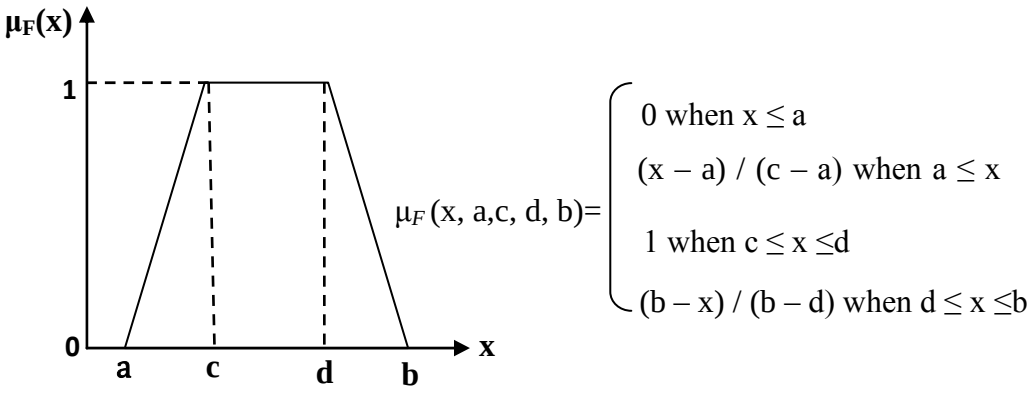

Figure 5.1(c) Trapezoidal membership function

5.2.2 Development of the fuzzy logic model using fuzzy rules

The input and output variables intricately depend on working domain of any real complex problem, so the optimization of input and output data is necessary for better solution of complex systems. Sometimes approximation of input and output variables of a complex application is preferable, rather than going through an elaborate process, which get more time to solve the same problem. The approximation of the input and output parameters in the fuzzy system has been performed using membership functions and fuzzy rules. The fuzzy membership functions are significant parameters of the fuzzy system, which are designed by suitable fuzzy linguistic terms and fuzzy rules. The conditional statements and fuzzy rules have been used for fuzzification of the input variables and defuzzification of the output variables. The conditional statements like fuzzy intersection, union and complement have been used to develop the membership functions of the fuzzy system. Hence, the fuzzy model takes the input variables from the working domain to an absolute state of condition and using the rules, it will provide an organized action as preferred by the system. A general model of a fuzzy controller has been shown in figure 5.2.

5.2.3 Analysis of defuzzification mechanism

The conversion of fuzzy outputs into crisp output in the fuzzy system is called defuzzification. Before an output is de-fuzzified, all the fuzzy outputs of the system are aggregated with conditional operator and de-fuzzifier gives the single crisp value. The selection of the defuzzification method depends on the structures of work domain. The relationship between the fuzzy output set (F_s), de-fuzzifier and crisp production (C_0) can be written in form of following equation:

C_0 = defuzzifier (F_s) (5.1)

There are some defuzzification methods available for development the fuzzy logic system, few of them are;

(1) Centroid of the area, (2) Mean of maximum

(3) Height method, (3) Weighted average method

5.3 Study of fuzzy logic system for detection of cracks

In the current analysis Triangular, Gaussian, and Trapezoidal membership functions have been used for development of fuzzy models. The six input data are fed into fuzzy model and four variables are received as output. The linguistic variables used for the inputs are as follows;

- "rfnf"= Relative first natural frequency;
- "rsnf"= Relative second natural frequency;
- "rtnf"= Relative third natural frequency;
- "rfmd"= Relative first mode shape difference;
- "rsmd"= Relative second mode shape difference;
- "rtmd"= Relative third mode shape difference.

The linguistic variables used for the outputs are as follows;

- "rfcl"= Relative first crack location;
- "rfcd"= Relative first crack depth;
- "rscl"=Relative second crack location;
- "rscd"=Relative second crack depth.

The illustrative view of the Triangular membership, Gaussian membership, Trapezoidal membership fuzzy models are shown in figures. 5.3(a), 5.3(b) and 5.3(c) respectively. Several fuzzy linguistic variables and fuzzy rules (Twenty four) used to design and train the knowledge-based fuzzy logic systems are shown in table 5.1 and table 5.2 respectively. The membership functions used in developing the fuzzy inference system for crack diagnosis have been shown in figures 5.4 to 5.6. Twelve membership functions have been used for each input parameters to the fuzzy model. In designing the output membership functions for the output parameter such as relative first crack location (rfcl) and relative second crack location (rscl), forty six membership functions has been taken. Whereas for relative first crack depth (rfcd) and relative second crack depth (rscd), nineteen membership functions have been used. The defuzzification process of the

Triangular, Gaussian, and Trapezoidal membership functions are presented in figures 5.7, 5.8 and 5.9 respectively by activating the rule no 6 and rule no 16 from table 5.2.

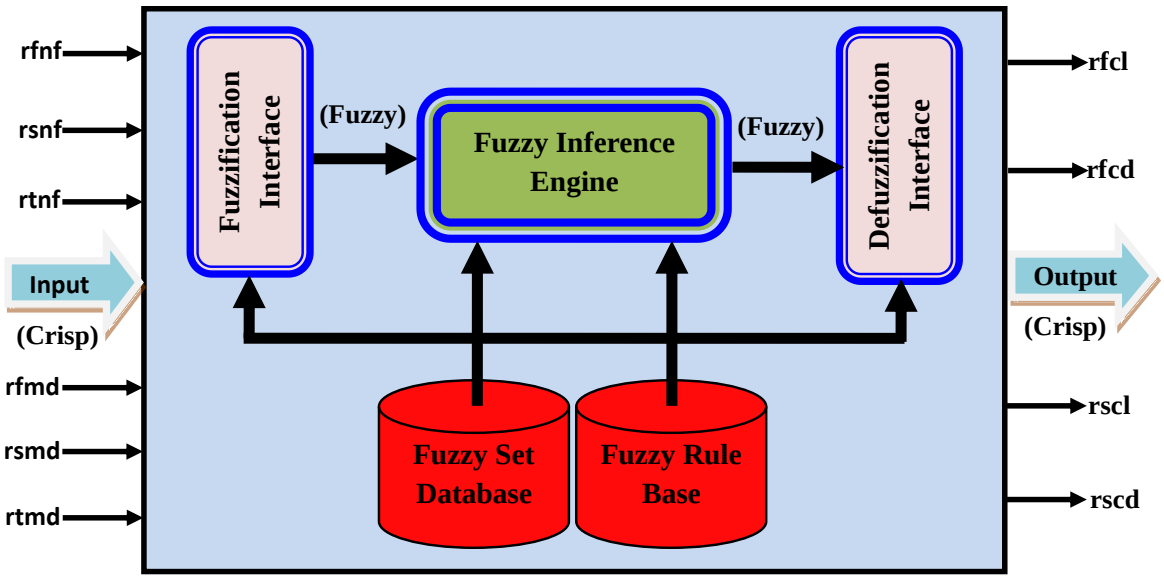

Figure 5.2, Fuzzy logic controller

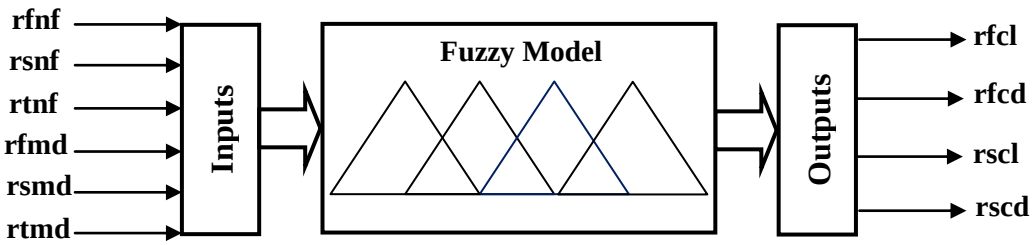

Figure 5.3(a) Triangular fuzzy model

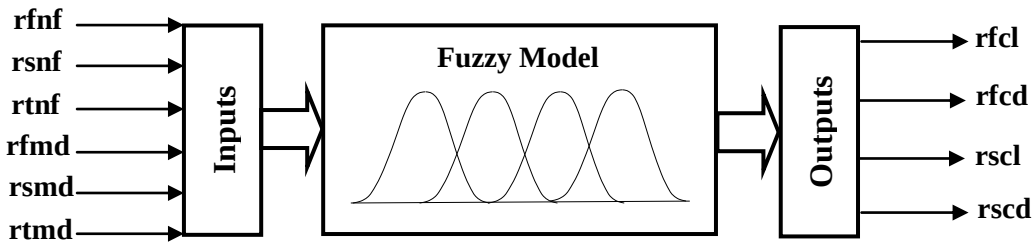

Figure 5.3 (b) Gaussian fuzzy model

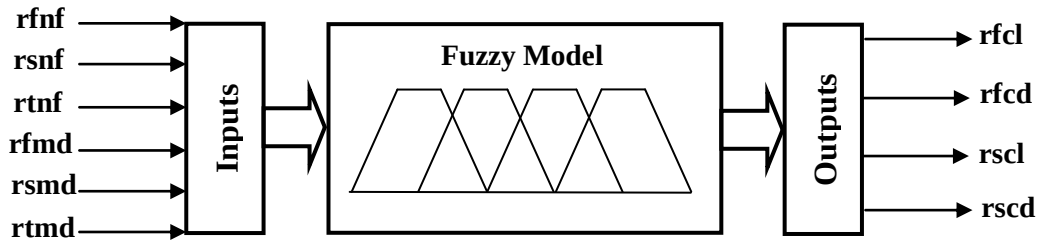

Figure 5.3 (c) Trapezoidal fuzzy model

5.3.1 Fuzzy logic mechanism for identification of crack

The rules for fuzzy mechanism can be defined, based on above fuzzy linguistic terms as follow:

$$\text{if}\begin{pmatrix} rfnf \text{ is } rfnf_a \text{ and } rsnf \text{ is } rsnf_b \text{ and } rtnf \text{ is } rtnf_c \\ rfmd \text{ is } rfmd_e \text{ and } rsmd \text{ is } rsmd_f \text{ and } rtmd \text{ is } rtmd_g \end{pmatrix} \tag{5.2}$$

Then rfcl is $\text{rfcl}_{\text{abcdefg}}$ and rfcd is $\text{rfcd}_{\text{abcdefg}}$ and rscl is $\text{rscl}_{\text{abcdefg}}$ and rscd is $\text{rfcl}_{\text{abcdefg}}$ where a, b, c, d, e, f, g=1to12

According to fuzzy methodology a factor, W_{abcefg} is defined in the rules as follows [66, 162]:

$$\begin{aligned} W_{abcefg} = {} & \mu\, rfnf_a\left(freq_a\right) \wedge \mu\, rsnf_a\left(freq_b\right) \wedge \mu\, rtnf_a\left(freq_c\right) \wedge \mu\, rfmd_e\left(\text{mod}\, shdif_e\right) \\ & \wedge \mu\, rsmd_f\left(\text{mod}\, shdif_f\right) \wedge \mu\, rtmd_g\left(\text{mod}\, shdif_g\right) \end{aligned} \tag{5.3}$$

Where: $freq_a$, $freq_b$ and $freq_c$ are the first, second and third relative natural frequencies of the cracked cantilever composite beam respectively; modshdif_e, modshdif_f and relative mode shape differences of the cracked cantilever composite beam. The membership values of the relative crack location and relative crack depth, $(\text{location})_{\text{rcli}}$ and $(\text{depth})_{\text{rcdi}}$ (i= 1, 2) by applying the composition rule of inference can be written as [66, 162];

$$\begin{aligned} \mu_{rcli_{abcefg}}(location) &= w_{abcefg} \wedge \mu_{rcli_{abcefg}}(location) \;\forall_{length} \in rcli \\ \mu_{rcdi_{abcefg}}(depth) &= w_{abcefg} \wedge \mu_{rcdi_{abcefg}}(depth) \qquad \forall_{depth} \in rcdi \end{aligned} \tag{5.4}$$

The outputs of all the fuzzy set rules combined to achieve the inclusive conclusions can be written as follows;

$$\mu_{rcli}(location) = \mu_{rcli_{11111}}(location) \vee .. \vee \mu_{rcli_{abcefg}}(location) \vee .. \vee \mu_{rcli_{121212121212}}(location)$$

$$\mu_{rcli}(depth) = \mu_{rcli_{11111}}(depth) \vee .... \vee \mu_{rcli_{abcefg}}(depth) \vee ..... \vee \mu_{rcli_{121212121212}}(depth)$$

The crisp values of the relative crack location and relative crack depth can be written with the help Centre of gravity method as [66,160]:

$$\left.\begin{aligned} \text{Re}\, lative\ crack\ location\ (rfcl, rscl) &= \frac{\int (location)\ .\ \mu_{rcl_{1,2}}(location)\ .\ d\ (location)}{\int \mu_{rcl_{1,2}}\ (location)\ .\ d\ (location)} \\ \text{Re}\, lative\ crack\ depth\ (rfcd, rscd) &= \frac{\int (depth)\ .\ \mu_{rcl_{1,2}}(depth)\ .\ d\ (depth)}{\int \mu_{rcl_{1,2}}\ (depth)\ .\ d\ (depth)} \end{aligned}\right\} \tag{5.5}$$

Table 5.1 Explanation of fuzzy linguistic variables.

Membership Functions	Linguistic Variables	Explanation of the Linguistic variables
L1NF1,L2NF1,L3NF1,L4NF1, L5NF1	$rfnf_{1-5}$	Low ranges of relative natural frequency of the first mode of vibration in descending order respectively
M1NF1,M2NF1	$rfnf_{6,7}$	Medium ranges of relative natural frequency of the first mode of vibration in ascending order respectively
H1NF1,H2NF1,H3NF1,H4NF1, H5NF1	$rfnf_{8-12}$	Higher ranges of relative natural frequency of the first mode of vibration in ascending order respectively
L1NF2,L2NF2,L3NF2,L4NF2, L5NF2	$rsnf_{1-5}$	Low ranges of relative natural frequency of the second mode of vibration in descending order respectively
M1NF2,M2NF2	$rsnf_{6,7}$	Medium ranges of relative natural frequency of the second mode of vibration in ascending order respectively
H1NF2,H2NF2,H3NF2,H4NF2, H5NF2	$rsnf_{8-12}$	Higher ranges of relative natural frequencies of the second mode of vibration in ascending order respectively
L1NF3,L2NF3,L3NF3,L4NF3, L5NF3	$rtnf_{1-5}$	Low ranges of relative natural frequencies of the third mode of vibration in descending order respectively
M1NF3,M2NF3	$rtnf_{6,7}$	Medium ranges of relative natural frequencies of the third mode of vibration in ascending order respectively
H1NF3,H2NF3,H3NF3,H4NF3, H5NF3	$rtnf_{8-12}$	Higher ranges of relative natural frequencies of the third mode of vibration in ascending order respectively
S1MS1,S2MS1,S3MS1,S4MS1, S5MS1	$rfmd_{1-5}$	Small ranges of first relative mode shape difference in descending order respectively
M1MS1,M2MS1	$rfmd_{6,7}$	medium ranges of first relative mode shape difference in ascending order respectively
H1MS1,H2MS1,H3MS1,H4MS1, H5MS1	$rfmd_{8-12}$	Higher ranges of first relative mode shape difference in ascending order respectively
S1MS2,S2MS2,S3MS2,S4MS2, S5MS2	$rsmd_{1-5}$	Small ranges of second relative mode shape difference in descending order respectively
M1MS2,M2MS2	$rsmd_{6,7}$	medium ranges of second relative mode shape difference in ascending order respectively
H1MS2,H2MS2,H3MS2,H4MS2, H5MS2	$rsmd_{8-12}$	Higher ranges of second relative mode shape difference in ascending order respectively
S1MS3,S2MS3,S3MS3,S4MS3, S5MS3	$rtmd_{1-5}$	Small ranges of third relative mode shape difference in descending order respectively
M1MS3,M2MS3	$rtmd_{6,7}$	medium ranges of third relative mode shape difference in ascending order respectively
H1MS3,H2MS3,H3MS3,H4MS3, H5MS3	$rtmd_{8-12}$	Higher ranges of third relative mode shape difference in ascending order respectively
S1CL1,S2CL1……S23CL1	$rfcl_{1-23}$	Small ranges of relative first crack location in descending order respectively
M1CL1,M2CL1, M3CL1	$rfcl_{24-26}$	Medium ranges of relative first crack location in ascending order respectively
B1CL1,B2CL1…….B23CL1	$rfcl_{27-49}$	Bigger ranges of relative first crack location in ascending order respectively
S1CD1,S2CD1……S10CD1	$rfcd_{1-10}$	Small ranges of relative first crack depth in descending order respectively
MCD1	$rfcd_{11}$	Medium relative first crack depth
L1CD1,L2CD1……L10CD1	$rfcd_{12-21}$	Larger ranges of relative second crack depth in ascending order respectively
S1CL2,S2CL2……S23CL2	$rscl_{1-23}$	Small ranges of relative second crack location in descending order respectively
M1CL2,M2CL2,M3CL2	$rscl_{24-26}$	Medium ranges of relative second crack location in ascending order respectively
B1CL2,B2CL2…….B23CL2	$rscl_{27-49}$	Bigger ranges of relative second crack location in ascending order respectively
S1CD2,S2CD2……S10CD2	$rscd_{1-10}$	Small ranges of relative second crack depth in descending order respectively
MCD2	$rscd_{11}$	Medium relative second crack depth
L1CD2,L2CD2……L10CD2	$rscd_{12-21}$	Larger ranges of relative second crack depth in ascending order respectively

Table 5.2 Examples of some fuzzy rules out of several hundred fuzzy rules for composite beam.

Sl. No.	Some Fuzzy Rules
1	If rfnf is M1NF1,rsnf is L2NF2,rtnf is L1NF3,rfmd is M2MS1,rsmd is M2MS2,rtmd is H1MS3, then rfcd is S1CD1,and rfcl is S6CL1 and rscd is S4CD2,and rscl is B5CL2
2	If rfnf is M2NF1,rsnf is M1NF2,rtnf is H2NF3,rfmd is H3MS1,rsmd is H3MS2,rtmd is H4MS3, then rfcd is S6CD1,and rfcl is S18CL1 and rscd is S5CD2,and rscl is M2CL2
3	If rfnf is M1NF1,rsnf is L1NF2,rtnf is L4NF3,rfmd is H3MS1,rsmd is H2MS2,rtmd is H3MS3, then rcd1 is S4CD1,and rfcl is S17CL1 and rscd is S6CD2,and rscl is S6CL2
4	If rfnf is M2NF1,rsnf is L1NF2,rtnf is L4NF3,rfmd is M1MS1,rsmd is H1MS2,rtmd is H2MS3, then rfcd is S4CD1,and rfcl is S11CL1 and rscd is S4CD2,and rscl is M2CL2
5	If rfnf is M1NF1,rsnf is L2NF2,rtnf is H5NF3,rfmd is H1MS1,rsmd is H1MS2,rtmd is H2MS3, then rfcd is S4CD1,and rfcl is S11CL1 and rscd is S1CD2,and rscl is B13CL2
6	If rfnf is L1NF4,rsnf is L2NF3,rtnf is M3NF2,rfmd is H2MS1,rsmd is H3MS2,rtmd is L1MS3, then rfcd is S3CD1,and rfcl is S16CL1 and rscd is S8CD2,and rscl is B3CL2
7	If rfnf is L4NF1,rsnf is H4NF2,rtnf is L2NF3,rfmd is M2MS1,rsmd is H1MS2,rtmd is H4MS3, then rfcd is L1CD1,and rfcl is S11CL1 and rscd is S4CD2,and rscl is B10CL2
8	If rfnf is H5NF1,rsnf is L1NF2,rtnf is M1NF3,rfmd is H2MS1,rsmd is H4MS2,rtmd is H5MS3, then rfcd is S6CD1,and rfcl is S6CL1 and rscd is S4CD2,and rscl is B5CL2
9	If rfnf is L1NF1,rsnf is L4NF2,rtnf is H1NF3,rfmd is M1MS1,rsmd is H1MS2,rtmd is M2MS3, then rfcd is L1CD1,and rfcl is S6CL1 and rscd is S1CD2,and rscl is B5CL2
10	If rfnf is H2NF1,rsnf is H4NF2,rtnf is H1NF3,rfmd is H4MS1,rsmd is H3MS2,rtmd is M1MS3, then rfcd is S7CD1,and rfcl is S17CL1 and rscd is S6CD2,and rscl is B18CL2
11	If rfnf is M1NF1,rsnf is L1NF2,rtnf is H2NF3,rfmd is L1MS1,rsmd is H2MS2,rtmd is H3MS3, then rfcd is S2CD1,and rfcl is S11CL1 and rscd is S6CD2,and rscl is B10CL2
12	If rfnf is L4NF1,rsnf is L4NF2,rtnf is L4NF3,rfmd is H2MS1,rsmd is L1MS2,rtmd is H2MS3, then rfcd is L1CD1,and rfcl is S17CL1 and rscd is S5CD2,and rscl is M2CL2
13	If rfnf is M1NF1,rsnf is L3NF2,rtnf is L1NF3,rfmd is L2MS1,rsmd is M1MS2,rtmd is S1MS3, then rfcd is S6D1,and rfcl is S12CL1 and rscd is MCD2,and rscl is M1CL2
14	If rfnf is L2NF1,rsnf is L1NF2,rtnf is L1NF3,rfmd is H2MS1,rsmd is H2MS2,rtmd is H2MS3, then rfcd is S2CD1,and rfcl is S12CL1 and rscd is S4CD2,and rscl is B14CL12
15	If rfnf is H2NF1,rsnf is H1NF2,rtnf is H1NF3,rfmd is H2MS1,rsmd is H3MS2,rtmd is H4MS3, then rfcd is S4CD1,and rfcl is B5CL1 and rscd is S6CD2,and rscl is B21CL2
16	If rfnf is L3NF1,rsnf is L1NF2,rtnf is H1NF3,rfmd is L2MS1,rsmd is M1MS2,rtmd is L3MS3, then rfcd is L5CD1,and rfcl is M2CL1 and rscd is L3CD2,and rscl is S10CL2
17	If rfnf is H1NF1,rsnf is M2NF2,rtnf is L1NF3,rfmd is H2MS1,rsmd is H4MS2,rtmd is L1MS3, then rfcd is S6CD1,and rfcl is S17CL1 and rscd is S4CD2,and rscl is S6CL2
18	If rfnf is L4NF1,rsnf is L4NF2,rtnf is L4NF3,rfmd is H1MS1,rsmd is H3MS2,rtmd is H5MS3, then rfcd is S2CD1,and the rifle is S17CL1 and rescued is S1CD2,and rscl is M2CL2
19	If rfnf is L3NF1,rsnf is L4NF2,rtnf is L5NF3,rfmd is M2MS1,rsmd is H2MS2,rtmd is H4MS3, then rfcd is MCD1,and rfcl is S17CL1 and rscd is S2CD2,and rscl is B19CL2
20	If rfnf is H2NF1,rsnf is H1NF2,rtnf is H4NF3,rfmd is H3MS1,rsmd is H4MS2,rtmd is H5MS3, then rfcd is S6CD1,and rfcl is S11CL1 and rscd is S4CD2,and rscl is M2CL2
21	If rfnf is H3NF1,rsnf is L2NF2,rtnf is M2NF3,rfmd is L2MS1,rsmd is H2MS2,rtmd is H1M3, then rfcd is S9CD1,and rfcl is S18CL1 and rscd is S11CD2,and rscl is S8CL2
22	If rfnf is M1NF1,rsnf is L3NF2,rtnf is H4NF3,rfmd is H2MS1,rsmd is L4MS2,rtmd is H3MS3, then rfcd is S12CD1,and rfcl is S18CL1 and rscd is S3CD2,and rscl is B10CL2
23	If rfnf is H3NF1,rsnf is M1NF2,rtnf is L1NF3,rfmd is M2MS1,rsmd is H3MS2,rtmd is H4MS3, then rfcd is MCD1,and rfcl is S14CL1 and rscd is S4CD2,and rscl is B4CL2
24	If rfnf is H4F1,rsnf is M1F2,rtnf is L4F3,rfmd is S4M1,rsmd is H1M2,rtmd is H4M3, then rfcd is S16CD1,and rfcl is B11L1 and rscd is M2CD2,and rscl is B22CL2

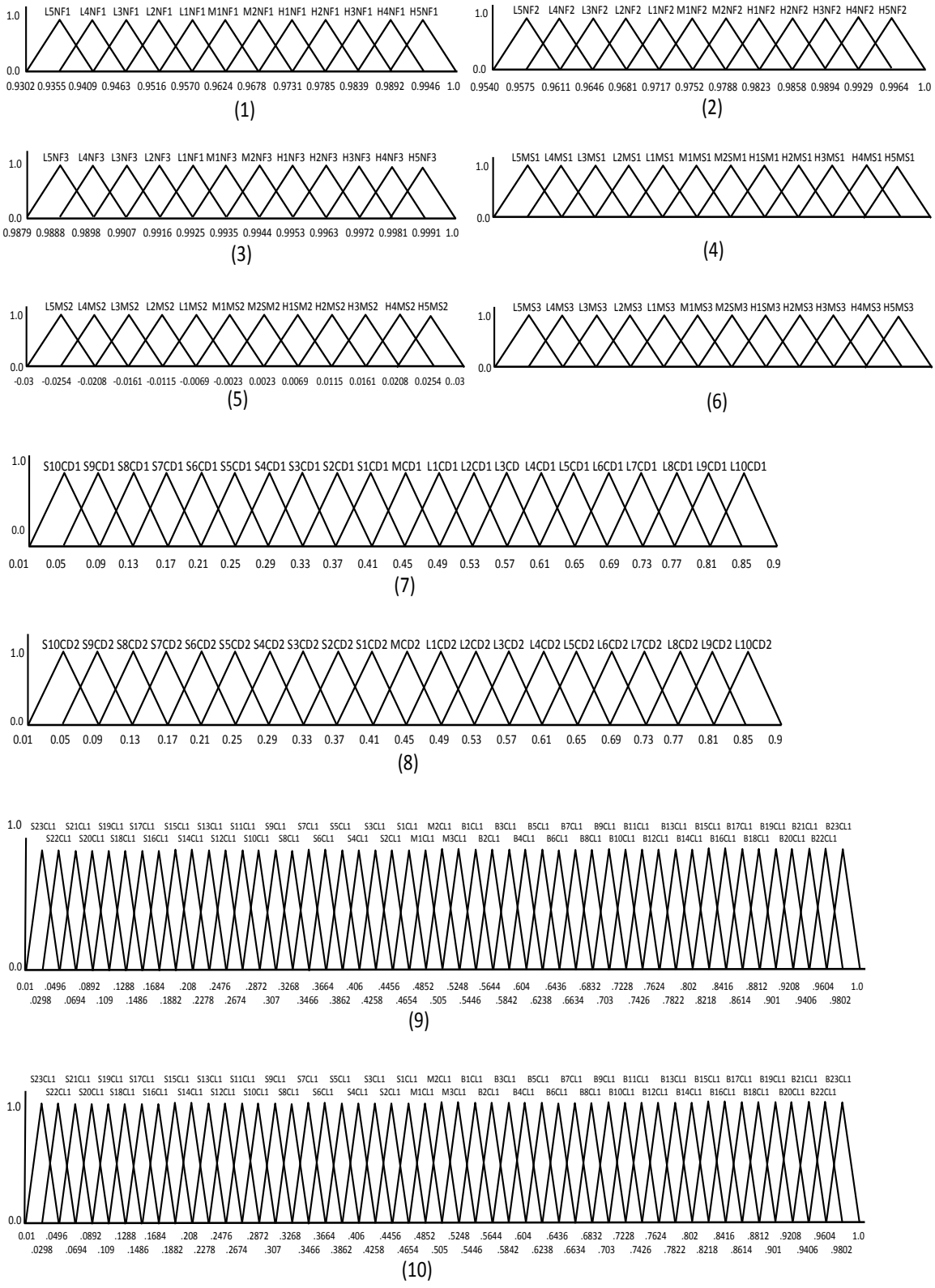

Figure 5.4 Triangular fuzzy membership functions for (1, 2, 3) relative natural frequency of first three bending mode of vibration, (4, 5, 6) relative mode shape difference of first three bending mode of vibration, (7, 8) first and second crack depth and (9, 10) first and second crack location for composite beam.

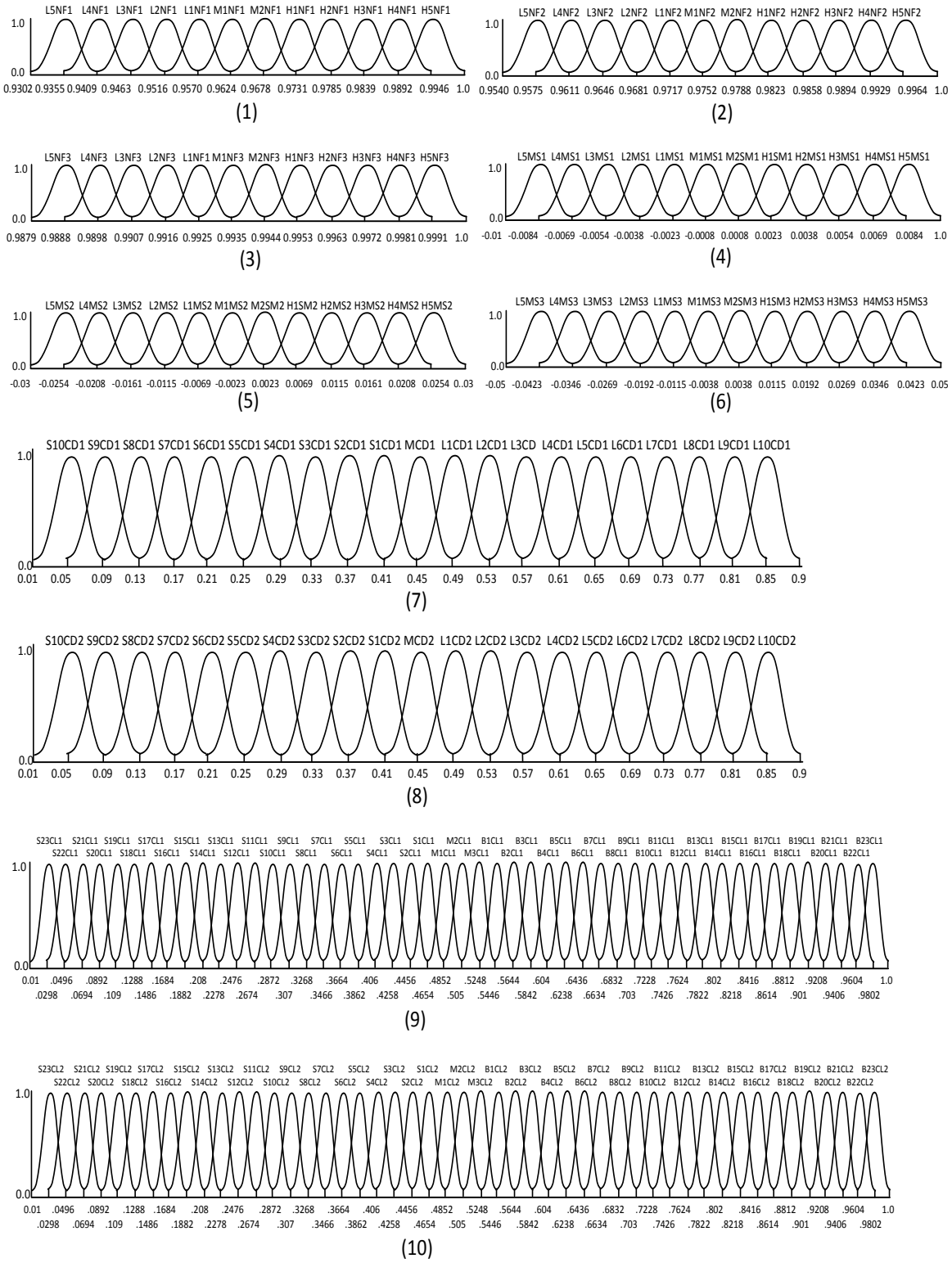

Figure 5.5 Gaussian fuzzy membership functions for (1, 2, 3) relative natural frequency of first three bending mode of vibration, (4, 5, 6) relative mode shape difference of first three bending mode of vibration, (7, 8) first and second crack depth and (9, 10) first and second crack location for composite beam.

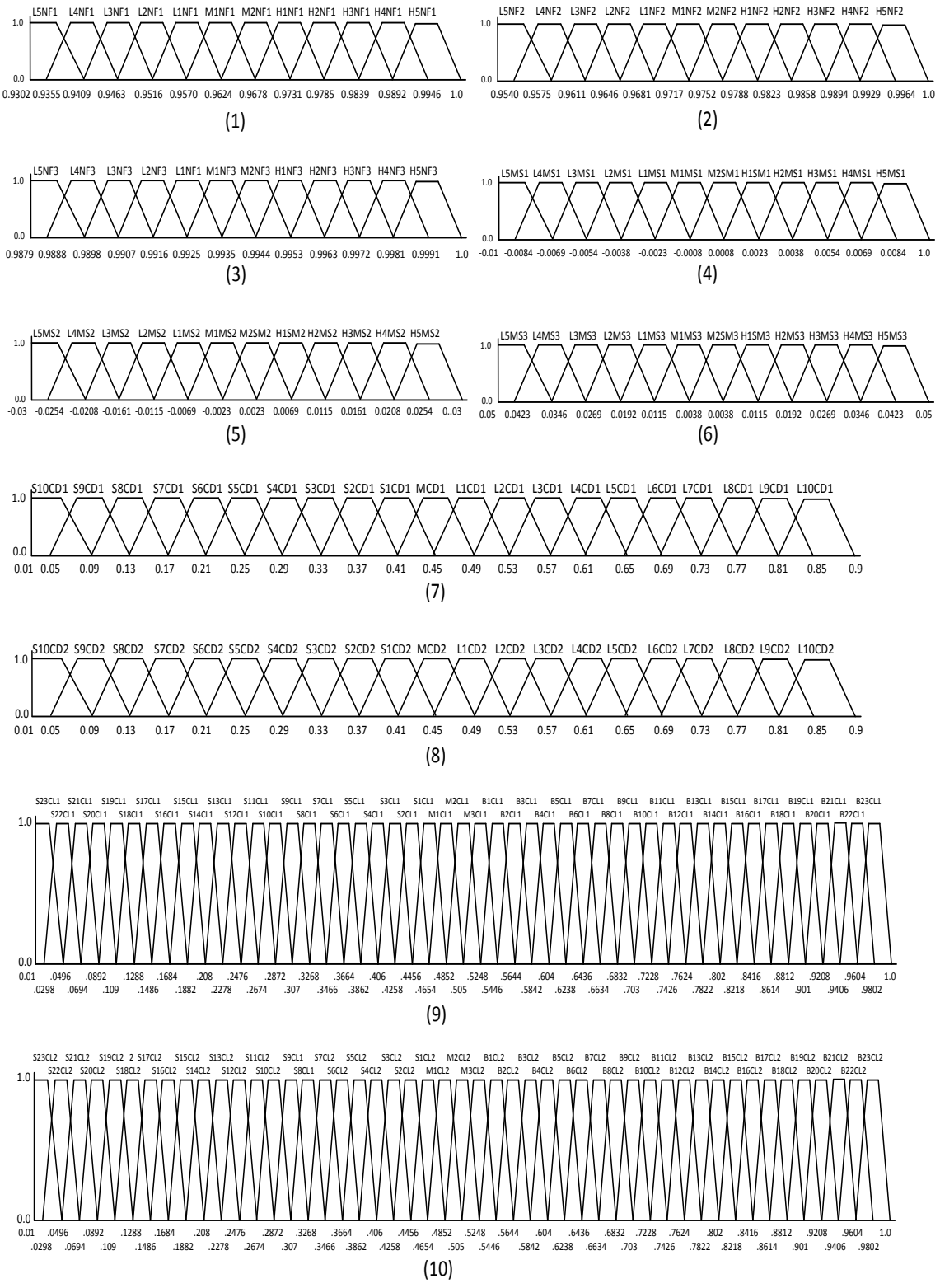

Figure 5.6 Trapezoidal fuzzy membership functions for (1, 2, 3) relative natural frequency of first three bending mode of vibration, (4, 5, 6) relative mode shape difference of first three bending mode of vibration, (7, 8) first and second crack depth and (9, 10) first and second crack location for composite beam.

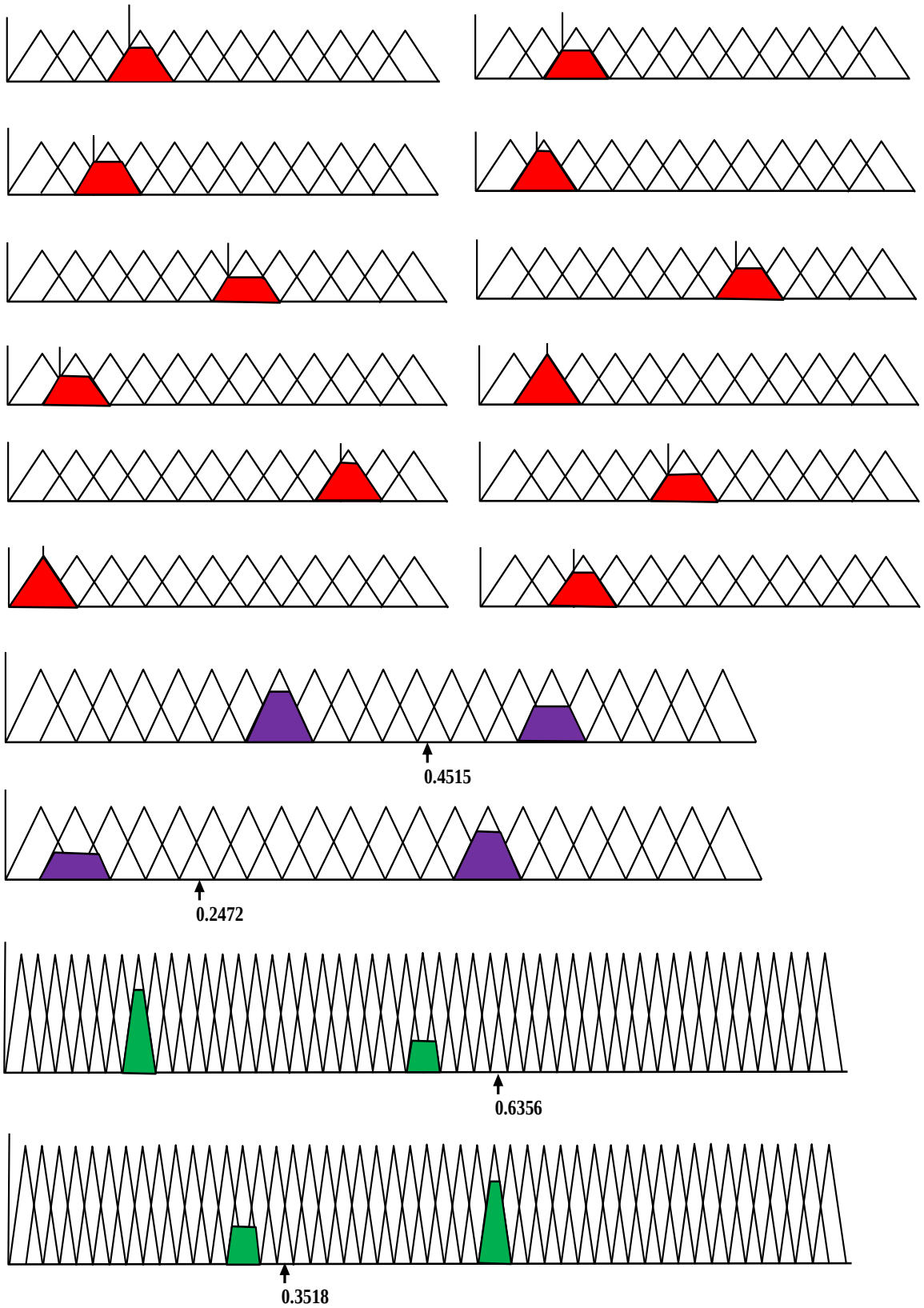

Figure 5.7 Aggregated values of first and second crack orientation (relative crack depths and relative crack locations) from triangular membership function when Rules 6 and 16 are activated of table 2 for composite beam.

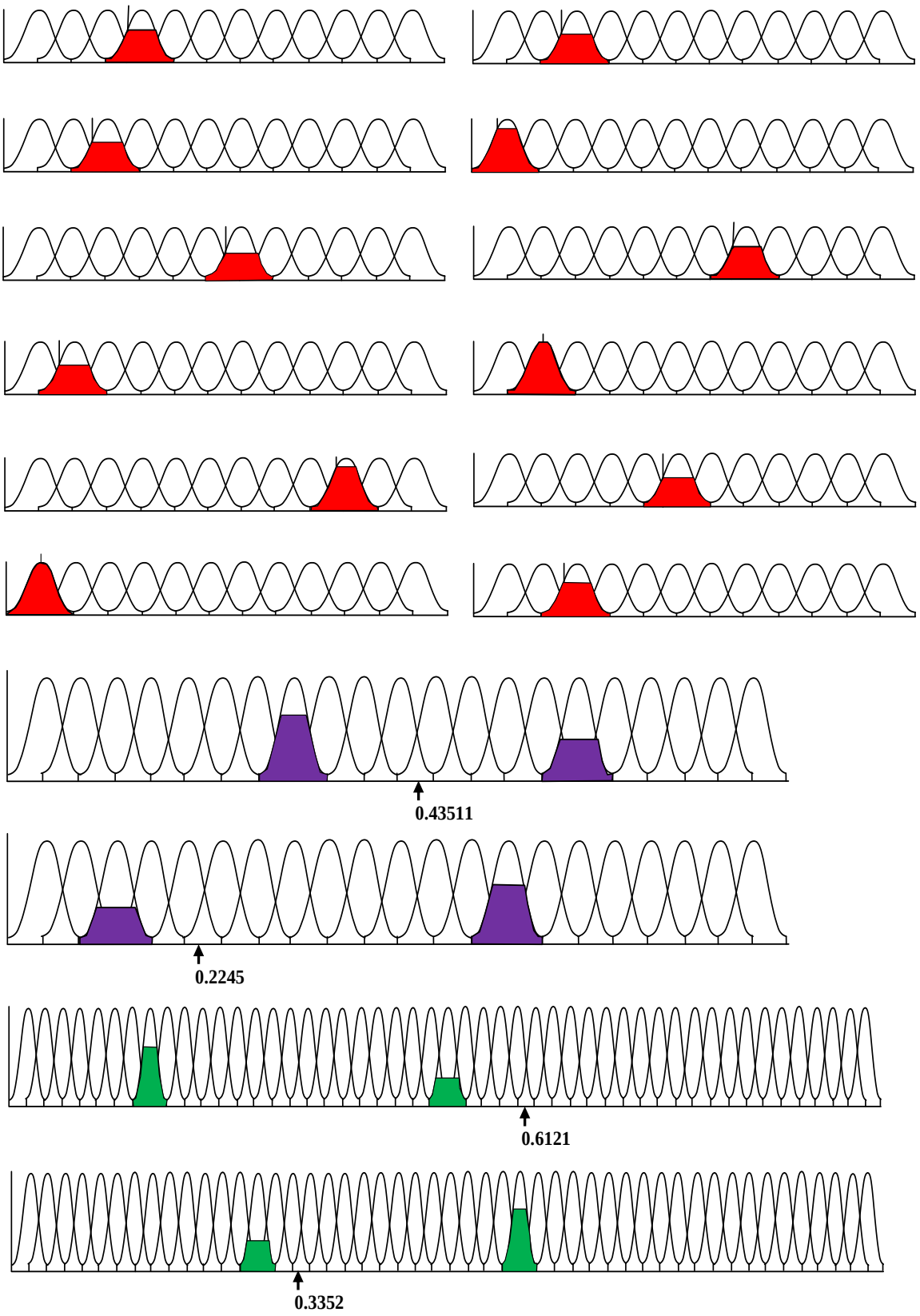

Figure 5.8 Aggregated values of first and second crack orientation (relative crack depths and relative crack locations) from Gaussian membership function when Rules 6 and 16 are activated of table 2 for composite beam.

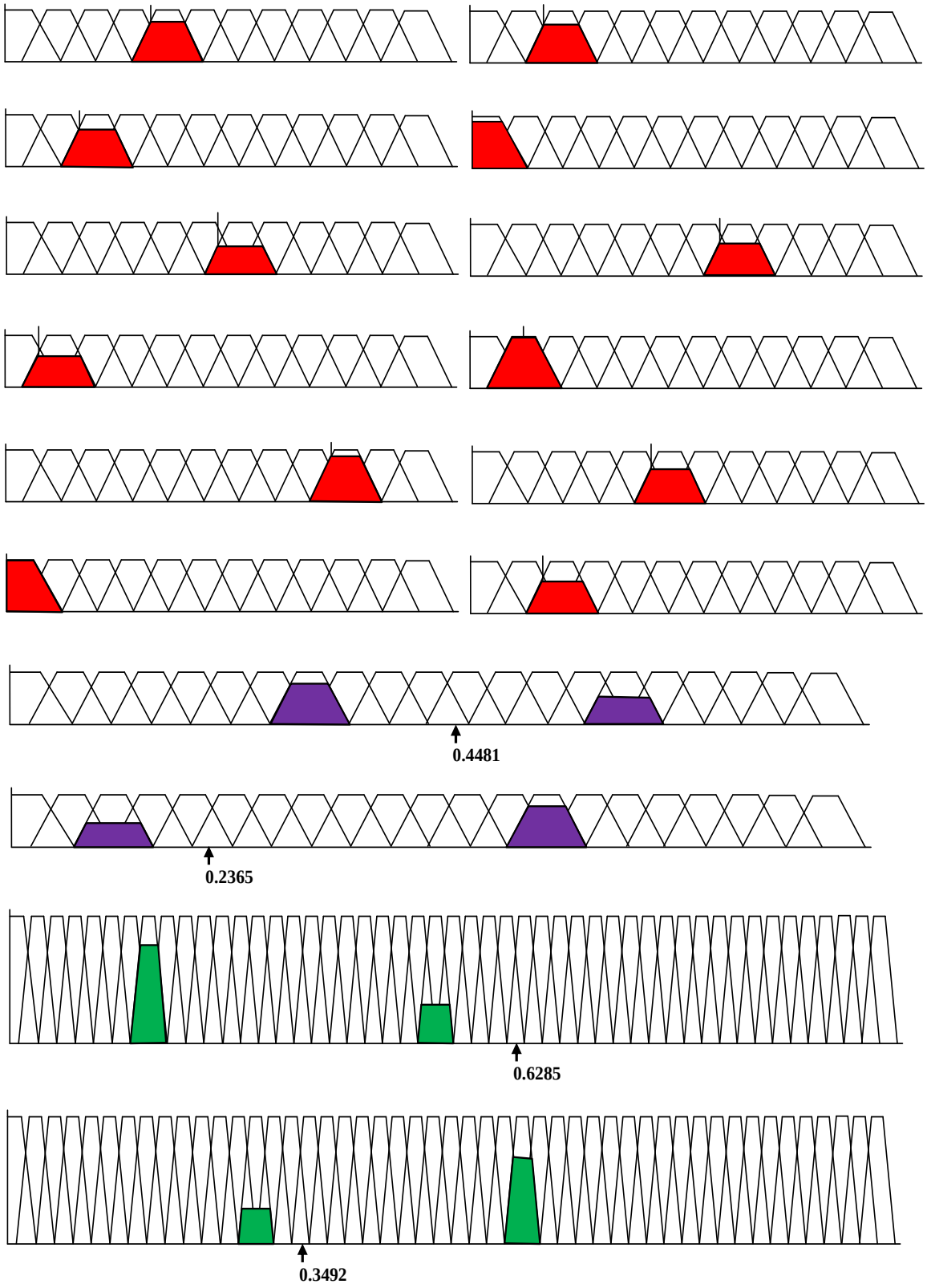

Figure 5.9 Aggregated values of first and second crack orientation (relative crack depths and relative crack locations) from trapezoidal membership function when Rules 6 and 16 are activated of table 2 for composite beam.

Table 5.3 Examples of some fuzzy rules out of several hundred fuzzy rules for steel beam.

Sl. No.	Some Fuzzy Rules
1	If rfnf is L1NF1,rsnf is H5NF2,rtnf is H3NF3,rfmd is H1MS1,rsmd is M1MS2,rtmd is H1MS3, then rfcd is S3CD1,and rfcl is S21CL1 and rscd is L1CD2,and rscl is S16CL2
2	If rfnf is L5NF1,rsnf is L2NF2,rtnf is L4NF3,rfmd is H1MS1,rsmd is M1MS2,rtmd is L2MS3, then rfcd is L1CD1,and rfcl is S21CL1 and rscd is L2CD2,and rscl is S16CL2
3	If rfnf is L5NF1,rsnf is L2NF2,rtnf is L5NF3,rfmd is M1MS1,rsmd is H1MS2,rtmd is M2MS3, then rcd1 is S7CD1,and rfcl is S16CL1 and rscd is L1CD2,and rscl is S9CL2
4	If rfnf is H5NF1,rsnf is L3NF2,rtnf is L4NF3,rfmd is M1MS1,rsmd is H2MS2,rtmd is M2MS3, then rfcd is S3CD1,and rfcl is S16CL1 and rscd is L1CD2,and rscl is S9CL2
5	If rfnf is H4NF1,rsnf is H4NF2,rtnf is H5NF3,rfmd is M1MS1,rsmd is M1MS2,rtmd is H2MS3, then rfcd is S7CD1,and rfcl is S3CL1 and rscd is S1CD2,and rscl is S2CL2
6	If rfnf is H4NF4,rsnf is H5NF3,rtnf is H3NF2,rfmd is M1MS1,rsmd is H2MS2,rtmd is L4MS3, then rfcd is S5CD1,and rfcl is S8CL1 and rscd is S7CD2,and rscl is S2CL2
7	If rfnf is H5NF1,rsnf is H5NF2,rtnf is L5NF3,rfmd is L2MS1,rsmd is M2MS2,rtmd is H1MS3, then rfcd is S8CD1,and rfcl is S3CL1 and rscd is S4CD2,and rscl is B2CL2
8	If rfnf is H3NF1,rsnf is L4NF2,rtnf is L3NF3,rfmd is H1MS1,rsmd is L2MS2,rtmd is L3MS3, then rfcd is L4CD1,and rfcl is S3CL1 and rscd is S6CD2,and rscl is B5CL2
9	If rfnf is L3NF1,rsnf is L4NF2,rtnf is L1NF3,rfmd is H1MS1,rsmd is L3MS2,rtmd is H1MS3, then rfcd is S2CD1,and rfcl is S2CL1 and rscd is L3CD2,and rscl is B3CL2
10	If rfnf is H1NF1,rsnf is M1NF2,rtnf is H2NF3,rfmd is L2MS1,rsmd is L1MS2,rtmd is L4MS3, then rfcd is MCD1,and rfcl is B8CL1 and rscd is S2CD2,and rscl is B22CL2
11	If rfnf is L3NF1,rsnf is M2NF2,rtnf is H4NF3,rfmd is L2MS1,rsmd is H3MS2,rtmd is L1MS3, then rfcd is S2CD1,and rfcl is B4CL1 and rscd is L2CD2,and rscl is B7CL2
12	If rfnf is H2NF1,rsnf is H3NF2,rtnf is H5NF3,rfmd is L2MS1,rsmd is M1MS2,rtmd is H1MS3, then rfcd is S4CD1,and rfcl is B6CL1 and rscd is L1CD2,and rscl is B9CL2
13	If rfnf is L3NF1,rsnf is L1NF2,rtnf is H3NF3,rfmd is L2MS1,rsmd is H1MS2,rtmd is H3MS3, then rfcd is B2CD1,and rfcl is B9CL1 and rscd is S3CD2,and rscl is B11CL2
14	If rfnf is H3NF1,rsnf is H3NF2,rtnf is H5NF3,rfmd is H2MS1,rsmd is L1MS2,rtmd is H3MS3, then rfcd is S3CD1,and rfcl is M3CL1 and rscd is L1CD2,and rscl is B7CL12
15	If rfnf is H4NF1,rsnf is M1NF2,rtnf is H3NF3,rfmd is L3MS1,rsmd is H1MS2,rtmd is H4MS3, then rfcd is S5CD1,and rfcl is B1CL1 and rscd is MCD2,and rscl is B7CL2
16	If rfnf is H4NF1,rsnf is H1NF2,rtnf is L3NF3,rfmd is H1MS1,rsmd is L4MS2,rtmd is H4MS3, then rfcd is S2CD1,and rfcl is B1CL1 and rscd is L3CD2,and rscl is B11CL2
17	If rfnf is H1NF1,rsnf is L3NF2,rtnf is H4NF3,rfmd is L3MS1,rsmd is H2MS2,rtmd is H3MS3, then rfcd is L3CD1,and rfcl is B7CL1 and rscd is S1CD2,and rscl is B12CL2
18	If rfnf is H5NF1,rsnf is H4NF2,rtnf is M1NF3,rfmd is L2MS1,rsmd is H2MS2,rtmd is H5MS3, then rfcd is S9CD1,and rfcl is B7CL1 and rscd is L1CD2,and rscl is B15CL2
19	If rfnf is H2NF1,rsnf is H5NF2,rtnf is L1NF3,rfmd is M1MS1,rsmd is H3MS2,rtmd is H4MS3, then rfcd is L4CD1,and rfcl is B11CL1 and rscd is S3CD2,and rscl is B16CL2
20	If rfnf is H1NF1,rsnf is L1NF2,rtnf is H4NF3,rfmd is L3MS1,rsmd is M1MS2,rtmd is H4MS3, then rfcd is S4CD1,and rfcl is B3CL1 and rscd is L1CD2,and rscl is B16CL2
21	If rfnf is H1NF1,rsnf is L3NF2,rtnf is H5NF3,rfmd is L4MS1,rsmd is L1MS2,rtmd is H3SM3, then rfcd is S5CD1,and rfcl is B9CL1 and rscd is L2CD2,and rscl is B17CL2
22	If rfnf is H3NF1,rsnf is L1NF2,rtnf is H3NF3,rfmd is L3MS1,rsmd is H1MS2,rtmd is H5MS3, then rfcd is S5CD1,and rfcl is S11CL1 and rscd is L1CD2,and rscl is B1CL2
23	If rfnf is H4NF1,rsnf is L1NF2,rtnf is H5NF3,rfmd is H1MS1,rsmd is L2MS2,rtmd is H3MS3, then rfcd is L1CD1,and rfcl is S12CL1 and rscd is S6CD2,and rscl is B6CL2
24	If rfnf is H1F1,rsnf is M2F2,rtnf is H4F3,rfmd is L4M1,rsmd is H2M2,rtmd is H5M3, then rfcd is S6CD1,and rfcl is B13L1 and rscd is S2CD2,and rscl is B21CL2

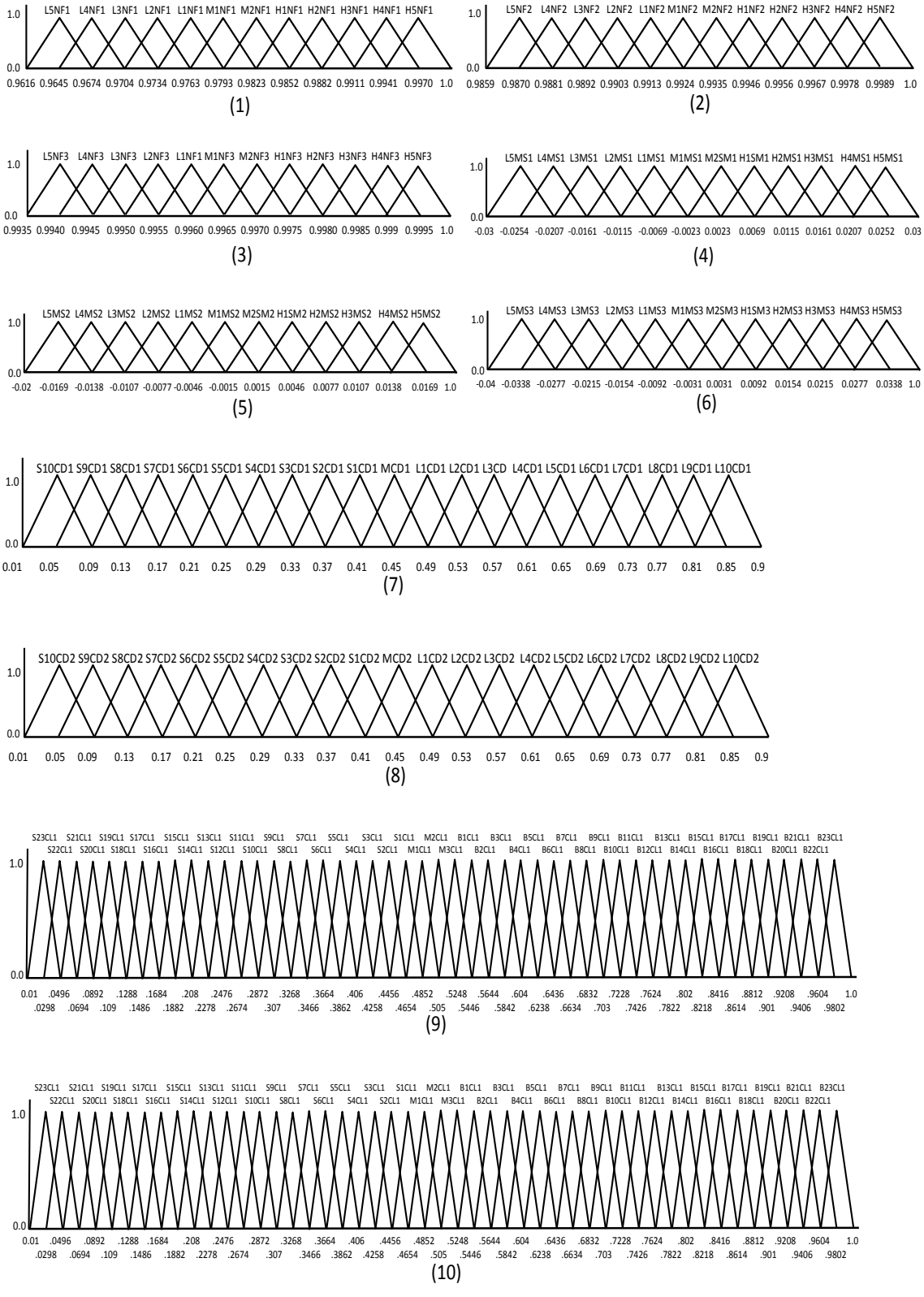

Figure 5.10 Triangular fuzzy membership functions for (1, 2, 3) relative natural frequency of first three bending mode of vibration, (4, 5, 6) relative mode shape difference of first three bending mode of vibration, (7, 8) first and second crack depth and (9, 10) first and second crack location for steel beam

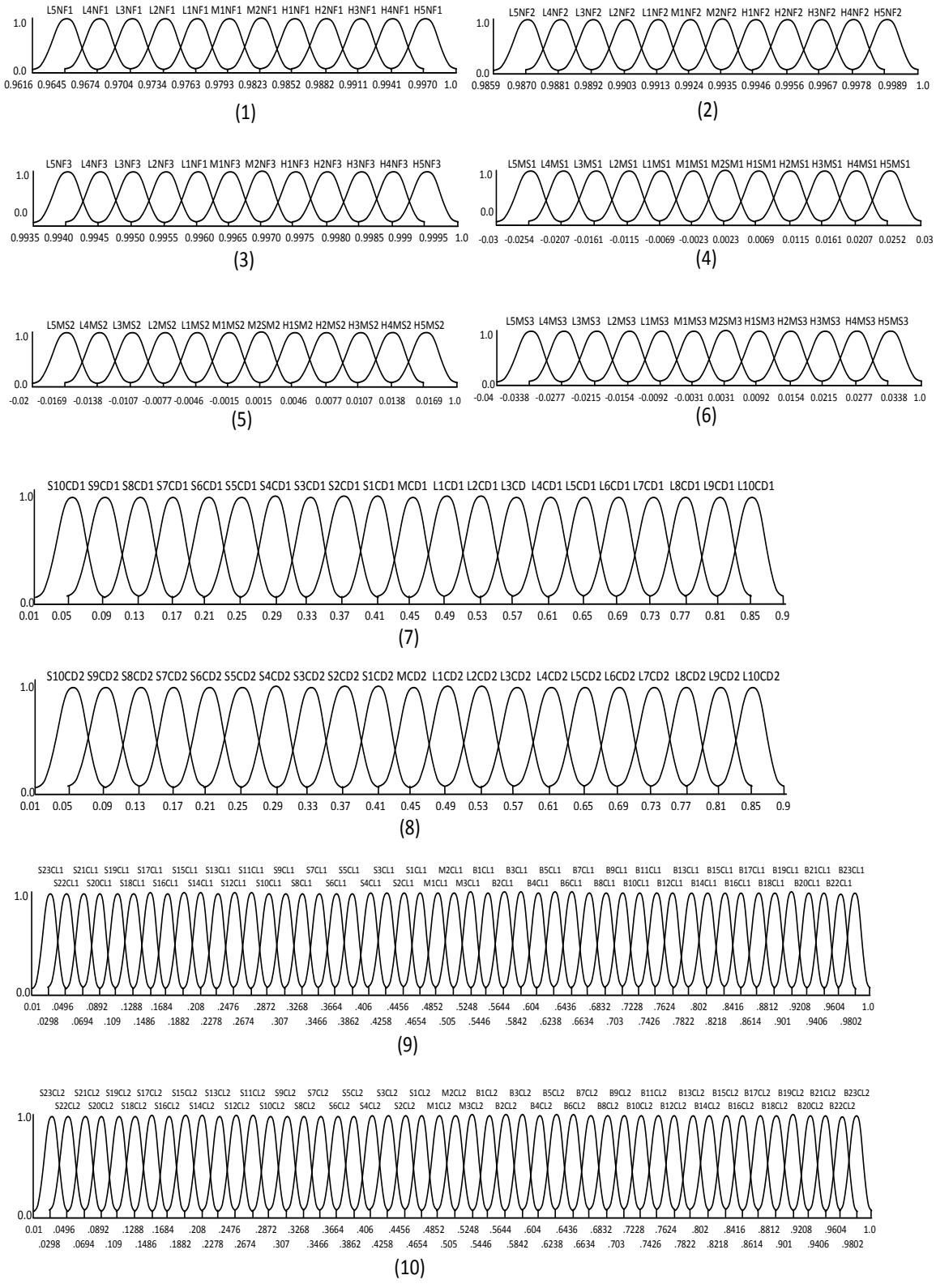

Figure 5.11 Gaussian fuzzy membership functions for (1, 2, 3) relative natural frequency of first three bending mode of vibration, (4, 5, 6) relative mode shape difference of first three bending mode of vibration, (7, 8) first and second crack depth and (9, 10) first and second crack location for steel beam

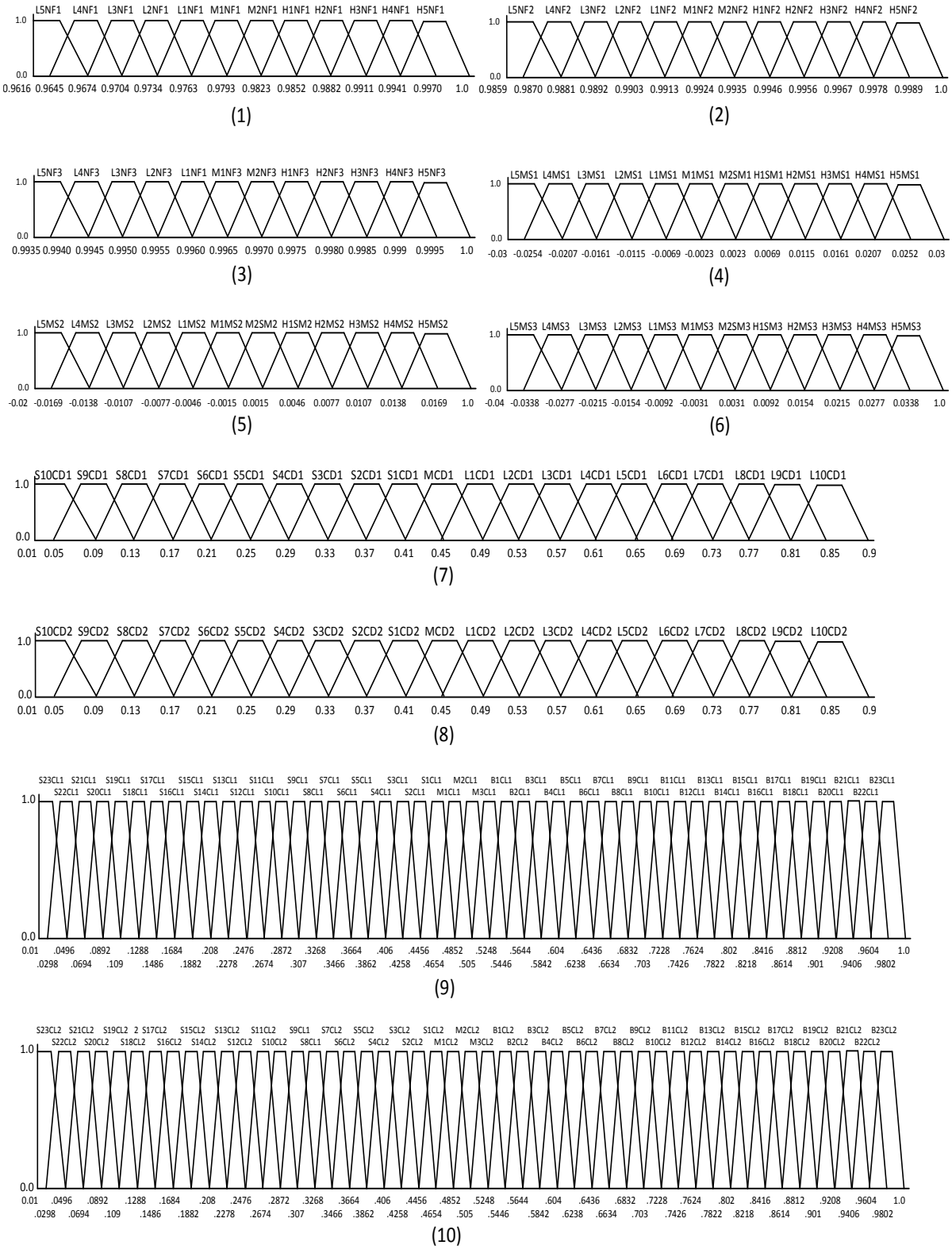

Figure 5.12 Trapezoidal fuzzy membership functions for (1, 2, 3) relative natural frequency of first three bending mode of vibration, (4, 5, 6) relative mode shape difference of first three bending mode of vibration, (7, 8) first and second crack depth and (9, 10) first and second crack location for steel beam

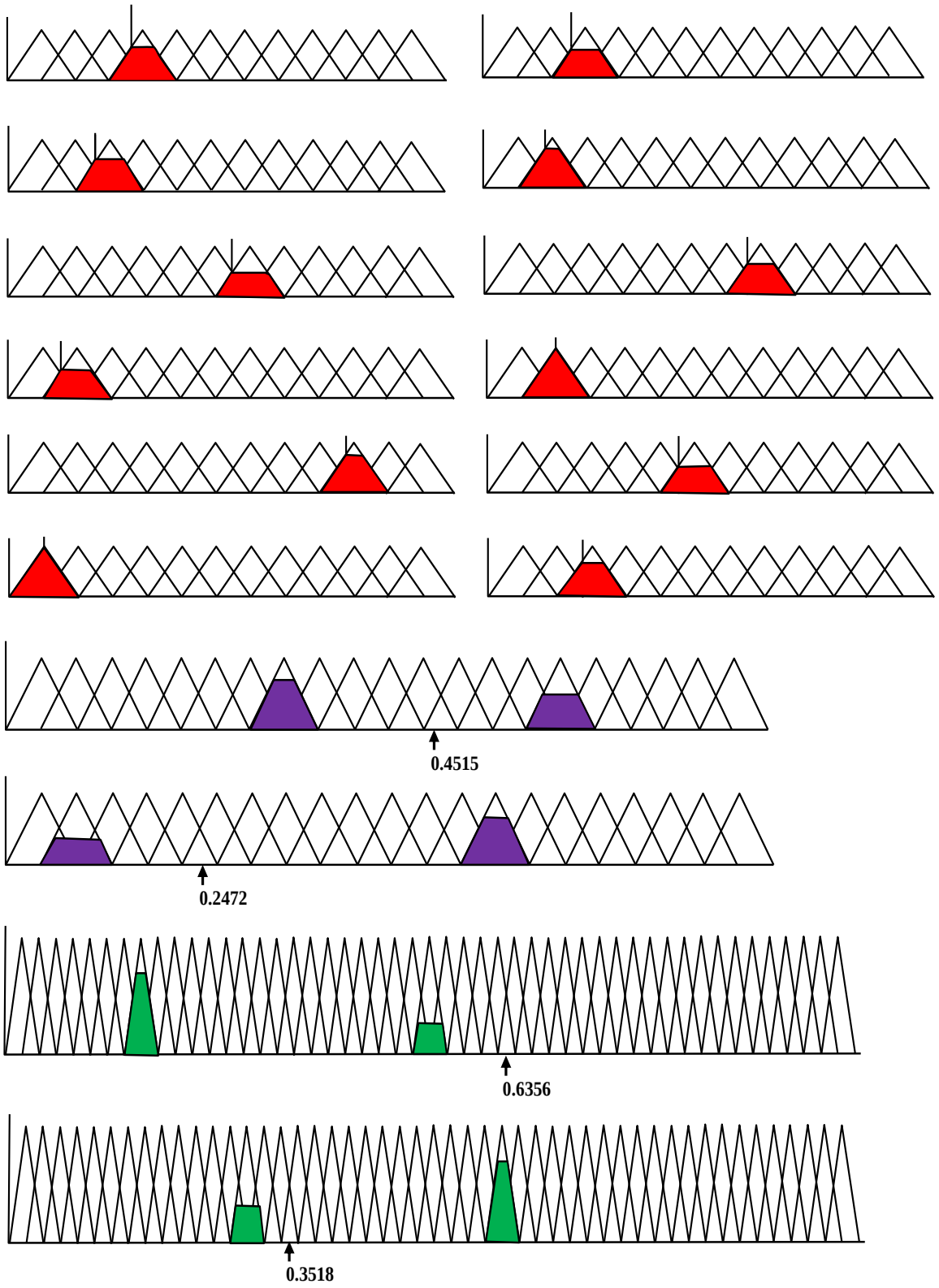

Figure 5.13 Aggregated values of first and second crack orientation (relative crack depths and relative crack locations) from triangular membership function when Rules 10 and 22 are activated of table 3 for steel beam.

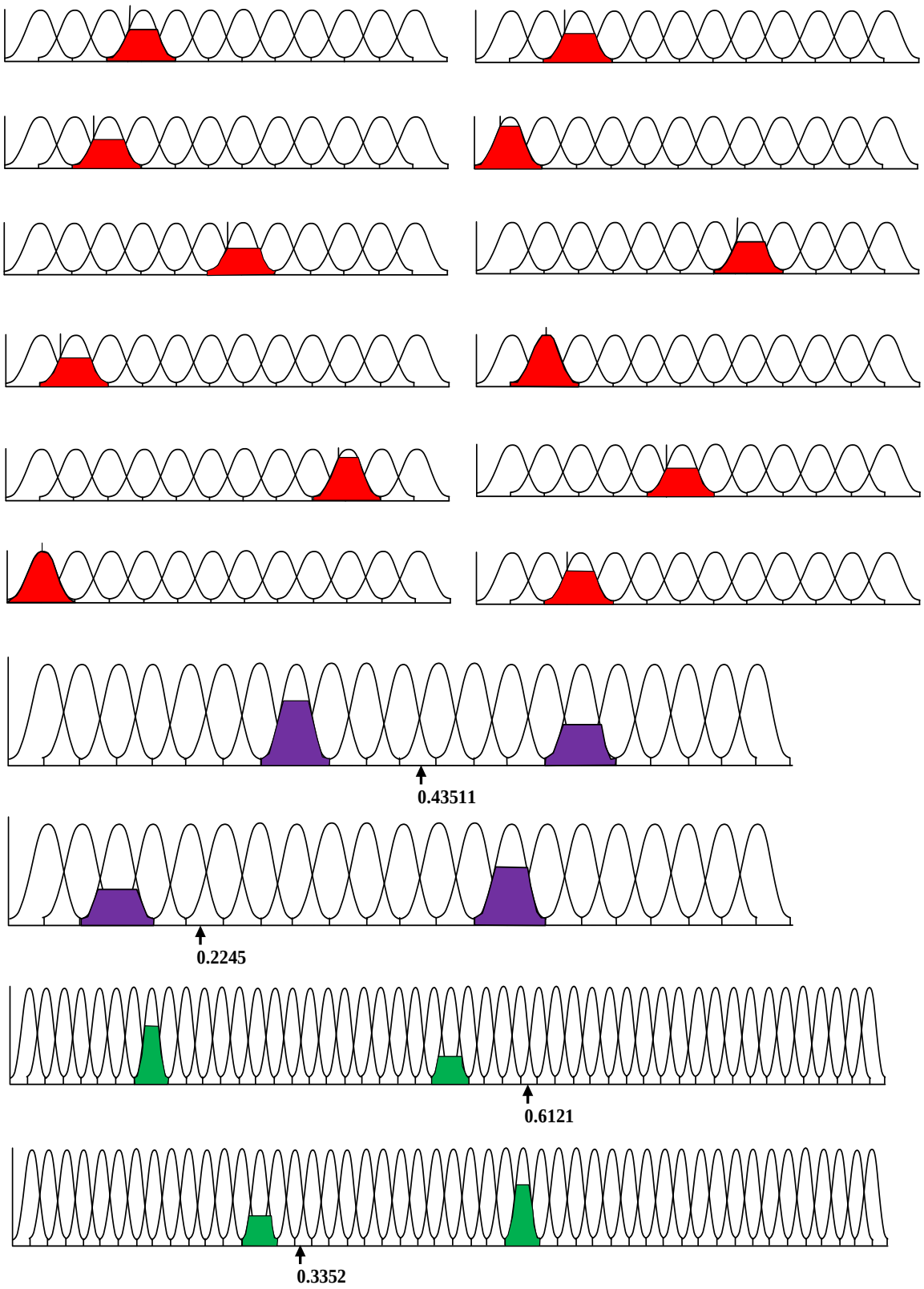

Figure 5.14 Aggregated values of first and second crack orientation (relative crack depths and relative crack locations) from Gaussian membership function when Rules10 and 22 are activated of table 3 for steel beam.

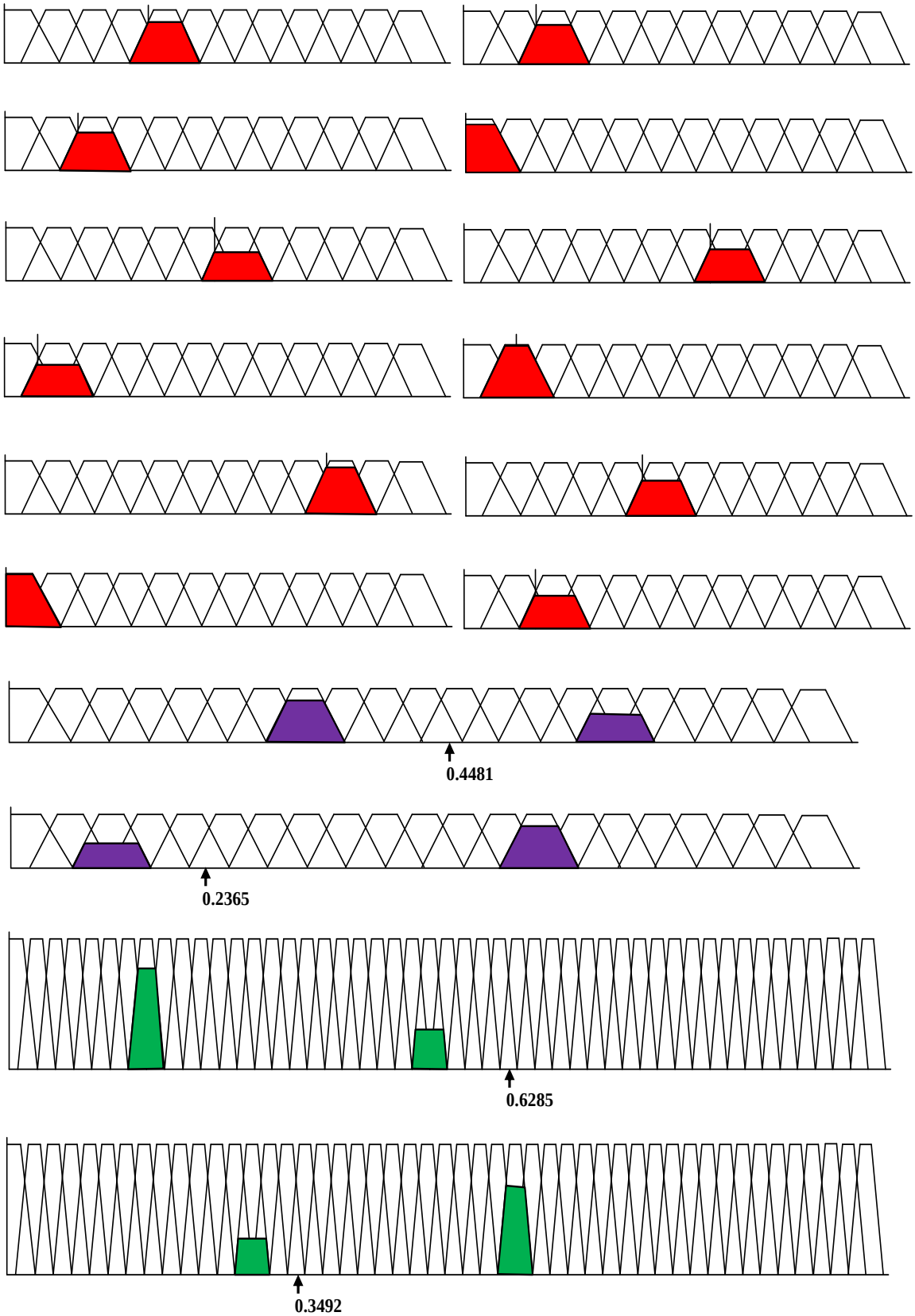

Figure 5.15 Aggregated values of first and second crack orientation (relative crack depths and relative crack locations) from trapezoidal membership function when Rules10 and 22 are activated of table 3 for steel beam.

5.4 Results and Discussion

The analysis of results derived from developed fuzzy models for identification of multiple cracks for composite and steel structure has been depicted in the current section. The fuzzy logic model has been developed with simple but effective architecture for six inputs variables (first three consecutive natural frequencies and mode shapes) and four outputs variables (relative first and second crack locations and depths). Three types of membership functions (Triangular, Gaussian and Trapezoidal) are used in the development of fuzzy system, presented in figures 5.1(a), 5.1(b) and 5.1(c). The various phase involved in the fuzzy logic system are shown in figure 5.2. Table 5.1 presents the various linguistic variables employed in the development of the fuzzy system. The membership functions (Triangular, Gaussian and Trapezoidal) with linguistic variables are shown in figures 5.3(a) to 5.3(c). The some fuzzy rule are presented in the table 5.2 for composite beam and table 5.3 for structural steel beam and are used for designing fuzzy logic based crack detection system. Figures 5.4 to 5.6 are represent Triangular, Gaussian and Trapezoidal membership functions for relative natural frequencies and mode shapes of first three modes of vibration, relative first and second crack depth and relative first and second crack location respectively for composite beam. Similarly figures 5.10 to 5.12 are represent membership functions for structural steel. The defuzzification of inputs using various membership functions (Triangular, Gaussian and Trapezoidal) have been performed with the help of activated rules 6 and 16 of table 5.2 and are presented in figures 5.7 to 5.9. Likewise for structural steel, it has been shown in the figures 5.13 to 5.15. The results derived from various fuzzy models (Triangular, Gaussian and Trapezoidal) and experimental test have been compared in table 5.4 for composite beam and likewise table 5.5 presents the comparison between results obtained from various method for structural steel. The tables 5.6 and 5.7 represent the comparison of results obtained from theoretical, finite element analysis and fuzzy Gaussian model for composite beam and structural beam respectively.

Table 5.4 Comparison of the results derived from Fuzzy Triangular, Fuzzy Gaussian, Fuzzy Trapezoidal model and Experimental (Composite beam)

Relative 1st natural frequency "rfnf"	Relative 2nd natural frequency "rsnf"	Relative 3rd natural frequency "rtnf"	Relative 1st mode shape difference "rfmd"	Relative 2nd mode shape difference "rsmd"	Relative 3rd mode shape difference "rtmd"	Experimental relative 1st crack location "rfcl" 1st crack depth "rfcd" 2nd crack location "rscl" 2nd crack depth "rscd"				Fuzzy Gaussian relative 1st crack location "rfcl" 1st crack depth "rfcd" 2nd crack location"rscl" 2nd crack depth "rscd"				Fuzzy Trapezoidal relative 1st crack location "rfcl" 1st crack depth "rfcd" 2nd crack location"rscl" 2nd crack depth "rscd"				Fuzzy Triangular relative 1st crack location "rfcl" 1st crack depth "rfcd" 2nd crack location "rscl" 2nd crack depth "rscd"			
						rfcl	rfcd	rscl	rscd	rfcl	rfcd	rscl	rscd	rfcl	rfcd	rscl	rscd	rfcl	rfcd	rscl	rscd
0.99607	0.99700	0.99829	0.00013	0.00203	0.00240	0.1875	0.1667	0.4375	0.250	0.178	0.158	0.415	0.237	0.174	0.154	0.405	0.232	0.172	0.153	0.402	0.230
0.98098	0.99557	0.99892	0.00275	0.00456	0.01064	0.125	0.4167	0.8750	0.333	0.119	0.395	0.830	0.316	0.116	0.386	0.810	0.308	0.115	0.383	0.804	0.306
0.99651	0.99425	0.99796	0.00079	0.00264	0.00101	0.3125	0.1667	0.5000	0.250	0.297	0.158	0.475	0.237	0.289	0.154	0.463	0.232	0.287	0.153	0.460	0.230
0.99001	0.99318	0.98710	0.00145	0.00571	0.00508	0.250	0.4167	0.5625	0.1667	0.237	0.395	0.534	0.158	0.232	0.386	0.521	0.154	0.230	0.383	0.517	0.153
0.98809	0.98584	0.98255	0.00288	0.01210	0.01352	0.375	0.5000	0.750	0.250	0.356	0.475	0.712	0.237	0.347	0.463	0.695	0.232	0.345	0.460	0.689	0.230
0.99672	0.98724	0.99719	0.00176	0.00332	0.00594	0.4375	0.2500	0.5625	0.333	0.415	0.237	0.534	0.316	0.405	0.232	0.521	0.308	0.402	0.230	0.517	0.306
0.99788	0.97843	0.97519	0.00284	0.01222	0.02349	0.5625	0.333	0.6875	0.500	0.534	0.316	0.652	0.475	0.521	0.308	0.637	0.463	0.517	0.306	0.632	0.460
0.99874	0.99877	0.99628	0.00026	0.00475	0.01519	0.625	0.0833	0.875	0.4167	0.593	0.079	0.830	0.395	0.579	0.077	0.810	0.386	0.574	0.077	0.804	0.383
0.99114	0.99799	0.99803	0.00010	0.00166	0.00183	0.1875	0.250	0.3125	0.250	0.178	0.237	0.297	0.237	0.174	0.232	0.289	0.232	0.172	0.230	0.287	0.230
0.99701	0.98999	0.99803	0.00153	0.00464	0.00239	0.4375	0.333	0.5625	0.1667	0.415	0.316	0.534	0.158	0.405	0.308	0.521	0.154	0.402	0.306	0.517	0.153
Average percentage of deviation										5.06	5.16	5.08	5.17	7.34	7.43	7.40	7.38	8.12	8.04	8.10	8.09
Total percentage of deviation										5.10				7.40				8.10			

Table 5.5 Comparison of the results derived from Fuzzy Gaussian model, Theoretical and FEA (Composite beam)

Relative 1st natural frequency "rfnf"	Relative 2nd natural frequency "rsnf"	Relative 3rd natural frequency "rtnf"	Relative 1st mode shape difference "rfmd"	Relative 2nd mode shape difference "rsmd"	Relative 3rd mode shape difference "rtmd"	Fuzzy Gaussian relative 1st crack location "rfcl" 1st crack depth "rfcd" 2nd crack location "rscl" 2nd crack depth "rscd"				Theoretical relative 1st crack location "rfcl" 1st crack depth "rfcd" 2nd crack location "rscl" 2nd crack depth "rscd"				FEA relative 1st crack location "rfcl" 1st crack depth "rfcd" 2nd crack location "rscl" 2nd crack depth "rscd"			
						rfcl	rfcd	rscl	rscd	rfcl	rfcd	rscl	rscd	rfcl	rfcd	rscl	rscd
0.99607	0.99700	0.99829	0.00013	0.00203	0.00240	0.178	0.158	0.415	0.237	0.180	0.160	0.421	0.241	0.182	0.162	0.424	0.242
0.98098	0.99557	0.99892	0.00275	0.00456	0.01064	0.119	0.395	0.830	0.316	0.120	0.401	0.842	0.320	0.121	0.404	0.848	0.323
0.99651	0.99425	0.99796	0.00079	0.00264	0.00101	0.297	0.158	0.475	0.237	0.301	0.160	0.481	0.241	0.303	0.162	0.485	0.242
0.99001	0.99318	0.98710	0.00145	0.00571	0.00508	0.237	0.395	0.534	0.158	0.241	0.401	0.541	0.160	0.242	0.404	0.545	0.162
0.98809	0.98584	0.98255	0.00288	0.01210	0.01352	0.356	0.475	0.712	0.237	0.361	0.481	0.722	0.241	0.363	0.485	0.727	0.242
0.99672	0.98724	0.99719	0.00176	0.00332	0.00594	0.415	0.237	0.534	0.316	0.421	0.241	0.541	0.320	0.424	0.242	0.545	0.323
0.99788	0.97843	0.97519	0.00284	0.01222	0.02349	0.534	0.316	0.652	0.475	0.541	0.320	0.661	0.481	0.545	0.323	0.666	0.485
0.99874	0.99877	0.99628	0.00026	0.00475	0.01519	0.593	0.079	0.830	0.395	0.601	0.080	0.842	0.401	0.606	0.081	0.848	0.404
0.99114	0.99799	0.99803	0.00010	0.00166	0.00183	0.178	0.237	0.297	0.237	0.180	0.241	0.301	0.241	0.182	0.242	0.303	0.242
0.99701	0.98999	0.99803	0.00153	0.00464	0.00239	0.415	0.316	0.534	0.158	0.421	0.320	0.541	0.160	0.424	0.323	0.545	0.162
Average percentage of deviation						5.06	5.16	5.08	5.17	3.82	3.83	3.78	3.77	3.08	2.99	3.06	3.15
Total percentage of deviation						5.10				3.80				3.10			

Table 5.6 Comparison of the results derived from Fuzzy Triangular, Fuzzy Gaussian, Fuzzy Trapezoidal model and Experimental (Steel beam)

Relative 1st natural frequency "rfnf"	Relative 2nd natural frequency "rsnf"	Relative 3rd natural frequency "rtnf"	Relative 1st mode shape difference "rfmd"	Relative 2nd mode shape difference "rsmd"	Relative 3rd mode shape difference "rtmd"	Experimental relative 1st crack location "rfcl" 1st crack depth "rfcd" 2nd crack location "rscl" 2nd crack depth "rscd"				Fuzzy Gaussian relative 1st crack location "rfcl" 1st crack depth "rfcd" 2nd crack location "rscl" 2nd crack depth "rscd"				Fuzzy Trapezoidal relative 1st crack location "rfcl" 1st crack depth "rfcd" 2nd crack location "rscl" 2nd crack depth "rscd"				Fuzzy Triangular relative 1st crack location "rfcl" 1st crack depth "rfcd" 2nd crack location "rscl" 2nd crack depth "rscd"			
						rfcl	rfcd	rscl	rscd	rfcl	rfcd	rscl	rscd	rfcl	rfcd	rscl	rscd	rfcl	rfcd	rscl	rscd
0.99939	0.99813	0.99978	0.00013	0.001063	0.004108	0.125	0.1667	0.250	0.3333	0.118	0.158	0.237	0.316	0.117	0.155	0.233	0.311	0.116	0.154	0.231	0.308
0.99980	0.99768	0.99664	0.00035	0.001084	0.000733	0.250	0.0833	0.500	0.1667	0.237	0.079	0.474	0.158	0.233	0.078	0.466	0.155	0.231	0.077	0.463	0.154
0.99952	0.97803	0.98418	0.00341	0.001338	0.02088	0.375	0.250	0.625	0.500	0.355	0.237	0.592	0.474	0.350	0.233	0.583	0.466	0.347	0.231	0.578	0.463
0.99889	0.99881	0.99932	0.00041	0.002245	0.003102	0.1875	0.3333	0.3125	0.1667	0.178	0.316	0.296	0.158	0.175	0.311	0.291	0.155	0.173	0.308	0.289	0.154
0.99906	0.98250	0.99800	0.00293	0.009652	0.00839	0.4375	0.500	0.6875	0.250	0.414	0.474	0.651	0.237	0.408	0.466	0.641	0.233	0.405	0.463	0.636	0.231
0.99958	0.99129	0.99869	0.00123	0.001865	0.006702	0.5625	0.3333	0.8125	0.0833	0.533	0.316	0.769	0.079	0.524	0.311	0.757	0.078	0.520	0.308	0.752	0.077
0.99971	0.98183	0.98589	0.00272	0.00638	0.00962	0.500	0.4167	0.75	0.500	0.474	0.395	0.710	0.474	0.466	0.388	0.699	0.466	0.463	0.385	0.694	0.463
0.99473	0.98761	0.98721	0.00239	0.007862	0.010996	0.3125	0.500	0.5625	0.3333	0.296	0.474	0.533	0.316	0.291	0.466	0.524	0.311	0.289	0.463	0.520	0.308
0.99230	0.99003	0.99182	0.00149	0.00455	0.00673	0.4375	0.250	0.6625	0.4167	0.414	0.237	0.627	0.395	0.408	0.233	0.617	0.388	0.405	0.231	0.613	0.385
0.99677	0.98931	0.99459	0.00152	0.00540	0.008654	0.625	0.4167	0.875	0.3333	0.592	0.395	0.829	0.316	0.583	0.388	0.816	0.311	0.578	0.385	0.809	0.308
Average percentage of deviation										5.32	5.26	5.28	5.22	6.73	6.77	6.80	6.82	7.49	7.56	7.5	5.4
Total percentage of deviation										5.3				6.8				7.5			

Table 5.7 Comparison of the results derived from Fuzzy Gaussian model, Theoretical and FEA (Steel beam)

Relative 1st natural frequency "rfnf"	Relative 2nd natural frequency "rsnf"	Relative 3rd natural frequency "rtnf"	Relative 1st mode shape difference "rfmd"	Relative 2nd mode shape difference "rsmd"	Relative 3rd mode shape difference "rtmd"	Fuzzy Gaussian relative 1st crack location "rfcl" 1st crack depth "rfcd" 2nd crack location "rscl" 2nd crack depth "rscd"				Theoretical relative 1st crack location "rfcl" 1st crack depth "rfcd" 2nd crack location "rscl" 2nd crack depth "rscd"				FEA relative 1st crack location "rfcl" 1st crack depth "rfcd" 2nd crack location "rscl" 2nd crack depth "rscd"			
						rfcl	rfcd	rscl	rscd	rfcl	rfcd	rscl	rscd	rfcl	rfcd	rscl	rscd
0.99939	0.99813	0.99978	0.00013	0.001063	0.004108	0.178	0.158	0.415	0.237	0.180	0.160	0.421	0.241	0.182	0.162	0.424	0.242
0.99980	0.99768	0.99664	0.00035	0.001084	0.000733	0.119	0.395	0.830	0.316	0.120	0.401	0.842	0.320	0.121	0.404	0.848	0.323
0.99952	0.97803	0.98418	0.00341	0.001338	0.02088	0.297	0.158	0.475	0.237	0.301	0.160	0.481	0.241	0.303	0.162	0.485	0.242
0.99889	0.99881	0.99932	0.000414	0.002245	0.003102	0.237	0.395	0.534	0.158	0.241	0.401	0.541	0.160	0.242	0.404	0.545	0.162
0.99906	0.98250	0.99800	0.00293	0.009652	0.00839	0.356	0.475	0.712	0.237	0.361	0.481	0.722	0.241	0.363	0.485	0.727	0.242
0.99958	0.99129	0.99869	0.00123	0.001865	0.006702	0.415	0.237	0.534	0.316	0.421	0.241	0.541	0.320	0.424	0.242	0.545	0.323
0.99971	0.98183	0.98589	0.00272	0.00638	0.00962	0.534	0.316	0.652	0.475	0.541	0.320	0.661	0.481	0.545	0.323	0.666	0.485
0.99473	0.98761	0.98721	0.00239	0.007862	0.010996	0.593	0.079	0.830	0.395	0.601	0.080	0.842	0.401	0.606	0.081	0.848	0.404
0.99230	0.99003	0.99182	0.00149	0.00455	0.00673	0.178	0.237	0.297	0.237	0.180	0.241	0.301	0.241	0.182	0.242	0.303	0.242
0.99677	0.98931	0.99459	0.00152	0.00540	0.008654	0.415	0.316	0.534	0.158	0.421	0.320	0.541	0.160	0.424	0.323	0.545	0.162
Average percentage of deviation						5.32	5.26	5.28	5.22	3.66	3.52	3.51	3.49	4.35	4.37	3.38	4.36
Total percentage of deviation						5.3				3.5				4.4			

5.5 Summary

The fuzzy logic method has been adopted in the current chapter to detect the fault in the both type of the cantilever beams and the following conclusions are drawn from present study.

The presence of the cracks in structural member upsets the vibration response of dynamic structures. The first three natural frequencies and mode shapes are fed as inputs to the fuzzy system and relative crack locations and relative crack depths are outputs of the developed fuzzy system. The robustness of proposed fuzzy models have been verified by comparing the results derived from fuzzy models with results derived from theoretical, finite element and experimental analysis. All results are in close proximity. Based on above study, it is found that fuzzy model with Gaussian membership function gives better results as comparison to theoretical, FEA, triangular and trapezoidal models for both types beams. Hence Gaussian fuzzy model can be effectively used for fault diagnosis. It is therefore the Gaussian fuzzy model results chosen to compare with other AI model, discussed in the next chapter to compare their effectiveness and performance in regard to Gaussian fuzzy model. The total percentage of deviation of results for triangular fuzzy model is 8.1%, for Gaussian fuzzy model is 5.1%, for Trapezoidal fuzzy model is 7.4% in the case of composite beam. Similarly for structural steel, total percentage of deviation of results for triangular fuzzy model is 7.5%, for Gaussian fuzzy model is 4.3 %, for Trapezoidal fuzzy model is 6.8%.

CHAPTER 6

Study of Neural Network for Identification of Multiple Cracks of Cantilever Beam

The presence of damage is a serious threat to proper functioning of structures and machines. Early detection of damage now has become the subject of serious concern for the researchers to secure the performance of systems. Since the last few years, many techniques have been applied to identify the fault in the engineering system. Few of them have used the sensors (Radiograph, Magnetic field, eddy current and thermal fields) to identify damage and others based on visual method (Dye penetration method). These methods consume much time to seize the fault in the system. Since last few years, some mathematical models and experimental investigations have been proposed by the researchers to determine the crack initiation and propagation.

In the current chapter, intelligent techniques have been applied based on artificial network techniques to locate the multiple cracks, present in the engineering system. The Back Propagation Neural Network (BPNN), Radial Basis Function Neural Network (RBFNN), and Kohonen Self-Organizing Maps (KSOM) have been used in the current study.

6.1 Introduction

The biological nervous system in a human body has massively parallel interconnected group of neurons enabled for the different type of output actions i.e. breathing, thinking and like other human activities. The ANN is robust and efficient due its novel structure of the information processing system.

The Artificial Neural Networks (ANNs) are simplified models of the biological central nervous system. ANN is a massively parallel distributed information processing system made up of highly interconnected neural computing elements that have the ability to learn and thereby acquire knowledge and make it available for use. Many researchers believe neural models offer a most promising integrated approach to build truly intelligent computer system. The biological network able to process millions of input stimuli in milisec even through the process is electrochemical in nature and, therefore, propagates relatively at slow milisec rate.

McCulloh and Pitts [163] have proposed several neural models and described how neurons worked with various assumptions. The proposed neural models based on the simple neurons, are considered as binary device with fixed threshold. Rosenblatt [164] has designed a novel perceptron. The proposed perceptron has three layers type of neural network, middle layer of perceptron is known as an associative layer. This perceptron could learn to connect with given input to a random output. Haykin [165] has defined that the neural network is highly parallel associated processing units called neurons, which has the ability to adopt the knowledge from available information and to make it available for use.

Since last few decades, many researchers have developed a health monitoring algorithm for the structural elements. The development of structural health monitoring techniques is a significant achievement of science fraternity because the presence of crack reduces the service life of the structural element and accountable for economic damage and in few cases may be loss of human life. The various non-destructive techniques are available in the literature for predicting the structural damage, that is not efficient in term of accuracy and computation time for real problems. Moreover the development of mathematical model for the complex problems is almost impossible. In the present analysis, application of ANN with adaptive learning, self-organization capacity, real time operation, fault tolerance ability and pattern recognition capability are suitable for design of an automated intelligent system. It is capable for fault recognition with very high accuracy and less are computation time for faulty dynamic structure. In the present scenario various scientist continuously engaged for developing a damage detection tool using ANNs.

In this section, three types of ANNs have been discussed (i.e. BPNN, RBFNN, and KSOM). All three types of ANNs are designed for six input variables (relative first three natural frequencies & relative first three mode shapes) and four output variables (relative first and second crack location and relative first and second crack depth). A comparison of results obtained from all three ANN models with results obtained from theoretical, numerical and experimental is done in current chapter. The RBFNN gives the best results as compared to other discussed ANNs models. Experimental investigation authenticates the fidelity of neural models.

6.2 Overview of Neural Network Technique

ANNs are computational parallel distributed information processing system. It is therefore effectively applied in many industrial applications such as fault diagnosis control & optimization, industrial process, and sale forecasting, etc. The ability to work

under challenging environment and parallel computing ability make ANNs most efficient and robust to solve the problem easily unlike using analytical methods.

An artificial neuron is acted like a device with many inputs and one output. The neuron is working on two modes of operation, one is training mode and another is using mode. The training mode of ANNs is more significant for potential and smooth results. In the training mode, neuron can be trained to fire (or not) for the specific input array. In the using mode, a learned input array is detected as the input, allied output becomes present output. If the input array does not belong in the learned input array list, the firing role is used to determine whether to fire or not.

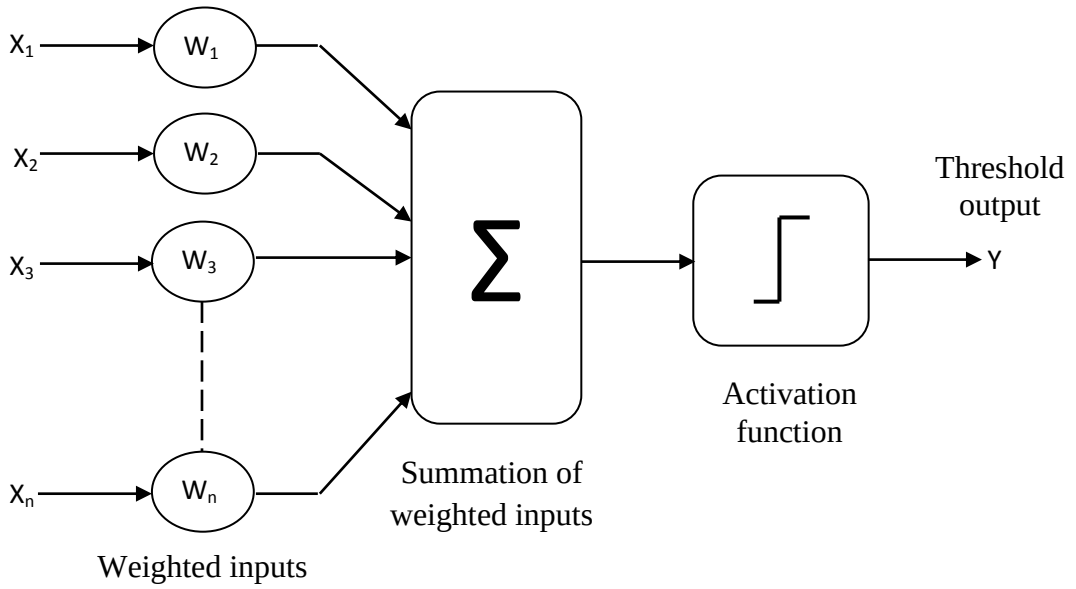

Figure 6.1 Simple model of an artificial neural network

The important characteristics of the neural network are depicted bellow.

(1) The input variables with synaptic weights are assigned to train neuron that turn upset the decision-making capacity of ANN. The inputs to the neuron with synaptic weight are also called weighted inputs.

(2) These weighted inputs are then summed together in summing point and if they exceed with pre-set threshold value, the neuron fires. Moreover, for any other cases neuron does not fire.

(3) For limiting the output of neuron, an activation function is provided. The most popular activation function is sigmoidal. Mostly the normalized amplitude range of the output of a neuron is given as closed unit interval [0, 1] or [-1, 1].

6.2.1 Type of learning process in ANNs

The learning process in ANNs is defined as adopted in an algorithm for updating the input weights to secure the adaptive nature of ANNs in the complex environments. The learning methods of ANN are broadly divided into the following three categories.

(a) Supervised learning

In the supervised learning both input and output data are provided to the network for proper training. When the inputs to the neuron of the network, the outputs of neuron have been compared to the target data through the learning process of the network, then weights are adjusted in order to bring the outputs closer to the targets.

(b) Unsupervised learning

This type of learning process does not require output data for the training of the network. The network modifies the weights as per the input response.

(c) Reinforcement learning

The learning of a score is provided with the help of algorithm instead of correct output for each input. The score represents the network performance over the sequence of inputs.
A neuron p can be described mathematically through the following equations:

$$u_p = \sum_{j=1}^{x} w_{pj} z_j \tag{6.1}$$

$$y_p = f(u_p) \tag{6.2}$$

Where: w_{p1}, w_{p2}... w_{px} are the synaptic weights of neuron p; z_1, z_2... z_x are the input signals; $f(\cdot)$ is the activation; u_p is the linear combined output; and y_p is the output signal of neuron.

6.3 Analysis of Back Propagation Neural Network

The multilayers neural network has been trained using back propagation algorithm and performance of the network is based on mean square error also called as approximate steepest gradient algorithm. The weights should be adjusted in such as way that the error between the actual output and desired output is minimum. This is the training process of neural network. The change in error has been calculated by managing the input weights.

6.3.1 Application of back propagation neural network for identification of crack

A back propagation neural network has been designed for identification of multiple crack of cantilever composite and steel beam. The BPNN model has been designed for six input and four output parameters. The input variables to the neural model are: 'rfnf', 'rsnf', 'rtnf', 'rfmd', 'rsmd' and 'rtmd'. The output variables of BPNN model are: 'rfcl', 'rfcd', 'rscl' and 'rscd'.

The BPNN model is made with one input layer, five hidden layers and one output layer. The input and output layer contain six and four neurons respectively. The input layer neurons represent the relative first, second & third natural frequencies and first, second & third mode shapes difference and similarly output layer neurons represent first & second crack location and first & second crack depth of the cantilever and steel beam. Figure 6.2 represents multiple layers back propagation neural network architecture for identification of multiple cracks.

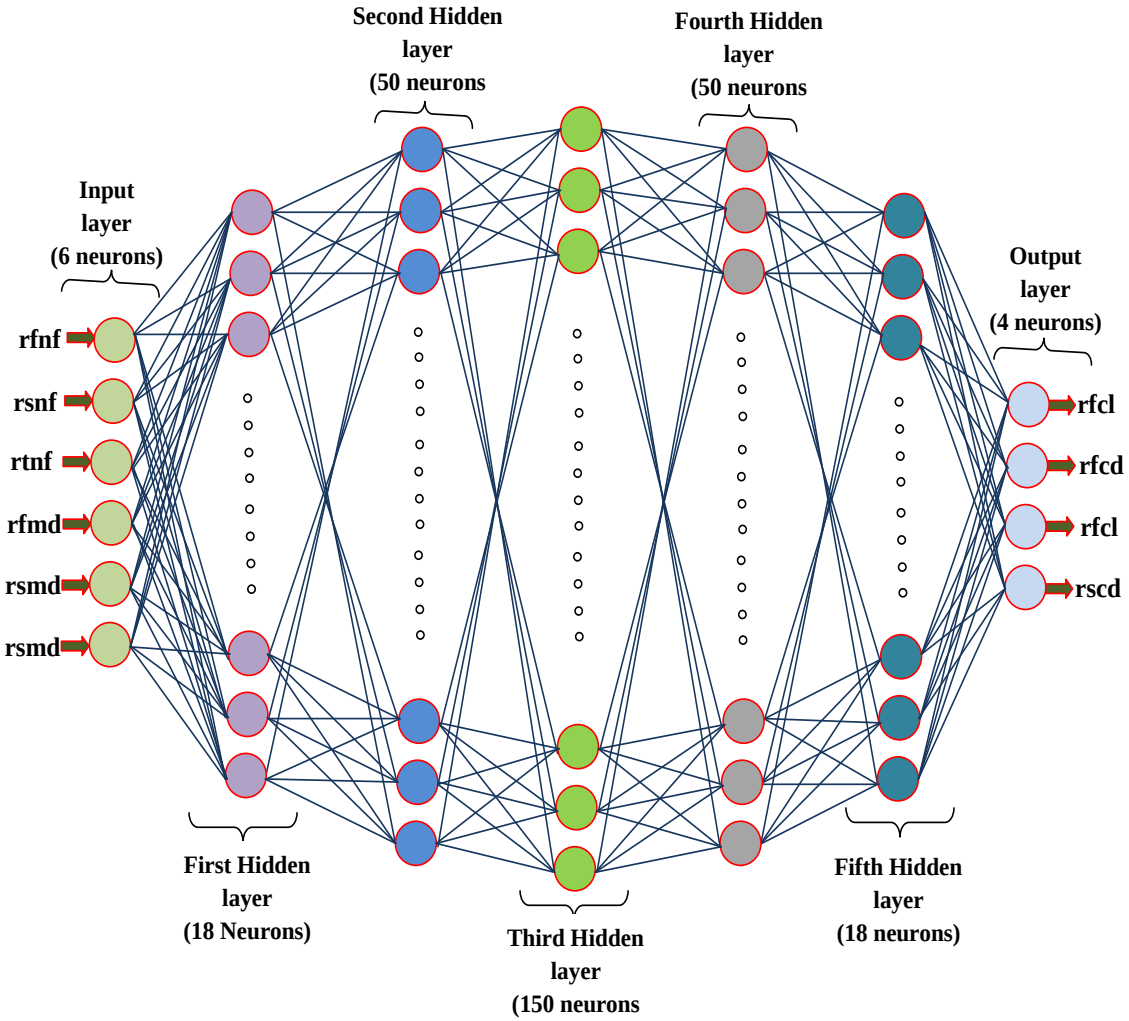

Figure 6.2 Multi layers back propagation neural network model for identification of multiple cracks

6.3.2 BPNN mechanism for prediction of crack

The neural network used in this section is seven layers feed forward neural model, trained with back propagation algorithm [165]. The number of layers has been chosen empirically. The input layer of BPNN represents the relative first three natural frequencies and relative first three mode shapes difference and relative first & second crack location and relative first & second crack depth are represented by output neuron of the BPNN. The number of neuron in hidden layers (1^{st}, 2^{nd}, 3^{rd}, 4^{th} and 5^{th}) is 18 neurons, 50 neurons, 150 neurons, 50 neurons and 18 neurons respectively. The number of neurons in hidden layers is decided using empirical relation. The designed BPNN model for prediction of crack is trained with 1000 data, obtained from various set of crack location and depth of the beam. The input parameters fed into BPNN associated with the following components.

$£_1$= deviation in first natural frequency.

$£_2$= deviation in second natural frequency.

$£_3$= deviation in third natural frequency.

$£_4$=deviation in first mode shape difference.

$£_5$=deviation in second mode shape difference.

$£_6$=deviation in third mode shape difference.

The output of BPNN due to sharing of input layer neuron to hidden layer neuron are given by [164]

$$f\left(V_j^{(L)}\right) = £_{\mathrm{i}}^{\mathrm{L}} \tag{6.4}$$

$$\text{Where: } V_j^{(L)} = \sum_i W_{ji}^{(L)} . £_{\mathrm{i}}^{(\mathrm{L\text{-}1})}, \tag{6.5}$$

Layer number (2 or 6) = L

j^{th} neuron in hidden layer labeled as 'L'= j

i^{th} neuron in hidden layer labeled as 'L-1'=i

$W_{ji}^{(L)}$= Weight of connection from 'i' neuron in layer 'L-1' to j neuron in layer 'L'

The activation function taken as

$$f(x) = \frac{e^x - e^{-x}}{e^x + e^{-x}} \tag{6.6}$$

In the training process output of the neural network $\Omega_{actual,n}(i = 1 to 4)$ may be differ from actual output $\Omega_{desired,n}(i = 1 to 4)$ as presented in training pattern of neural network. The

measure of the performance of neural network is instantaneous sum-squared difference between $\Omega_{actual,n}$ and $\Omega_{desired,n}$ for the set of given training patterns.

$$E_{error} = \frac{1}{2} \sum_{\substack{all\ training \\ pattern}} \left(\Omega_{desired,n} - \Omega_{actual,n}\right)^2 \tag{6.7}$$

Where;

Relative first crack location (rfcl) is represented by parameter $\Omega_{actual,n(n=1)}$

Relative second crack location (rscl) is represented by parameter $\Omega_{actual,n(n=2)}$

Relative first crack depth (rfcd) is represented by parameter $\Omega_{actual,n(n=3)}$

Relative second crack depth (rscd) is represented by parameter $\Omega_{actual,n(n=4)}$

BPNN model, error back propagation method is employed to train the network [164]. This model computes local error gradients to determine appropriate corrections to reduce error. The error gradient for output layer is:

$$\delta^{(7)} = f\left(V_1^7\right)\left(\Omega_{desired,n} - \Omega_{actual,n}\right) \tag{6.8}$$

Hence local gradients for hidden layer (L) neuron is represented by

$$\delta_j^{(L)} = f'\left(V_J^{(L)}\right)\left(\sum_k \delta_k^{(L+1)} W_{kj}^{(L+1)}\right) \tag{6.9}$$

The weights are modified as per the following terms:

$$W_{ji}(\tau+1) = W_{ji}(\tau) + \Delta W_{ji}(\tau+1) \tag{6.10}$$

$$\Delta W_{ji}(\tau+1) = \alpha \Delta W_{ji}(\tau) + \eta \Delta W_{ji}(\tau) + \eta \delta_j^L £_j^{(L-1)} \tag{6.11}$$

Where

α (momentum co-efficient) =0.2 (chosen statically)

η (learning rate)= 0.35 (chosen statically)

τ= iteration number

The final output of the BPNN can be expressed as:

$$\Omega_{actual,n} = f\left(V_n^7\right) \tag{6.12}$$

Where $\left(V_n^7\right) = \sum_i W_{ni}^7 £_i^6$

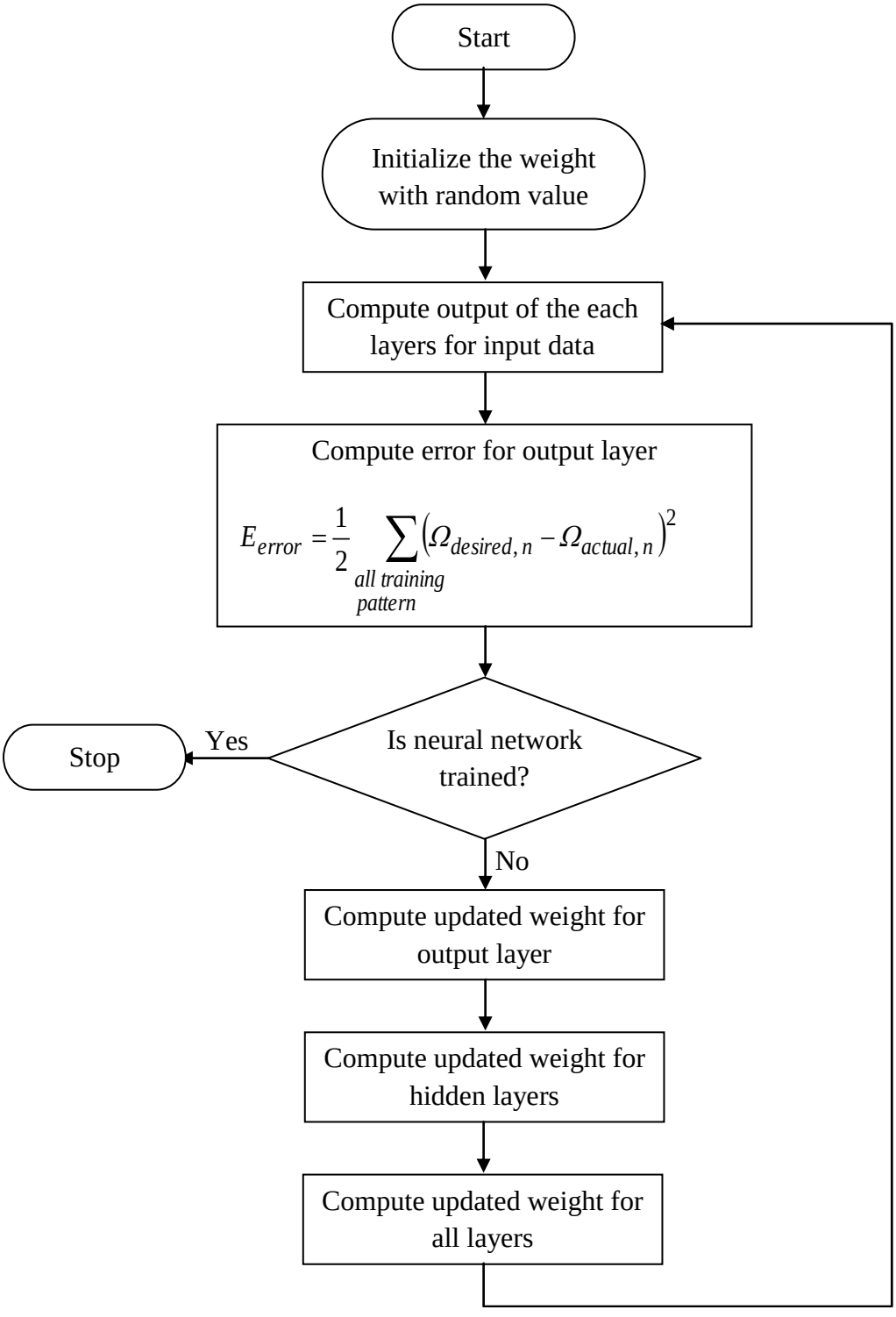

Figure 6.3 Flow chart for training process of BPNN

6.4 Analysis Radial basis function neural network

The radial basis function neural network, as a type of feed-forward neural network has recently attracted extensive research interest because of its simple architecture, high approximation and regularization capability, and good local specialization and global generalization ability. RBFNN is a powerful technique for interpolation in multi-dimensional space. The RBFNN chosen is usually a Gaussian-kernel transfer function, the response of such a function is positive for all input values. The RBF neural network consists of three layers: an input layer, a hidden layer, an output layer. Hidden units provide asset of functions that constitute an arbitrary basis for the input patterns.

1. Hidden units are known as radial centers. Each radial center can be represented by a vector.
2. The transformation from the input space to be hidden unit space is non-linear whereas the transformation from the hidden unit space to the output space is linear.

6.4.1 RBFNN Mechanism for identification of damage

A RBFNN is symmetrical about a center (RBF center) point in a multi-dimensional space. In the RBFNN, a number of hidden unit nodes with activation functions are connected in a feed forward parallel construction. The parameters associated with the RBFs are optimized during training. It is not, essentially, the value of these parameters is same throughout the network and also they are not directly related to or constrained by the actual training vectors.

RBF type of neural network is capable of universal approximation with one hidden layer. The expression for output of RBFNN can be presented as;

$$y_j(x) = \sum_{i=1}^{K} w_{ji} \exp\ (-\|c_i - z\|/\sigma_i^{\,2}) \qquad (6.13)$$

Where $y_j(x)$ = j^{th} output, w_{ji} = weight from the i^{th} RBF node to the j^{th} output node, c_i = center of the i^{th} RBF node, $\sigma_{i=}$ width of i^{th} RBF node, K= numbers of RBF nodes.

The RBF parameters w_{ji}, c_i and σ_i are commonly selected by random or regularly the c_i and then w_{ji} and σ_i are solved by singular value decomposition (SVD) method. Mostly this approach is found not satisfactory. An improved and satisfactory approach, proposed by Leonard et al [164], the RBF parameters $c_{i,}$ w_{ji} and σ_i can be determined by using K-means clustering, multiple linear regression and K-nearest heuristic respectively. A set of cluster centers and a share of the training data into subsets are determined by K-means

clustering algorithm. Each cluster center is then associated with one of the RBF centers in the hidden layer. After the establishment of centers, the width of each center is determined to shield the training points to allow a smooth and desirable RBFN controller outputs. The width is carefully chosen in this way, the σ_i is greater than the distance to the nearest RBF center, but also try to keep its distance as small as possible to influence, its local region. Details of the algorithm used for designing the RBF are discussed below.

Assume that the r-input for the training of the present RBFNN model. Because all inputs are connected to the hidden node, each node has an r -dimensional center, but only one width value is used to scale all r -dimensions. The setting of the value of these centers and widths is discussed below.

Assume x_{1L}, x_{2L}, x_{3L} …..... x_{rL} are the component of the incoming vector $X_{L.}$ The $v_i(x_L)$ is the output of i^{th} unit in the hidden layer for given input pattern, can be present as

$$v_i(x_L) = \exp\left[-\sum_{j=l}^{r} (x_{ji} - c_{ji})^2 \right] / \sigma_i^2 \qquad (6.14)$$

Where c_{ji} is the center of the RBF unit for input variables, σ_i is the width of i^{th} RBF unit, x_{ji} is j^{th} variable of input patterns.

The output "y_{mt}" of the m^{th} output node is equal to the summation of the weighted outputs of the hidden units, given by;

$$y_{mt} = \sum_{i=1}^{K} w_{im} v_i(x_L) \qquad (6.15)$$

Where k is the number of hidden layer nodes, y_{mt} is the output value of m^{th} node in output layer for the i^{th} incoming pattern, w_{im} is the weight between the i^{th} RBF unit and the m^{th} output node.

6.4.1.1 Determination of the RBF centers

A set of clusters has been found by 'K-means' clustering algorithm, each cluster with r-dimensional centers from the given training data. The dimensions of the centers are calculated by the number of variables or nodes of the input layer. The cluster centers then become the centers of the RBF units. The number of clusters, k, is a design parameter and calculates the number of RBF units (nodes in the hidden layer). The 'K-means' clustering algorithm proceeds as follows;

(1) Different randomly selected training pattern has been used to initialize the progress of each cluster.

(2) The Euclidean distance between the training patterns and the cluster centers can be calculated through assigning each training pattern to a nearest cluster.

(3) Determine the average position for each other center after assigning each training pattern to a nearest cluster. They then become new cluster centers.

(4) The steps 2 and 3 repeat, until the new cluster centers do not change during the successive iterations.

6.4.1.2 Determination of the RBF unit widths

The widths of each RBF can be determined after locating the RBF centers. The width of any RBF distance to the nearest β RBF units, where β is a design parameter for the RBFNN, for unit is given by

$$\sigma_i = \sqrt{\left[\frac{1}{\beta}\sum_{j=1}^{\beta}\sum_{K=1}^{K}(\hat{x}_{ki} - \hat{x}_{kj})^2\right]} \tag{6.16}$$

Where $\hat{x}_{ki}$ and $\hat{x}_{kj}$ are the k[th] entries of the centers of the i [th] and j [th] hidden units.

6.4.1.3 Determination of the weights

The calculation of the weights depends on the selection of centers and widths of the RBF units, then the M training patterns are moved through the hidden RBFN nodes and produced a B=K ×M matrix. Assumed S = T× M desired output matrix for the training patterns and T be the number of output nodes. The main objective is to find the weights that minimize the error between the actual output and the desired output of the network. Basically, we are trying to minimize the objective function

$$\|S - WB\| \tag{6.17}$$

Where W is the T × K matrix of weights on the connections between the hidden and output nodes of the network. The selection of weights between the hidden layer and the output layer is computed by linear least square regression. The solution to the previous equation can be obtained using the pseudo-inverse of B and is given by;

$$W = S\,B^{T}(B\,B^{T})^{-1} \tag{6.18}$$

6.4.1.4 Selection of K and β

The design parameters, i.e. the number of RBF units in the hidden layer 'K' and the value of overlap parameter 'β' for the nearest neighbor method, are selected by the model builder to achieve the optimal RBF network structure for better performance. The

parameters can be easily determined by using an S-fold cross-validation method (SFCV) [165], the procedure is as follows:

(1) Training data are randomly divided into P equal sized sets.

(2) For a given K and β, RBFNN is trained using P -1 data sets.

(3) The remaining subset is used to test the network's local specialization and global generalization ability.

(4) The mean square difference between the target output and the predicted output is the error associated with test subsets.

(5) This procedure is repeated S times using different P– 1 subsets for training and a different subset for testing at each time.

(6) The mean square error is the error for all the testing set for the proposed RBF network.

(7) This procedure is repeated several times with different values of K and β to obtain the optimum network structure with minimum mean square error.

6.4.2 Application of radial basis function neural network for identification of crack

A radial basis function neural network is designed for identification of multiple cracks of cantilever composite and structural steel beam. The RBFNN model has been designed for six input and four output variables. The input variables to the neural model are: 'rfnf', 'rsnf', 'rtnf', 'rfmd', 'rsmd' and 'rtmd'. The output variables are: 'rfcl', 'rfcd', 'rscl' and 'rscd'.

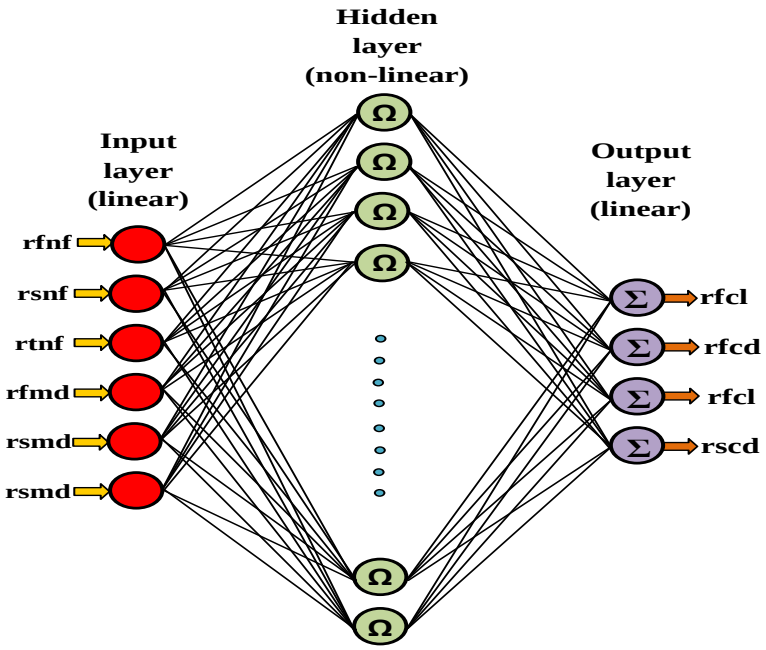

Figure 6.4 RBFNN models for identification of multiple cracks

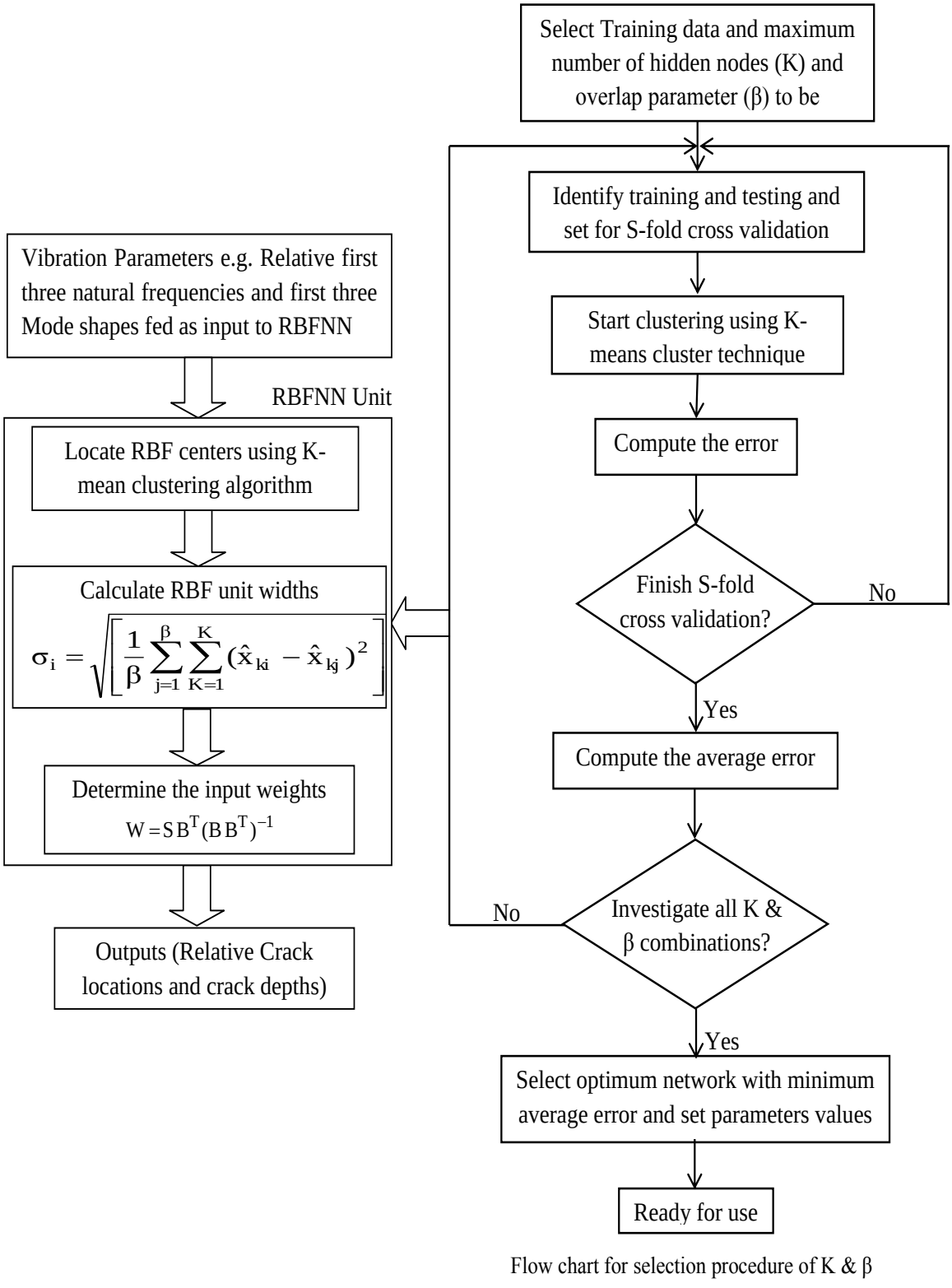

Flow chart for selection procedure of K & β

Figure 6.5 Flowchart for damage detection using RBFNN technique

6.5 Analysis of Kohonen self-organizing maps

Kohonen Self-Organizing Maps in sort Self-Organizing Maps (SOMs) and can be defined as a competitive unsupervised learning type of neural network, invented by Finnish Professor Tuevo Kohonen in 1982 [168]. The invention of the SOM was motivated by way of microbiological structure of different sensory inputs like visual, motion, auditory and acoustic inputs are mapped on their respective area of cerebral cortex topographically ordered computational map. The SOMs differ from other artificial neural networks in the sense that they use a neighborhood function to prevent the topological properties of the input space. This type of neural network is a popular nonlinear technique for dimensionality reduction and data visualization.

6.5.1 Kohonen Self-organizing Maps Mechanism

The training of the Kohonen's self-organizing maps is performed by using a specific algorithm. The algorithm responsible for formation of self-organizing maps proceeds first by synaptic weight in network. The complete process or mechanism can be categorized into four parts, i.e. Initialization; Competition Mechanism; Co-operative Mechanism and Adaptive Mechanism**.**

(a) Initialization:

Each node weights present in the lattice are initialized. An input vector is randomly chosen from a set of training data. When the input vector is presented in the map; the distance of the weight vector to each node is computed. The map returns the closest node which is called the Best Matching Unit (BMU) or winner neuron as shown figure 6.6.

(b) Competition Mechanism:

For each input pattern the neurons in the network compute their respective value that is a discriminant function. This discriminant function provides the platform for competition among the neuron. The particular neuron with largest value of discriminant function is declared winner of competition or best match unit. A best match unit (BMU) also called winner neuron has been found from output neurons in this part of the mechanism.

$$[\vec{a}] = [a_1, a_2, ..., a_m]^T \tag{6.19}$$

Where, $\vec{a}$ = input vectors, m= dimensional input

$$[\vec{w}_i] = [w_{i1}, w_{i2}, ..., w_{il}] \tag{6.20}$$

Where, i= 1,2,3,4,...,l, l= Number of output neurons

$[\vec{w}_i]$=Weight vector

Every output is connected to all inputs. There will be $m \times 1$ number of arrays. We have to determine the best match between $\vec{a}$ and $\vec{w}_i$. Compute $w_i^T.x$ for i=1, 2 …l.

Winner neuron= arg maximize $(w_i^T.a)$,

The Euclidian distance can be defined as $\left(\|\vec{a} - w_i\|\right)$

Winner neuron= arg max $(w_i^T.\vec{a})$=arg min $\left(\|\vec{a} - w_i\|\right)$ (6.21)

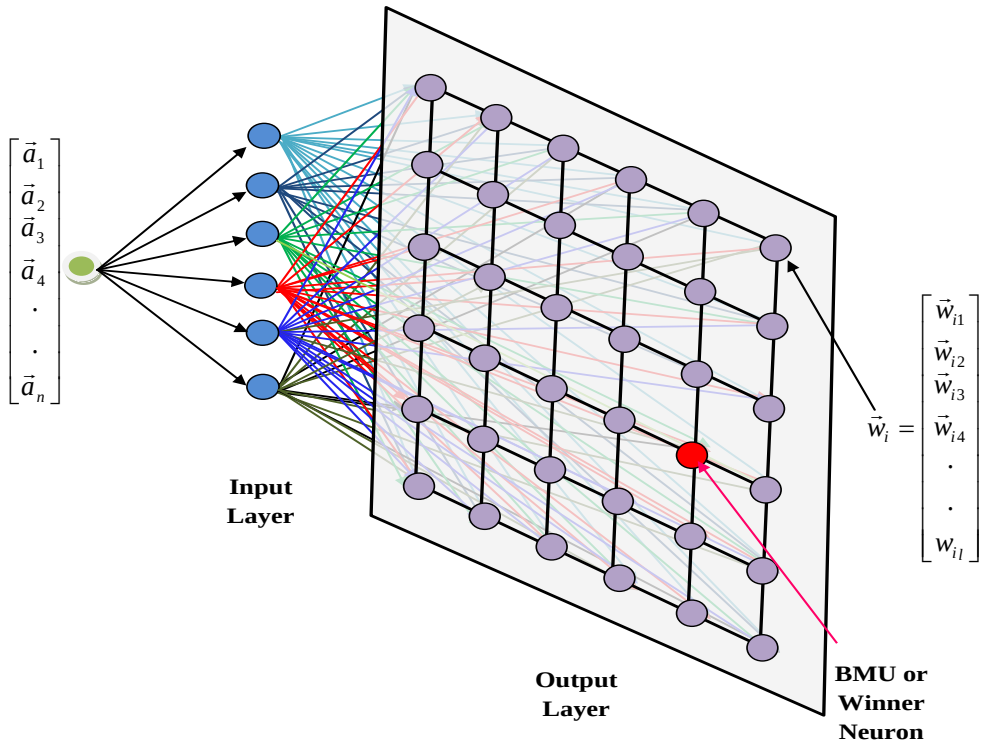

Figure 6.6 Initialization process in Kohonen SOM Network

(c) Co-operative Mechanism:

The winning neuron locates the center of a topological neighborhood of co-operating neurons. All the neighborhood neuron of the winner neuron should adjust their weights in this step.

If the winner neuron is 'j' then topological neighborhood:

$c_{i,j}$:Topological neighborhood centered on j; encompassing neuron i.

$x_{i,j}$:Lateral distance between the winning neuron 'j'and excited neuron 'i'.

Satisfying two properties:

Symmetric about $x_{i,j} \rightarrow 0$ and considering monotonically decaying function, we can get

$$c_{i,j}(\vec{a}) = \exp\left(\frac{-x_{i,j}^2}{2\sigma}\right) \quad (6.22)$$

Where σ=width of Gaussian function, σ is not constant with time/iteration. As the iteration

Processes, σ is going to be decreased. The topological neighborhood $c_{i,j}$ shrinks and narrow down with time.

$$\sigma(t) = \sigma_0 \exp\left(-\frac{t}{\lambda_l}\right), \quad (6.23)$$

t= number of iterations, $\sigma_{0=}$Initial, σ (at t=0), λ_l=time constant

σ is a function of iteration number. When $t=\lambda_l$, σ(t)decreases to 0.37 of its maximum value. t= 0, 1, 2. .

$$c_{i,j}(\vec{a}) = \exp\left(\frac{-x_{i,j}^2}{2\sigma^2(t)}\right) \quad (6.24)$$

$c_{i,j}$ ($\vec{a}$) is called the neighborhood function (the more a node is far from the BMU the smaller value is returned by this function).

(d) Adaptive Mechanism

This process enables the excited neuron to increase their individual value of discriminant function in relation with input pattern through suitable adjustment applied to their synaptic weight. The adjustments are made such that the response of BMU to subsequent application of similar input pattern is enhanced. This step has been done to update the weight in relation with input data.

$$\vec{w}_i(t+1) = \vec{w}_i(t) + \psi(t)\, c_{i,j}(t)\, (\vec{a}\text{-}\vec{w}_i(t)) \;\&\; \psi(t) = \psi_0 \exp\left(-\frac{t}{\lambda_2}\right) \quad (6.25)$$

Where $\psi(t)$ = leaning rate and λ_2= another time constant

6.5.2 Application of Kohonen Self Organizing Maps for identification of Damage

The relative first three natural frequencies (relative 1st natural frequency="rfnf", relative 2nd natural frequency= "rsnf" and relative 3rd natural frequency="rtnf") and first three relative mode shape difference (relative 1st mode shape difference= "rfmd", relative 2nd mode shape difference="rsmd" and relative 3rd mode shape difference="rtmd") are the input parameters for Kohonen self-organizing maps network and relative first crack location= "rfcl", relative first crack depth="rfcd", relative second crack location= "rscd"

and relative second crack depth= “rscd” are the outputs of the KSOM. The architecture of KSOM for identification of cracks is shown in figure 6.7.

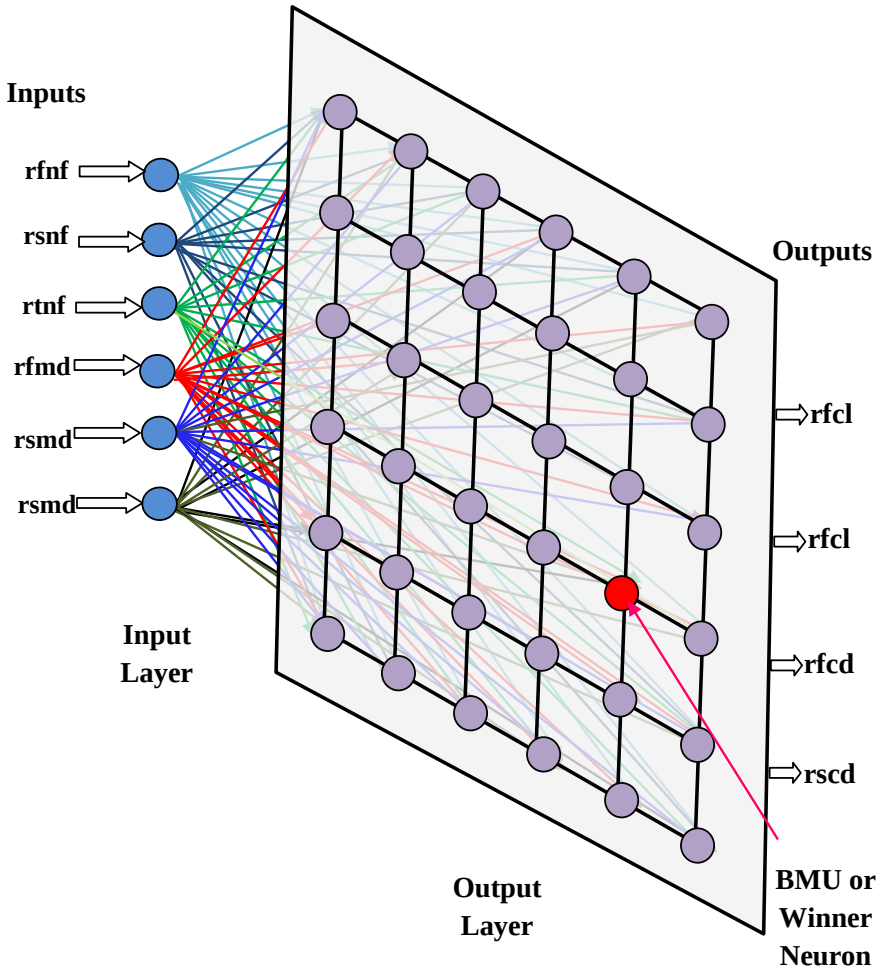

Figure 6.7 KSOM neural model for identification of multiple cracks

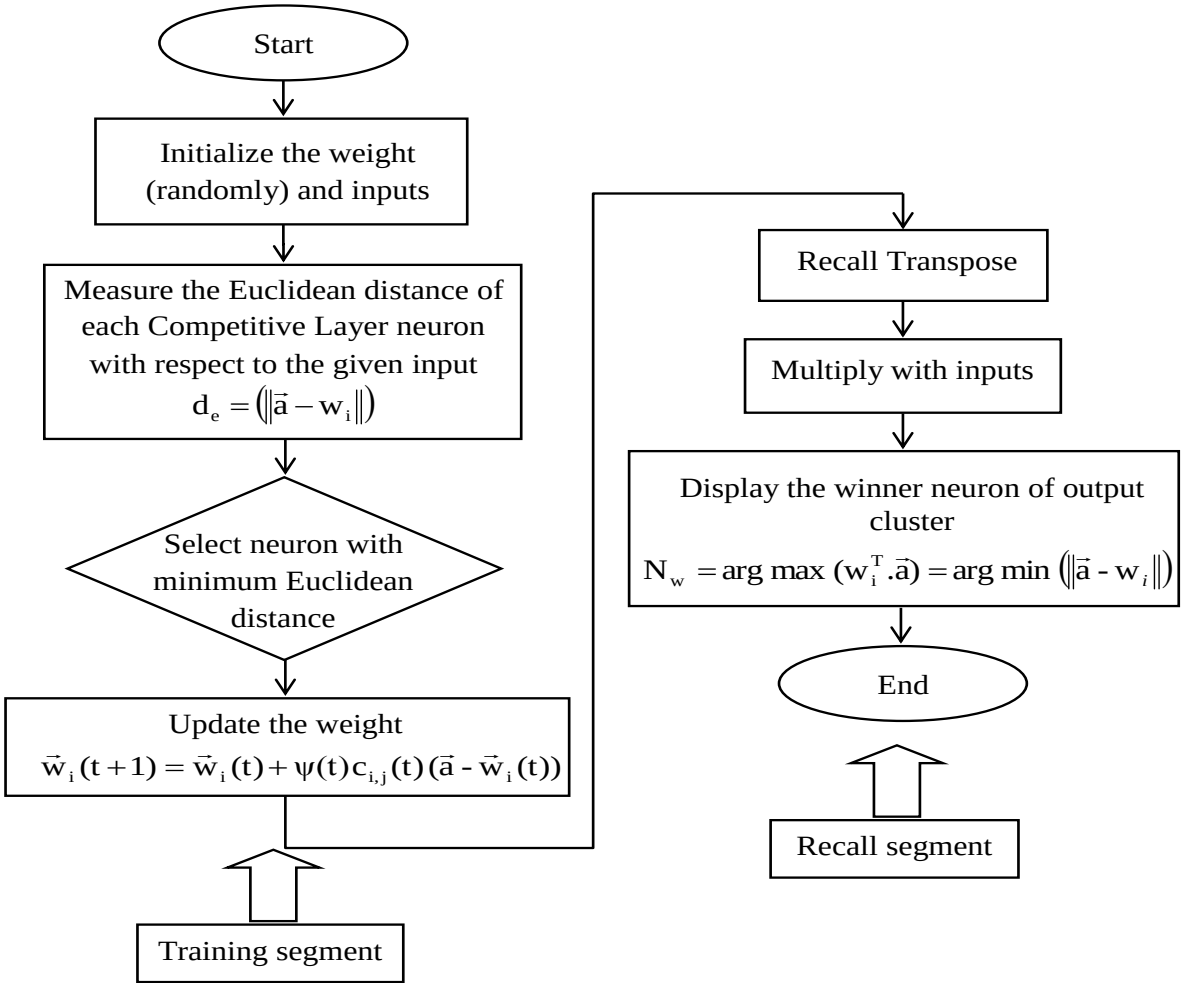

Figure 6.8 Flowchart for Kohonen SOM process

6.6 Results and Discussion

This section depictes the discussion on analysis of results derived from various neural models such as BPNN, RBFNN and KSOM. Figure 6.1 presents the simple architecture of an artificial neural network. The seven layered back propagation neural network technique for recognition of first and second crack locations and depths is presented in figure 6.2. First three natural frequencies and mode shapes of bending mode of vibration have been used as input variables to input layer of BPNN model. These input variables process through five hidden layers then output layer gives relative first and second crack depths and locations. The Flow chart for training process of BPNN has been shown in figure 6.3. The RBFNN is a feed forward, supervised learning type of neural network. It has approximation and regularization capacity. In present work, the RBFNN has been employed for localization and quantification of cracks present in the cantilever composite and structural steel beam. Similar to BPNN model, RBFNN consist of one input layer and

output layer but RBFNN has only one hidden layer. The input data is fed into input layer. Output layer gives relative crack locations and crack depths. Figure 6.4 presents RBFNN model for identification of multiple cracks. The procedure of damage detection of beam using RBFNN model has been displayed in the flowchart (figure 6.5). Likewise BPNN and RBFNN model, Kohonen SOM type of neural network has been discussed in this chapter for estimation of multiple cracks present in the composite and steel beam. KSOM is a competitive un-supervised learning type neural network. The complete working procedure of KSOM can be characterized in four steps: Initialization phase, competition mechanism, co-operation mechanism and adaptive mechanism. The initialization and competition process of KSOM for identification of multiple cracks are shown in figures 6.6 and 6.7 respectively. The flowchart for KSOM mechanism is shown in the figure 6.8. The results obtained from neural network techniques (BPNN, RBFNN, and KSOM) and experimental test are compared and close agreement is observed between each other. The results derived from BPNN, RBFNN and KSOM model are compared with experimental analysis results and are presented in table 6.1 and table 6.3 for composite beam and steel beam respectively. The results obtained from RBFNN, fuzzy Gaussian model, theoretical and finite element method have been compared in tables 6.2 and 6.4 for composite and steel beam respectively. It is observed that the RBFNN model gives better results as compared to fuzzy Gaussian model for composite as well as structural steel beam.

Table 6.1 Comparison of the results derived from RBFNN, BPNN, KSOM model and experimental (Composite beam)

Relative 1st natural frequency "rfnf"	Relative 2nd natural frequency "rsnf"	Relative 3rd natural frequency "rtnf"	Relative 1st mode shape difference "rfmd"	Relative 2nd mode shape difference "rsmd"	Relative 3rd mode shape difference "rtmd"	Experimental relative 1st crack location "rfcl" 1st crack depth "rfcd" 2nd crack location "rscl" 2nd crack depth "rscd"				RBFNN relative 1st crack location "rfcl" 1st crack depth "rfcd" 2nd crack location "rscl" 2nd crack depth "rscd"				BPNN relative 1st crack location "rfcl" 1st crack depth "rfcd" 2nd crack location "rscl" 2nd crack depth "rscd"				KSOM relative 1st crack location "rfcl" 1st crack depth "rfcd" 2nd crack location "rscl" 2nd crack depth "rscd"			
						rfcl	rfcd	rscl	rscd	rfcl	rfcd	rscl	rscd	rfcl	rfcd	rscl	rscd	rfcl	rfcd	rscl	rscd
0.99607	0.99700	0.99829	0.00013	0.00203	0.00240	0.1875	0.1667	0.4375	0.250	0.179	0.159	0.417	0.239	0.178	0.159	0.416	0.238	0.177	0.158	0.414	0.237
0.98098	0.99557	0.99892	0.00275	0.00456	0.01064	0.125	0.4167	0.8750	0.333	0.119	0.398	0.835	0.318	0.119	0.396	0.832	0.317	0.118	0.394	0.828	0.315
0.99651	0.99425	0.99796	0.00079	0.00264	0.00101	0.3125	0.1667	0.5000	0.250	0.298	0.159	0.477	0.239	0.297	0.159	0.476	0.238	0.296	0.158	0.473	0.237
0.99001	0.99318	0.98710	0.00145	0.00571	0.00508	0.250	0.4167	0.5625	0.1667	0.239	0.398	0.537	0.159	0.238	0.396	0.535	0.159	0.237	0.394	0.532	0.158
0.98809	0.98584	0.98255	0.00288	0.01210	0.01352	0.375	0.5000	0.750	0.250	0.358	0.477	0.716	0.239	0.357	0.476	0.713	0.238	0.355	0.473	0.710	0.237
0.99672	0.98724	0.99719	0.00176	0.00332	0.00594	0.4375	0.2500	0.5625	0.333	0.417	0.239	0.537	0.318	0.416	0.238	0.535	0.317	0.414	0.237	0.532	0.315
0.99788	0.97843	0.97519	0.00284	0.01222	0.02349	0.5625	0.333	0.6875	0.500	0.537	0.318	0.656	0.477	0.535	0.317	0.654	0.476	0.532	0.315	0.650	0.473
0.99874	0.99877	0.99628	0.00026	0.00475	0.01519	0.625	0.0833	0.875	0.4167	0.596	0.079	0.835	0.398	0.594	0.079	0.832	0.396	0.591	0.079	0.828	0.394
0.99114	0.99799	0.99803	0.00010	0.00166	0.00183	0.1875	0.250	0.3125	0.250	0.179	0.239	0.298	0.239	0.178	0.238	0.297	0.238	0.177	0.237	0.296	0.237
0.99701	0.98999	0.99803	0.00153	0.00464	0.00239	0.4375	0.333	0.5625	0.1667	0.417	0.318	0.537	0.159	0.416	0.317	0.535	0.159	0.414	0.315	0.532	0.158
Average percentage of deviation										4.62	4.58	4.63	4.57	4.93	4.88	4.90	4.94	5.43	5.44	5.39	5.33
Total percentage of deviation										4.60				4.91				5.40			

Table 6.2 Comparison of the results derived from RBFNN, Fuzzy Gaussian model, Theoretical and FEA (Composite)

Relative 1st natural frequency "rfnf"	Relative 2nd natural frequency "rsnf"	Relative 3rd natural frequency "rtnf"	Relative 1st mode shape difference "rfmd"	Relative 2nd mode shape difference "rsmd"	Relative 3rd mode shape difference "rtmd"	RBFNN controller relative 1st crack location "rfcl" 1st crack depth "rfcd" 2nd crack location "rscl" 2nd crack depth "rscd"				Fuzzy Gaussian relative 1st crack location "rfcl" 1st crack depth "rfcd" 2nd crack location "rscl" 2nd crack depth "rscd"				Theoretical relative 1st crack location "rfcl" 1st crack depth "rfcd" 2nd crack location "rscl" 2nd crack depth "rscd"				FEA relative 1st crack location "rfcl" 1st crack depth "rfcd" 2nd crack location "rscl" 2nd crack depth "rscd"			
						rfcl	rfcd	rscl	rscd	rfcl	rfcd	rscl	rscd	rfcl	rfcd	rscl	rscd	rfcl	rfcd	rscl	rscd
0.99607	0.99700	0.99829	0.00013	0.00203	0.00240	0.179	0.159	0.417	0.239	0.178	0.158	0.415	0.237	0.180	0.160	0.421	0.241	0.182	0.162	0.424	0.242
0.98098	0.99557	0.99892	0.00275	0.00456	0.01064	0.119	0.398	0.835	0.318	0.119	0.395	0.830	0.316	0.120	0.401	0.842	0.320	0.121	0.404	0.848	0.323
0.99651	0.99425	0.99796	0.00079	0.00264	0.00101	0.298	0.159	0.477	0.239	0.297	0.158	0.475	0.237	0.301	0.160	0.481	0.241	0.303	0.162	0.485	0.242
0.99001	0.99318	0.98710	0.00145	0.00571	0.00508	0.239	0.398	0.537	0.159	0.237	0.395	0.534	0.158	0.241	0.401	0.541	0.160	0.242	0.404	0.545	0.162
0.98809	0.98584	0.98255	0.00288	0.01210	0.01352	0.358	0.477	0.716	0.239	0.356	0.475	0.712	0.237	0.361	0.481	0.722	0.241	0.363	0.485	0.727	0.242
0.99672	0.98724	0.99719	0.00176	0.00332	0.00594	0.417	0.239	0.537	0.318	0.415	0.237	0.534	0.316	0.421	0.241	0.541	0.320	0.424	0.242	0.545	0.323
0.99788	0.97843	0.97519	0.00284	0.01222	0.02349	0.537	0.318	0.656	0.477	0.534	0.316	0.652	0.475	0.541	0.320	0.661	0.481	0.545	0.323	0.666	0.485
0.99874	0.99877	0.99628	0.00026	0.00475	0.01519	0.596	0.079	0.835	0.398	0.593	0.079	0.830	0.395	0.601	0.080	0.842	0.401	0.606	0.081	0.848	0.404
0.99114	0.99799	0.99803	0.00010	0.00166	0.00183	0.179	0.239	0.298	0.239	0.178	0.237	0.297	0.237	0.180	0.241	0.301	0.241	0.182	0.242	0.303	0.242
0.99701	0.98999	0.99803	0.00153	0.00464	0.00239	0.417	0.318	0.537	0.159	0.415	0.316	0.534	0.158	0.421	0.320	0.541	0.160	0.424	0.323	0.545	0.162
Average percentage of deviation										4.62	4.58	4.63	4.57	3.82	3.83	3.78	3.77	3.08	2.99	3.06	3.15
Total percentage of deviation										4.60				3.80				3.10			

Table 6.3 Comparison of the results derived from RBFNN, BPNN, KSOM model and experimental (Composite beam)

Relative 1st natural frequency "rfnf"	Relative 2nd natural frequency "rsnf"	Relative 3rd natural frequency "rtnf"	Relative 1st mode shape difference "rfmd"	Relative 2nd mode shape difference "rsmd"	Relative 3rd mode shape difference "rtmd"	Experimental relative 1st crack location "rfcl" 1st crack depth "rfcd" 2nd crack location "rscl" 2nd crack depth "rscd"				RBFNN relative 1st crack location "rfcl" 1st crack depth "rfcd" 2nd crack location"rscl" 2nd crack depth "rscd"				BPNN relative 1st crack location "rfcl" 1st crack depth "rfcd" 2nd crack location"rscl" 2nd crack depth "rscd"				KSOM relative 1st crack location "rfcl" 1st crack depth "rfcd" 2nd crack location "rscl" 2nd crack depth "rscd"			
						rfcl	rfcd	rscl	rscd	rfcl	rfcd	rscl	rscd	rfcl	rfcd	rscl	rscd	rfcl	rfcd	rscl	rscd
0.99607	0.99700	0.99829	0.00013	0.00203	0.00240	0.125	0.1667	0.250	0.3333	0.119	0.159	0.238	0.318	0.118	0.157	0.236	0.314	0.117	0.156	0.234	0.313
0.98098	0.99557	0.99892	0.00275	0.00456	0.01064	0.250	0.0833	0.500	0.1667	0.238	0.079	0.477	0.159	0.236	0.079	0.472	0.157	0.234	0.078	0.469	0.156
0.99651	0.99425	0.99796	0.00079	0.00264	0.00101	0.375	0.250	0.625	0.500	0.357	0.238	0.596	0.477	0.354	0.236	0.589	0.472	0.352	0.234	0.586	0.469
0.99001	0.99318	0.98710	0.00145	0.00571	0.00508	0.1875	0.3333	0.3125	0.1667	0.179	0.318	0.298	0.159	0.177	0.314	0.295	0.157	0.176	0.313	0.293	0.156
0.98809	0.98584	0.98255	0.00288	0.01210	0.01352	0.4375	0.500	0.6875	0.25	0.417	0.477	0.655	0.238	0.413	0.472	0.648	0.236	0.410	0.469	0.645	0.234
0.99672	0.98724	0.99719	0.00176	0.00332	0.00594	0.5625	0.3333	0.8125	0.0833	0.536	0.318	0.774	0.079	0.530	0.314	0.766	0.079	0.528	0.313	0.762	0.078
0.99788	0.97843	0.97519	0.00284	0.01222	0.02349	0.500	0.4167	0.75	0.500	0.477	0.397	0.715	0.477	0.472	0.393	0.707	0.472	0.469	0.391	0.703	0.469
0.99874	0.99877	0.99628	0.00026	0.00475	0.01519	0.3125	0.500	0.5625	0.3333	0.298	0.477	0.536	0.318	0.295	0.472	0.530	0.314	0.293	0.469	0.528	0.313
0.99114	0.99799	0.99803	0.00010	0.00166	0.00183	0.4375	0.250	0.6625	0.4167	0.417	0.238	0.631	0.397	0.413	0.236	0.625	0.393	0.410	0.234	0.621	0.391
0.99701	0.98999	0.99803	0.00153	0.00464	0.00239	0.625	0.4167	0.875	0.3333	0.596	0.397	0.834	0.318	0.589	0.393	0.825	0.314	0.586	0.391	0.821	0.313
Average percentage of deviation										4.68	4.72	4.70	7.69	5.68	5.75	5.69	5.67	6.23	6.24	6.22	6.19
Total percentage of deviation										4.69				5.7				6.21			

Table 6.4 Comparison of the results derived from RBFNN, Fuzzy Gaussian model, Theoretical and FEA (Steel)

Relative 1st natural frequency "rfnf"	Relative 2nd natural frequency "rsnf"	Relative 3rd natural frequency "rtnf"	Relative 1st mode shape difference "rfmd"	Relative 2nd mode shape difference "r smd"	Relative 3rd mode shape difference "rtmd"	RBFNN controller relative 1st crack location "rfcl" 1st crack depth "rfcd" 2nd crack location "rscl" 2nd crack depth "rscd"				Fuzzy Gaussian relative 1st crack location "rfcl" 1st crack depth "rfcd" 2nd crack location "rscl" 2nd crack depth "rscd"				Theoretical relative 1st crack location "rfcl" 1st crack depth "rfcd" 2nd crack location "rscl" 2nd crack depth "rscd"				FEA relative 1st crack location "rfcl" 1st crack depth "rfcd" 2nd crack location "rscl" 2nd crack depth "rscd"			
						rfcl	rfcd	rscl	rscd	rfcl	rfcd	rscl	rscd	rfcl	rfcd	rscl	rscd	rfcl	rfcd	rscl	rscd
0.99939	0.99813	0.99978	0.00013	0.00106	0.00411	0.119	0.159	0.238	0.318	0.118	0.158	0.237	0.316	0.120	0.159	0.239	0.319	0.121	0.161	0.241	0.322
0.99980	0.99768	0.99664	0.00035	0.00108	0.00073	0.238	0.079	0.477	0.159	0.237	0.079	0.474	0.158	0.239	0.080	0.478	0.159	0.241	0.080	0.483	0.161
0.99952	0.97803	0.98418	0.00341	0.00134	0.02088	0.357	0.238	0.596	0.477	0.355	0.237	0.592	0.474	0.359	0.239	0.598	0.478	0.362	0.241	0.603	0.483
0.99889	0.99881	0.99932	0.00041	0.00224	0.00310	0.179	0.318	0.298	0.159	0.178	0.316	0.296	0.158	0.179	0.319	0.299	0.159	0.181	0.322	0.302	0.161
0.99906	0.98250	0.99800	0.00293	0.00965	0.00839	0.417	0.477	0.655	0.238	0.414	0.474	0.651	0.237	0.418	0.478	0.657	0.239	0.422	0.483	0.663	0.241
0.99958	0.99129	0.99869	0.00123	0.00187	0.00670	0.536	0.318	0.774	0.079	0.533	0.316	0.769	0.079	0.538	0.319	0.777	0.080	0.543	0.322	0.784	0.080
0.99971	0.98183	0.98589	0.00272	0.00638	0.00962	0.477	0.397	0.715	0.477	0.474	0.395	0.710	0.474	0.478	0.398	0.717	0.478	0.483	0.402	0.724	0.483
0.99473	0.98761	0.98721	0.00239	0.00786	0.01099	0.298	0.477	0.536	0.318	0.296	0.474	0.533	0.316	0.299	0.478	0.538	0.319	0.302	0.483	0.543	0.322
0.99230	0.99003	0.99182	0.00149	0.00455	0.00673	0.417	0.238	0.631	0.397	0.414	0.237	0.627	0.395	0.418	0.239	0.633	0.398	0.422	0.241	0.639	0.402
0.99677	0.98931	0.99459	0.00152	0.00540	0.00865	0.596	0.397	0.834	0.318	0.592	0.395	0.829	0.316	0.598	0.398	0.837	0.319	0.603	0.402	0.844	0.322
Average percentage of deviation						4.68	4.72	4.70	7.69	5.32	5.26	5.28	5.22	3.66	3.52	3.51	3.49	4.35	4.37	3.38	4.36
Total percentage of deviation						4.69				5.3				3.5				4.4			

6.7 Summary

This section deals with the conclusions drawn from analysis of results derived from various neural network techniques. In this chapter three types of neural network techniques such as BPNN, RBFNN and KSOM have been discussed to localize and quantify the cracks severities and intensities for composite and structural steel beam. The first three modal frequencies and curvature mode shapes have been employed as inputs to neural network model and the final outputs of the neural model are relative first and second crack location and crack depth. Several hundred of training data have been extracted to train the RBFNN and BPFNN model. KSOM model does not require training data because it is unsupervised type of the neural network. The BPNN model contained different numbers of neural in seven layers for processing the input data into outputs with the help of back propagation algorithm. The RBFNN model consists of only three layers. In the hidden layer Gaussian kernel activation function has been employed to locate RBF units (RBF centers). The RBFNN proceed input space to hidden space non-linearly and hidden space to output space linearly. Similarly KSOM type of neural model has been used to predict cracks location and depth for composite and steel beam. The results derived from developed three type neural model have been compared with experimental test results to verify the effectiveness of proposed neural models. The total percentage of deviation for BPNN is 4.91%, for RBFNN is 4.6% and for KSOM is 5.4% in the case of composite beam. Similarly for the structural steel beam the total percentage of deviation for BPNN is 5.7%, for RBFNN is 4.69% and for KSOM is 6.21%. It is observed that there is well agreement between them for both composite and steel beam. The results obtained from neural models are also compared with the results of fuzzy Gaussian model, theoretical and finite element method and a close proximity found between them. These developed neural models have been used to develop the hybrid models in the next chapter.

CHAPTER 7

Study of Hybrid Fuzzy-Neuro Technique for Identification of Multiple Cracks of Cantilever Beam

Different fault diagnostics techniques are required to observe the health of various machine components and structural elements for acquiring the un-interrupted service. The detection of faults before failure of the structures not only prevents loss of economy but also saves the human life. Various nondestructive techniques have been applied by researchers to locate the damage but they are costly and time consuming. The vibration based method along with artificial intelligent techniques can be used to effectively identify the damage. The hybridization of fuzzy system and neural models has been done by engineers and researchers from various fields of science and technology for developing intelligent systems for identification of damage. The fuzzy model has potential to solve various engineering problems based on concepts of fuzzy sets, fuzzy reasoning and fuzzy rules. The neural models have ability to learn and diagnose any type of problems by adjusting the synaptic weights of neuron between the layers. Advantages of integration of fuzzy model and neural models have utilized the properties of the both models to get more synchronized results. The fuzzy and neural models have ability to adopt the challenges present in system and mimic the human behavior. In this chapter fuzzy and neural techniques (BPNN, RBFNN &KSOM) have been adopted to develop the fault diagnostics tool for condition monitoring of the structures.

7.1 Introduction

The hybrid fuzzy-neuro soft computing technique is a powerful tool for solving the complex and real time problems. The fuzzy logic system can be developed, if the system variables are expressed in terms of linguistic term and fuzzy rules. If training data is available for simulation, a neural model can be developed. It is observed from the comprehensive study of fuzzy and neural models. The disadvantage of both methods is correlative to the each other. Consequently, it is attract to hybridize and to solve the any problems by combining the capabilities of fuzzy and neural models. The advantage of

fuzzy logic is formation of linguistic rules and learning capability is the advantage of the neural method. Therefore integrated fuzzy-neuro method can be used to design condition monitoring techniques for identification of multiple cracks present in the composite and structural steel beam. In this chapter, a fault diagnosis technique has been developed using vibration responses of cracked cantilever beams. The integrated intelligent model has been fabricated for localizing and quantifying the crack positions and depths by fusion of capacity of fuzzy and neural models. The performance of hybrid model is verified by comparing the results derived from fuzzy-neuro model and experimental analysis. The well agreement between the results is ascertained.

7.2 Analysis of the hybrid fuzzy-neuro technique

In this chapter, an intelligent integrated fuzzy-neuro models has been designed for detection of transverse cracks present on the cantilever composite and structural steel beam using vibration responses. The first three modal frequencies and curvature mode shapes of the cracked and non-cracked cantilever beam for different crack orientation are measured using theoretical and numerical method and verified by experimental examination. The calculated vibrational modal response are used as input variables to fuzzy section of the hybrid model and outputs of fuzzy section are relative first and second crack location ($rfcl_{fuzzy,}$ $rscl_{fuzzy}$) and relative first and second crack depth ($rfcd_{fuzzy,}$ $rscd_{fuzzy}$). The first three relative modal frequencies and first three relative mode shapes and output of fuzzy segment are fed as input variables to the neural segment of hybrid model and modified final relative crack depths and crack location are output parameters of hybrid model. The modal responses are used to generate fuzzy rules for fuzzy model and training pattern for the neural model. The robustness of developed hybrid model has been verified by experimental analysis. The fuzzy section has used Triangular, Gaussian and Trapezoidal membership for prediction of transverse cracks. In the neural section three types of neural models (BPNN, RBFNN and KSOM) have been employed to develop hybrid model. The Triangular fuzzy-BPNN model, Gaussian fuzzy-BPNN model and Trapezoidal fuzzy-BPNN model have been shown in figures 7.1(a), 7.1(b) and 7.1(c) respectively. Figures 7.2(a), 7.2(b) and 7.2(c) represent Triangular fuzzy-RBFNN model, Gaussian fuzzy-RBFNN model and Trapezoidal fuzzy-RBFNN model respectively. The Triangular fuzzy-KSOM model, Gaussian fuzzy-KSOM model and Trapezoidal fuzzy-KSOM model have been presented in figures 7.3(a), 7.3(b) and 7.3(c) respectively. Each

fuzzy membership fuction hybridized with BPNN, RBFNN and KSOM neural model for composite and steel beam (shown in figures 7.1, 7.2 and 7.3).

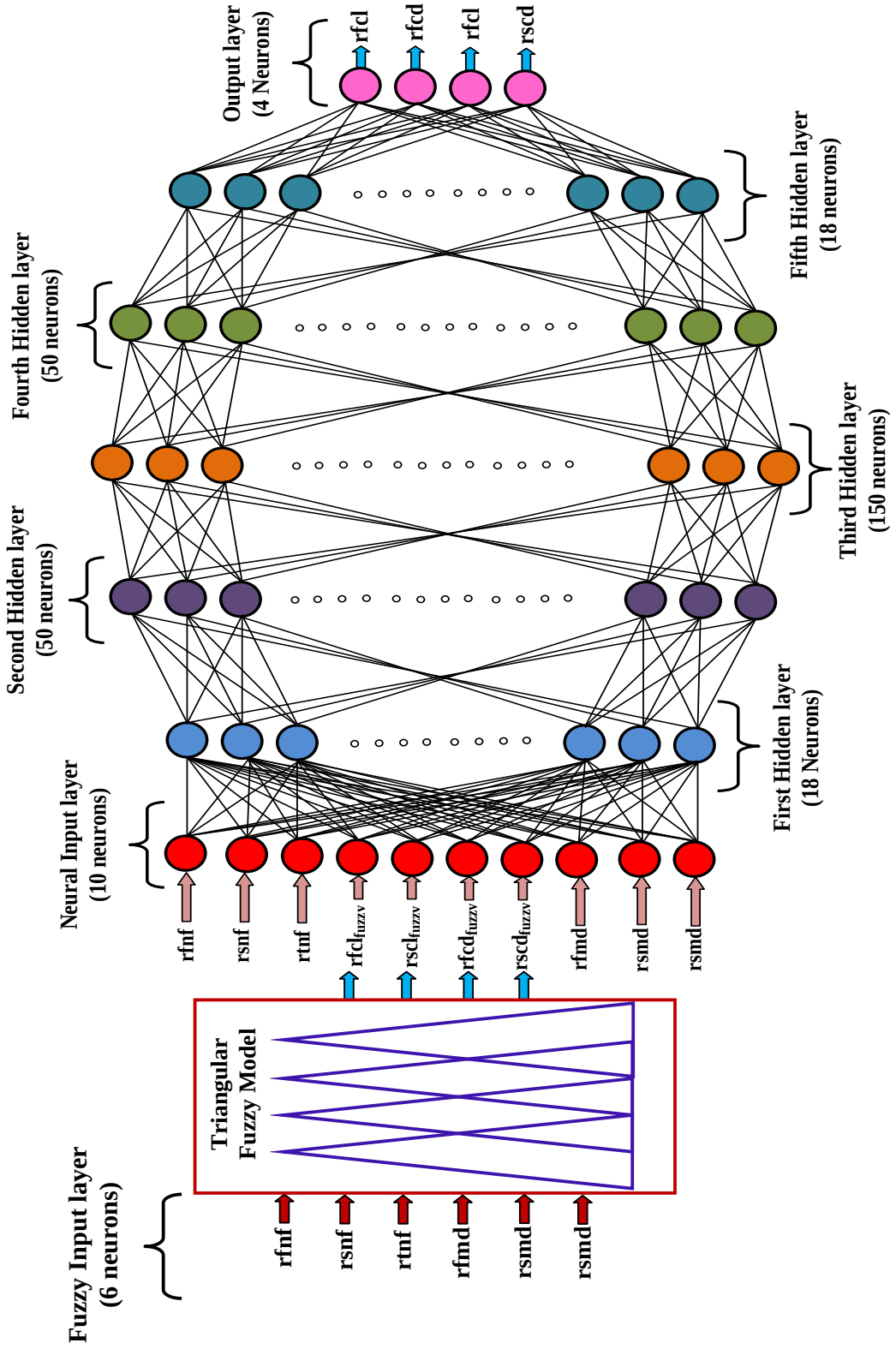

Figure 7.1(a) Triangular fuzzy-Neuro (BPNN) hybrid model for identification of multiple cracks

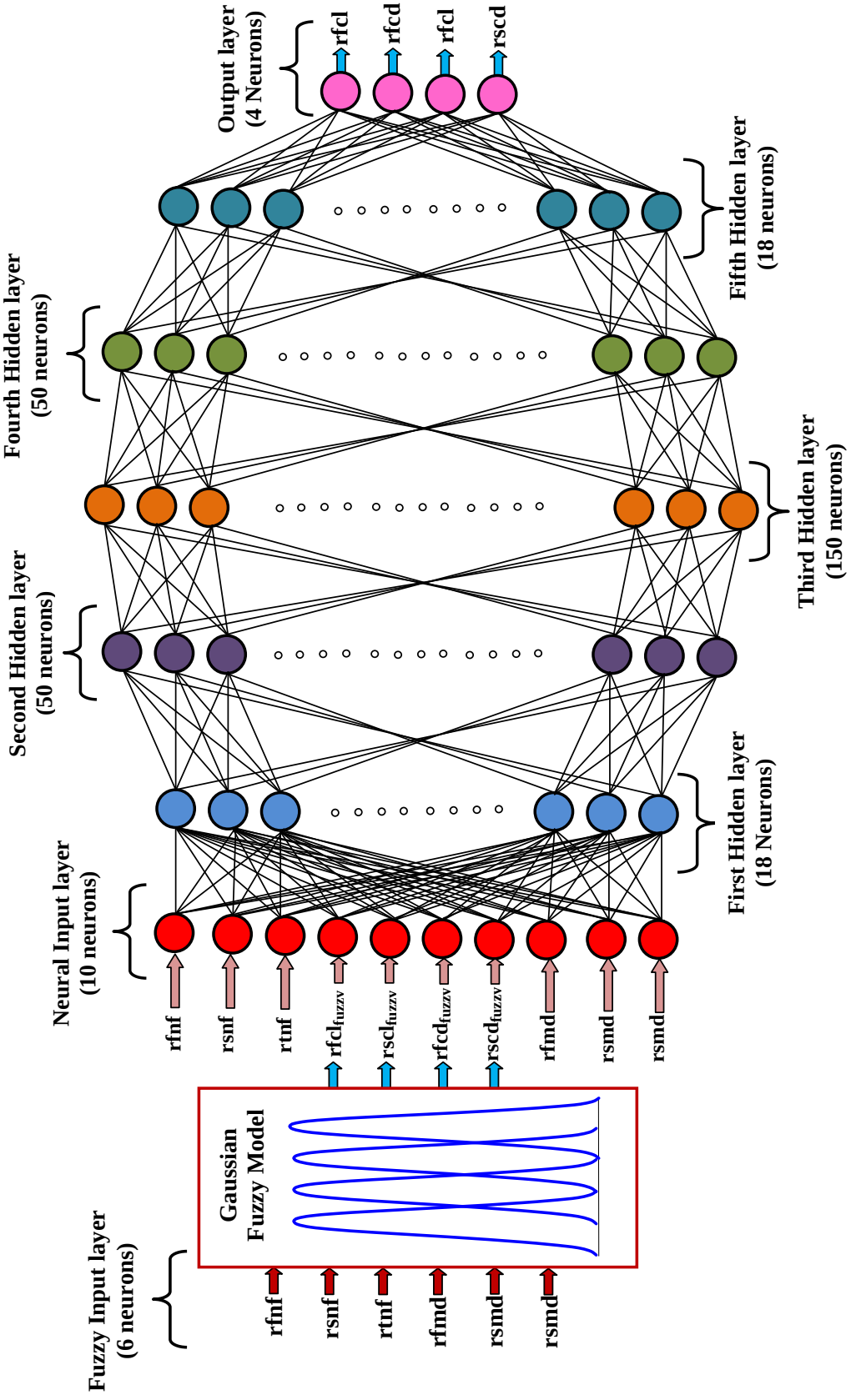

Figure 7.1(b) Gaussian fuzzy-Neuro (BPNN) hybrid model for identification of multiple cracks

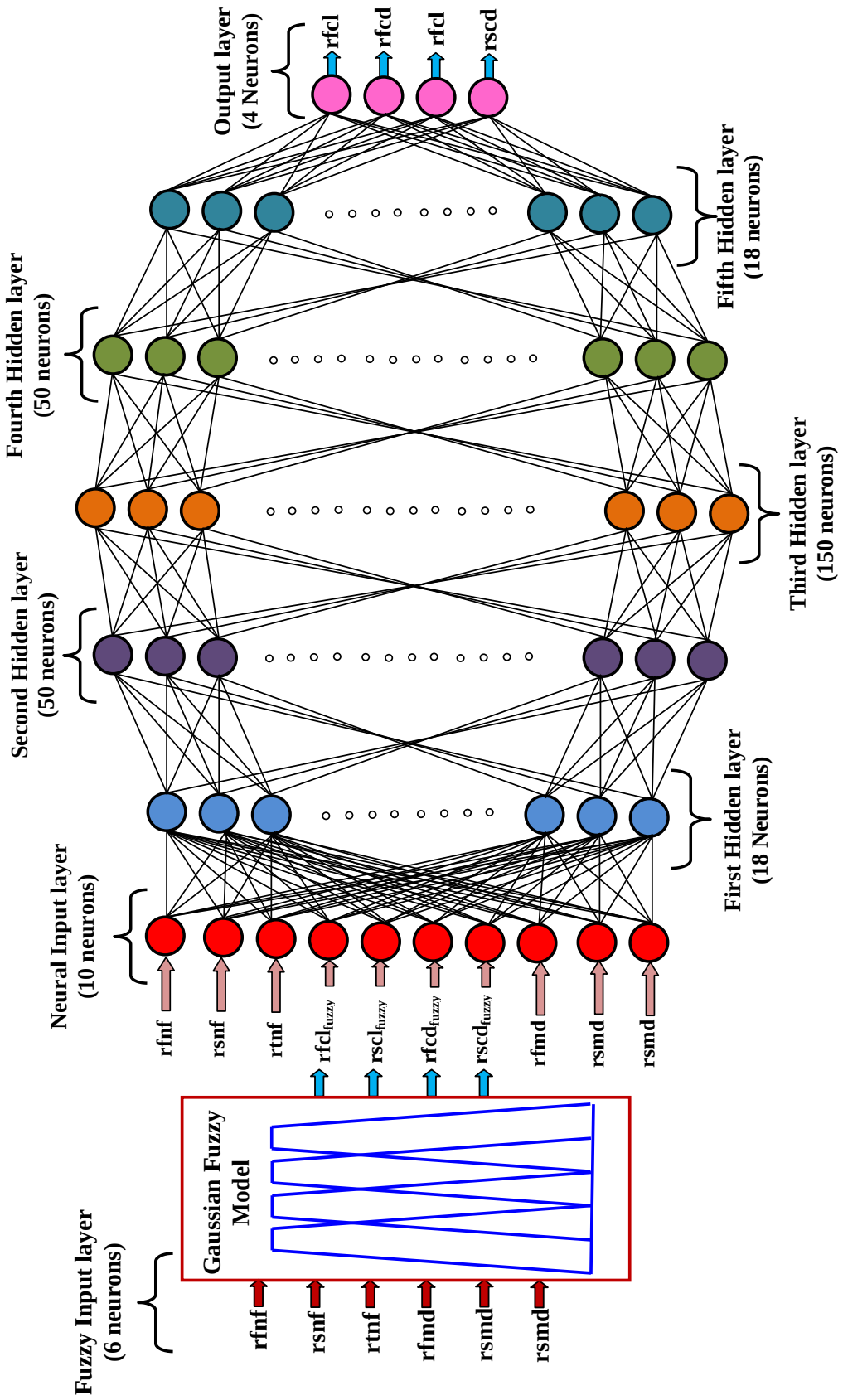

Figure 7.1(c) Trapezoidal fuzzy-Neuro (BPNN) hybrid model for identification of multiple cracks

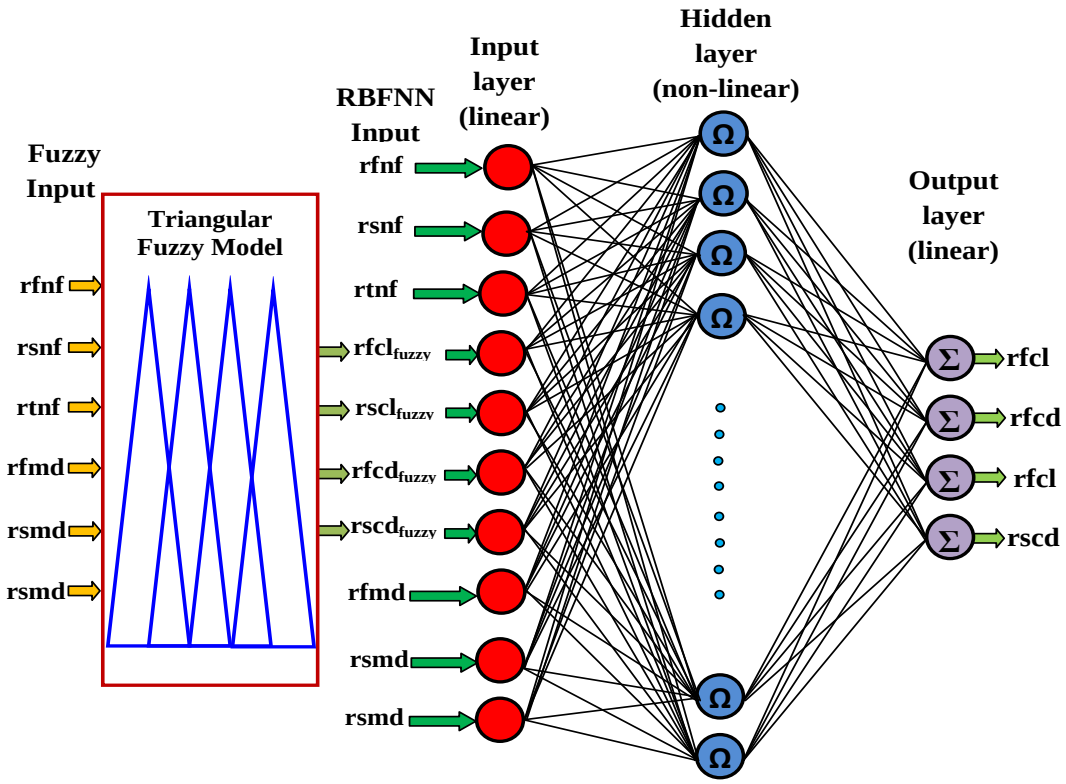

Figure 7.2(a) Triangular fuzzy-Neuro (RBFNN) hybrid model for identification of multiple cracks

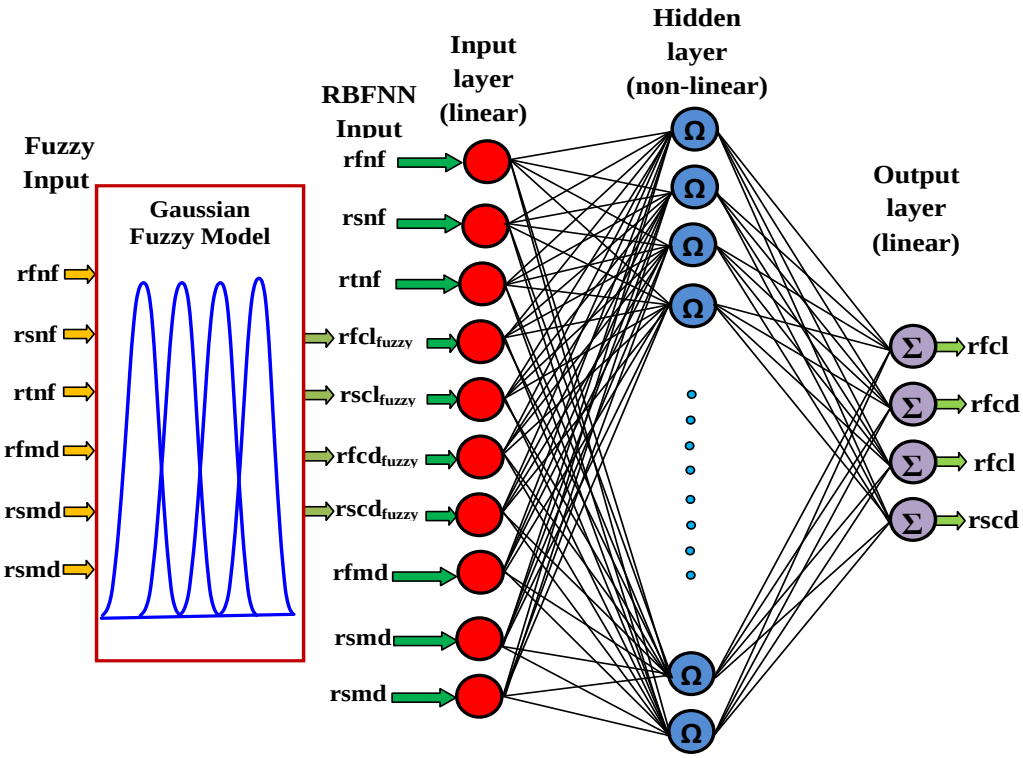

Figure 7.2(b) Gaussian fuzzy-Neuro (RBFNN) hybrid model for identification of multiple cracks

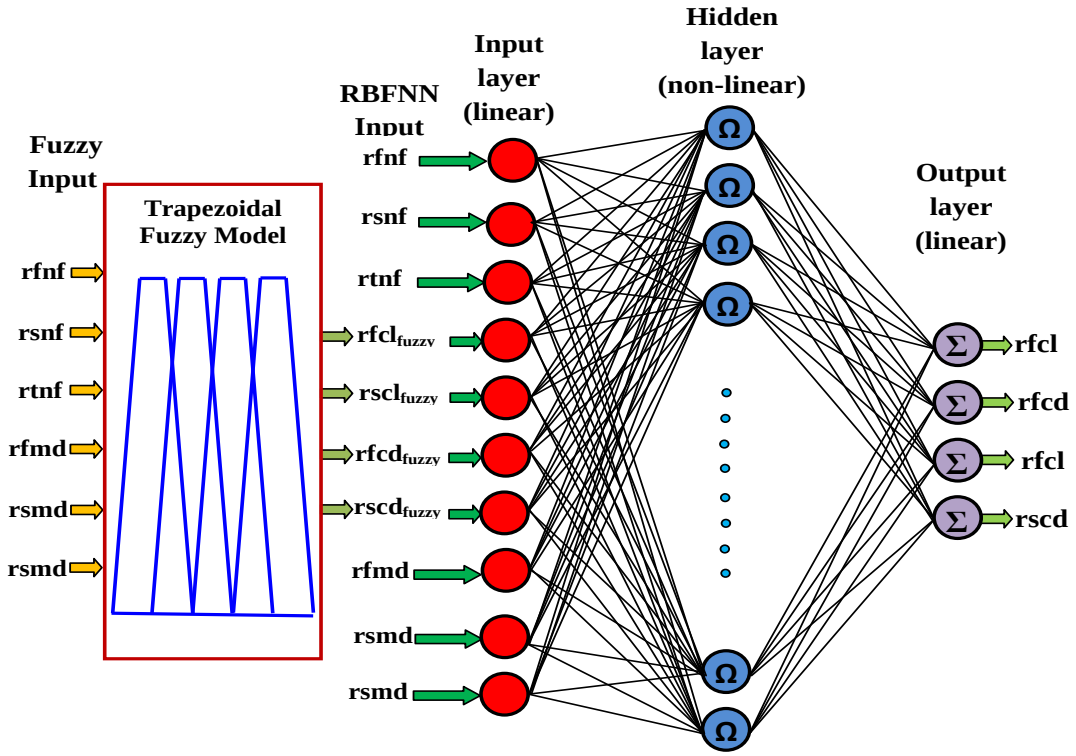

Figure 7.2(c) Trapezoidal fuzzy-Neuro (RBFNN) hybrid model for identification of multiple cracks

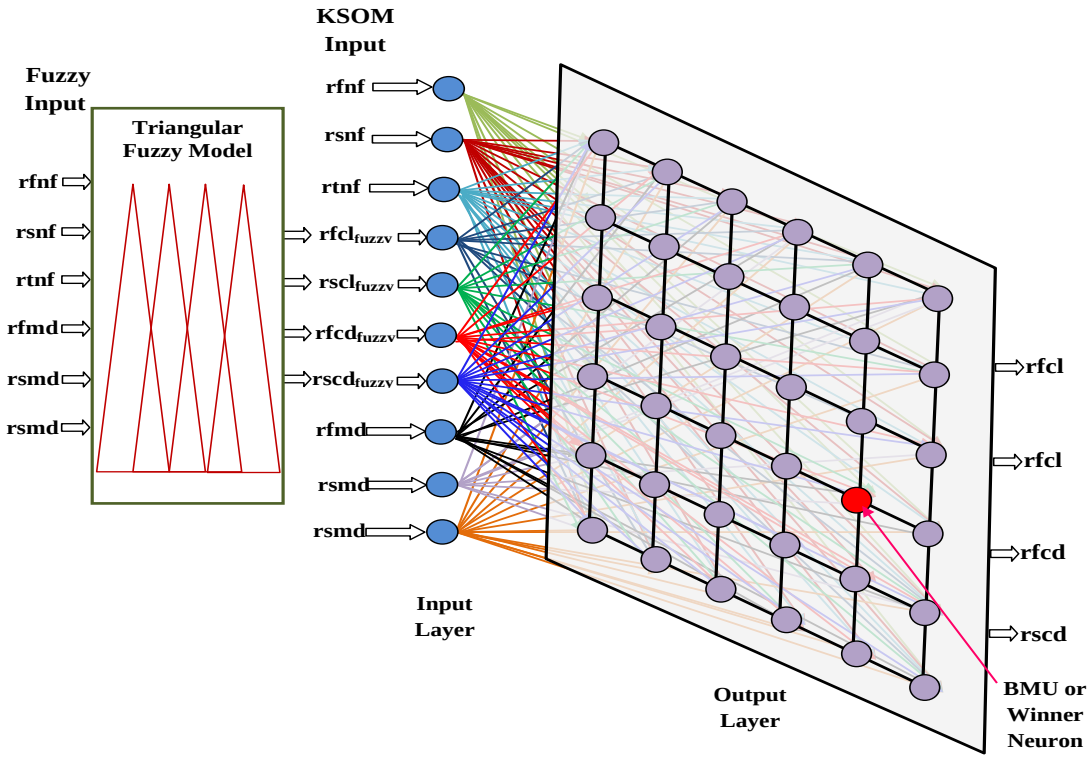

Figure 7.3(a) Triangular fuzzy-Neuro (KSOM) hybrid model for identification of multiple cracks

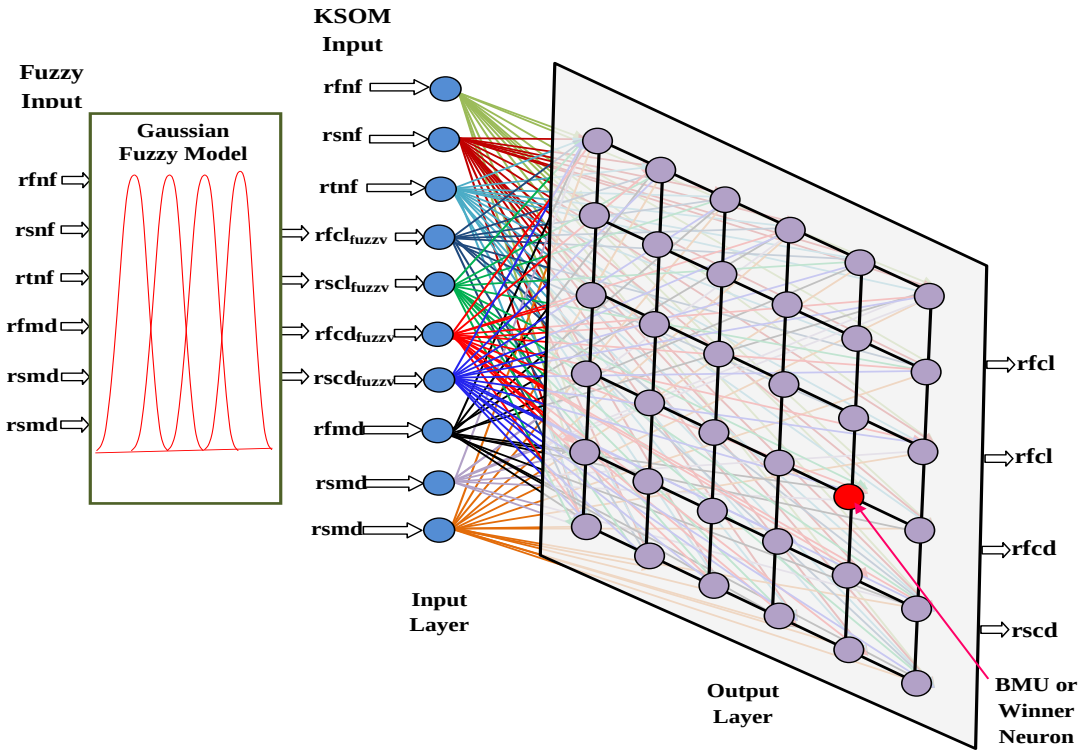

Figure 7.3(b) Gaussian fuzzy-Neuro (KSOM) hybrid model for identification of multiple cracks

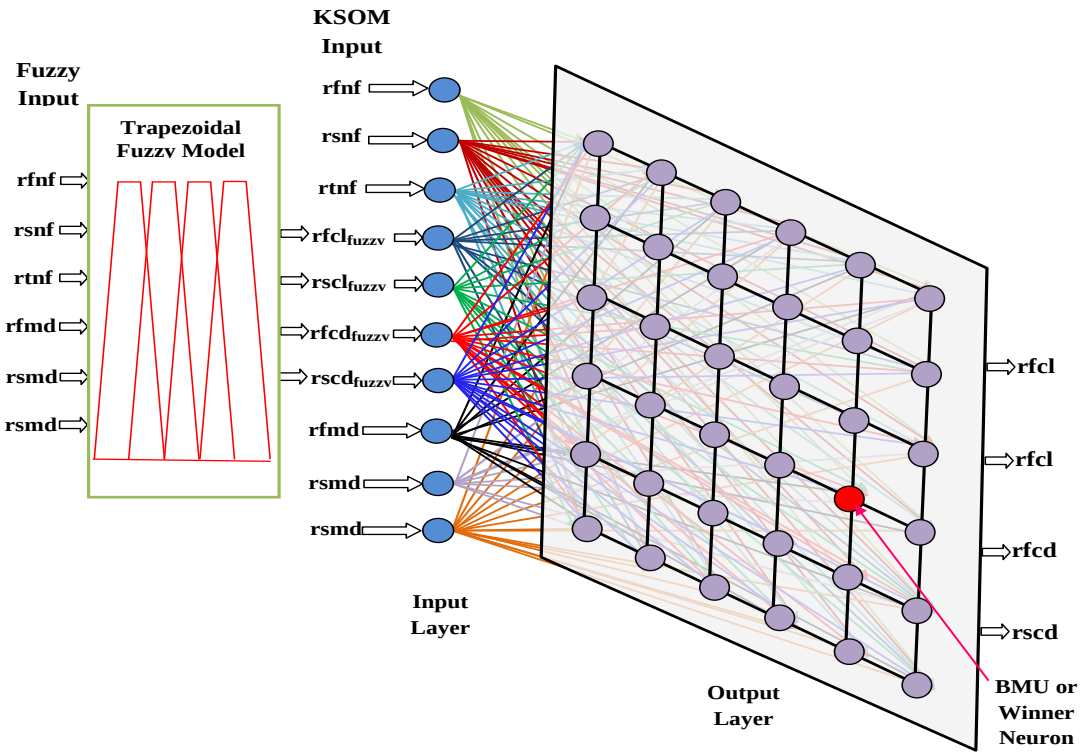

Figure 7.3(c) Trapezoidal fuzzy-Neuro (KSOM) hybrid model for identification of multiple cracks

7.2.1 Analysis of fuzzy part of hybrid model

The fuzzy part of hybrid fuzzy-neuro models has been computed for six input variables and four interim output variables. The linguistic terminologies have been used for input variables such as relative first natural frequency (rfnf), relative second natural frequency (rsnf), relative third natural frequency (rtnf), relative first mode shape difference (rtmd), relative second mode shape difference (rsmd) and relative third mode shape difference (rtmd). The linguistic terminologies for interim outputs from fuzzy part are: fuzzy relative first crack location ($rfcl_{fuzzy}$), fuzzy relative second crack location ($rscl_{fuzzy}$), fuzzy relative first crack depth ($rfcd_{fuzzy}$) and fuzzy relative first crack depth ($rscd_{fuzzy}$). Various type of membership functions (Triangular, Gaussian and Trapezoidal) have been used for constructing the fuzzy segment of fuzzy-neuro models. The fuzzy rules and fuzzy linguistic terminologies have been used for computing the fuzzy segment of the hybrid model as presented in tables 5.1, 5.2 (composite beam) and table 5.3 (steel beam) in chapter 5. The fuzzy mechanism for constructing fuzzy-neuro hybrid crack detection tool has been already discussed in chapter 5.

7.2.2 Analysis of neural part of hybrid model

The neural part of hybrid fuzzy-neuro model has been discussed in this section. Three types of neural techniques such as BPNN, RBFNN and KSOM have been integrated with fuzzy system. The BPNN based neural model of integrated fuzzy-neuro system has seven layers feed forward network trained back propagation algorithm. The working mechanism of BPNN has been presented in section 6.3 of chapter 6. The RBFNN based neural system is also used to develop hybrid fuzzy-neuro system for identification of multiple cracks present in the cantilever beam. The detail working principle of RBFNN has already been discussed in the section 6.4 of the chapter 6. Similarly KSOM type of neural model is integrated with fuzzy system for development of crack identification tool for structures. The results derived from fuzzy part have been used as inputs to the neural segment of hybrid model. The input variables of neural part are rfnf, rsnf, rtnf, rfmd, rsmd, rtmd and $rfcl_{fuzzy}$, $rscl_{fuzzy}$, $rfcd_{fuzzy}$, $rscd_{fuzzy}$. The final outputs of hybrid model obtained from neural segment are as follow: relative first crack location (rfcl), relative second crack location (rscl), relative first crack depth (rfcd) and relative second crack depth (rscd).

7.3 Results and discussion

In this section, discussion has been given from the analysis of results obtained from hybrid fuzzy-neuro system. The fuzzy system with Triangular, Gaussian and Trapezoidal membership function has been integrated with neural network models (BPNN, RBFNN & KSOM) for designing the smart crack identification mechanism for composite and structural beam. The Triangular fuzzy-BPNN hybrid model, Gaussian fuzzy-BPNN hybrid system and Trapezoidal fuzzy-BPNN hybrid model have been shown in figures 7.1(a), 7.1(b) and 7.1(c) respectively. Figures 7.2(a), 7.2(b) and 7.2(c) represent Triangular fuzzy-RBFNN hybrid model, Gaussian fuzzy- RBFNN hybrid system and Trapezoidal fuzzy- RBFNN hybrid model respectively. Similarly triangular fuzzy-KSOM hybrid model, Gaussian fuzzy- KSOM hybrid system and trapezoidal fuzzy- KSOM hybrid technique have been presented in Figures 7.3(a), 7.3(b) and 7.3(c) respectively. The comparison of results derived from various hybrid fuzzy-neuro systems have been displayed in tables 7.1, 7.2 and 7.3 for composite beam. After the study of results, it is observed that Gaussian fuzzy-BPNN, Gaussian fuzzy-RBFNN and Gaussian fuzzy-KSOM hybrid system provides least deviation from that of experimental data. Therefore Gaussian fuzzy model integrated with BPNN, RBFNN and KSOM compared with Gaussian fuzzy model in table 7.4. Similar patterns have been observed for structural steel. The comparison of results obtained from various hybrid models have been presented in tables 7.5, 7.6, 7.7 and 7.8.

Table 7.1 Comparison of the results derived from Gaussian Fuzzy -BPNN, Trapezoidal Fuzzy –BPNN, Triangular Fuzzy -BPNN model

Relative 1st natural frequency "rfnf"	Relative 2nd natural frequency "rsnf"	Relative 3rd natural frequency "rtnf"	Relative 1st mode shape difference "rfmd"	Relative 2nd mode shape difference "rsmd"	Relative 3rd mode shape difference "rtmd"	Experimental relative 1st crack location "rfcl" 1st crack depth "rfcd" 2nd crack location "rscl" 2nd crack depth "rscd"				Gaussian Fuzzy-BPNN relative 1st crack location "rfcl" 1st crack depth "rfcd" 2nd crack location"rscl" 2nd crack depth "rscd"				Trapezoidal fuzzy-BPNN relative 1st crack location "rfcl" 1st crack depth "rfcd" 2nd crack location"rscl" 2nd crack depth "rscd"				Triangular Fuzzy-BPNN relative 1st crack location "rfcl" 1st crack depth "rfcd" 2nd crack location "rscl" 2nd crack depth "rscd "			
						rfcl	rfcd	rscl	rscd	rfcl	rfcd	rscl	rscd	rfcl	rfcd	rscl	rscd	rfcl	rfcd	rscl	rscd
0.99607	0.99700	0.99829	0.00013	0.00203	0.00240	0.1875	0.1667	0.4375	0.250	0.180	0.160	0.421	0.241	0.179	0.159	0.418	0.239	0.179	0.159	0.417	0.238
0.98098	0.99557	0.99892	0.00275	0.00456	0.01064	0.125	0.4167	0.8750	0.333	0.120	0.401	0.842	0.320	0.119	0.398	0.836	0.318	0.119	0.397	0.833	0.317
0.99651	0.99425	0.99796	0.00079	0.00264	0.00101	0.3125	0.1667	0.5000	0.250	0.301	0.160	0.481	0.241	0.299	0.159	0.478	0.239	0.298	0.159	0.476	0.238
0.99001	0.99318	0.98710	0.00145	0.00571	0.00508	0.250	0.4167	0.5625	0.1667	0.241	0.401	0.541	0.160	0.239	0.398	0.538	0.159	0.238	0.397	0.536	0.159
0.98809	0.98584	0.98255	0.00288	0.01210	0.01352	0.375	0.5000	0.750	0.250	0.361	0.481	0.722	0.241	0.358	0.478	0.717	0.239	0.357	0.476	0.714	0.238
0.99672	0.98724	0.99719	0.00176	0.00332	0.00594	0.4375	0.2500	0.5625	0.333	0.421	0.241	0.541	0.320	0.418	0.239	0.538	0.318	0.417	0.238	0.536	0.317
0.99788	0.97843	0.97519	0.00284	0.01222	0.02349	0.5625	0.333	0.6875	0.500	0.541	0.320	0.661	0.481	0.538	0.318	0.657	0.478	0.536	0.317	0.655	0.476
0.99874	0.99877	0.99628	0.00026	0.00475	0.01519	0.625	0.0833	0.875	0.4167	0.601	0.080	0.842	0.401	0.597	0.080	0.836	0.398	0.595	0.079	0.833	0.397
0.99114	0.99799	0.99803	0.00010	0.00166	0.00183	0.1875	0.250	0.3125	0.250	0.180	0.241	0.301	0.241	0.179	0.239	0.299	0.239	0.179	0.238	0.298	0.238
0.99701	0.98999	0.99803	0.00153	0.00464	0.00239	0.4375	0.333	0.5625	0.1667	0.421	0.320	0.541	0.160	0.418	0.318	0.538	0.159	0.417	0.317	0.536	0.159
Average percentage of deviation										3.82	3.83	3.78	3.79	4.49	4.44	4.40	4.47	4.78	4.84	4.74	4.76
Total percentage of deviation										3.80				4.45				4.75			

Table 7.2 Comparison of the results derived from Gaussian Fuzzy - RBFNN, Trapezoidal Fuzzy - RBFNN model, Triangular Fuzzy - RBFNN and Experimental (Composite beam)

Relative 1st natural frequency "rfnf"	Relative 2nd natural frequency "rsnf"	Relative 3rd natural frequency "rtnf"	Relative 1st mode shape difference "rfmd"	Relative 2nd mode shape difference "rsmd"	Relative 3rd mode shape difference "rtmd"	Experimental relative 1st crack location "rfcl" 1st crack depth "rfcd" 2nd crack location "rscl" 2nd crack depth "rscd"				Gaussian Fuzzy-RBFNN relative 1st crack location "rfcl" 1st crack depth "rfcd" 2nd crack location "rscl" 2nd crack depth "rscd"				Trapezoidal fuzzy-RBFNN relative 1st crack location "rfcl" 1st crack depth "rfcd" 2nd crack location "rscl" 2nd crack depth "rscd"				Triangular Fuzzy-RBFNN relative 1st crack location "rfcl" 1st crack depth "rfcd" 2nd crack location "rscl" 2nd crack depth "rscd"			
						rfcl	rfcd	rscl	rscd	rfcl	rfcd	rscl	rscd	rfcl	rfcd	rscl	rscd	rfcl	rfcd	rscl	rscd
0.99607	0.99700	0.99829	0.00013	0.00203	0.00240	0.1875	0.1667	0.4375	0.250	0.182	0.161	0.424	0.242	0.181	0.161	0.422	0.241	0.180	0.160	0.419	0.240
0.98098	0.99557	0.99892	0.00275	0.00456	0.01064	0.125	0.4167	0.8750	0.333	0.121	0.403	0.847	0.322	0.121	0.402	0.844	0.321	0.120	0.399	0.838	0.319
0.99651	0.99425	0.99796	0.00079	0.00264	0.00101	0.3125	0.1667	0.5000	0.250	0.303	0.161	0.484	0.242	0.301	0.161	0.482	0.241	0.299	0.160	0.479	0.240
0.99001	0.99318	0.98710	0.00145	0.00571	0.00508	0.250	0.4167	0.5625	0.1667	0.242	0.403	0.545	0.161	0.241	0.402	0.543	0.161	0.240	0.399	0.539	0.160
0.98809	0.98584	0.98255	0.00288	0.01210	0.01352	0.375	0.5000	0.750	0.250	0.363	0.484	0.726	0.242	0.362	0.482	0.723	0.241	0.359	0.479	0.719	0.240
0.99672	0.98724	0.99719	0.00176	0.00332	0.00594	0.4375	0.2500	0.5625	0.333	0.424	0.242	0.545	0.322	0.422	0.241	0.543	0.321	0.419	0.240	0.539	0.319
0.99788	0.97843	0.97519	0.00284	0.01222	0.02349	0.5625	0.333	0.6875	0.500	0.545	0.322	0.666	0.484	0.543	0.321	0.663	0.482	0.539	0.319	0.659	0.479
0.99874	0.99877	0.99628	0.00026	0.00475	0.01519	0.625	0.0833	0.875	0.4167	0.605	0.081	0.847	0.403	0.603	0.080	0.844	0.402	0.599	0.080	0.838	0.399
0.99114	0.99799	0.99803	0.00010	0.00166	0.00183	0.1875	0.250	0.3125	0.250	0.182	0.242	0.303	0.242	0.181	0.241	0.301	0.241	0.180	0.240	0.299	0.240
0.99701	0.98999	0.99803	0.00153	0.00464	0.00239	0.4375	0.333	0.5625	0.1667	0.424	0.322	0.545	0.161	0.422	0.321	0.543	0.161	0.419	0.319	0.539	0.160
Average percentage of deviation										3.15	3.24	3.14	3.27	3.50	3.59	3.55	3.56	4.15	4.16	4.22	4.17
Total percentage of deviation										3.20				3.55				4.18			

Table 7.3 Comparison of the results derived, Gaussian Fuzzy - KSOM, Trapezoidal Fuzzy - KSOM model, from Triangular Fuzzy - KSOM and Experimental (Composite beam)

Relative 1st natural frequency "rfnf"	Relative 2nd natural frequency "rsnf"	Relative 3rd natural frequency "rtnf"	Relative 1st mode shape difference "rfmd"	Relative 2nd mode shape difference "rsmd"	Relative 3rd mode shape difference "rtmd"	Experimental relative 1st crack location "rfcl" 1st crack depth "rfcd" 2nd crack location "rscl" 2nd crack depth "rscd"				Gaussian Fuzzy - KSOM relative 1st crack location "rfcl" 1st crack depth "rfcd" 2nd crack location"rscl" 2nd crack depth "rscd"				Trapezoidal Fuzzy - KSOM relative 1st crack location "rfcl" 1st crack depth "rfcd" 2nd crack location"rscl" 2nd crack depth "rscd"				Triangular Fuzzy - KSOM relative 1st crack location "rfcl" 1st crack depth "rfcd" 2nd crack location "rscl" 2nd crack depth "rscd"			
						rfcl	rfcd	rscl	rscd	rfcl	rfcd	rscl	rscd	rfcl	rfcd	rscl	rscd	rfcl	rfcd	rscl	rscd
0.99607	0.99700	0.99829	0.00013	0.00203	0.00240	0.1875	0.1667	0.4375	0.250	0.179	0.159	0.418	0.239	0.179	0.159	0.417	0.238	0.178	0.158	0.414	0.237
0.98098	0.99557	0.99892	0.00275	0.00456	0.01064	0.125	0.4167	0.8750	0.333	0.119	0.398	0.836	0.318	0.119	0.397	0.834	0.317	0.118	0.395	0.829	0.315
0.99651	0.99425	0.99796	0.00079	0.00264	0.00101	0.3125	0.1667	0.5000	0.250	0.298	0.159	0.478	0.239	0.298	0.159	0.477	0.238	0.296	0.158	0.474	0.237
0.99001	0.99318	0.98710	0.00145	0.00571	0.00508	0.250	0.4167	0.5625	0.1667	0.239	0.398	0.537	0.159	0.238	0.397	0.536	0.159	0.237	0.395	0.533	0.158
0.98809	0.98584	0.98255	0.00288	0.01210	0.01352	0.375	0.5000	0.750	0.250	0.358	0.478	0.716	0.239	0.357	0.477	0.715	0.238	0.355	0.474	0.710	0.237
0.99672	0.98724	0.99719	0.00176	0.00332	0.00594	0.4375	0.2500	0.5625	0.333	0.418	0.239	0.537	0.318	0.417	0.238	0.536	0.317	0.414	0.237	0.533	0.315
0.99788	0.97843	0.97519	0.00284	0.01222	0.02349	0.5625	0.333	0.6875	0.500	0.537	0.318	0.657	0.478	0.536	0.317	0.655	0.477	0.533	0.315	0.651	0.474
0.99874	0.99877	0.99628	0.00026	0.00475	0.01519	0.625	0.0833	0.875	0.4167	0.597	0.080	0.836	0.398	0.596	0.079	0.834	0.397	0.592	0.079	0.829	0.395
0.99114	0.99799	0.99803	0.00010	0.00166	0.00183	0.1875	0.250	0.3125	0.250	0.179	0.239	0.298	0.239	0.179	0.238	0.298	0.238	0.178	0.237	0.296	0.237
0.99701	0.98999	0.99803	0.00153	0.00464	0.00239	0.4375	0.333	0.5625	0.1667	0.418	0.318	0.537	0.159	0.417	0.317	0.536	0.159	0.414	0.315	0.533	0.158
Average percentage of deviation										4.54	4.44	4.52	4.47	4.68	4.77	4.66	4.74	5.28	5.26	5.33	5.34
Total percentage of deviation										4.50				4.70				5.31			

Table 7.4 Comparison of the results derived from Gaussian Fuzzy -BPNN, Gaussian Fuzzy - RBFNN, Gaussian Fuzzy-KSOM and Gaussian Fuzzy model (Composite beam)

Relative 1st natural frequency "rfnf"	Relative 2nd natural frequency "rsnf"	Relative 3rd natural frequency "rtnf"	Relative 1st mode shape difference "rfmd"	Relative 2nd mode shape difference "rsmd"	Relative 3rd mode shape difference "rtmd"	Gaussian Fuzzy – KSOM relative 1st crack location "rfcl" 1st crack depth "rfcd" 2nd crack location "rscl" 2nd crack depth "rscd"				Gaussian Fuzzy-RBFNN relative 1st crack location "rfcl" 1st crack depth "rfcd" 2nd crack location "rscl" 2nd crack depth "rscd"				Gaussian Fuzzy-BPNN relative 1st crack location "rfcl" 1st crack depth "rfcd" 2nd crack location "rscl" 2nd crack depth "rscd"				Gaussian Fuzzy relative 1st crack location "rfcl" 1st crack depth "rfcd" 2nd crack location "rscl" 2nd crack depth "rscd"			
						rfcl	rfcd	rscl	rscd	rfcl	rfcd	rscl	rscd	rfcl	rfcd	rscl	rscd	rfcl	rfcd	rscl	rscd
0.99607	0.99700	0.99829	0.00013	0.00203	0.00240	0.179	0.159	0.418	0.239	0.182	0.161	0.424	0.242	0.180	0.160	0.421	0.241	0.178	0.158	0.415	0.237
0.98098	0.99557	0.99892	0.00275	0.00456	0.01064	0.119	0.398	0.836	0.318	0.121	0.403	0.847	0.322	0.120	0.401	0.842	0.320	0.119	0.395	0.830	0.316
0.99651	0.99425	0.99796	0.00079	0.00264	0.00101	0.298	0.159	0.478	0.239	0.303	0.161	0.484	0.242	0.301	0.160	0.481	0.241	0.297	0.158	0.475	0.237
0.99001	0.99318	0.98710	0.00145	0.00571	0.00508	0.239	0.398	0.537	0.159	0.242	0.403	0.545	0.161	0.241	0.401	0.541	0.160	0.237	0.395	0.534	0.158
0.98809	0.98584	0.98255	0.00288	0.01210	0.01352	0.358	0.478	0.716	0.239	0.363	0.484	0.726	0.242	0.361	0.481	0.722	0.241	0.356	0.475	0.712	0.237
0.99672	0.98724	0.99719	0.00176	0.00332	0.00594	0.418	0.239	0.537	0.318	0.424	0.242	0.545	0.322	0.421	0.241	0.541	0.320	0.415	0.237	0.534	0.316
0.99788	0.97843	0.97519	0.00284	0.01222	0.02349	0.537	0.318	0.657	0.478	0.545	0.322	0.666	0.484	0.541	0.320	0.661	0.481	0.534	0.316	0.652	0.475
0.99874	0.99877	0.99628	0.00026	0.00475	0.01519	0.597	0.080	0.836	0.398	0.605	0.081	0.847	0.403	0.601	0.080	0.842	0.401	0.593	0.079	0.830	0.395
0.99114	0.99799	0.99803	0.00010	0.00166	0.00183	0.179	0.239	0.298	0.239	0.182	0.242	0.303	0.242	0.180	0.241	0.301	0.241	0.178	0.237	0.297	0.237
0.99701	0.98999	0.99803	0.00153	0.00464	0.00239	0.418	0.318	0.537	0.159	0.424	0.322	0.545	0.161	0.421	0.320	0.541	0.160	0.415	0.316	0.534	0.158
Average percentage of deviation						4.54	4.44	4.52	4.47	3.15	3.24	3.14	3.27	3.82	3.83	3.78	3.79	5.06	5.16	5.08	5.17
Total percentage of deviation						4.50				3.20				3.80				5.10			

Table 7.5 Comparison of the results derived from Gaussian Fuzzy -BPNN, Trapezoidal Fuzzy –BPNN, Triangular Fuzzy -BPNN model and Experimental (Steel beam)

Relative 1st natural frequency "rfnf"	Relative 2nd natural frequency "rsnf"	Relative 3rd natural frequency "rtnf"	Relative 1st mode shape difference "rfmd"	Relative 2nd mode shape difference "rsmd"	Relative 3rd mode shape difference "rtmd"	Experimental relative 1st crack location "rfcl" 1st crack depth "rfcd" 2nd crack location "rscl" 2nd crack depth "rscd"				Gaussian Fuzzy-BPNN relative 1st crack location "rfcl" 1st crack depth "rfcd" 2nd crack location"rscl" 2nd crack depth "rscd"				Trapezoidal fuzzy-BPNN relative 1st crack location "rfcl" 1st crack depth "rfcd" 2nd crack location"rscl" 2nd crack depth "rscd"				Triangular Fuzzy-BPNN relative 1st crack location "rfcl" 1st crack depth "rfcd" 2nd crack location "rscl" 2nd crack depth "rscd "			
						rfcl	rfcd	rscl	rscd	rfcl	rfcd	rscl	rscd	rfcl	rfcd	rscl	rscd	rfcl	rfcd	rscl	rscd
0.99607	0.99700	0.99829	0.00013	0.00203	0.00240	0.125	0.1667	0.250	0.3333	0.119	0.159	0.239	0.318	0.119	0.159	0.238	0.318	0.118	0.158	0.236	0.315
0.98098	0.99557	0.99892	0.00275	0.00456	0.01064	0.250	0.0833	0.500	0.1667	0.239	0.079	0.477	0.159	0.238	0.079	0.476	0.159	0.236	0.079	0.473	0.158
0.99651	0.99425	0.99796	0.00079	0.00264	0.00101	0.375	0.250	0.625	0.500	0.358	0.239	0.596	0.477	0.357	0.238	0.596	0.476	0.355	0.236	0.591	0.473
0.99001	0.99318	0.98710	0.00145	0.00571	0.00508	0.1875	0.3333	0.3125	0.1667	0.179	0.318	0.298	0.159	0.179	0.318	0.298	0.159	0.177	0.315	0.295	0.158
0.98809	0.98584	0.98255	0.00288	0.01210	0.01352	0.4375	0.500	0.6875	0.25	0.417	0.477	0.656	0.239	0.417	0.476	0.655	0.238	0.414	0.473	0.650	0.236
0.99672	0.98724	0.99719	0.00176	0.00332	0.00594	0.5625	0.3333	0.8125	0.0833	0.537	0.318	0.775	0.079	0.536	0.318	0.774	0.079	0.532	0.315	0.768	0.079
0.99788	0.97843	0.97519	0.00284	0.01222	0.02349	0.500	0.4167	0.750	0.500	0.477	0.398	0.716	0.477	0.476	0.397	0.715	0.476	0.473	0.394	0.709	0.473
0.99874	0.99877	0.99628	0.00026	0.00475	0.01519	0.3125	0.500	0.5625	0.3333	0.298	0.477	0.537	0.318	0.298	0.476	0.536	0.318	0.295	0.473	0.532	0.315
0.99114	0.99799	0.99803	0.00010	0.00166	0.00183	0.4375	0.250	0.6625	0.4167	0.417	0.239	0.632	0.398	0.417	0.238	0.631	0.397	0.414	0.236	0.626	0.394
0.99701	0.98999	0.99803	0.00153	0.00464	0.00239	0.625	0.4167	0.875	0.3333	0.596	0.398	0.835	0.318	0.596	0.397	0.834	0.318	0.591	0.394	0.827	0.315
Average percentage of deviation										4.61	4.59	4.57	4.63	4.85	4.79	4.72	4.82	5.47	5.43	5.39	5.44
Total percentage of deviation										4.60				4.79				5.44			

Table 7.6 Comparison of the results derived from Gaussian Fuzzy - RBFNN, Trapezoidal Fuzzy – RBFNN, Triangular Fuzzy - RBFNN model and Experimental (Steel beam)

Relative 1st natural frequency "rfnf"	Relative 2nd natural frequency "rsnf"	Relative 3rd natural frequency "rtnf"	Relative 1st mode shape difference "rfmd"	Relative 2nd mode shape difference "rsmd"	Relative 3rd mode shape difference "rtmd"	Experimental relative 1st crack location "rfcl" 1st crack depth "rfcd" 2nd crack location "rscl" 2nd crack depth "rscd"				Gaussian Fuzzy-RBFNN relative 1st crack location "rfcl" 1st crack depth "rfcd" 2nd crack location"rscl" 2nd crack depth "rscd"				Trapezoidal fuzzy-RBFNN relative 1st crack location "rfcl" 1st crack depth "rfcd" 2nd crack location"rscl" 2nd crack depth "rscd"				Triangular Fuzzy-RBFNN relative 1st crack location "rfcl" 1st crack depth "rfcd" 2nd crack location "rscl" 2nd crack depth "rscd "			
						rfcl	rfcd	rscl	rscd	rfcl	rfcd	rscl	rscd	rfcl	rfcd	rscl	rscd	rfcl	rfcd	rscl	rscd
0.99607	0.99700	0.99829	0.00013	0.00203	0.00240	0.125	0.1667	0.250	0.3333	0.121	0.161	0.242	0.323	0.120	0.161	0.241	0.321	0.120	0.160	0.240	0.320
0.98098	0.99557	0.99892	0.00275	0.00456	0.01064	0.250	0.0833	0.500	0.1667	0.242	0.081	0.484	0.161	0.241	0.080	0.482	0.161	0.240	0.080	0.480	0.160
0.99651	0.99425	0.99796	0.00079	0.00264	0.00101	0.375	0.250	0.625	0.500	0.363	0.242	0.605	0.484	0.361	0.241	0.602	0.482	0.360	0.240	0.601	0.480
0.99001	0.99318	0.98710	0.00145	0.00571	0.00508	0.1875	0.3333	0.3125	0.1667	0.182	0.323	0.303	0.161	0.181	0.321	0.301	0.161	0.180	0.320	0.300	0.160
0.98809	0.98584	0.98255	0.00288	0.01210	0.01352	0.4375	0.500	0.6875	0.25	0.424	0.484	0.666	0.242	0.422	0.482	0.663	0.241	0.420	0.480	0.661	0.240
0.99672	0.98724	0.99719	0.00176	0.00332	0.00594	0.5625	0.3333	0.8125	0.0833	0.545	0.323	0.787	0.081	0.542	0.321	0.783	0.080	0.540	0.320	0.781	0.080
0.99788	0.97843	0.97519	0.00284	0.01222	0.02349	0.500	0.4167	0.750	0.500	0.484	0.403	0.726	0.484	0.482	0.402	0.723	0.482	0.480	0.400	0.721	0.480
0.99874	0.99877	0.99628	0.00026	0.00475	0.01519	0.3125	0.500	0.5625	0.3333	0.303	0.484	0.545	0.323	0.301	0.482	0.542	0.321	0.300	0.480	0.540	0.320
0.99114	0.99799	0.99803	0.00010	0.00166	0.00183	0.4375	0.250	0.6625	0.4167	0.424	0.242	0.641	0.403	0.422	0.241	0.638	0.402	0.420	0.240	0.637	0.400
0.99701	0.98999	0.99803	0.00153	0.00464	0.00239	0.625	0.4167	0.875	0.3333	0.605	0.403	0.847	0.323	0.602	0.402	0.843	0.321	0.601	0.400	0.841	0.320
Average percentage of deviation										3.15	3.19	3.17	3.18	3.65	3.62	3.64	3.62	3.98	3.99	3.92	4.10
Total percentage of deviation										3.17				3.63				3.99			

Table 7.7 Comparison of the results derived from, Gaussian Fuzzy - KSOM, Trapezoidal Fuzzy – KSOM, Triangular Fuzzy - KSOM model and Experimental (Steel beam)

Relative 1st natural frequency "rfnf"	Relative 2nd natural frequency "rsnf"	Relative 3rd natural frequency "rtnf"	Relative 1st mode shape difference "rfmd"	Relative 2nd mode shape difference "rsmd"	Relative 3rd mode shape difference "rtmd"	Experimental relative 1st crack location "rfcl" 1st crack depth "rfcd" 2nd crack location "rscl" 2nd crack depth "rscd"				Gaussian Fuzzy - KSOM relative 1st crack location "rfcl" 1st crack depth "rfcd" 2nd crack location"rscl" 2nd crack depth "rscd"				Trapezoidal Fuzzy - KSOM relative 1st crack location "rfcl" 1st crack depth "rfcd" 2nd crack location"rscl" 2nd crack depth "rscd"				Triangular Fuzzy - KSOM relative 1st crack location "rfcl" 1st crack depth "rfcd" 2nd crack location "rscl" 2nd crack depth "rscd"			
						rfcl	rfcd	rscl	rscd	rfcl	rfcd	rscl	rscd	rfcl	rfcd	rscl	rscd	rfcl	rfcd	rscl	rscd
0.99607	0.99700	0.99829	0.00013	0.00203	0.00240	0.125	0.1667	0.250	0.3333	0.119	0.158	0.237	0.316	0.118	0.158	0.236	0.315	0.118	0.157	0.235	0.314
0.98098	0.99557	0.99892	0.00275	0.00456	0.01064	0.250	0.0833	0.500	0.1667	0.237	0.079	0.475	0.158	0.236	0.079	0.473	0.158	0.235	0.078	0.471	0.157
0.99651	0.99425	0.99796	0.00079	0.00264	0.00101	0.375	0.250	0.625	0.500	0.356	0.237	0.593	0.475	0.354	0.236	0.591	0.473	0.353	0.235	0.588	0.471
0.99001	0.99318	0.98710	0.00145	0.00571	0.00508	0.1875	0.3333	0.3125	0.1667	0.178	0.316	0.297	0.158	0.177	0.315	0.295	0.158	0.176	0.314	0.294	0.157
0.98809	0.98584	0.98255	0.00288	0.01210	0.01352	0.4375	0.500	0.6875	0.250	0.415	0.475	0.652	0.237	0.413	0.473	0.650	0.236	0.412	0.471	0.647	0.235
0.99672	0.98724	0.99719	0.00176	0.00332	0.00594	0.5625	0.3333	0.8125	0.0833	0.534	0.316	0.771	0.079	0.532	0.315	0.768	0.079	0.529	0.314	0.765	0.078
0.99788	0.97843	0.97519	0.00284	0.01222	0.02349	0.500	0.4167	0.750	0.500	0.475	0.395	0.712	0.475	0.473	0.394	0.709	0.473	0.471	0.392	0.706	0.471
0.99874	0.99877	0.99628	0.00026	0.00475	0.01519	0.3125	0.500	0.5625	0.3333	0.297	0.475	0.534	0.316	0.295	0.473	0.532	0.315	0.294	0.471	0.529	0.314
0.99114	0.99799	0.99803	0.00010	0.00166	0.00183	0.4375	0.250	0.6625	0.4167	0.415	0.237	0.629	0.395	0.413	0.236	0.626	0.394	0.412	0.235	0.623	0.392
0.99701	0.98999	0.99803	0.00153	0.00464	0.00239	0.625	0.4167	0.875	0.3333	0.593	0.395	0.830	0.316	0.591	0.394	0.827	0.315	0.588	0.392	0.823	0.314
Average percentage of deviation										5.06	5.16	5.08	5.18	5.58	5.48	5.49	5.39	5.89	5.92	5.91	5.89
Total percentage of deviation										5.11				5.50				5.90			

Table 7.8 Comparison of the results derived from Gaussian Fuzzy -BPNN, Gaussian Fuzzy - RBFNN, Gaussian Fuzzy-KSOM and Gaussian Fuzzy model (Steel beam)

Relative 1st natural frequency "rfnf"	Relative 2nd natural frequency "rsnf"	Relative 3rd natural frequency "rtnf"	Relative 1st mode shape difference "rfmd"	Relative 2nd mode shape difference "rsmd"	Relative 3rd mode shape difference "rtmd"	Gaussian-Fuzzy-KSOM relative 1st crack location "rfcl" 1st crack depth "rfcd" 2nd crack location "rscl" 2nd crack depth "rscd				Gaussian-Fuzzy-RBFNN relative 1st crack location "rfcl" 1st crack depth "rfcd" 2nd crack location "rscl" 2nd crack depth "rscd"				Gaussian Fuzzy-BPNN relative 1st crack location "rfcl" 1st crack depth "rfcd" 2nd crack location "rscl" 2nd crack depth "rscd"				Fuzzy Gaussian relative 1st crack location "rfcl" 1st crack depth "rfcd" 2nd crack location "rscl" 2nd crack depth "rscd"			
						rfcl	rfcd	rscl	rscd	rfcl	rfcd	rscl	rscd	rfcl	rfcd	rscl	rscd	rfcl	rfcd	rscl	rscd
0.99939	0.99813	0.99978	0.00013	0.00106	0.00411	0.119	0.158	0.237	0.316	0.121	0.161	0.242	0.323	0.119	0.159	0.239	0.318	0.118	0.158	0.237	0.316
0.99980	0.99768	0.99664	0.00035	0.00108	0.00073	0.237	0.079	0.475	0.158	0.242	0.081	0.484	0.161	0.239	0.079	0.477	0.159	0.237	0.079	0.474	0.158
0.99952	0.97803	0.98418	0.00341	0.00134	0.02088	0.356	0.237	0.593	0.475	0.363	0.242	0.605	0.484	0.358	0.239	0.596	0.477	0.355	0.237	0.592	0.474
0.99889	0.99881	0.99932	0.00041	0.00224	0.00310	0.178	0.316	0.297	0.158	0.182	0.323	0.303	0.161	0.179	0.318	0.298	0.159	0.178	0.316	0.296	0.158
0.99906	0.98250	0.99800	0.00293	0.00965	0.00839	0.415	0.475	0.652	0.237	0.424	0.484	0.666	0.242	0.417	0.477	0.656	0.239	0.414	0.474	0.651	0.237
0.99958	0.99129	0.99869	0.00123	0.00187	0.00670	0.534	0.316	0.771	0.079	0.545	0.323	0.787	0.081	0.537	0.318	0.775	0.079	0.533	0.316	0.769	0.079
0.99971	0.98183	0.98589	0.00272	0.00638	0.00962	0.475	0.395	0.712	0.475	0.484	0.403	0.726	0.484	0.477	0.398	0.716	0.477	0.474	0.395	0.710	0.474
0.99473	0.98761	0.98721	0.00239	0.00786	0.01099	0.297	0.475	0.534	0.316	0.303	0.484	0.545	0.323	0.298	0.477	0.537	0.318	0.296	0.474	0.533	0.316
0.99230	0.99003	0.99182	0.00149	0.00455	0.00673	0.415	0.237	0.629	0.395	0.424	0.242	0.641	0.403	0.417	0.239	0.632	0.398	0.414	0.237	0.627	0.395
0.99677	0.98931	0.99459	0.00152	0.00540	0.00865	0.593	0.395	0.830	0.316	0.605	0.403	0.847	0.323	0.596	0.398	0.835	0.318	0.592	0.395	0.829	0.316
Average percentage of deviation						5.06	5.16	5.08	5.18	3.15	3.19	3.17	3.18	4.61	4.59	4.57	4.63	5.32	5.26	5.28	5.22
Total percentage of deviation						5.11				3.17				4.60				5.30			

7.4 Summary

The following conclusions can be drawn by analyzing the results in terms of crack locations and crack depths derived from hybrid fuzzy-neuro models. In this section an intelligent hybrid fuzzy-neuro model have been presented. The modal characteristics derived from theoretical and numerical analysis for various crack depths and crack locations for composite and steel beam. These modal data is fed as inputs to the integrated fuzzy-neuro model and outputs are relative first and second crack depth and location. The feasibility of hybrid fuzzy-neuro models have been verified by experimental examination. It is observed that there is a close agreement between them. The Gaussian fuzzy-neuro models produce best results in term of first and second crack location and crack depth in comparison to other hybrid model. The Gaussian fuzzy-RBFNN model gives most efficient results. It is suggested that the Gaussian fuzzy integrated with neural models can be used as health monitoring algorithm for structural elements. It is observed that percentage of deviation is least in hybrid Gaussian fuzzy-RBFNN model with experiment. It is 3.2 % in case of composite beam and 3.17% for the structural steel.

CHAPTER 8

Analysis & Description of Experimental Investigation

The experimental investigation has been carried out to evaluate the modal characteristics (natural frequencies and mode shapes) of cracked and non-cracked beam (composite and steel) for different combination of crack depths and crack locations. The modal response derived from experimental test has been compared with that of theoretical, numerical and various AI techniques data as discussed in previous chapters. This chapter addresses the experimental investigation procedure and required vibration measuring instruments for measuring vibration response of cantilever beam.

8.1 Analysis and Specification of instruments required in vibration measurement

Experiments have been performed using established Bruel & kjaer experimental procedure for composite beam (figure 8.1(a)) and for structural steel (figure 8.1(b)). The experiments are conducted for both types of beams (composite and steel). Ten cracked beam specimens have been taken for each material in experimental analysis with different crack locations and depths. The cantilever beam was clamped on a vibrating table one by one for each material. The cracked and non-cracked cantilever beams have been vibrated with the help of an exciter and a signal generator. The modal responses such as natural frequencies and mode shapes of the beams corresponding to 1^{st}, 2^{nd} and 3^{rd} mode of vibration have been recorded by placing the accelerometer along the length of the beams and displayed on the vibration indicator. Accelerometer received the signals from vibrating beam in term of modal signatures and vibration analyzer analyzed the signals and then displaced on the vibration indicator. The following instruments used in experimental analysis have been shown in table 8.1 with their specification in detail.

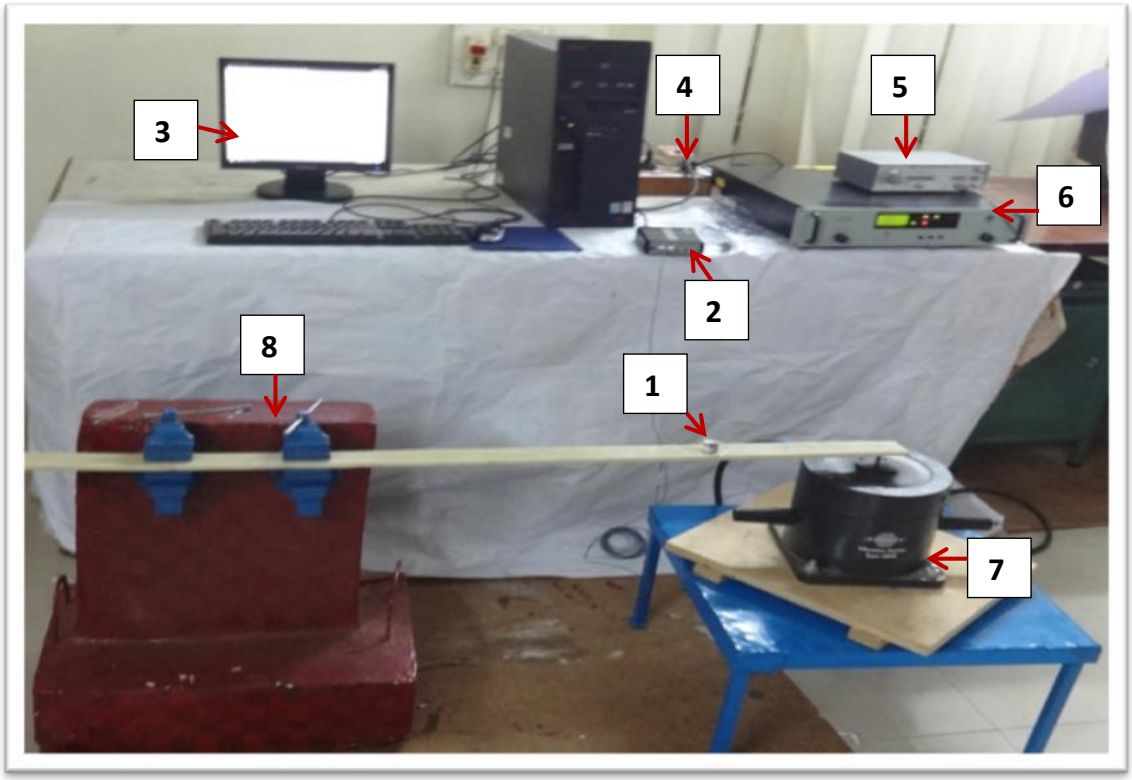

Figure 8.1(a) Photographic view of experimental setup for composite beam

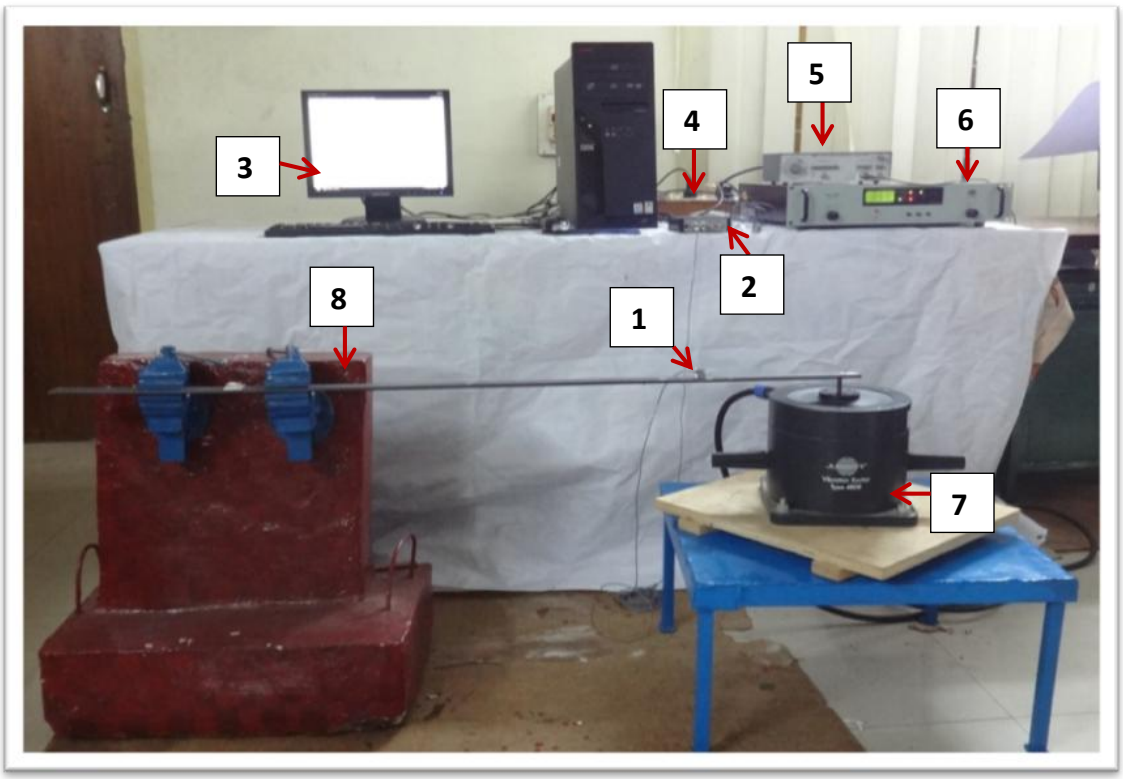

Figure 8.1(b) Photographic view of experimental setup for steel beam

Table 8.1 Description and Specifications of the instruments used in the experiments

Sl. No	**Name of the Instrument**	**Description of Instruments**	
1	**Vibration Analyzer**	Product Name	Pocket front end
		Product Type	3560L
		Manufacturer	Bruel & kjaer
		Frequency Range	7 Hz to 20 Khz
		Channels	2 Inputs, 2 Tachometer
		Input Type	Direct/CCLD
2	**Delta Tron Accelerometer**	Manufacture	Bruel & kjaer
		Product Type	4513-001
		Sensitivity	10mv/g-500mv/g
		Frequency Range	1Hz-10KHz
		Supply voltage	24volts
		Operating temperature range	-50^0C to $+100^0$c
3	**Vibration Indicator**	Manufacture	Bruel & kjaer (PULSE LabShop Software Version 12)
4	**Vibration shaker**	Product Type	4808, Permanent Magnetic Vibration shaker
		Manufacture	Bruel & kjaer
		Frequency Range	5Hz to 10 kHz
		1^{st} t axial resonance	10 kHz
		Maximum bare Table acceleration	700 m/s2 (71 g)
5	**Power Amplifier**	Product Type	2719
		Manufacture	Bruel & kjaer
		Power Amplifier	180VA
6	**Test specimen**	Double crack cantilever beam with dimension 800mmx50mmx6mm	
7	**Power Distribution box**	220V power supply, 50Hz	
8	**Signal Generator**	Product Model	FG200K
		Manufacturer	Aplab
		Frequency Rang	0.2Hz to 200 KHz
		Output Level	15Vp-p into 600 ohms
		Rise/Fall Time	<300nSec

8.2 Systematic experimental procedure

The experimental investigation has been performed on the cracked and non-cracked cantilever beams of layered composite and structural steel to verify the robustness of the results derived from theoretical, numerical and various AI techniques. The cracks at various locations and different depths are introduced in the specimen with the help of wire cut EDM for structural steel beam and for layered composite by putting the slips during the fabrication of composite beam. The test specimens have been clamped one by one of each material in the vibrating table as shown in figure 8.1. The test specimen are excited by signal generator at desirable signal and power amplifier is used for amplify the signal. The specimens have been excited at their first three consecutive modes of vibration and corresponding vibration response (natural frequency and mode shape) received by Deltatron accelerometer by suitable positioning of accelerometer and tuning the vibration shaker at the corresponding resonance frequencies. The vibration analyzer examined the vibration signal received from intact and cracked cantilever beam and displayed in the vibration indicator loaded with the Pulse labshop software. Vibration analyzer is connected with Pulse labshop software with the PCMCIA card. The snapshot of various instruments used in experimental test shown in figures 8.2(a) to 8.2(h).

Figure 8.2(a) Delta Tron Accelerometer

Figure 8.2(b) PCMCIA card

Figure 8.2(c) Vibration analyzer

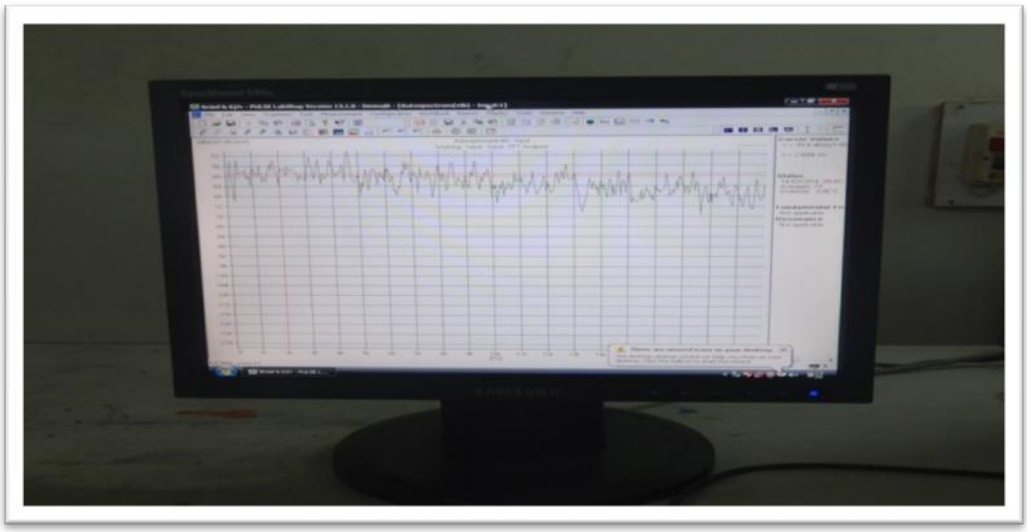

Figure 8.2(d) Vibration indicator imbedded with PULSE lap Shop software

Figure 8.2(e) Signal generator

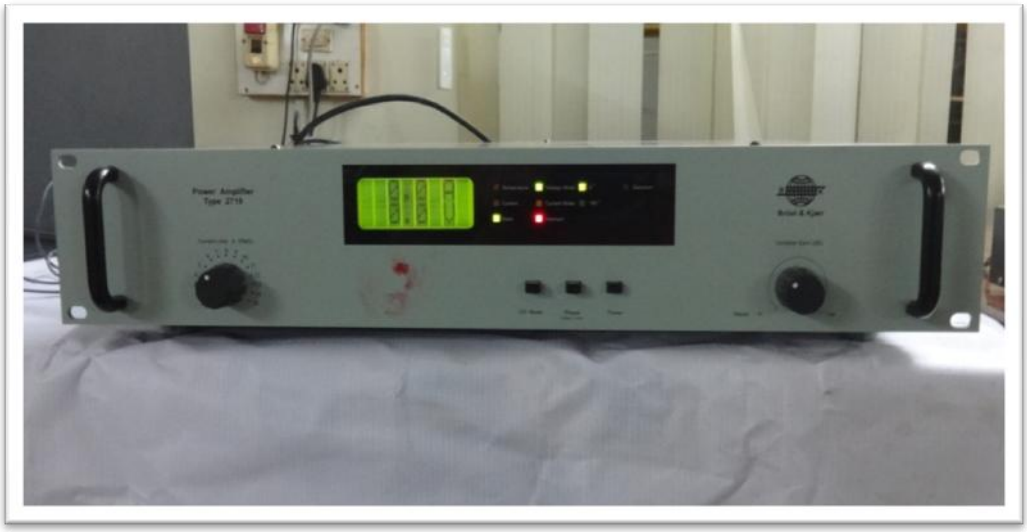

Figure 8.2(f) Power amplifier

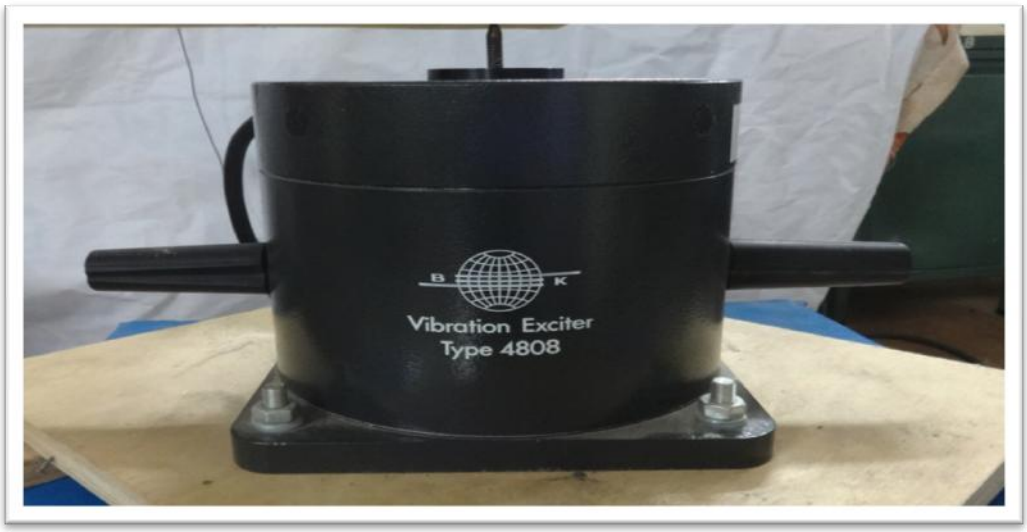

Figure 8.2(g) Vibration Shaker

Figure 8.2(h) Concrete foundation with specimen

8.3 Results and discussion

This section depicts the analysis of results derived from experimental investigation.

The intact and cracked beams with various crack locations and different crack depths have been examined in experimental bed to get vibration response. This is used to verify the robustness of results obtained from various techniques discussed in the previous chapters. A comparison and verification of the results derived from theoretical model for multiple cracks beam with orientation of cracks (β_1=0.25, β_2=0.5, ψ_1=0.1667 and ψ_2=0.5) are shown in chapter 3 and It is plotted with results of experimental examination in the figures 3.13 to 3.15 (for composite) and figures 3.16 to 3.18 (for structural steel). The results derived from theoretical and experimental observation are displayed in tabular form with first three modal parameters (natural frequencies and mode shapes) and relative crack location and crack depth in the table 3.1 and table 3.2 for composite beam and steel bream respectively. Good agreement between the results is observed. The total percentage of deviation of the theoretical analysis is 3.8% for composite beam and 4.4% for structural steel. The results for first three consecutive mode shapes are obtained from numerical analysis for multiple cracks beam with orientation of cracks (β_1=0.25, β_2=0.5, ψ_1=0.1667 and ψ_2=0.5) in chapter 4. It is plotted with corresponding mode shapes derived from theoretical and experimental diagnosis for cracked composite beam and have been shown in figures 4.2a-4.2c. Similarly graph plotted for structural steel has been shown in figures 4.4a to 4.4c. The results for relative first crack depth and crack position and relative second crack depth and crack position are derived from theoretical, numerical and

experimental examination corresponding to relative 1st, 2nd & 3rd natural frequencies and mode shapes. And it is presented in table 4.2 and table 4.4 for composite and steel beam respectively. The total percentages of deviation of numerical analysis are 3.10% for composite beam and 3.50% for structural steel. In chapter 5, the results derived from various fuzzy models (Triangular, Gaussian and Trapezoidal) and experimental test have been compared in table 5.4 for composite beam and likewise table 5.5 presents the comparison of results obtained from various method for structural steel. The total percentage of deviation of results for triangular fuzzy model is 8.1%, for Gaussian fuzzy model is 4.6%, for Trapezoidal fuzzy model is 7.4% for the case of composite beam. Similarly for structural steel, total percentage of deviation of results for triangular fuzzy model is 7.5%, for Gaussian fuzzy model is 4.3 %, for Trapezoidal fuzzy model is 6.8%. In chapter 6 presents discussion about various neural models. The results derived from BPNN, RBFNN and KSOM model compared with experimental analysis results and has been presented in tables 6.1 and 6.3 for composite beam and steel beam respectively. The percentage of total deviation for BPNN is 4.9%, for RBFNN is 4.6% and for KSOM is 5.4%for composite beam. Similarly for the structural steel beam the total percentage of deviation for BPNN is 5.7%, for RBFNN is 4.3% and for KSOM is 6.21%. The comparison of results derived from various hybrid fuzzy-neuro systems have been displayed in tables 7.1, 7.2 and 7.3 for composite beam. After the study of results, it is observed that Gaussian fuzzy-BPNN, Gaussian fuzzy-RBFNN and Gaussian fuzzy-KSOM hybrid system provides least deviation in the results. A similar pattern is observed for structural steel. The comparison of results obtained from various hybrid models have been presented in tables 7.5, 7.6 and 7.7. A close proximity is found between the results.

CHAPTER 9

Results and Discussion

9.1 Introduction

This chapter describes the systematic analysis of performance of various techniques used for identification of multiple damages of cantilever beams cited in the above chapters. The vibration responses of faulty structures have been used for development of damage assessment tool. Various techniques are discussed in current dissertation for assessment of multiple damages of cantilever beams. These techniques are: theoretical method (chapter 3), Finite element method (chapter 4), fuzzy logic system (chapter 5), and artificial neural network (chapter 6), hybrid fuzzy-neuro methods (chapter 7) and experimental investigation (chapter 8).

9.2 Analysis of results derived from various methods

The seven techniques have been employed in current research for development of crack identification tool of structures as discussed in introduction (chapter 1). This dissertation comprises two introductory chapters (Chapter 1- Introduction and chapter 2 - Literature review) besides seven chapters. This section addressed the analysis of results derived from various methods cited in different chapters. The introduction section (chapter 1) of the thesis addressed aim and objective along with the motivation factors to carry out current research. The outline of the dissertation is also discussed in last section of chapter 1. The literature review (chapter 2) part addresses the various methodologies that have been presented by researchers and engineers for prediction of cracks in structures and machine components. Finally this section provides the knowledge to conclude the direction of research.

The vibration response has been measured by theoretical analysis of intact and cracked cantilever layered composite and structural steel beam cited in chapter 3. The variations of natural frequencies for the first three consecutive modes of vibration with different crack locations and depths have been shown in figures 3.2(a), 3.2(b) and 3.2(c). It is seen

that the relative natural frequency for first mode of vibration is on increasing trend while for other two modes, it attains minimum and maximum value at different crack location.

Figures 3.3 to 3.5 represents noticeable deviation in first three consecutive mode shapes of cracked and intact composite beam and magnified view at the vicinity of first crack (figures 3.3(b), 3.4(b) & 3.5(b)) and second crack (figures 3.3(c), 3.4(c) & 3.5(c)). An unexpected jump is observed in mode shape behavior at the crack position. There is a signal of noticeable change in the mode shape behavior due to presence of a crack in the structure. The significant variation in the mode shapes can be observed with increase in crack depth in figures 3.3(a) to 3.3 (c). It is observed that the dimensionless compliance constant increases with increase in the depth of crack due to a reduction in stiffness at the crack location in case of steel beam. Similar to the composite structure, steel beam also depicts the variation in the mode shapes for cracked and intact beam and are displayed in the figures 3.9 to 3.11. Magnified view near the first and second crack position are shown in the figures 3.9(b), 3.10(b), 3.11(b), 3.9(c), 3.10(c) & 3.11(c). It is found that there is significant deviation in the mode shapes due to the presence of a crack. A comparison and verification of the results derived from theoretical model are plotted with results from experimental examination in the figures 3.13 to 3.15 (for composite) and figures 3.16 to 3.18 (for structural steel). The results derived from theoretical and experimental observation are displayed in tabular form with first three modal parameters (natural frequencies and mode shapes) and relative crack location and crack depth in the table 3.1 and table 3.2 for composite beam and steel bream respectively. The total percentages of deviation of the theoretical analysis are 3.8% for composite beam and 4.4% for structural steel.

The finite element based simulation software package ANSYS has been used to extract vibrational features of cantilever composite and structural steel beam (in chapter 4). It is noticed that presence of damage in the form of crack in the structure can alter the vibration responses. The various steps involved in the ANSYS to solve any problem has been discussed. The results obtained from the finite element method have been authenticated by results of experimental analysis for the composite structure as well as a structural steel beam. The results for first three consecutive mode shapes obtained from the finite element analysis have been plotted with corresponding mode shapes are derived from theoretical and experimental diagnosis for cracked composite and are shown in figures 4.2(a)-4.2(c). Similarly, graphs plotted for structural steel are presented in figures 4.4(a) to 4.4(c). The results for relative first crack depth and crack position and relative

second crack depth and crack position are derived from theoretical, finite element analysis and experimental test corresponding to relative 1^{st}, 2^{nd} & 3^{rd} natural frequencies and mode shapes and presented in tables 4.3 and 4.4 for composite and steel beam respectively. It is observed that results have good agreement with each other. The total percentages of deviation of finite element analysis are 3.10% for composite beam and 3.50% for structural steel.

The analysis of results derived from the developed fuzzy model for identification of multiple cracks in composite and steel structure has been depicted in chapter 5. The fuzzy logic system has been developed with simple but effective architecture for six input variables (first three consecutive natural frequencies and mode shapes) and four output variables (relative first and second natural frequencies and mode shapes). Three types of membership functions (Triangular, Gaussian and Trapezoidal) are employed in the development of the fuzzy system and are presented in figures 5.1(a), 5.1(b) and 5.1(c). The various phase involved in the fuzzy logic system has been shown in figure 5.2. The defuzzification of inputs using various membership functions (Triangular, Gaussian and Trapezoidal) have been performed with the help of activated rules 6, and 16 of Table 5.2 are presented in figures 5.7 to 5.9. Similarly for structural steel, it has been shown in the figures 5.13 to 5.15. The results derived from various fuzzy models (Triangular, Gaussian and Trapezoidal) and experimental test have been compared in table 5.4 for composite beam and likewise table 5.5 presents the comparison between results derived from various method for structural steel. The tables 5.6 and 5.7 represent the comparison of results obtained from theoretical, finite element analysis and Fuzzy Gaussian model for composite beam and structural beam respectively. The total percentage of deviation of results for the triangular fuzzy model is 8.1%, for Gaussian fuzzy model is 5.1%, for the Trapezoidal fuzzy model is 7.4% in case of composite beam. Similarly the total percentage of deviation of results for the Triangular fuzzy model is 7.5%, for Gaussian fuzzy model is 4.3 %, for the Trapezoidal fuzzy model is 6.8% for structural steel.

Chapter 6 depicts the discussion on the analysis of results derived from various neural models such as BPNN, RBFNN, and KSOM. Figure 6.1 presents the simple architecture of an artificial neural network. The seven layered back propagation neural network technique is analysed from diagnosis of first and second crack locations, and crack depths and are presented in figure 6.2. First three natural frequencies and mode shapes of bending mode of vibration have been used as input variables to input layer of BPNN model. These input variables process through five hidden layers then output layer gives

relative first and second crack depth and location. The RBFNN is a feed forward, supervised learning type of neural network. In present work, RBFNN is employed for localization and quantification of cracks, present in the cantilever composite and structural steel beam. Similar to BPNN model, RBFNN consists of one input layer and output layer. But RBFNN has only one hidden layer. Moreover, output layer gives relative crack locations and crack depths. Figure 6.3 denotes architecture of radial basis function neural network for identification of multiple cracks. The procedure of damage detection of the beam using RBFNN model has been displayed in the flowchart (figure 6.4). Likewise BPNN and RBFNN model, Kohonen SOM type of neural network has been discussed in chapter 6 for prediction of multiple cracks presence in the composite and steel beam. KSOM is a competitive un-supervised learning type neural network. The flowchart for KSOM mechanism has been shown in figure 6.7. The results obtained from neural network techniques (BPNN, RBFNN, and KSOM) and the experimental test is compared and close agreement between each other is observed. The flowchart for KSOM mechanism has shown in figure 6.7. The results derived from BPNN, RBFNN, and KSOM model compared with experimental analysis results are presented in tables 6.1 and 6.3 for composite beam and steel beam respectively. The total percentage of deviation for BPNN is 4.9%, for RBFNN is 4.6% and for KSOM is 5.4%for the composite beam. Similarly for the structural steel beam the total percentage of deviation for BPNN is 5.7%, for RBFNN is 4.3% and for KSOM is 6.21%. The results obtained from RBFNN, fuzzy Gaussian model, theoretical and finite element method have been compared in tables 6.2 and 6.4 for composite and steel beam respectively. It is observed that the RBFNN model gives better results as compared to the Fuzzy Gaussian model for the composite as well as structural steel beam.

Chapter 7 describes the analysis of results obtained from the hybrid fuzzy-neuro system. The fuzzy system with Triangular, Gaussian and Trapezoidal membership function are integrated with neural network models (BPNN, RBFNN & KSOM) for designing the smart crack identification mechanism for composite and structural beam. The Triangular fuzzy-BPNN hybrid model, Gaussian fuzzy-BPNN hybrid system, and Trapezoidal fuzzy-BPNN hybrid model have been shown in figures 7.1(a), 7.1(b) and 7.1(c) respectively. Figures 7.2(a), 7.2(b) and 7.2(c) represent the Triangular fuzzy-RBFNN hybrid model, Gaussian fuzzy- RBFNN hybrid system and Trapezoidal fuzzy- RBFNN hybrid model respectively. Similarly Triangular fuzzy-KSOM hybrid model, Gaussian fuzzy- KSOM hybrid system and Trapezoidal fuzzy- KSOM hybrid technique has been

presented in figures 7.3(a), 7.3(b) and 7.3(c) respectively. The comparisons of results derived from various hybrid fuzzy-neuro systems have been displayed in tables 7.1, 7.2 and 7.3 for the composite beam. After the study of results, it is observed that Gaussian fuzzy-BPNN, Gaussian fuzzy-RBFNN and Gaussian fuzzy-KSOM hybrid system provide the least deviation in the results. Therefore Gaussian fuzzy model is integrated with BPNN, RBFNN and KSOM. A similar pattern is observed for structural steel. The comparisons of results obtained from various hybrid models have been presented in tables 7.5, 7.6, 7.7 and 7.8.

The experimental investigation is performed to verify the robustness of the results derived from the theoretical model, finite element method, fuzzy logic system, neural network techniques and hybrid fuzzy-neuro model and is discussed in chapter 8. The schematic and snapshot view of the experimental set up with all desired instruments and test specimen are shown in figure 3.12 and fig. 8.1 respectively. The systematic experimental procedure described in the section 8.2 of chapter 8.

9.3 Summary

After the comprehensive investigation of current chapter it is observed that the hybrid model fuzzy-neuro models provide better results as compared to the results derived from standalone AI techniques. Among all proposed hybrid models, Gaussian fuzzy-RBFNN gives far better results. The total percentage for Gaussian fuzzy-RBFNN is 3.2% (composite beam) and 3.17% (steel beam).

CHAPTER 10

Conclusions and Scope for future work

10.1 Introduction

In the present study, localization and quantification of crack locations and depths present in the engineering structures using vibration response have been addressed. The effects of multiple transverse cracks on composite and steel beams are analyzed using the intelligent fault diagnosis system. The vibration responses of cantilever structures have been measured using theoretical, finite element and experimental analysis. The vibration response has been adopted to design inverse intelligent damage identification tool such as fuzzy logic system, neural network and fuzzy-neuro hybrid models for assessment of relative crack locations and relative crack depths.

10.2 Contributions

The presence of the crack in the structural members and machines induces local flexibility. This flexibility changes the integrity of the structural such as frequency response and amplitude of vibration. In previous research, the researchers have analyzed the effect of crack on the modal parameters (natural frequencies and mode shapes) in the domain of identification of damage in beam like dynamic structures, whereas in the present thesis effort has been made to design computational AI techniques based models to identify the crack locations and depths present in structural using the natural frequencies and mode shapes.

In the present thesis multiple faults recognition algorithm has been developed, a theoretical model has been developed using stress intensity factors and strain energy release rate to find out changes in the modal parameters due to presence of the cracks in the vibrating structures. Finite element analysis and experimental analysis have also been carried out on the cracked steel and composite beam to find out the influence of cracks on the modal parameters on vibrating structures. Different AI models have been designed and developed for multiple crack identification using fuzzy inference system, artificial neural network such as BPNN, RBFNN and KSOM and various hybrid models such as fuzzy-BPNN, Fuzzy-RBFNN and Fuzzy-KSOM.

10.3 Conclusions

The conclusions are drawn on the basis of results derived from various methods as discussed in the above chapters and are as follows;

- The theoretical and finite element analysis for cantilever composite and steel beam containing multiple cracks has been derived to measure the modal parameters (natural frequencies and mode shapes) of the system.
- The location and size of the crack strongly influence the natural frequencies and mode shapes of damaged engineering structures. The noticeable changes in mode shapes are observed at the vicinity of cracks.
- The positions of the cracks affect significantly the changes in the natural frequencies of vibrations in the case of constant relative depth of the cracks. When the cracks are located near to each other, the changes in the natural frequencies tend to increase.
- In the case of two cracks of different depths, the larger crack has the most significant effect on the natural frequencies of vibration. This is evident for the first natural vibration of a cantilever beam. For other modes of vibration this is not so clear, because the influence of a crack location at a node is negligible. These changes in mode shapes and natural frequencies will be helpful in prediction of crack location and its intensity and can further be extended to any multiple cracked systems.
- It is observed from the analysis that change in frequencies due to presence of cracks have no substantial influence especially for least crack depth ratio (if less than 0.1). Therefore it is decreasing the chance of localization and quantification of crack effectively. But the crack depths have noticeable influence on mode shapes even with presence of small crack depth ratios. So, it can be concluded that if there is change in natural frequencies and mode shapes of vibrating structures, crack locations and its depths can be efficiently recognized.
- The comparison of mode shape contours drawn from the theoretical analysis of cracked and non-cracked composite beam (figures 3.3 to 3.5) and steel beam (figures 3.9 to 3.11) have been articulated the deviations in mode shape contours. From the investigation of mode shape profiles of the cracked cantilever beams at different crack locations and crack depths, a substantial pattern has been recognized (A sudden jump in the magnitudes of mode shapes have been observed at crack locations and the magnitude of mode shapes increase with increase in crack depth).

- The experimental test on cracked cantilever composite and steel beams with different crack orientations has been performed to verify the authentication of the modal parameters obtained from theoretical and numerical methods for composite beam (shown in figures 3.13 to 3.15) and for steel beam (shown in figures 3.16 to 3.18). The results are in close agreement.
- The natural frequencies and mode shapes for first three consecutive modes of vibration corresponding to different crack locations and its size have been used as a platform to design the fuzzy logic system for multiple cracks identification of structural system.
- The Triangular, Gaussian, and Trapezoidal membership functions have been used to design and develop the fuzzy logic system with six input and four output parameters. From the analysis of results, it is reported that fuzzy system can be efficiently used for identification of crack locations and depths.
- The fuzzy model with Gaussian membership function provides better results as compared to Triangular and Trapezoidal fuzzy models. It is reported by the analysis of results from the fuzzy models. Hence, a fuzzy model with Gaussian membership function is found most suitable for identification of faults present in the vibrating structures.
- The artificial neural network techniques such as BPNN, RBFNN and KSOM have been used as fault diagnosis tool with six input and four output parameters in current research. The training data for developed neural models have been derived from theoretical, numerical and experimental investigations. The results predicted by neural network techniques in terms of relative crack locations and its size have good agreement with the experimental results. The results predicted by proposed RBFNN model provides least deviation from experimental results. Thereby RBFNN model can be used more effectively than BPNN and KSOM models for the diagnosis of damages in the vibrating structures.
- From the investigation of results predicted from fuzzy models and neural models, Gaussian fuzzy model and RBFNN model are closer to real results (experimental) as compared to other proposed fuzzy and neural models.
- The fuzzy-neuro hybrid models have been designed to predict the damage present in the composite and steel beam. The fuzzy model with Triangular, Gaussian and Trapezoidal membership functions have been individually integrated with the three

types of neural models i. e. BPNN, RBFNN & KSOM. Total nine fuzzy-neural models have been discussed in current research.

- From the analysis of results, Gaussian fuzzy-neural (BPNN, RBFNN & KSOM) model provides better results as compared to others fuzzy-neuro models and individual fuzzy and neural models. It is concluded that fuzzy-neuro model with Gaussian membership function and RBFNN give excellent results than other fuzzy-neuro models. The Fuzzy-neuro model with Gaussian membership function and RBFNN model can be used as potential damage identification tools.
- The results predicted from proposed AI techniques have been compared with the results obtained from theoretical, numerical and experimental analysis. The results predicted from Gaussian fuzzy- RBFNN hybrid model provides more accurate results as compared to other AI techniques discussed in above chapters. It is concluded that this hybrid technique can be used as an efficient fault diagnosis tool in the engineering system.
- The developed intelligent fault diagnosis system can be used for identification of damages present in cantilever type of bridges and cranes, turbine shafts, mechanical systems, marine structures, various engineering systems etc.

10.2 Future scope of the work

- The application of AI techniques may be extended to estimation of damage present in the complex engineering system.
- The AI techniques may be utilized for identification of multiple faults present in the different FRC materials with different ply sequence.
- The hybridization of AI techniques can be used as efficient, accurate and robust fault detection technique for identification of damage present in various vibrating dynamic systems such as crushers, turbine shafts, helicopter rotors, bridges, rails etc.

REFERENCES

1. Doebling, S. W., Farrar, C. R., Prime, M. B., & Shevitz, D. W. (1996). Damage identification and health monitoring of structural and mechanical systems from changes in their vibration characteristics: a literature review (No. LA--13070-MS). *Los Alamos National Laboratory*.
2. Dimarogonas, A. D. (1996). Vibration of cracked structures: a state of the art review. *Engineering fracture mechanics*, *55*(5), 831-857.
3. Sohn, H., Farrar, C. R., Hemez, F. M., & Czarnecki, J. J. (2002). A Review of Structural Health Review of Structural Health Monitoring Literature 1996-2001(No. LA-UR-02-2095). *Los Alamos National Laboratory*.
4. Carden, E. P., & Fanning, P. (2004). Vibration based condition monitoring: a review. *Structural health monitoring*, *3*(4), 355-377.
5. Dessi, D., & Camerlengo, G. (2015). Damage identification techniques via modal curvature analysis: Overview and comparison. *Mechanical Systems and Signal Processing*, *52*, 181-205.
6. Cao, M., Radzieński, M., Xu, W., & Ostachowicz, W. (2014). Identification of multiple damage in beams based on robust curvature mode shapes. *Mechanical Systems and Signal Processing*, *46*(2), 468-480.
7. Wang, Y. L. (2014). New damage localization indicator based on curvature for single-span beams. *Structural Engineering and Mechanics*, *51*(6), 1037-1046.
8. Kargarnovin, M. H., Jafari-Talookolaei, R. A., & Ahmadian, M. T. (2013). Vibration analysis of de-laminated Timoshenko beams under the motion of a constant amplitude point force traveling with uniform velocity. *International Journal of Mechanical Sciences*, *70*, 39-49.
9. Argatov, I., & Butcher, E. A. (2011). On the separation of internal and boundary damage in slender bars using longitudinal vibration frequencies and equivalent linearization of damaged bolted joint response. *Journal of Sound and Vibration*, *330*(13), 3245-3256.
10. Casini, P., & Vestroni, F. (2011). Characterization of bifurcating nonlinear normal modes in piecewise linear mechanical systems. *International Journal of Non-Linear Mechanics*, *46*(1), 142-150.

11. Carr, G. E., & Chapetti, M. D. (2011). On the detection threshold for fatigue cracks in welded steel beams using vibration analysis. *International Journal of Fatigue*, *33* (4), 642-648.
12. Farshidi, R., Trieu, D., Park, S. S., & Freiheit, T. (2010). Non-contact experimental modal analysis using air excitation and a microphone array. *Measurement*, *43*(6), 755-765.
13. Rezaee, M., & Hassannejad, R. (2010). Free vibration analysis of simply supported beam with breathing crack using perturbation method. *Acta Mechanica Solida Sinica*, *23*(5), 459-470.
14. Faverjon, B., & Sinou, J. J. (2009). Identification of an open crack in a beam using an a posteriori error estimator of the frequency response functions with noisy measurements. *European journal of mechanics-A/Solids*, *28*(1), 75-85.
15. Mazanoglu, K., Yesilyurt, I., & Sabuncu, M. (2009). Vibration analysis of multiple-cracked non-uniform beams. *Journal of sound and vibration*, *320*(4), 977-989.
16. Lee, J. (2009). Identification of multiple cracks in a beam using natural frequencies. *Journal of sound and vibration*, *320*(3), 482-490.
17. He, Y., Ye, J., Chen, X., & He, Z. (2009). Discussion on calculation of the local flexibility due to the crack in a pipe. *Mechanical systems and signal processing*, *23*(3), 804-810.
18. Ebersbach, S., & Peng, Z. (2008). Expert system development for vibration analysis in machine condition monitoring. *Expert systems with applications*, *34*(1), 291-299.
19. Cerri, M. N., Dilena, M., & Ruta, G. C. (2008). Vibration and damage detection in undamaged and cracked circular arches: experimental and analytical results. *Journal of sound and vibration*, *314*(1), 83-94.
20. Shin, Y. J., Kwon, K. M., & Yun, J. H. (2008). Vibration analysis of a circular arc with variable cross-section using differential transformation and generalized differential quadrature. *Journal of Sound and Vibration*, *309* (1), 9-19.
21. Babu, T. R., & Sekhar, A. S. (2008). Detection of two cracks in a rotor-bearing system using amplitude deviation curve. *Journal of sound and vibration*, *314*(3), 457-464.
22. Benfratello, S., Cacciola, P., Impollonia, N., Masnata, A., & Muscolino, G. (2007). Numerical and experimental verification of a technique for locating a

fatigue crack on beams vibrating under Gaussian excitation. *Engineering Fracture Mechanics*, *74*(18), 2992-3001

23. Sinha, J. K. (2007). Higher order spectra for crack and misalignment identification in the shaft of a rotating machine. *Structural Health Monitoring*, *6*(4), 325-334.
24. Viola, E., Dilena, M., & Tornabene, F. (2007). Analytical and numerical results for vibration analysis of multi-stepped and multi-damaged circular arches. *Journal of Sound and Vibration*, *299* (1), 143-163.
25. Humar, J., Bagchi, A., & Xu, H. (2006). Performance of vibration-based techniques for the identification of structural damage. *Structural Health Monitoring*, *5*(3), 215-241.
26. Loutridis, S., Douka, E., & Hadjileontiadis, L. J. (2005). Forced vibration behavior and crack detection of cracked beams using instantaneous frequency. *Ndt & E International*, *38*(5), 411-419
27. Wang, K., Inman, D. J., & Farrar, C. R. (2005). Modeling and analysis of a cracked composite cantilever beam vibrating in coupled bending and torsion. *Journal of sound and vibration*, *284*(1), 23-49.
28. Douka, E., & Hadjileontiadis, L. J. (2005). Time–frequency analysis of the free vibration response of a beam with a breathing crack. *NDT & E International*, *38*(1), 3-10.
29. Douka, E., Bamnios, G., & Trochidis, A. (2004). A method for determining the location and depth of cracks in double-cracked beams. *Applied acoustics*, *65*(10), 997-1008.
30. Cerri, M. N., & Ruta, G. C. (2004). Detection of localised damage in plane circular arches by frequency data. *Journal of sound and vibration*, *270*(1), 39-59.
31. Owolabi, G. M., Swamidas, A. S. J., & Seshadri, R. (2003). Crack detection in beams using changes in frequencies and amplitudes of frequency response functions. *Journal of sound and vibration*, *265*(1), 1-22.
32. Song, O., Ha, T. W., & Librescu, L. (2003). Dynamics of anisotropic composite cantilevers weakened by multiple transverse open cracks. *Engineering Fracture Mechanics*, *70*(1), 105-123.
33. Zou, J., Chen, J., Niu, J. C., & Geng, Z. M. (2003). Discussion on the local flexibility due to the crack in a cracked rotor system. *Journal of sound and vibration*, *262*(2), 365-369.

34. Patil, D. P., & Maiti, S. K. (2003). Detection of multiple cracks using frequency measurements. *Engineering Fracture Mechanics*, *70*(12), 1553-1572.
35. Kim, J. T., & Stubbs, N. (2002). An improved damage identification method based on modal information. *Journal of Sound and Vibration*, *252*(2), 223-238.
36. Chinchalkar, S. (2001). Determination of crack location in beams using natural frequencies. *Journal of Sound and vibration*, *247*(3), 417-429.
37. Xia, Y., & Hao, H. (2000). Measurement selection for vibration-based structural damage identification. *Journal of Sound and Vibration*, *236*(1), 89-104.
38. Messina, A., Williams, E. J., & Contursi, T. (1998). Structural damage detection by a sensitivity and statistical-based method. *Journal of sound and vibration*, *216*(5), 791-808.
39. Xu, Y. F., Zhu, W. D., Liu, J., & Shao, Y. M. (2014). Identification of embedded horizontal cracks in beams using measured mode shapes. *Journal of Sound and Vibration*, *333*(23), 6273-6294.
40. Wang, W., Wan, X., Zhou, J., Zhao, M., Li, Y., Shang, S., & Gao, X. (2012). Damage and Failure of Laminated Carbon-Fiber-Reinforced Composite under Low-Velocity Impact. *Journal of Aerospace Engineering*, *27*(2), 308-317.
41. Ariaei, A., Ziaei-Rad, S., & Ghayour, M. (2009). Vibration analysis of beams with open and breathing cracks subjected to moving masses. *Journal of sound and vibration*, *326*(3), 709-724.
42. Panigrahi, S. K. (2009). Damage analyses of adhesively bonded single lap joints due to de-laminated FRP composite adherents. *Applied Composite Materials*, *16*(4), 211-223.
43. Potirniche, G. P., Hearndon, J., Daniewicz, S. R., Parker, D., Cuevas, P., Wang, P. T., & Horstemeyer, M. F. (2008). A two-dimensional damaged finite element for fracture applications. *Engineering Fracture Mechanics*, *75*(13), 3895-3908.
44. Hearndon, J. L., Potirniche, G. P., Parker, D., Cuevas, P. M., Rinehart, H., Wang, P. T., & Horstemeyer, M. F. (2008). Monitoring structural damage of components using an effective modulus approach. *Theoretical and applied fracture mechanics*, *50*(1), 23-29.
45. Al-Said, S. M. (2007). Crack identification in a stepped beam carrying a rigid disk. *Journal of sound and vibration*, *300*(3), 863-876.

46. Andreaus, U., Casini, P., & Vestroni, F. (2007). Non-linear dynamics of a cracked cantilever beam under harmonic excitation. *International journal of non-linear mechanics*, *42*(3), 566-575.
47. Kisa, M., & Gurel, M. A. (2007). Free vibration analysis of uniform and stepped cracked beams with circular cross sections. *International Journal of Engineering Science*, *45*(2), 364-380.
48. Karthikeyan, M., Tiwari, R., & Talukdar, S. (2007). Crack localization and sizing in a beam based on the free and forced response measurements. *Mechanical Systems and Signal Processing*, *21*(3), 1362-1385.
49. Chasalevris, A. C., & Papadopoulos, C. A. (2006). Identification of multiple cracks in beams under bending. *Mechanical Systems and Signal Processing*, *20*(7), 1631-1673.
50. Nahvi, H., & Jabbari, M. (2005). Crack detection in beams using experimental modal data and finite element model. *International Journal of Mechanical Sciences, 47* (10), 1477-1497.
51. Law, S. S., & Lu, Z. R. (2005). Crack identification in beam from dynamic responses. *Journal of Sound and Vibration*, *285* (4), 967-987.
52. Zheng, D. Y., & Kessissoglou, N. J. (2004). Free vibration analysis of a cracked beam by finite element method. *Journal of Sound and vibration*, *273*(3), 457-475.
53. Kim, J. T., & Stubbs, N. (2003). Crack detection in beam-type structures using frequency data. *Journal of Sound and Vibration*, *259*(1), 145-160.
54. Saavedra, P. N., & Cuitino, L. A. (2001). Crack detection and vibration behavior of cracked beams. *Computers & Structures*, *79*(16), 1451-1459.
55. Viola, E., Federici, L., & Nobile, L. (2001). Detection of crack location using cracked beam element method for structural analysis. *Theoretical and Applied Fracture Mechanics*, *36*(1), 23-35.
56. Sugumaran, V., & Ramachandran, K. I. (2011). Fault diagnosis of roller bearing using fuzzy classifier and histogram features with focus on automatic rule learning. *Expert Systems with Applications*, *38*(5), 4901-4907.
57. Hasanzadeh, R. P., Sadeghi, S. H. H., Ravan, M., Moghaddamjoo, A. R., & Moini, R. (2011). A fuzzy alignment approach to sizing surface cracks by the AC field measurement technique. *NDT & E International*, *44*(1), 75-83.

58. Wu, Q., & Law, R. (2010). Complex system fault diagnosis based on a fuzzy robust wavelet support vector classifier and an adaptive Gaussian particle swarm optimization. *Information Sciences*, *180*(23), 4514-4528.
59. Chandrashekhar, M., & Ganguli, R. (2009). Damage assessment of structures with uncertainty by using mode-shape curvatures and fuzzy logic. *Journal of Sound and Vibration*, *326*(3), 939-957.
60. Saravanan, N., Cholairajan, S., & Ramachandran, K. I. (2009). Vibration-based fault diagnosis of spur bevel gear box using fuzzy technique. *Expert systems with applications*, *36*(2), 3119-3135.
61. Angelov, P., Lughofer, E., & Zhou, X. (2008). Evolving fuzzy classifiers using different model architectures. *Fuzzy Sets and Systems*, *159*(23), 3160-3182.
62. Kim, Y. M., Kim, C. K., & Hong, G. H. (2007). Fuzzy set based crack diagnosis system for reinforced concrete structures. *Computers & structures*, *85*(23), 1828-1844.
63. Reza, H. P., Rezaie, A. H., Sadeghi, S. H. H., Moradi, M. H., & Ahmadi, M. (2007). A density-based fuzzy clustering technique for non-destructive detection of defects in materials. *NDT & E International*, *40*(4), 337-346.
64. Boutros, T., & Liang, M. (2007). Mechanical fault detection using fuzzy index fusion. *International Journal of Machine Tools and Manufacture*, *47*(11), 1702-1714.
65. De Miguel, L. J., & Blázquez, L. F. (2005). Fuzzy logic-based decision-making for fault diagnosis in a DC motor. *Engineering Applications of Artificial Intelligence*, *18*(4), 423-450.
66. Parhi, D. R. (2005). Navigation of mobile robots using a fuzzy logic controller. *Journal of intelligent and robotic systems*, *42*(3), 253-273.
67. Mohanta, D. K., Sadhu, P. K., & Chakrabarti, R. (2005). Fuzzy Markov model for determination of fuzzy state probabilities of generating units including the effect of maintenance scheduling. *IEEE Transactions on Power Systems*, *20*(4), 2117-2124.
68. Rakideh, M., Dardel, M., & Pashaei, M. H. (2013). Crack detection of Timoshenko beams using vibration behavior and neural network. *Int. J. Eng*, *26*(12), 1433-1444.

69. Eski, I., Erkaya, S., Savas, S., & Yildirim, S. (2011). Fault detection on robot manipulators using artificial neural networks. *Robotics and Computer-Integrated Manufacturing*, *27*(1), 115-123.
70. Schlechtingen, M., & Santos, I. F. (2011). Comparative analysis of neural network and regression based condition monitoring approaches for wind turbine fault detection. *Mechanical systems and signal processing*, *25*(5), 1849-1875.
71. Ghate, V. N., & Dudul, S. V. (2010). Optimal MLP neural network classifier for fault detection of three phase induction motor. *Expert Systems with Applications*, *37*(4), 3468-3481.
72. Fan, B., Du, Z., Jin, X., Yang, X., & Guo, Y. (2010). A hybrid FDD strategy for local system of AHU based on artificial neural network and wavelet analysis. *Building and environment*, *45*(12), 2698-2708.
73. Saravanan, N., Siddabattuni, V. K., & Ramachandran, K. I. (2010). Fault diagnosis of spur bevel gear box using artificial neural network (ANN), and proximal support vector machine (PSVM). *Applied soft computing*, *10*(1), 344-360.
74. Paviglianiti, G., Pierri, F., Caccavale, F., & Mattei, M. (2010). Robust fault detection and isolation for proprioceptive sensors of robot manipulators. *Mechatronics*, *20* (1), 162-170.
75. Wang, C. C., Kang, Y., Shen, P. C., Chang, Y. P., & Chung, Y. L. (2010). Applications of fault diagnosis in rotating machinery by using time series analysis with neural network. *Expert Systems with Applications*, *37*(2), 1696-1702.
76. Wu, J. D., & Chan, J. J. (2009). Faulted gear identification of a rotating machinery based on wavelet transform and artificial neural network. *Expert Systems with Applications*, *36*(5), 8862-8875.
77. Mehrjoo, M., Khaji, N., Moharrami, H., & Bahreininejad, A. (2008). Damage detection of truss bridge joints using Artificial Neural Networks. *Expert Systems with Applications*, *35*(3), 1122-1131.
78. Just-Agosto, F., Serrano, D., Shafiq, B., & Cecchini, A. (2008). Neural network based nondestructive evaluation of sandwich composites. *Composites Part B: Engineering*, *39*(1), 217-225
79. Wu, J. D., & Liu, C. H. (2008). Investigation of engine fault diagnosis using discrete wavelet transform and neural network. *Expert Systems with Applications*, *35*(3), 1200-1213.

80. Bakhary, N., Hao, H., & Deeks, A. J. (2007). Damage detection using artificial neural network with consideration of uncertainties. *Engineering Structures*, *29*(11), 2806-2815.
81. Oberholster, A. J., & Heyns, P. S. (2006). On-line fan blade damage detection using neural networks. *Mechanical systems and signal processing*, *20*(1), 78-93.
82. Yeung, W. T., & Smith, J. W. (2005). Damage detection in bridges using neural networks for pattern recognition of vibration signatures. *Engineering Structures*,*27*(5), 685-698
83. Suresh, S., Omkar, S. N., Ganguli, R., and Mani, V. (2004). Identification of crack location and depth in a cantilever beam using a modular neural network approach. *Smart Materials and Structures*, *13*(4), 907.
84. Kao, C. Y., & Hung, S. L. (2003). Detection of structural damage via free vibration responses generated by approximating artificial neural networks. *Computers & structures*, *81*(28), 2631-2644.
85. Zheng, S., Liang, X., Wang, H., & Fan, D. (2014) Detecting multiple cracks in beams using hierarchical genetic algorithms. *Journal of Vibro-engineering*, *16* (1), 341-350.
86. Mehrjoo, M., Khaji, N., & Ghafory-Ashtiany, M. (2013). The application of genetic algorithm in crack detection of beam-like structures using a new cracked Euler–Bernoulli beam element. *Applied Soft Computing*, *13*(2), 867-880
87. Meruane, V., & Heylen, W. (2011). A hybrid real genetic algorithm to detect structural damage using modal properties. *Mechanical Systems and Signal Processing*, *25*(5), 1559-1573.
88. Li, B., Zhang, P. L., Tian, H., Mi, S. S., Liu, D. S., & Ren, G. Q. (2011). A new feature extraction and selection scheme for hybrid fault diagnosis of gearbox. *Expert Systems with Applications*, *38*(8), 10000-10009.
89. Nobahari, M., & Seyedpoor, S. M. (2011). Structural damage detection using an efficient correlation-based index and a modified genetic algorithm. *Mathematical and Computer modelling*, *53*(9), 1798-1809.
90. Buezas, F. S., Rosales, M. B., & Filipich, C. P. (2011). Damage detection with genetic algorithms taking into account a crack contact model. *Engineering Fracture Mechanics*, *78*(4), 695-712.

91. Hussain, S., & Gabbar, H. A. (2011). A novel method for real time gear fault detection based on pulse shape analysis. *Mechanical Systems and Signal Processing*, *25*(4), 1287-1298.
92. Han, H., Gu, B., Wang, T., & Li, Z. R. (2011). Important sensors for chiller fault detection and diagnosis (FDD) from the perspective of feature selection and machine learning. *International journal of refrigeration*, *34*(2), 586-599.
93. Singh, S. K., & Tiwari, R. (2010). Identification of a multi-crack in a shaft system using transverse frequency response functions. *Mechanism and Machine Theory*, *45*(12), 1813-1827.
94. Lei, Y., Zuo, M. J., He, Z., & Zi, Y. (2010). A multidimensional hybrid intelligent method for gear fault diagnosis. *Expert Systems with Applications*, *37*(2), 1419-1430.
95. Zhang, Y., & Randall, R. B. (2009). Rolling element bearing fault diagnosis based on the combination of genetic algorithms and fast kurtogram. *Mechanical Systems and Signal Processing*, *23*(5), 1509-1517.
96. Perera, R., Ruiz, A., & Manzano, C. (2009). Performance assessment of multi-criteria damage identification genetic algorithms. *Computers & Structures*, *87*(1), 120-127.
97. Xiang, J., Zhong, Y., Chen, X., & He, Z. (2008). Crack detection in a shaft by combination of wavelet-based elements and genetic algorithm. *International Journal of Solids and Structures*, *45*(17), 4782-4795.
98. Vakil-Baghmisheh, M. T., Peimani, M., Sadeghi, M. H., & Ettefagh, M. M. (2008). Crack detection in beam-like structures using genetic algorithms. *Applied Soft Computing*, *8*(2), 1150-1160.
99. Zhang, L., Jack, L. B., & Nandi, A. K. (2005). Fault detection using genetic programming. *Mechanical Systems and Signal Processing*, *19*(2), 271-289.
100. He, Y., Guo, D., & Chu, F. (2001). Using genetic algorithms and finite element methods to detect shaft crack for rotor-bearing system. *Mathematics and computers in simulation*, *57*(1), 95-108.
101. Friswell, M. I., Penny, J. E. T., & Garvey, S. D. (1998). A combined genetic an eigensensitivity algorithm for the location of damage in structures. *Computers & Structures*, *69*(5), 547-556.

102. Güneri, A. F., Ertay, T., & YüCel, A. (2011). An approach based on ANFIS input selection and modeling for supplier selection problem. *Expert Systems with Applications*, *38*(12), 14907-14917.
103. Boyacioglu, M. A., & Avci, D. (2010). An adaptive network-based fuzzy inference system (ANFIS) for the prediction of stock market return: the case of the Istanbul stock exchange. *Expert Systems with Applications*, *37*(12), 7908-7912.
104. Vairappan, C., Tamura, H., Gao, S., & Tang, Z. (2009). Batch type local search-based adaptive neuro-fuzzy inference system (ANFIS) with self-feedbacks for time-series prediction. *Neurocomputing*, *72*(7), 1870-1877.
105. Çaydaş, U., Hasçalık, A., & Ekici, S. (2009). An adaptive neuro-fuzzy inference system (ANFIS) model for wire-EDM. *Expert Systems with Applications*, *36*(3), 6135-6139.
106. Jassar, S., Liao, Z., & Zhao, L. (2009). Adaptive neuro-fuzzy based inferential sensor model for estimating the average air temperature in space heating systems. *Building and environment*, *44*(8), 1609-1616.
107. Lei, Y., He, Z., Zi, Y., & Hu, Q. (2007). Fault diagnosis of rotating machinery based on multiple ANFIS combination with GAs. *Mechanical Systems and Signal Processing*, *21*(5), 2280-2294.
108. Ellithy, K., & Al-Naamany, A. (2000). A hybrid neuro-fuzzy static var compensator stabilizer for power system damping improvement in the presence of load parameters uncertainty. *Electric Power Systems Research*, *56*(3), 211-223.
109. Zhu, F., Deng, Z., & Zhang, J. (2013). An integrated approach for structural damage identification using wavelet neuro-fuzzy model. *Expert Systems with Applications*, *40*(18), 7415-7427.
110. Mitchell, R., Kim, Y., & El-Korchi, T. (2012). System identification of smart structures using a wavelet neuro-fuzzy model. *Smart Materials and Structures*, *21*(11), 115009-115021.
111. Beena, P., & Ganguli, R. (2011). Structural damage detection using fuzzy cognitive maps and Hebbian learning. *Applied Soft Computing*, *11*(1), 1014-1020.
112. Salahshoor, K., Khoshro, M. S., & Kordestani, M. (2011). Fault detection and diagnosis of an industrial steam turbine using a distributed configuration of

adaptive neuro-fuzzy inference systems. *Simulation Modelling Practice and Theory*, *19*(5), 1280-1293.

113. Sadeghian, M., & Fatehi, A. (2011). Identification, prediction and detection of the process fault in a cement rotary kiln by locally linear neuro-fuzzy technique. *Journal of Process Control*, *21*(2), 302-308.
114. Eslamloueyan, R. (2011). Designing a hierarchical neural network based on fuzzy clustering for fault diagnosis of the Tennessee–Eastman process.*Applied soft computing*, *11*(1), 1407-1415.
115. Zhang, L., Xiong, G., Liu, H., Zou, H., & Guo, W. (2010). Bearing fault diagnosis using multi-scale entropy and adaptive neuro-fuzzy inference. *Expert Systems with Applications*, *37*(8), 6077-6085.
116. Simon, L. L., & Hungerbuhler, K. (2010). Industrial batch dryer data mining using intelligent pattern classifiers: neural network, neuro-fuzzy and Takagi–Sugeno fuzzy models. *Chemical Engineering Journal*, *157*(2), 568-578.
117. Zio, E., & Gola, G. (2009). A neuro-fuzzy technique for fault diagnosis and its application to rotating machinery. *Reliability Engineering & System Safety*, *94*(1), 78-88.
118. Yang, B. S., Oh, M. S., & Tan, A. C. C. (2009). Fault diagnosis of induction motor based on decision trees and adaptive neuro-fuzzy inference. *Expert Systems with Applications*, *36*(2), 1840-1849.
119. Quteishat, A., & Lim, C. P. (2008). A modified fuzzy min–max neural network with rule extraction and its application to fault detection and classification. *Applied Soft Computing*, *8*(2), 985-995.
120. Fang, X., Luo, H., & Tang, J. (2005). Structural damage detection using neural network with learning rate improvement. *Computers & structures*, *83*(25), 2150-2161.
121. Hajnayeb, A., Ghasemloonia, A., Khadem, S. E., & Moradi, M. H. (2011). Application and comparison of an ANN-based feature selection method and the genetic algorithm in gearbox fault diagnosis. *Expert Systems with Applications*, *38*(8), 10205-10209.
122. Firpi, H., & Vachtsevanos, G. (2008). Genetically programmed-based artificial features extraction applied to fault detection. *Engineering Applications of Artificial Intelligence*, *21*(4), 558-568.

123. Han, T., Yang, B. S., Choi, W. H., & Kim, J. S. (2006). Fault diagnosis system of induction motors based on neural network and genetic algorithm using stator current signals. *International Journal of Rotating Machinery*, *2006*, 1-13.
124. Samanta, B. (2004). Gear fault detection using artificial neural networks and support vector machines with genetic algorithms. *Mechanical Systems and Signal Processing*, *18*(3), 625-644.
125. Samanta, B., Al-Balushi, K. R., & Al-Araimi, S. A. (2003). Artificial neural networks and support vector machines with genetic algorithm for bearing fault detection. *Engineering Applications of Artificial Intelligence*, *16*(7), 657-665.
126. Jack, L. B., & Nandi, A. K. (2002). Fault detection using support vector machines and artificial neural networks, augmented by genetic algorithms.*Mechanical systems and signal processing*, *16*(2), 373-390.
127. Aydin, K., & Kisi, O. (2015). Applicability of a Fuzzy Genetic System for Crack Diagnosis in Timoshenko Beams. *Journal of Computing in Civil Engineering*, *29(*5), 1-15.
128. Wu, Q. (2011). Hybrid fuzzy support vector classifier machine and modified genetic algorithm for automatic car assembly fault diagnosis. *Expert Systems with Applications*, *38*(3), 1457-1463.
129. Pawar, P. M., & Ganguli, R. (2007). Genetic fuzzy system for online structural health monitoring of composite helicopter rotor blades. *Mechanical Systems and Signal Processing*, *21*(5), 2212-2236.
130. Yuan, S., & Chu, F. (2007). Fault diagnosis based on support vector machines with parameter optimisation by artificial immunisation algorithm. *Mechanical Systems and Signal Processing*, *21*(3), 1318-1330.
131. Pawar, P. M., & Ganguli, R. (2003). Genetic fuzzy system for damage detection in beams and helicopter rotor blades. *Computer methods in applied mechanics and engineering*, *192*(16), 2031-2057.
132. Hosseinabadi, H. Z., Nazari, B., Amirfattahi, R., Mirdamadi, H. R., & Sadri, A. R. (2014). Wavelet Network Approach for Structural Damage Identification Using Guided Ultrasonic Waves. *IEEE Transactions on Instrumentation and Measurement*, *63*(7), 1680-1692.
133. Mandal, S. K., Chan, F. T., & Tiwari, M. K. (2012). Leak detection of pipeline: An integrated approach of rough set theory and artificial bee colony trained SVM. *Expert Systems with Applications*, *39*(3), 3071-3080.

134. Bacha, K., Souahlia, S., & Gossa, M. (2012). Power transformer fault diagnosis based on dissolved gas analysis by support vector machine. *Electric power systems research*, *83*(1), 73-79.
135. Kim, H. E., Tan, A. C., Mathew, J., & Choi, B. K. (2012). Bearing fault prognosis based on health state probability estimation. *Expert Systems with Applications*, *39*(5), 5200-5213.
136. Yiakopoulos, C. T., Gryllias, K. C., & Antoniadis, I. A. (2011). Rolling element bearing fault detection in industrial environments based on a K-means clustering approach. *Expert Systems with Applications*, *38*(3), 2888-2911.
137. Jun, B. H. (2011). Fault detection using dynamic time warping (DTW) algorithm and discriminant analysis for swine wastewater treatment. *Journal of hazardous materials*, *185*(1), 262-268.
138. Fagerholt, E., Dørum, C., Børvik, T., Laukli, H. I., & Hopperstad, O. S. (2010). Experimental and numerical investigation of fracture in a cast aluminium alloy. *International Journal of Solids and Structures*, *47*(24), 3352-3365.
139. Cusido, J., Romeral, L., Ortega, J. A., Garcia, A., & Riba, J. R. (2010). Wavelet and PDD as fault detection techniques. *Electric Power Systems Research*, *80*(8), 915-924.
140. Bachschmid, N., Pennacchi, P., & Tanzi, E. (2010). A sensitivity analysis of vibrations in cracked turbogenerator units versus crack position and depth.*Mechanical Systems and Signal Processing*, *24*(3), 844-859.
141. Dilena, M., & Morassi, A. (2009). Structural health monitoring of rods based on natural frequency and antiresonant frequency measurements. *Structural health monitoring*, *8*(2), 149-173.
142. Cao, M., & Qiao, P. (2009). Novel Laplacian scheme and multiresolution modal curvatures for structural damage identification. *Mechanical Systems and Signal Processing*, *23*(4), 1223-1242.
143. Curadelli, R. O., Riera, J. D., Ambrosini, D., & Amani, M. G. (2008). Damage detection by means of structural damping identification. *Engineering Structures*, *30*(12), 3497-3504.
144. Friswell, M. I. (2007). Damage identification using inverse methods. *Philosophical Transactions of the Royal Society of London A: Mathematical, Physical and Engineering Sciences*, *365*(1851), 393-410.

145. Peng, Z. K., Lang, Z. Q., & Billings, S. A. (2007). Crack detection using nonlinear output frequency response functions. *Journal of Sound and Vibration*, *301*(3), 777-788.
146. Rus, G., & Gallego, R. (2007). Hypersingular shape sensitivity boundary integral equation for crack identification under harmonic elasto dynamic excitation. *Computer methods in applied mechanics and engineering*, *196*(25), 2596-2618.
147. Pakrashi, V., Basu, B., & O'Connor, A. (2007). Structural damage detection and calibration using a wavelet–kurtosis technique. *Engineering Structures*, *29*(9), 2097-2108.
148. Hadjileontiadis, L. J., Douka, E., & Trochidis, A. (2005). Crack detection in beams using kurtosis. *Computers & structures*, *83*(12), 909-919.
149. Kyriazoglou, C., Le Page, B. H., & Guild, F. J. (2004). Vibration damping for crack detection in composite laminates. *Composites Part A: Applied Science and Manufacturing*, *35*(7), 945-953.
150. Agrawalla, D. (2013). Diagnosis of Damages in Beam Structures using Vibration Parameters and Artificial Intelligence Techniques. http://ethesis.nitrkl.ac.in/4869.
151. Dash, A., K. (2012). Multiple Damage Identification of Beam Structure using Vibration Analysis and Artificial Intelligence Techniques. http://ethesis.nitrkl.ac.in/4430/1.
152. Przemieniecki, J.S. (1967).Theory of matrix structural analysis. 1st edition. London: McGraw-Hill.
153. Krawczuk, M., & Ostachowicz, W. M. (1995). Modelling and vibration analysis of a cantilever composite beam with a transverse open crack. *Journal of Sound and Vibration*, *183*(1), 69-89.
154. Vinson, J. R., & Sierakowski, R. L. (2012). *The behavior of structures composed of composite materials* (Vol. 5). Springer Science & Business Media.
155. Nikpur, K., & Dimarogonas, A. (1988). Local compliance of composite cracked bodies. *Composites science and technology*, *32*(3), 209-223.
156. Tada, H., Paris, P. C., & Irwin, G. R. (2000). The *Theory of matrix structural analysis alysis of cracks handbook*. New York: ASME Press.
157. Bao, G., Ho, S., Suo, Z., & Fan, B. (1992). The role of material orthotropy in fracture specimens for composites. *International Journal of Solids and Structures*, *29*(9), 1105-1116.

158. Tada H, Paris PC and Irwin GR (1985) *the stress analysis of cracks handbook 2nd ed. St. Louis*, MO: Paris production incorporated and Del Research Corporation.
159. http://www.ansys.com/staticassets/ansys/staticassets/resourcelibrary/presentation/ate-shells-14218.pdf.
160. Mamdani, E. M., & Assilian, S. (1975). An experiment in linguistic synthesis with fuzzy logic controller*" International journal of man-machine studies*, *7*(1), 1-13.
161. Zadeh, L. A. (1965). Fuzzy sets. *Information and control*, *8*(3), 338-353.
162. Takagi, T., & Sugeno, M. (1985). Fuzzy identification of systems and its applications to modeling and control. *Systems, Man and Cybernetics, IEEE Transactions on*, (1), 116-132.
163. Mcculloch, W., and Pitts, W. (1947). A logical calculus of the ideas immanent in nervous activity. *Bulletin of Mathematical Biophysics*, *5*(4), 115-133.
164. Rosenblatt, F. (1958). The perceptron: A probabilistic model for information storage and organization in the brain, *Psychological Review*, *65*(6), 386-408.
165. Haykin, S. (2006). *Neural Networks*: *A comprehensive foundation*. Pearson Education.
166. Leonard, J. A., Kramer, M. A., & Ungar, L. H. (1991). Using radial basis functions to approximate a function and its error bounds. *IEEE transactions on neural networks/a publication of the IEEE Neural Networks Council*, *3*(4), 624-627.
167. Weiss, S., & Kulikowski, C. (1991). Computer systems that learn. Morgan Kaufmann, San Mateo.
168. Kohonen, T. (1982), Self-organized formations of topologically correct feature maps. *Biological cybernetics*, *43*(1), 59-69.

.

Paper Published/Accepted in International/National Journals /Conferences

(1) **Irshad A. Khan,** and Dayal R. Parhi, "Fault detection of composite beam by using the modal parameters and RBFNN technique."*Journal of Mechanical Science and Technology* 29 (4) (2015):1637-1648.

(2) **Irshad A**. **Khan**, and Dayal R. Parhi, "Damage Identification in Composite Beam by Vibration Measurement and Fuzzy Inference System". *Journal of Mechanical Design* and *Vibration* 3(1) (2015): 8-23.

(3) **Irshad A**. **Khan**, Adik Yadao, and Dayal R. Parhi, "Fault Diagnosis of Cracked Cantilever Composite Beam by Vibration Measurement and RBFNN." *Journal of Mechanical Design and Vibration*1 (1) (2014): 1-4.

(4) Dayal R. Parhi and **Irshad A. Khan**, "Damage Identification Methodologies for Dynamic Structures: A Review" *International Journal of Applied Artificial Intelligence in Engineering System (IJAAIES)* 5 (2013): 141-149.

(5) Dayal R. Parhi and **Irshad A. Khan**; "Finite Element Analysis of Multi Cracked Cantilever Beam" *International Journal of Applied Artificial Intelligence in Engineering System (IJAAIES)* 5 (2013):105-112.

(6) Adik Yadao, **Irshad A. Khan** and Dayal R.Parhi, Modal Analysis of a Multiple Cracked Cantilever Bar" *IOSR Journal of Mechanical and Civil Engineering*, (2014):12-15.

(7) **Irshad A. Khan**, Adik Yadao and Dayal R. Parhi, "Diagnosis of Multiple Crack of Cantilever Composite Beam by Vibration analysis and Hybrid AI technique" *International Journal of Artificial Intelligence and Computational Research (IJAICR)*, 6(1) (2014): 25-31.

(8) Dayal R. Parhi, Adik Yadao and **Irshad A. khan**, "Vibration analysis of spinning cantilever shaft with a disc in viscous fluid" *International Journal of Artificial Intelligence and Computational Research (IJAICR)*, 6(1) (2014):17-24.

(9) Dayal R. Parhi and **Irshad A. Khan,** "Damage assessment of cantilever beam using vibration response and Kohonen Self Organizing Map network" *International Journal of Applied Artificial Intelligence in Engineering System* (Accepted).

(10) **Irshad A. Khan** and Dayal R. Parhi, "An intelligent fault diagnosis technique using hybrid Gaussian fuzzy and RBFNN" *Applied Soft Computing* (Communicated).

(11) **Irshad A. Khan** and Dayal R. Parhi, "An online condition monitoring technique using hybrid trapezoidal fuzzy-KSOM", *Structural Health Monitoring* (Communicated).

(12) **Irshad A. Khan**, Dayal R. Parhi, "Fault diagnosis of cantilever composite beam using vibration characteristics and Self organizing map neural network" *Steel and Composite Structures* (Communicated).

(13) **Irshad A. Khan**, Dayal R. Parhi, "Finite Element Analysis of Double Cracked Beam and its Experimental Validation" Procedia Engineering 51 (2013): 703 – 708.

(14) **Irshad A. Khan** and Dayal R. Parhi, "Diagnosis of Multiple Crack of Dynamic Cantilever Composite Beam using Vibration Signatures and Fuzzy Controller" Proceedings of International Conference on Advances in Mechanical Engineering; May 29-31, 2013.

(15) **Irshad A. Khan** and Dayal R. Parhi; "Application of Neural Network for Diagnosis of Damage of Multiple Cracked Cantilever Composite Beam" Proceedings of International Conference on Intelligent Robotics, Automation and Manufacturing; Dec 16-18, 2013.

(16) **Irshad A Khan**, Adik Yadao and Dayal R Parhi; "Application of Neural Network for Identification of Cracks on Cantilever Composite Beam" Internation Conference on Industrial Engineering Science and Applications; April 2-4, 2014

APPENDIX A

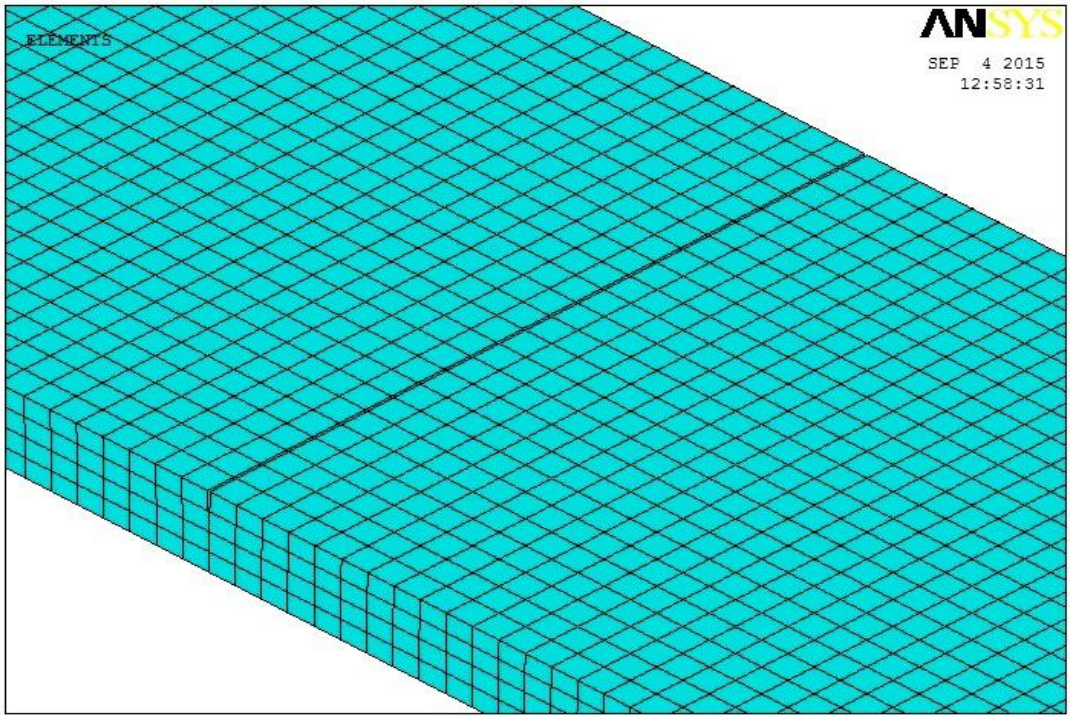

Figure A1 Finite element model of cracked composite beam for crack depth 0.166

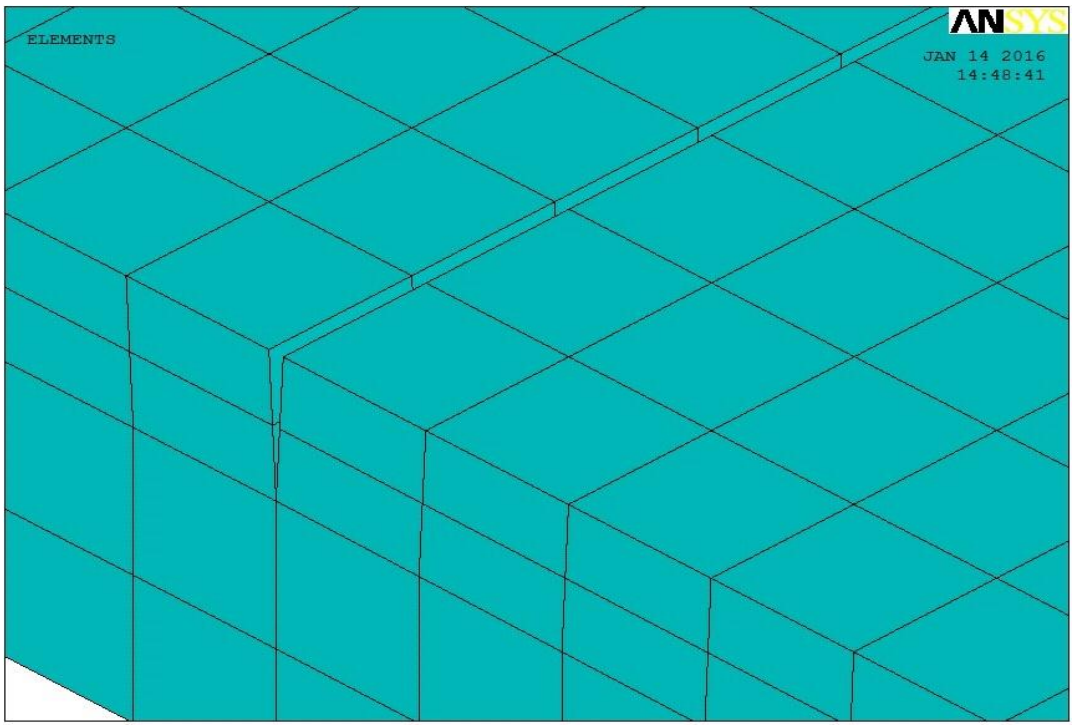

Figure A2 Finite element model of cracked composite beam for crack depth 0.333

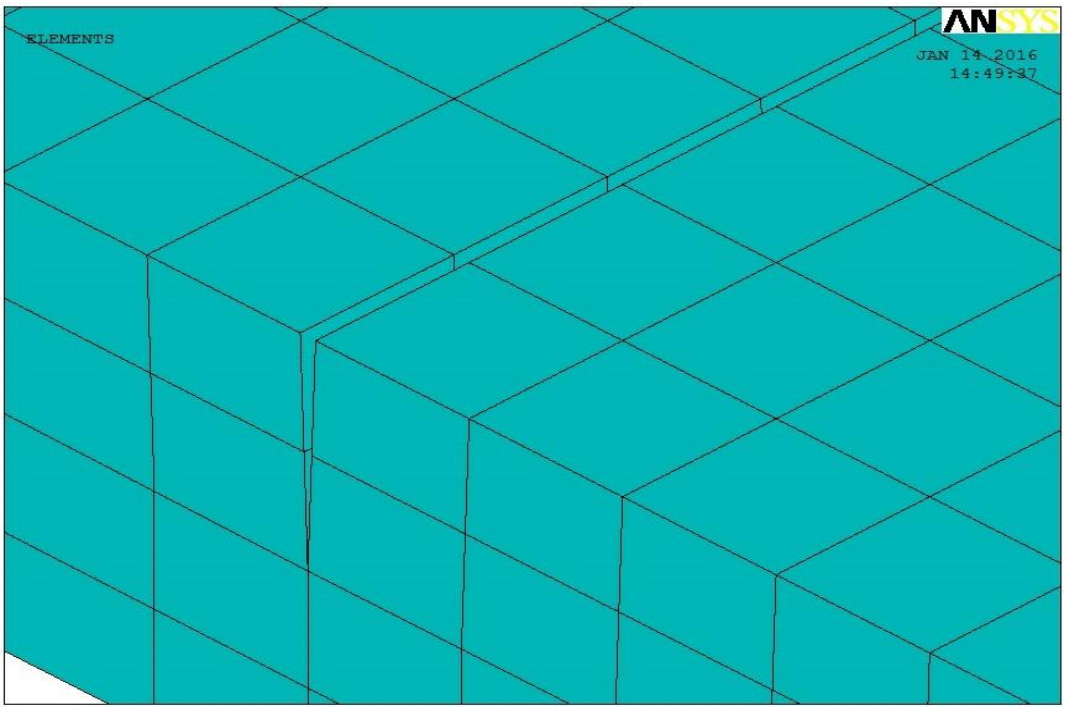

Figure A3 Finite element model of cracked composite beam for crack depth 0.5

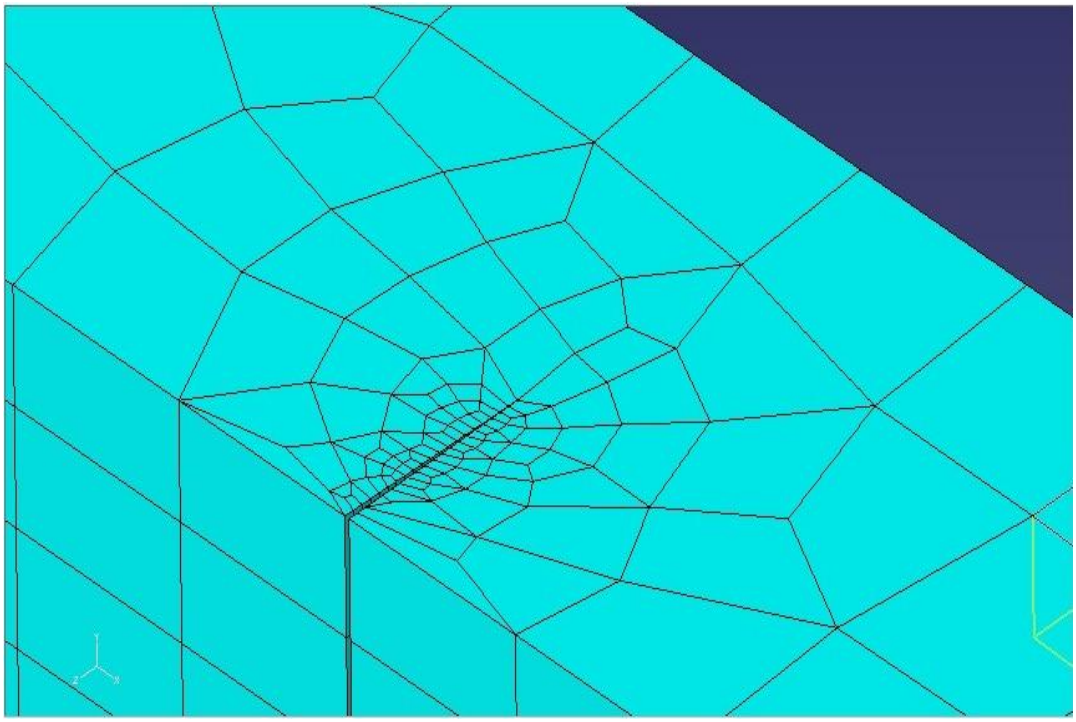

Figure A4 Meshing at the crack tip

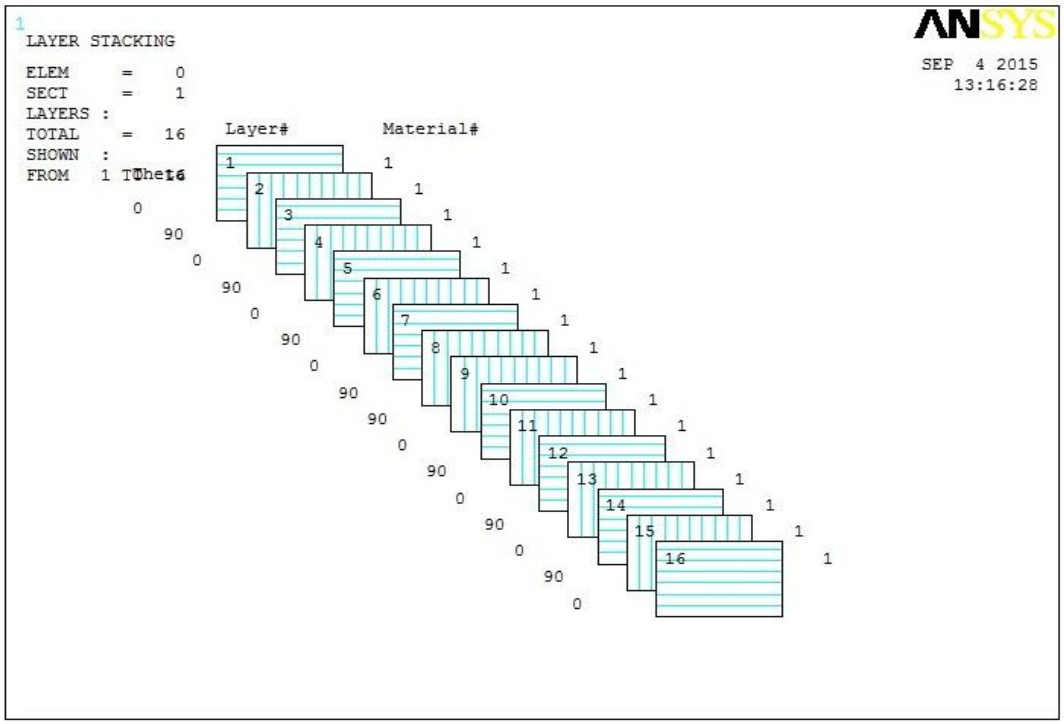

Figure A5 Layers stacking in composite beam

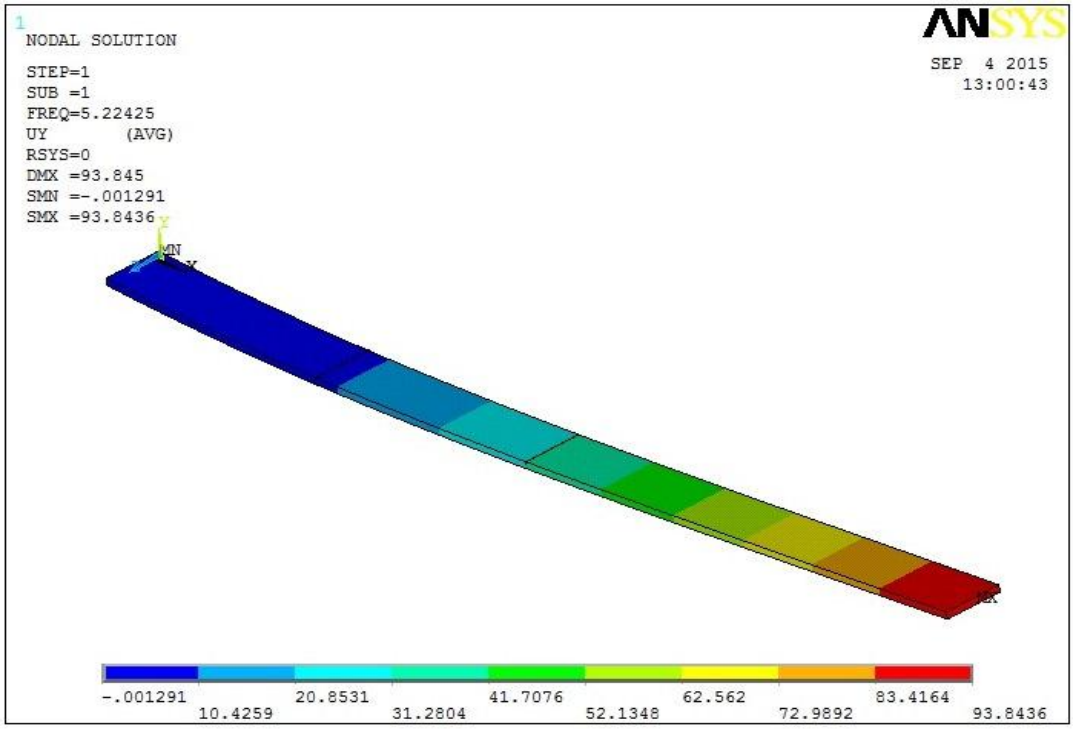

Figure A6 (a) ANSYS generated I mode shape of cantilever beam

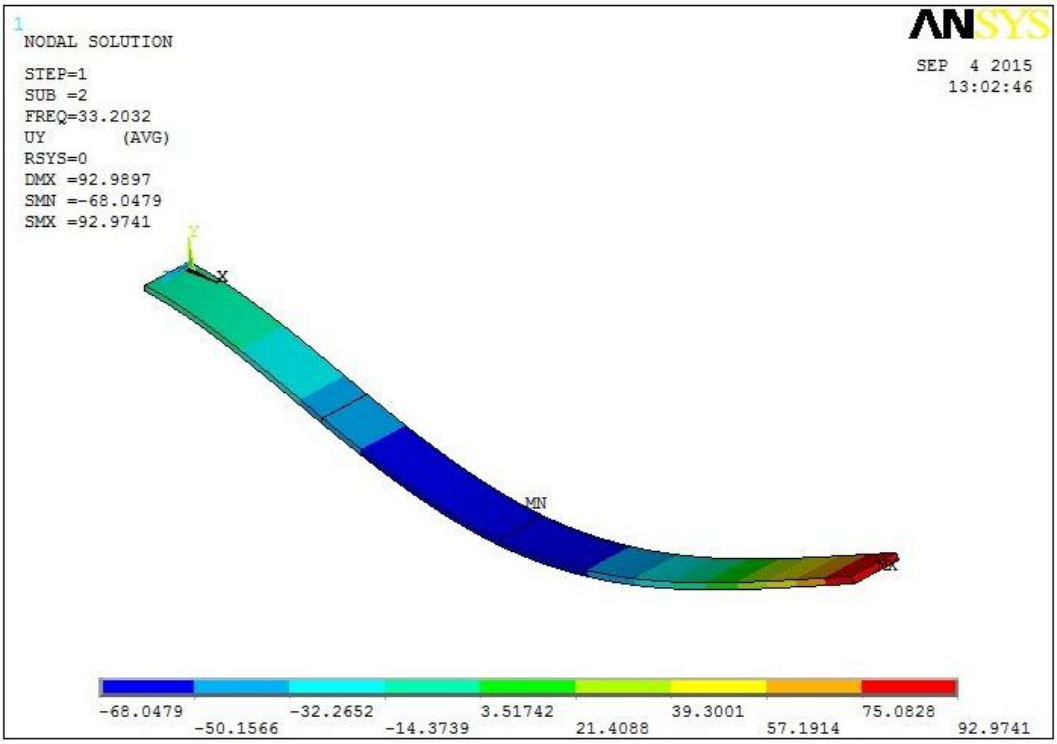

Figure A6 (b) ANSYS generated II mode shape of cantilever beam

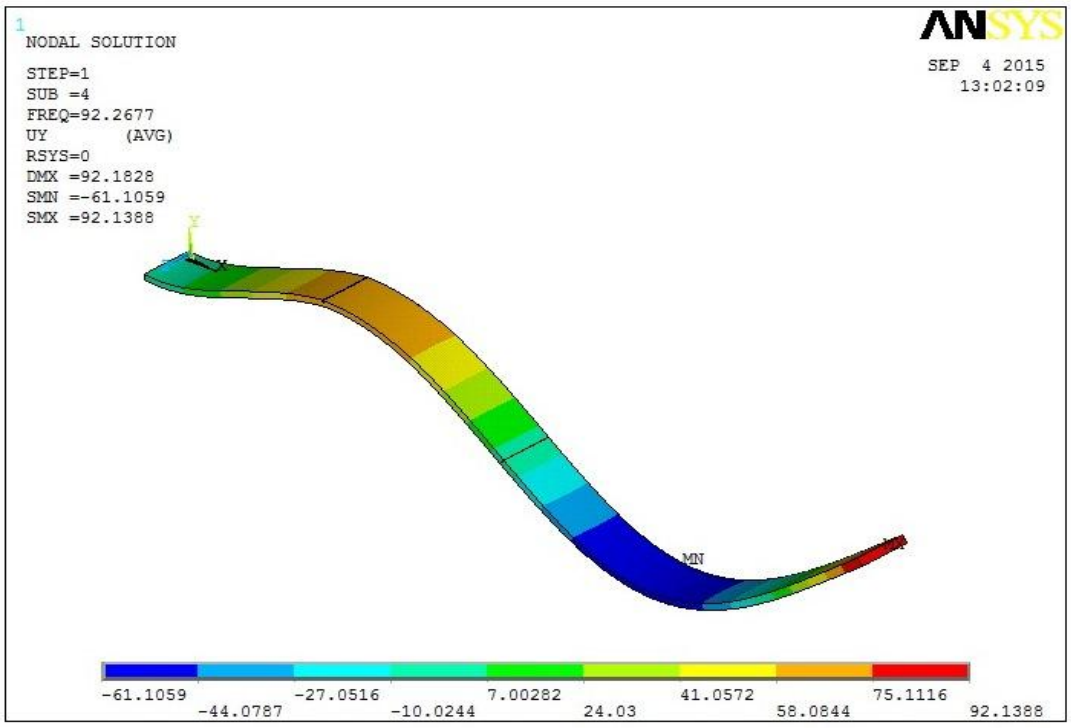

Figure A6 (c) ANSYS generated III mode shape of cantilever beam

APPENDIX B

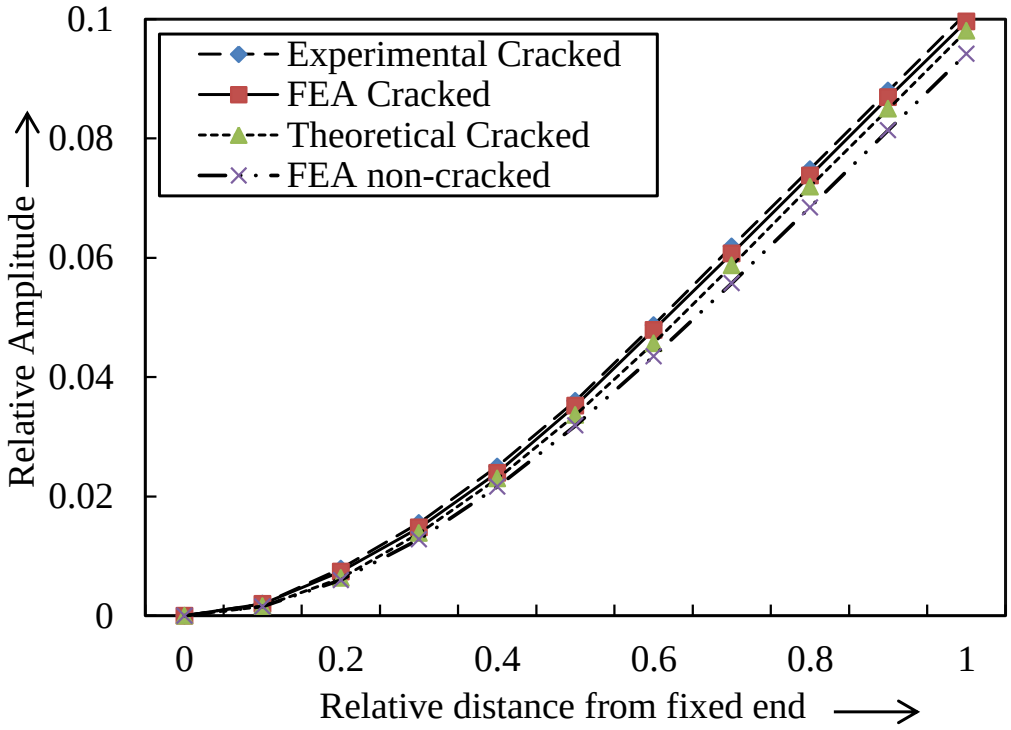

Figure B1 (a) Relative Amplitude vs. Relative distance from fixed end (1st mode of vibration) β1=0.25, β2=0.5, ψ1=0.1667 & ψ2=0.5 (Composite)

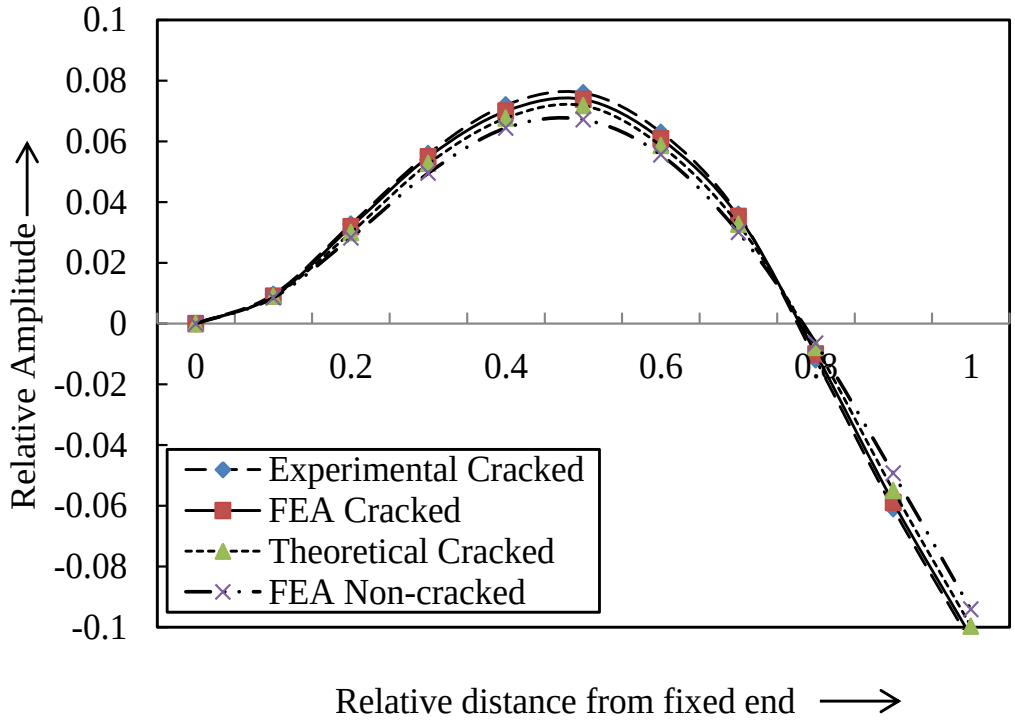

Figure B1 (b) Relative Amplitude vs. Relative distance from fixed end (2^{nd} mode of vibration) β_1=0.25, β_2=0.5, ψ_1=0.1667 & ψ_2=0.5 (Composite)

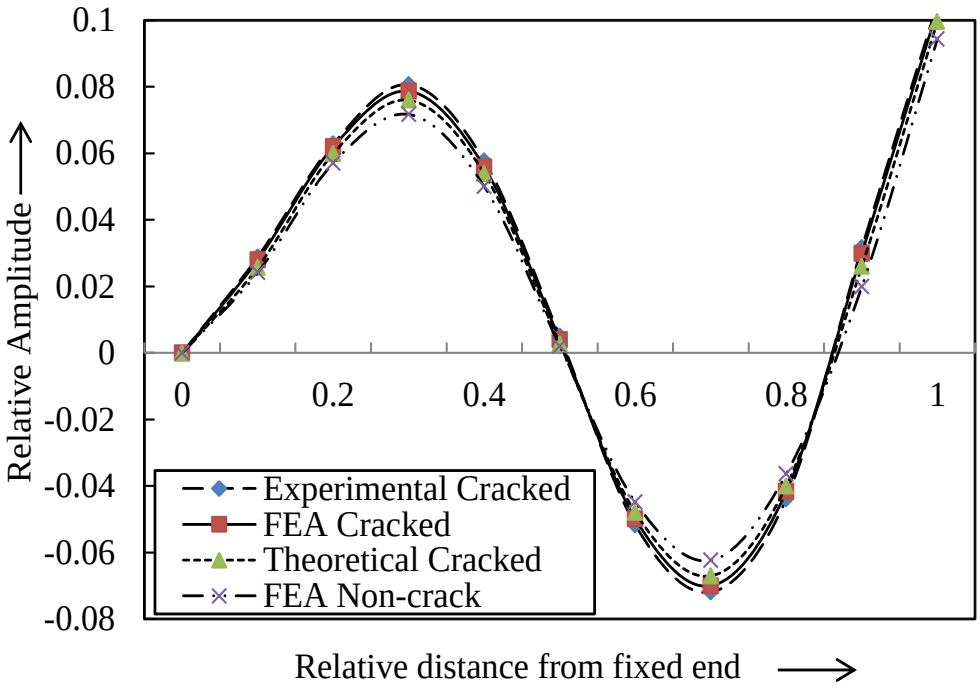

Figure B1(c) Relative Amplitude vs. Relative distance from fixed end (3rd mode of vibration) β_1=0.25, β_2=0.5, ψ_1=0.1667 & ψ_2=0.5 (Composite)

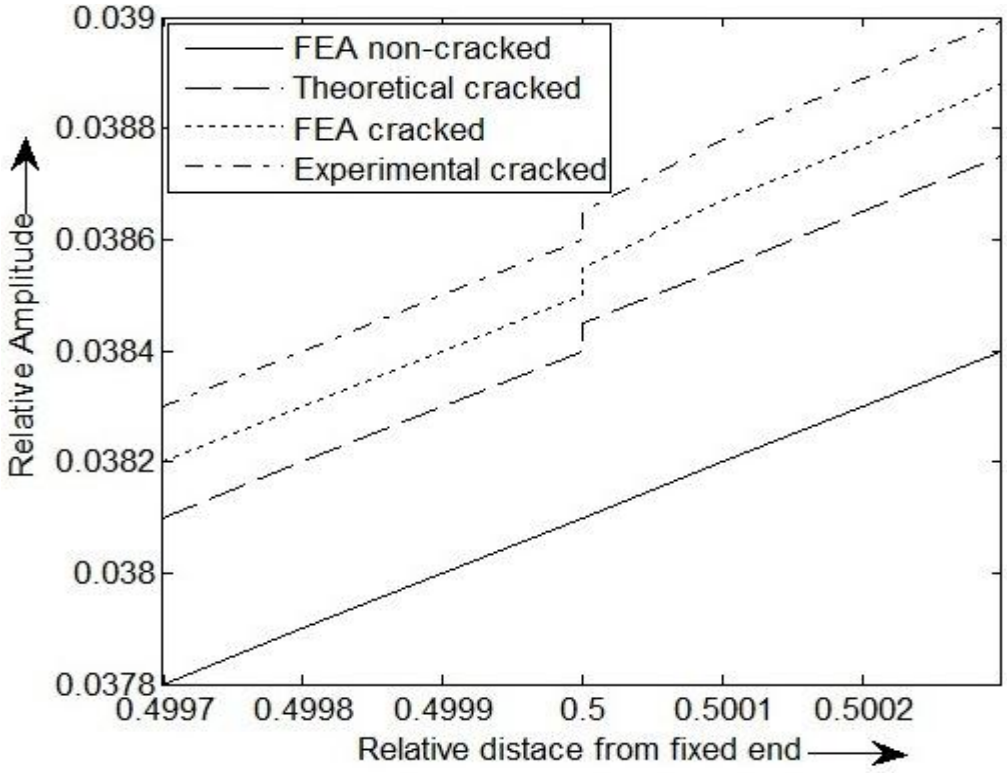

Figure B2 (a) Magnified view at the second crack location (β_1=0.5) for the first mode shape (Composite)

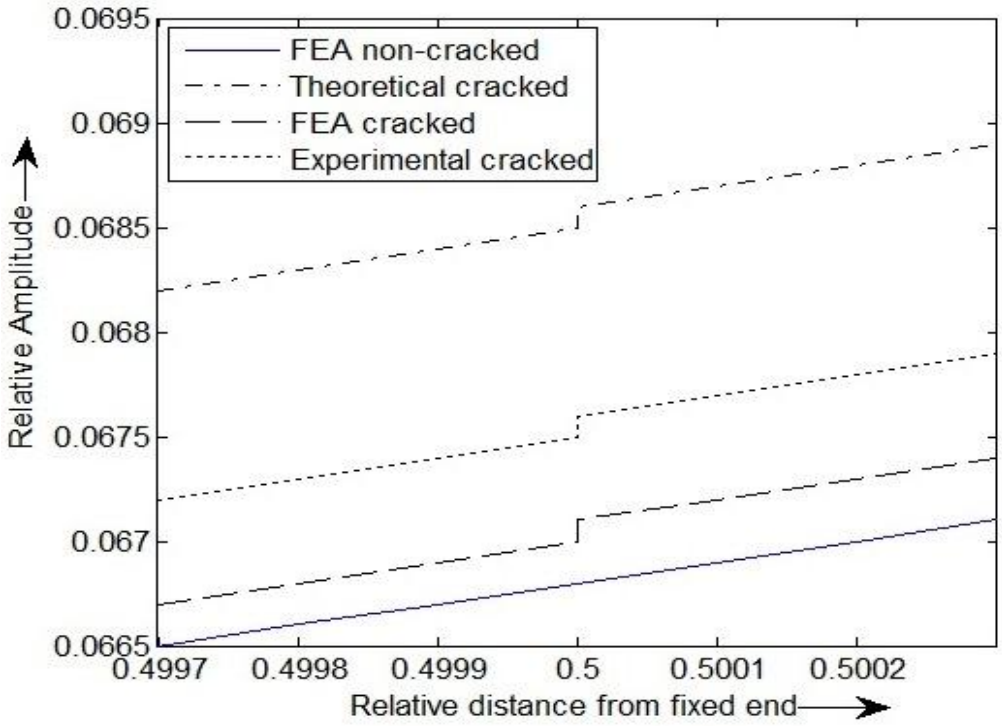

Figure B2 (b) Magnified view at the second crack location (β_1=0.5) for the second mode shape (Composite)

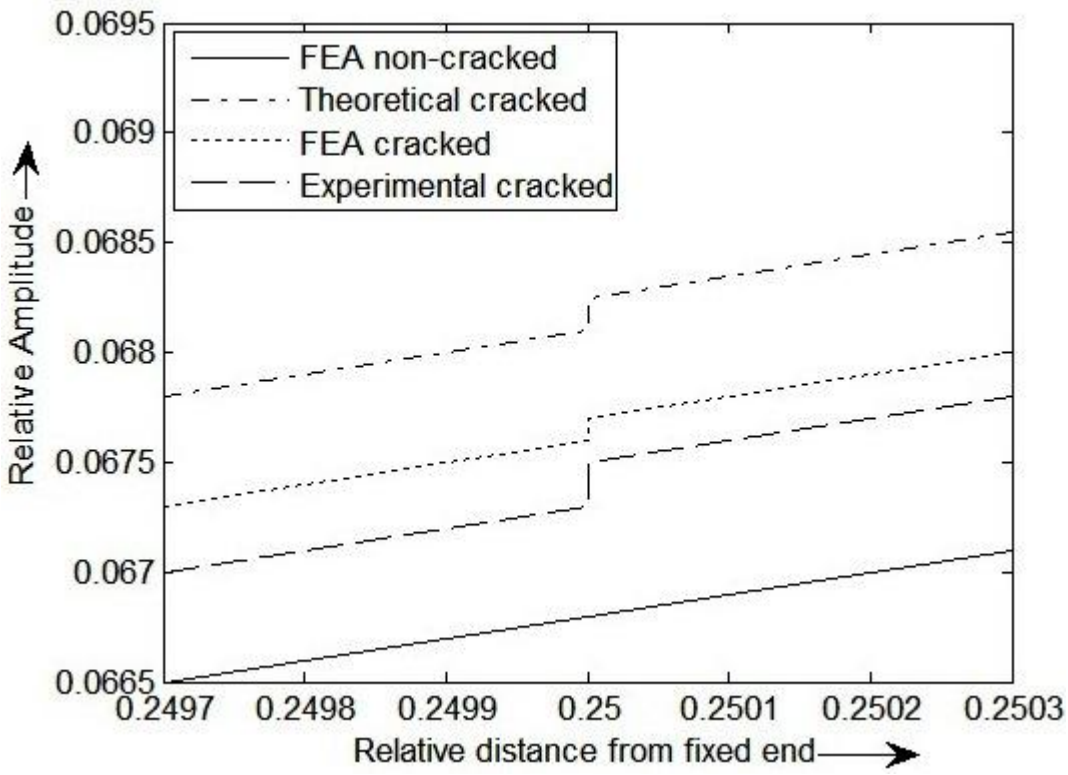

Figure B2(c) Magnified view at the third crack location (β_1=0.25) for the third mode shape (Composite)

APPENDIX C

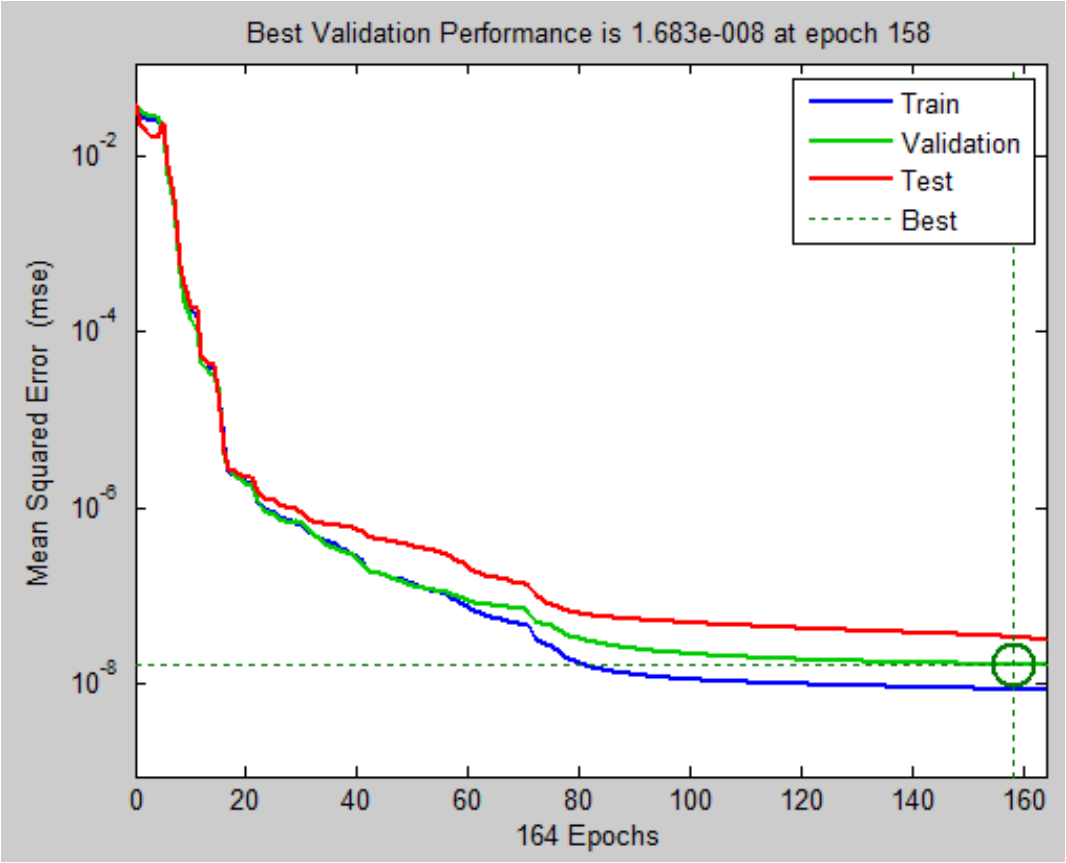

Figure C1 Epochs vs mean square error for BPNN model

APPENDIX D

Figure D1 Relative first three natural frequencies and mode shapes derived from FEA (Composite)

Relative 1st natural frequency "rfnf" (Cracked)	Relative 1st natural frequency "rfnf" (Non-cracked)	Relative 2nd natural frequency "rsnf" (Cracked)	Relative 2nd natural frequency "rsnf" (Non-cracked)	Relative 3rd natural frequency "rtnf" (Cracked)	Relative 3rd natural frequency "rtnf" (Non-cracked)	Relative 1st mode shape difference "rfmd" (Cracked)	Relative 1st mode shape difference "rfmd" ((Non-cracked)	Relative 2nd mode shape difference "rsmd"(Cracked)	Relative 2nd mode shape difference "rsmd" (Non-cracked)	Relative 3rd mode shape difference "rtmd"(Cracked)	Relative 3rd mode shape difference "rtmd" (Non-cracked)	FEA relative 1st crack location "rfcl" 1st crack depth "rfcd" 2nd crack location "rscl" 2nd crack depth "rscd"			
												rfcl	rfcd	rscl	rscd
0.99607	1	0.99700	1	0.99829	1	0.00013	0	0.00203	0	0.00240	0	0.182	0.162	0.424	0.242
0.98098	1	0.99557	1	0.99892	1	0.00275	0	0.00456	0	0.01064	0	0.121	0.404	0.848	0.323
0.99651	1	0.99425	1	0.99796	1	0.00079	0	0.00264	0	0.00101	0	0.303	0.162	0.485	0.242
0.99001	1	0.99318	1	0.98710	1	0.00145	0	0.00571	0	0.00508	0	0.242	0.404	0.545	0.162
0.98809	1	0.98584	1	0.98255	1	0.00288	0	0.01210	0	0.01352	0	0.363	0.485	0.727	0.242
0.99672	1	0.98724	1	0.99719	1	0.00176	0	0.00332	0	0.00594	0	0.424	0.242	0.545	0.323
0.99788	1	0.97843	1	0.97519	1	0.00284	0	0.01222	0	0.02349	0	0.545	0.323	0.666	0.485
0.99874	1	0.99877	1	0.99628	1	0.00026	0	0.00475	0	0.01519	0	0.606	0.081	0.848	0.404
0.99114	1	0.99799	1	0.99803	1	0.00010	0	0.00166	0	0.00183	0	0.182	0.242	0.303	0.242
0.99701	1	0.98999	1	0.99803	1	0.00153	0	0.00464	0	0.00239	0	0.424	0.323	0.545	0.162

Figure D2 Relative first three natural frequencies and mode shapes derived from FEA (Steel)

Relative 1st natural frequency "rfnf" (Cracked)	Relative 1st natural frequency "rfnf" (Non-cracked)	Relative 2nd natural frequency "rsnf" (Cracked)	Relative 2nd natural frequency "rsnf" (Non-cracked)	Relative 3rd natural frequency "rtnf"(Cracked)	Relative 3rd natural frequency "rtnf"(Non-cracked)	Relative 1st mode shape difference "rfmd"(Cracked)	Relative 1st mode shape difference "rfmd" ((Non-cracked)	Relative 2nd mode shape difference "rsmd"(Cracked)	Relative 2nd mode shape difference "rsmd"(Non-cracked)	Relative 3rd mode shape difference "rtmd"(Cracked)	Relative 3rd mode shape difference "rtmd"(Non-cracked)	FEA relative 1st crack location "rfcl" 1st crack depth "rfcd" 2nd crack location "rscl" 2nd crack depth "rscd"			
												rfcl	rfcd	rscl	rscd
0.99939	1	0.99813	1	0.99978	1	0.00013	0	0.00106	0	0.00411	0	0.121	0.161	0.241	0.322
0.99980	1	0.99768	1	0.99664	1	0.00035	0	0.00108	0	0.00073	0	0.241	0.080	0.483	0.161
0.99952	1	0.97803	1	0.98418	1	0.00341	0	0.00134	0	0.02088	0	0.362	0.241	0.603	0.483
0.99889	1	0.99881	1	0.99932	1	0.00041	0	0.00224	0	0.00310	0	0.181	0.322	0.302	0.161
0.99906	1	0.98250	1	0.99800	1	0.00293	0	0.00965	0	0.00839	0	0.422	0.483	0.663	0.241
0.99958	1	0.99129	1	0.99869	1	0.00123	0	0.00187	0	0.00670	0	0.543	0.322	0.784	0.080
0.99971	1	0.98183	1	0.98589	1	0.00272	0	0.00638	0	0.00962	0	0.483	0.402	0.724	0.483
0.99473	1	0.98761	1	0.98721	1	0.00239	0	0.00786	0	0.01099	0	0.302	0.483	0.543	0.322
0.99230	1	0.99003	1	0.99182	1	0.00149	0	0.00455	0	0.00673	0	0.422	0.241	0.639	0.402
0.99677	1	0.98931	1	0.99459	1	0.00152	0	0.00540	0	0.00865	0	0.603	0.402	0.844	0.322